JOINT EUROPEAN TORUS JET

JET JOINT UNDERTAKING

PROGRESS REPORT 1990

Volume II

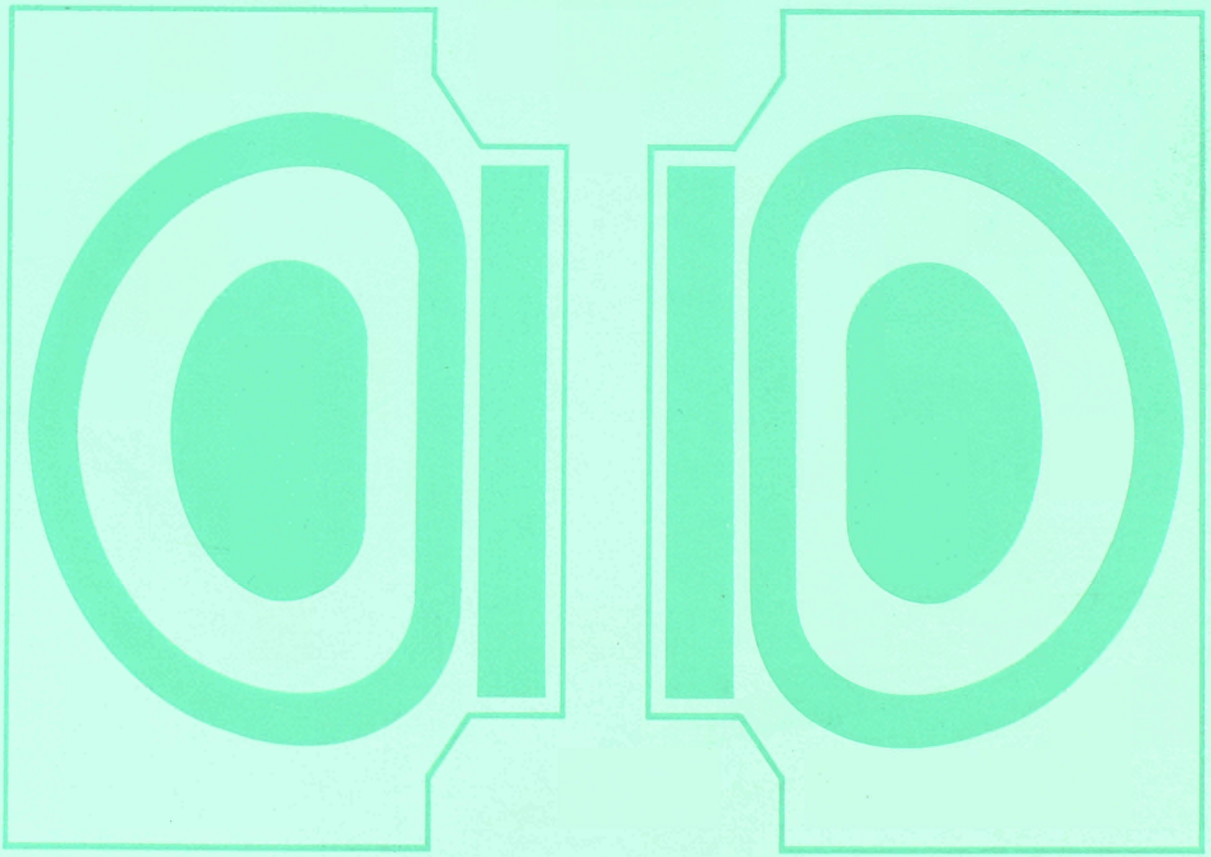

EUR 13493 EN

EUR-JET-PR8

JET JOINT UNDERTAKING

PROGRESS REPORT 1990

Volume II

March 1991

This document is intended for information only
and should not be used as a technical reference.

EUR13493 EN (EUR-JET-PR8)March 1991.
Editorial work on this report was carried out by B.E.Keen.
The preparation for publication was undertaken by JET
Reprographic Service, JET Joint Undertaking, Abingdon, UK.

Catalogue number : CD-NB-13493-EN-C for the report EUR 13493 Volume II

Printed in England

Contents

Appendix III

Reprints of JET Papers

* Copies of these papers can be obtained from JET Publications Office, K1/1/20a, Ext. 4646

Contributed Papers to 17th EPS Conference on Controlled Fusion and Plasma Heating

Amsterdam, the Netherlands, 25th-29th June 1990

Many Authors

JET PAPERS TO 17TH EPS CONFERENCE ON CONTROLLED FUSION & PLASMA HEATING (AMSTERDAM, NETHERLANDS, 25TH-29TH JUNE 1990)

Title	Responsible Author
Oral Papers	
^{3}He-D Fusion Studies and α-Particle Simulations using MeV Ions Created by ICRH in the JET Tokamak	D.F.H. Start
Particle and Heat Deposition in the X-Point Region at JET	D.P. O'Brien
High-Beta Regimes in JET	P. Smeulders
ICRH Produced H-Modes in the JET Tokamak	V.P. Bhatnagar
JET Neutron Emission Profiles and Fast Ion Redistribution from Sawteeth	F.B. Marcus
Effect of Limiter and Wall Composition on Z_{eff} and Recycling in JET	J.P. Coad
First Measurements of the JET Electron Density Profile with the Multichannel Reflectometer	R. Prentice
Poster Contributions	
Sawtooth Stabilisation by Fast Ions: Comparison BetweenTheory and Experiments	F. Porcelli
A Unified Physical Scaling Law for Tokamak Confinement	J.P. Christiansen
Electron Absorption of Fast Magnetosonic Wave by TTMP in JET	F. Rimini

Title	Responsible Author
Fast Ion Orbit Effects in High Power ICRH Modulation Experiments in the JET Tokamak	D.F.H. Start
Evidence of Coupling of Thermal and Particle Transport from Heat and Density Pulse Measurements at JET	G.M.D. Hogeweij
Vertical Instabilities in JET	P. Noll
Magnetic Island Self-Sustainment by Finite Larmor Radius Effect	M. Hugon
Transport of Impurities during H-Mode Pulses in JET	L. Lauro-Taroni
Determination of Local Transport Coefficients by Heat Flux Analysis and Comparisons with Theoretical Models	B. Balet
Extrapolation of the High Performance JET Plasmas to D-T Operation	J.G. Cordey
On Global H-Mode Scalings Based on JET and ASDEX	O. Kardaun
Analysis of Simultaneous Evolution of Temperature and Density Perturbations following Pellet Injection	A. Gondhalekar
Assessment of Transport Models on the Basis of JET Ohmic and L-Mode Discharges	Ch. Sack
Charge Exchange Spectroscopy Measurements of Light Impurity Behaviour in the JET Beryllium Phase	H. Weisen

Title	Responsible Author
A Regime Showing Anomalous Triton Burnup in JET	S. Conroy
Retention of Gaseous (Ar,He) Impurities in the JET X-Point Configuration	G. Janeschitz
The Spontaneous Growth and Resulting Topology of the m=1 Instability in the JET Sawtooth Collapse	S.W. Wolfe
Modelling Impurity Control in the JET Pumped Divertor	R. Simonini
On Diffusion of Magnetic Field Lines	D.F. Düchs
Measurements of Deuteron Density Profiles in JET	W. Mandl
Scrape-Off Layer Parameters at JET During Density Limit Discharges	S. Clement
The Compatibility of The JET H-Mode with Other Regimes of Improved Performance	A. Tanga
D-D Neutron Production from JET Plasmas	G. Sadler
Peaked Profiles in Low q High Current Limiter Plasmas in JET	P.J. Lomas
Density Limits in JET with Beryllium	C.G. Lowry
Stabilisation of Drift-Tearing Modes at the Breakdown of the Constant- ψ Approximation	F. Porcelli
Faraday Rotation Meaurements on JET, and the Change in the Safety Factor Profile at a Sawtooth Collapse	J. O'Rourke

Title	Responsible Author
The Fusion Performance of JET Limiter Plasmas using Be Coated Graphite and Solid Be Surfaces	T.T.C. Jones
Toroidal Plasma Rotation in JET	H.P.L. de Esch
A Quantitative Assessment of Ion-Temperature-Gradient-Driven Turbulence Theory based on JET Experimental Data	F. Tibone
Temperatures and Densities in the JET Plasma Boundary Deduced from Deuterium and Beryllium Spectra	M.F. Stamp
Radiation Asymmetries and H-Modes	N. Gottardi
Ion Temperatures at JET	H.W. Morsi
Dynamic Response of Plasma Energy and Broad-Band Magnetic Fluctuations to Additional Heating in JET	C. Nardone
Formation of Detached Plasmas During High Power Discharges in JET	G.M. McCracken
Sawtooth Triggered Disruptions at the DITE Density Limit	G.M. Fishpool
A Method for the Determination of the Total Internal Magnetic Field in JET	L. Porte
An Investigation into the Possibility of High Ion Temperatures in the edge of JET	S.K. Erents

Appendix III (b)
JET-P(90)33

Fusion Relevant Performance in JET

The JET Team
(presented by A.Gibson)

Invited Paper presented to the 17th European Conference on Controlled Fusion and Plasma Heating, Amsterdam, the Netherlands, 25th-29th June 1990

Fusion Relevant Performance in JET

The JET Team[1]
(Presented by A. Gibson[2])
JET Joint Undertaking, Abingdon, Oxon, OX14 3EA, UK

ABSTRACT

An overview is given of fusion relevant performance in a number of JET operational regimes. It is shown that in most areas JET provides a suitable platform on which to base the design and predict the performance of a next step device. The main outstanding problem area is that of controlling impurity influxes and plasma exhaust, these are to be studied in a new phase programme under consideration for JET. The fusion performance already obtained in JET is described with 100kW of fusion power being generated in charged particles from the D-He^3 reaction and more than 10 MW of fusion power predicted from present discharges if operated in D-T.

1. INTRODUCTION

The Joint European Torus (JET) routinely produces plasmas whose main parameters lie clearly within the reactor regime.

In this paper we describe some of the important reactor relevant properties of these plasmas, especially in the following areas:

(a) Operation near the Density Limit
(b) Operation near the β Limit
(c) The Production of High Temperatures
(d) Confinement Times
(e) Limitations due to Impurity Influxes
(f) Fusion Product Confinement
(g) Fusion Performance

2. OPERATION NEAR THE DENSITY LIMIT

Operation near the density limit has been systematically studied in JET for limiter discharges, with Carbon limiters, with evaporated Beryllium layers and with Beryllium limiters (see Lowry et al, 1990).

The operating density in tokamaks is usually presented in the form given in Fig 1. Each point represents the maximum obtained normalised density during a discharge with either Ohmic (OH), Neutral Beam (NBI), Ion Cyclotron (ICRH) or combined heating. The broken lines marked by OH (C) and NBI(C) are the highest limits obtained in the previous campaigns with Carbon walls and limiters (nRq/B = 12 for ohmic heating and 20 with additional heating in units of 10^{19} m^{-3}, m, T). There are clear improvements due to the Be

[1]See Appendix I
[2]Paper prepared by A Gibson and P Smeulders

limiters and Be coated walls, so that nRq/B ~33 is reached with combined heating, ICRH heating and NBI. Furthermore the limiting density increases with the applied power as we shall see shortly. The limit at low q however is unchanged and is still set by major current disruptions. It corresponds to unstable plasma conditions at $q_\psi < 2$ for all densities.

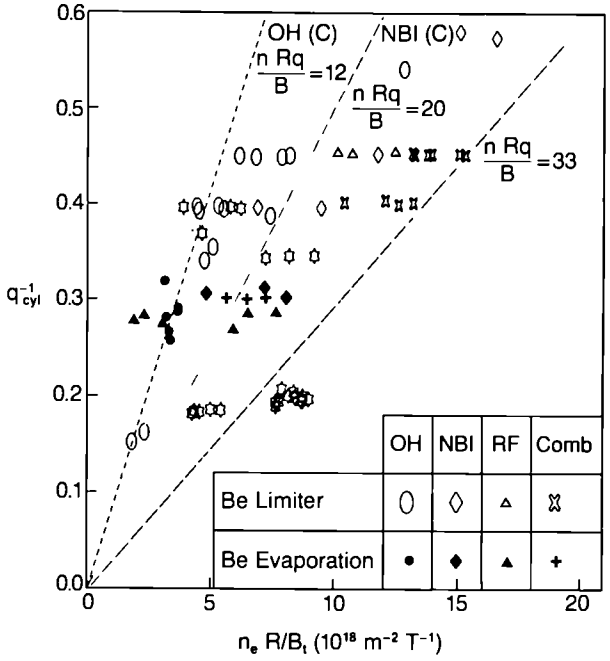

Fig. 1 The operating density range for JET shown as normalised current $q_{cyl}^{-1} = \pi R I_p / 5 A B_\varphi \left[m, MA, m^2, T\right]$ *versus normalised density* $n_e R/B_\varphi$ *[m^{-3}, m, T]. The broken lines with nRq/B = 12 and 20 respectively. represent the maximum density values obtained before the introduction of Beryllium into the vacuum vessel for ohmic heating (OH (C)) and for Neutral Beam heating (NBI (C)). The symbols are the maxima obtained after the introduction of Be for various heating scenarios.*

There has not yet been such a systematic study for X-point discharges, but it is clear that the behaviour is similar, perhaps with somewhat smaller density limits. The highest densities so far in X-point discharge are obtained in H-mode with $\bar{n}Rq_{cyl} / B_t \sim 20 \times 10^{19}$ m^{-2}T^{-1}. At higher densities, typically when $P_{rad}/P_t \sim 60\%$, an H to L-mode transition occurs and the density falls without causing a disruption.

In limiter discharges the nature of the limit is different for C and Be limiters. Whereas with C limiters the limit is marked by a radiative collapse and hard disruption. With Be limiters it is generally marked by the appearance of an asymmetrical edge radiation (MARFE) which, with gas fuelled discharges, is accompanied by a fall in recycling and reduction in density, typically leading to a soft density limit with a relaxation oscillation of density and radiation near the limit. It is also clear that the highest densities are obtained for the points with the highest additional heating. This point is emphasised in Fig. 2.

A number of papers (Gibson, 1976) have suggested that the density limit is determined by a radiation power balance especially in the edge regions of the discharge (Rebut and Green, 1976, Campbell et al, 1986, Wesson et al, 1989). These models suggest that the density limit should increase approximately as $P_t^{1/2}$. Fig 2 shows this type of behaviour for gas and pellet fuelled discharges with Beryllium coated walls.

A number of discharges on Fig. 2 show a MARFE density limit while the other points are existence points where no density limit occured. The MARFE points on this diagram fall in the middle of the existence region. However the MARFE limit for pellet and gas fuelled discharges does lie at the boundary of the existence region if the edge density is used

instead of the line average density. That is MARFE's occur only close to the curve $n_{edge} R/B_t = 2.37 P^{1/2}$, see Fig. 3.

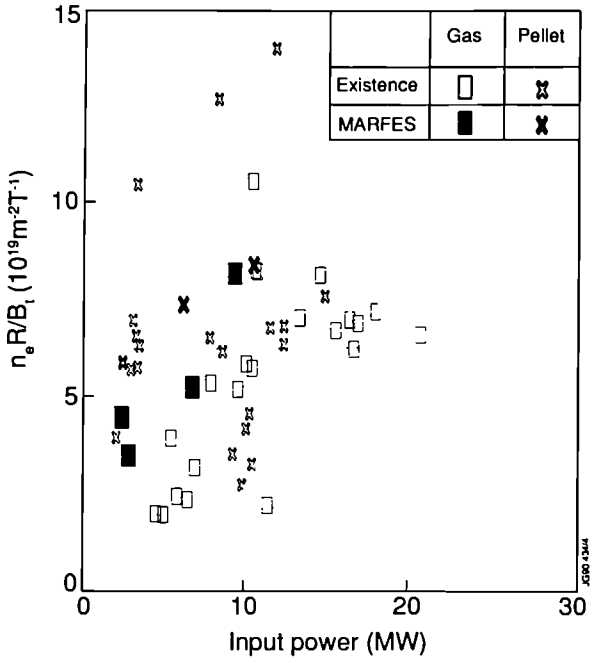

Fig. 2 The normalised line density as function of the input power, the limiting density cases (MARFES) occur throughout the existence region shown in the figure.

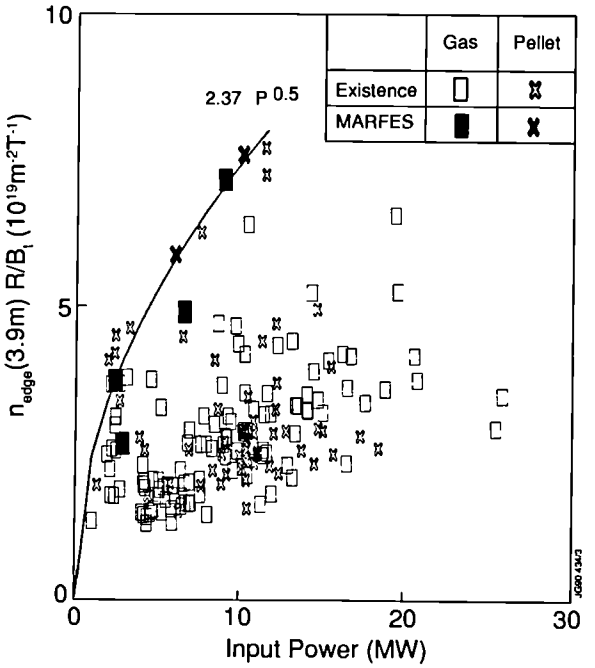

Fig.3 The normalised edge density versus input power showing that the MARFE density limit now occurs at the boundary of the existence region. In this diagram B varies in the range 1.4 to 2.6 T.

Operation near the density limit in JET can thus be summarised as follows :

(a) The density limit for additionally heated discharges in JET, with Beryllium limiters in clean conditions, exceeds $nRq_{cyl}/B_t = 33 \times 10^{19} m^{-2} T^{-1}$;

(b) The density limit in gas and pellet fuelled discharges increases with input power approximately as $P_t^{1/2}$ and is determined by edge parameters, particularly the edge density;

(c) The radiative nature of the limit and the difference between Carbon and Beryllium walls make it clear that the limit is determined by impurity content and hence wall interaction and material type;

(d) The high value obtained for the limit in JET means that an acceptable limit will be obtained in next step devices provided that a sufficient degree of impurity exclusion can be obtained.

3. OPERATION NEAR THE BETA LIMIT

Troyon established computationally a quantitative estimate for the β limit in tokamaks for reasonable profiles (Troyon et al, 1984) :

$$\beta_{Troy} = 2.8 \times 10^{-2} I_p / B_\varphi a \text{ (MA, T, m)} \qquad (2.1)$$

Many experiments have shown steady state high β operation close to this limit and even at somewhat higher values. (ASDEX, Ryter et al, 1990; DIII-D, Ferron et al, 1990; PBX, Takahashi et al, 1990)

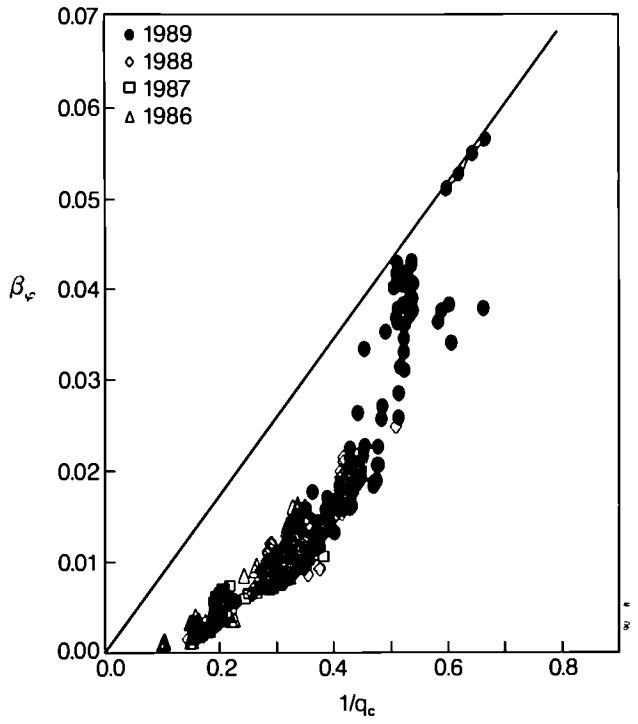

Fig. 4 The maximum toroidal beta ($\beta_\varphi = 2\mu_0 <p>/B_\varphi^2$) as function of the normalised current $q_{cyl}^{-1} = \pi R I_p / 5 A B_\varphi$ for all JET discharges from 1986-1989 with the poloidal beta β_φ>0.4. The line is approximately the Troyon limit, $\beta_{Troyon} = 0.028\, I_p/aB_\varphi$ [MA,m,T]. The highest β of 5.5% is obtained in a 2 MA, Double-Null H-mode discharge at 0.9T with $T_e(0)$=3.7 keV, $T_i(0)$ =6.3 keV, $n_e(0)=3x10^{19}m^{-3}$, τ_E = 0.35 s, q_{cyl} = 1.6, q_ψ = 2.2, P_{NB} = 11 MW, 80 kV D-injection in a H-plasma.

In JET, the Troyon limit has been reached within the available heating power at reduced toroidal field in Double Null H-mode discharges. (Smeulders et al, 1990). Fig. 4 shows for a number of JET discharges the maximum β obtained as a function of q_c^{-1}. Values within a factor of two of the Troyon value are readily obtained and the highest values reach the Troyon limit.

These values were obtained for a discharge where the toroidal magnetic field was lowered from 1.1 to 0.9T at a constant neutral beam (NB) power of 11 MW while the β remained close to the Troyon value limit as shown in Fig. 5. The discharge is already sawtoothing before the β limit is reached. NBI is switched on progressively from t = 13s, β increases

progressively until Troyon limit is reached at t = 14.3s. The β value then falls from the limit value by ~10% at each sawtooth crash and climbs back between the crashes.

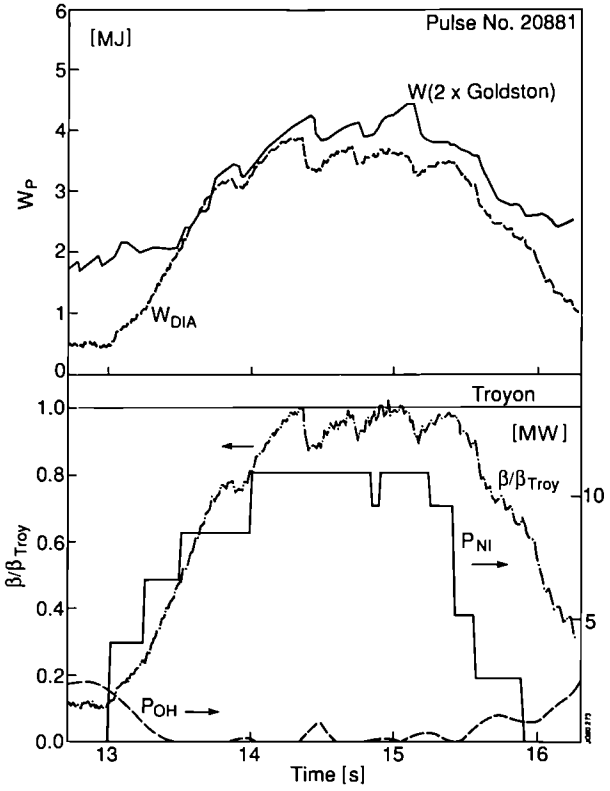

Fig. 5 The observed plasma energy W_{DIA} and the energy W_G calculated from the effective input power (P_t–dW/dt) and $\tau_E = 2\tau_G$ for the highest beta discharge as a function of time. Also shown are the normalised beta β β_{Troy}, NBI and OH powers.

This discharge like other H-mode discharges in JET has $\tau_E \sim 2 \times \tau_G$ (Eq. 4.1). Fig. 5 also shows the observed plasma energy W_{DIA} and the energy W_G calculated from the power input and $\tau_E = 2x\tau_G$. When the β limit is reached W_{DIA} is close to or below W_G This could be because the confinement time has degraded to give a soft limit, or it could be because the power applied in this discharge is only just enough to reach the limit. Clearly an important experiment to do in JET is to increase the input power significantly above the value needed to reach β_{Troy} and see whether the confinement time does indeed degrade to maintain a soft limit.

4. CONFINEMENT TIMES

The confinement time in JET discharges generally degrades with increasing power flow through the plasma. An example for H-Mode discharges is shown in Fig. 6. The energy confinement time is defined in the usual way as $\tau_E = W/(P_t - dW/dt)$, where P_t is the total power input to the plasma and W is the plasma kinetic energy content (usually measured by a diamagnetic loop). The experimental values roughly follow a scaling of the Goldston type (Goldston et al, 1984) with a multiplier, H of ~2 :

$$\tau_E(G) = 3.7 \times 10^{-2} H I_p (P_t - [dW/dt])^{-0.5} R^{1.38} (a/R)^{-0.37} (b/a)^{0.5} \quad (MA, MW, m) \qquad (4.1)$$

It should be noted that for a power-flow of 10 MW the energy confinement time can reach ~1 s and for 20 MW can exceed ~0.5 s.

The inclusion of the (dW/dt) term in the definition of $\tau_E(G)$ permits the inclusion on Fig. 6 of a number of data which have not reached steady state. However more than 90% of the

data have (dW/dt) < 0.5 P_t and more than 60% have (dW/dt) < 0.3 P_t. The term (dW/dt) thus always has the nature of a correction but it does significantly improve the fit to the scaling relation.

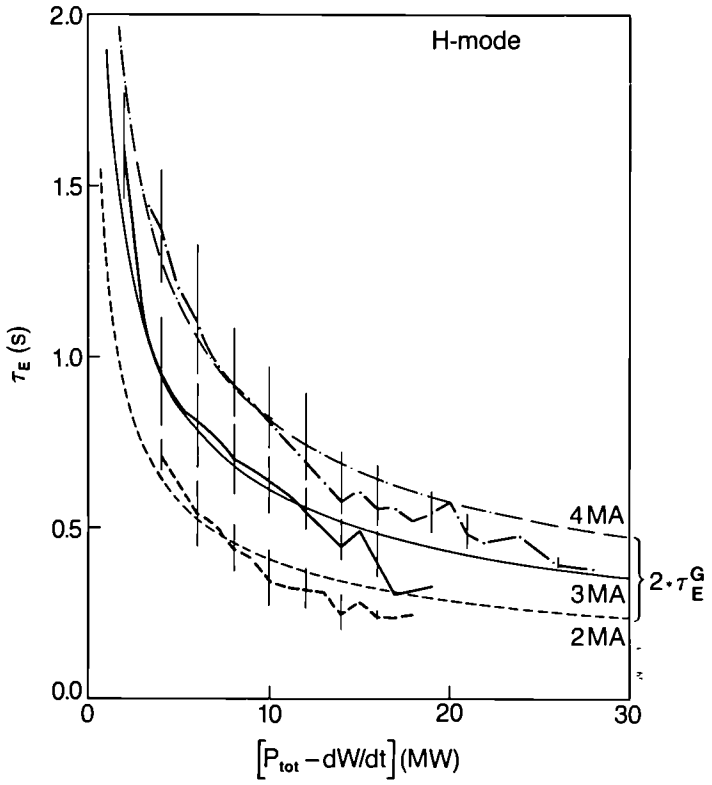

Fig. 6 Energy confinement time τ_E as a function of the effective input power $P_{eff} = (P_{tot} - dW/dt)$ for H-mode plasmas with currents of 2,3 and 4 MA. The smooth curves are twice the Goldston scaling for each current. The bars represent the scatter of the experimental data (being ± one standard deviation).

5. THE PRODUCTION OF HIGH TEMPERATURES

The observed confinement time τ_E and the available power P_t limit the plasma energy that can be obtained. Thus for a JET H-mode discharge at 4 MA with an input power around 20MW and a confinement $\tau_E \sim 0.5$ s, the average temperature <T> would be around 6keV at average densities around $3 \times 10^{19} m^{-3}$. Consequently strong temperature profile peaking of $(T_i(0)/<T>) \geq 5$ is required to get the central temperatures of ~30 keV which are of fusion interest.

Such strong temperature profile peaking factors are indeed observed for the ion temperatures in low density discharges. Central ion temperatures $T_i(0)$ of 28 keV have been obtained at high power levels per particle as shown in Fig. 7(a). Note that there is a steady increase in $T_i(0)$ with increasing $P_t/<n>$, but also a large spread. Thus the highest $T_i(0)$ values are obtained for $P_t/<n>$ in the range 5 - 10 while for $P_t/<n> = 5$, $T_i(0)$ ranges from 12 to 28keV. The quantity $P_t/<n>$ is thus an indicator rather than a true scale parameter. The high $T_i(0)$ values are associated with a progressive increase in the peaking factor $(T_i(0)/<T>)$ which reaches a value of 6 for those values of $P_t/<n>$ that have the highest $T_i(0)$ values (see Fig. 7(b)).

The slope of the increase of $T_i(0)$ with $P_t/<n>$ represents a central confinement time and the fact that $T_i(0)$ increases roughly linearly with $P_t/<n>$ means that the energy confinement of the ions in the plasma centre does not degrade with $P_t/<n>$. The same is not true for the electrons as can be seen in Fig. 7(c). There is a strong saturation at $T_e(0)$ of around 8keV implying a strong decrease in the central electron confinement time as $P_t/<n>$ increases.

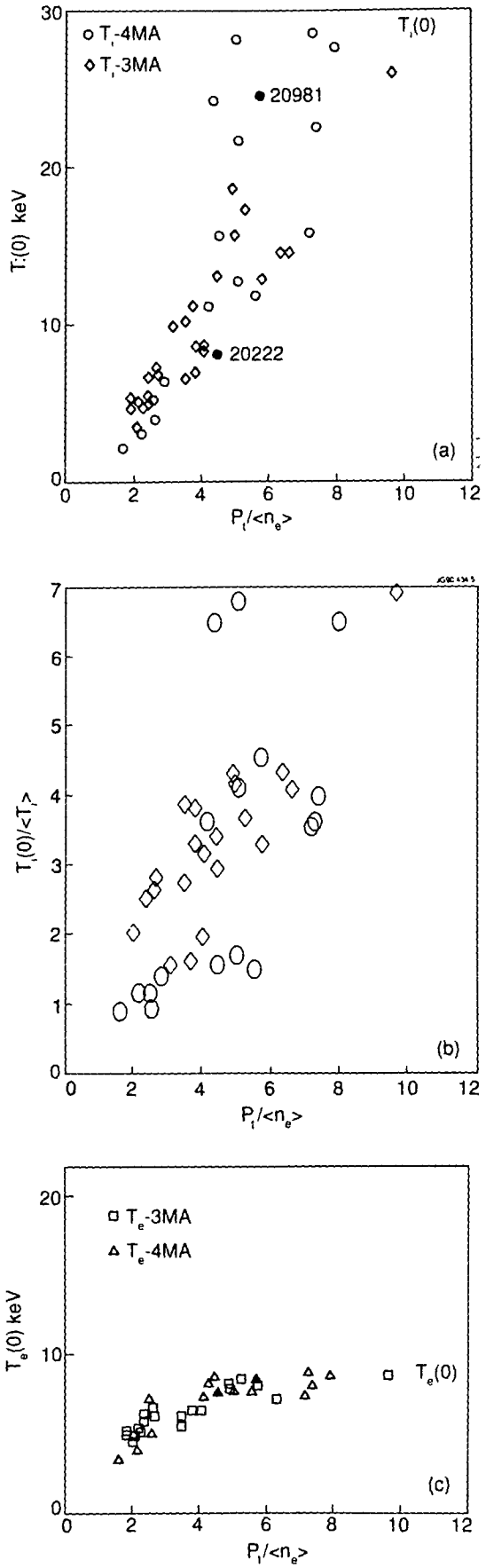

Fig. 7 (a) The dependence of the highest central ion temperature $T_i(0)$ reached in each pulse ratio of the total input power P_t to the averaged electron density $<n_e>$, at the same time, for (□,◊) and 4 MA (o,Δ) H-mode discharges with NBI heating and gas fuelling.

(b) The temperature profile peaking factor $T_i(0)/<T_i>$ versus $P_t/<n_e>$ for the same disc

(c) The central electron temperature $T_e(0)$ versus $P_t/<n_e>$.

Of course it has to be remembered that rather little power goes to the electrons in these discharges. In the central region (~a/3), typically 90% of the neutral beam power goes to the ions. Nevertheless there is a marked difference in behaviour between the $T_i(0)$ and $T_e(0)$ in going between the indicated Pulse Nos: 20222 and 20981, as shown in Table. I. Both pulses have I_p = 4MA, B = 2.8T, but for Pulse No: 20222 the applied NB power has mainly 80kV acceleration (13.8 MW at 80 kV; 1.8 MW at 140 kV), whereas Pulse No: 20981 has appreciable power with 140 kV acceleration (12.1 MW at 80 kV; 5.8 MW at 140 kV).

Table I

Parameters	Pulse No: 20222 (t = 9.9 s)	Pulse No: 20981 (t = 11.4 s)	Units
$\hat{P}_i$ (r<a/3)	3.5	4.5	MW
$\hat{P}_i/\hat{n}$	0.6	1.1	10^{-19} MW m^3
$T_i(0)$	8	22	keV
$\hat{P}_e$ (r<a/3)	0.7	1.5	MW
$\hat{P}_e/\hat{n}$	0.1	0.4	10^{-19} MW m^3
$T_e(0)$	8	9	keV
$\hat{n}_e$	6	4	10^{19} m^{-3}

A change of a factor of about 2 in the ion input power per particle $P_t/\langle n\rangle$ leads to a large change in $T_i(0)$ presumably because the ion losses do not increase with P_t. For the electrons the situation is less clear due to the low power given to them, consequently there are large errors in the electron power balance. Nevertheless the $P_t/\langle n\rangle$ changes appreciably (estimated to be by about a factor of 4) without a significant change in $T_e(0)$ presumably because of a strong degradation of the electron confinement time with power.

A more precise analysis of the energy balance in the central region of these discharges was not possible because of the difficulty in obtaining sufficiently accurate data on temperature and deposition profiles.

Electron Heating

Ion cyclotron resonance heating produces energetic (MeV) ions in the plasma and by this means, in contrast to neutral beams,primarily heats the electrons (typically > 90% of ICRH power goes to the electrons). An obvious next step is to apply centrally deposited ICRH power to the hot ion discharges described above in order to attempt to increase the central T_e which is important in order to get reactor like plasmas with $T_e(0) \sim T_i(0)$.

The introduction of Be antenna screens has solved previous ICRF heating impurity production problems. Consequently effective ICRF electron heating is now possible in both limiter and H-mode discharges. Electron temperatures as high as 12 keV have been obtained. However, initial experiments in limiter configuration (Lomas, et al, 1990) show saturation at this value as $P_{ICRF}(0)/n_e$ is increased above 2 x 10^{19} MW m^3. Further experiments are required in order to establish whether this saturation is due to transport or possibly a difference in the deposition profile.

High temperature operation in JET can thus be summarised, as follows:

(a) Application of high power beam and ICRF heating to JET has produced

$T_i(0) > 28$ keV

$T_e(0) > 12$ keV

Discharges have been produced in which $T_i(0)$ and $T_e(0)$ are simultaneously in excess of 10keV.

(b) Experiments to use ICRF heating to heat the electrons in the present hot ion discharges have begun, but need further development.

6. LIMITATIONS DUE TO IMPURITY FLUXES

The highest performance conditions in JET are obtained in X-point and H-mode discharges. The duration of these conditions is limited to ~ 1s or less by a large influx of Carbon impurity released from local hot spots which form on the X-point dump plates (carbon-carbon fibre composite). A similar behaviour occurs for discharges limited on the inner wall of JET.

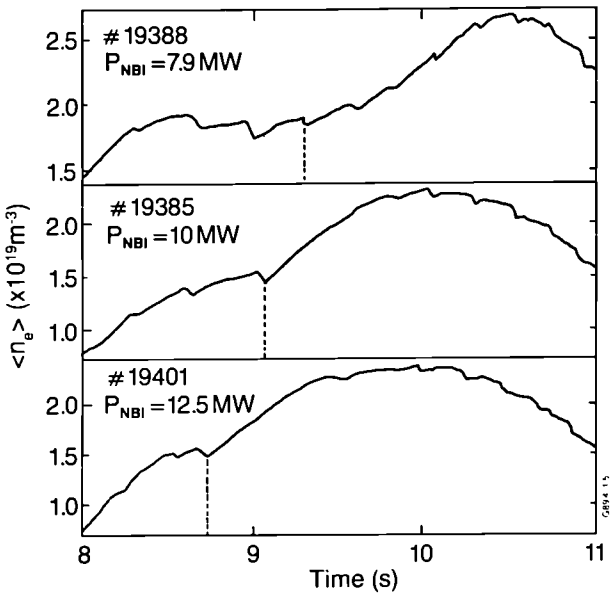

Fig. 8 Effect of varying the additional heating power P on the onset of the high carbon influx. The onset is readily visible on the line average electron density $<n_e>$ for the Pulse Nos: 19388, 19385, and 19401, it is marked by the vertical broken lines. The product P.t(onset) is about 10 MJ : the higher the heating power the shorter the time delay for the carbon influx.

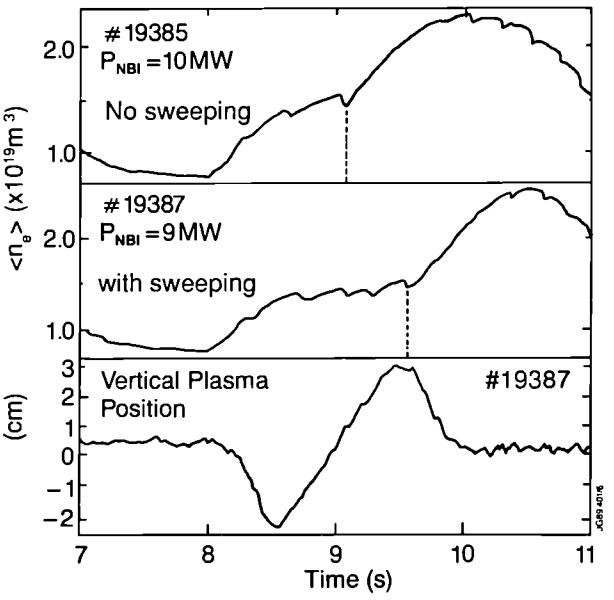

Fig. 9 The dependence of the onset of the carbon influx on the sweeping of the plasma contact position on the inner wall limiter. Comparison of a discharge Pulse No: 19385 without and with sweeping Pulse No:19387. Sweeping of the plasma on the inner wall delays the carbon influx by a few hundreds of ms.

Measurements by Pasini et al (1989) in Figs. 8 and 9 show this effect. In Fig. 8, n_e is given as a function of time for 3 shots with different power levels. The sharp increase in n_e is a direct indication of the carbon influx. The onset of the influx can be delayed by sweeping the position of the plasma-wall contact over the carbon tiles, so that a wider distribution of

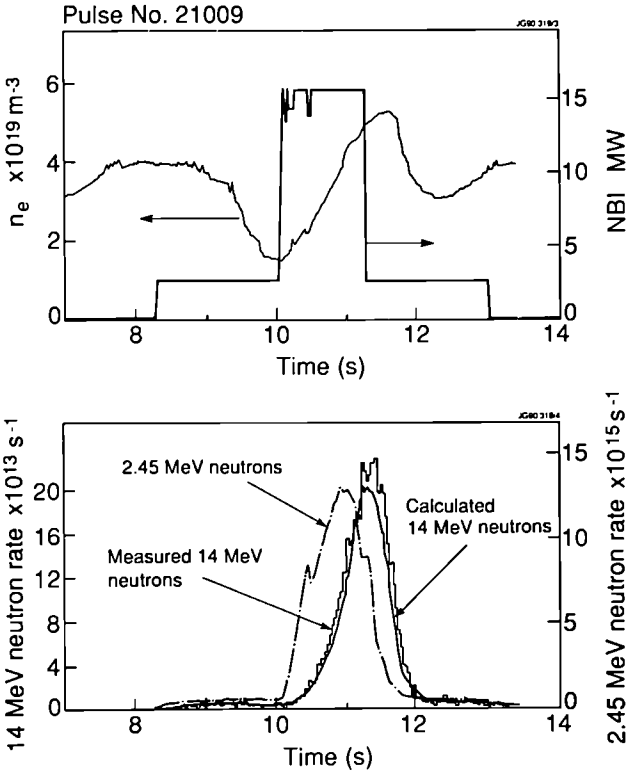

Fig. 10 The upper part shows the time evolution of the electron density <n_e> and that of the NBI power. In the lower part the measured 2.45 MeV neutron (originating from D-D reactions) and the 14 MeV neutron (coming from D-T reactions) rates are shown. Also shown is the calculated neutron rate by the D-T reactions resulting from the tritons produced by the D-D reactions and an assumed triton loss time of 2s.

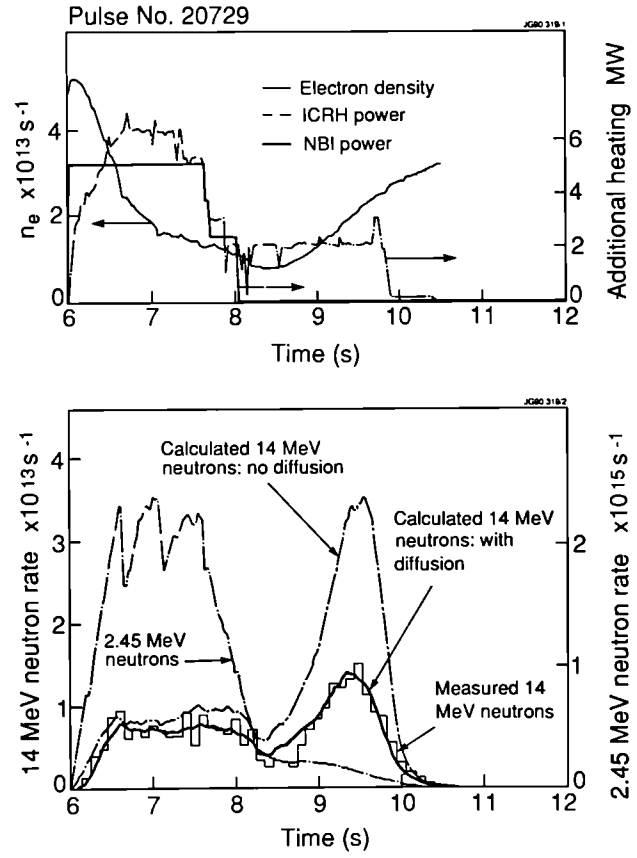

Fig. 11 The upper figure gives the NBI and ICRH powers versus time together with the electron density <n_e>. In the lower half the measured 2.45 and 14 MeV neutron rates are given as a function of time. Also shown are calculated 14 MeV neutron emission rates with and without the triton diffusion model.

the heat over the tiles occurs. In Fig. 9, this can be seen for Pulse No: 19387, for which the vertical position has been changed from -2 to +3 cm thus sweeping the interaction area and giving an extra delay of around 0.5 s. This demonstrates that if one can devise an X-point target chamber, which can accept the heat flux without excessive wall temperatures the plasma can be kept clean and undiluted. This excessive wall loading behaviour which limits the performance of JET is a serious problem which must be overcome before a long burn ignition experiment can be designed.

A new phase program has been formulated for JET to address this problem using an internal pumped divertor with a radiating plasma channel to spread the heat load, impurities are expected to be kept away from the main discharge by plasma flow along the channel.

7. CONFINEMENT OF FUSION PRODUCTS

The slowing down and confinement behaviour of 1 MeV tritons generated in D-D fusion reactions in JET has been studied by comparing the 2.45 MeV neutron emission, which has the same time profile as the triton generation, with the 14 MeV neutron emission emitted as the tritons slow down to the peak D-T reactivity energy of 0.18 MeV (Conroy et al,1990). The observed time profile of 14 MeV emission is compared with that calculated from a multi-group test particle, slowing down model. The model includes a diffusive loss mechanism which can also be represented by a simpler exponential loss time applied to each group.

For a typical JET discharge (4MA, X-point with NBI), the classical triton slowing down time is ~0.7s and the model gives a good fit to the observations with a triton loss time of about 2s (determined by the quality of the fit). An example is shown in Fig.10, which also shows the NBI power and the central electron density n_e as a function of time.

The triton confinement time can be determined more accurately in certain extreme discharges with high T_e (~ 7keV) and low n_e ($\sim 10^{19}$ m^{-3}), and hence long triton slowing times (>2s), as shown in Fig. 11. A good agreement between the calculated and measured 14 MeV neutron rate can only be obtained if a diffusive transport of $D = 0.1 \pm 0.05$ m^2s^{-1} is included, this is also modelled by an exponential loss time of $\tau = 2$ s.

Alpha-Particle Simulation

High energy (several MeV) minority ions (H and He^3 in D plasma) generated by ICRH in JET provide a good simulation for the behaviour of α-particles to be expected in the D-T phase of JET and in a reactor. In some JET discharges, the energy in these fast particles can reach 50% of the total plasma energy.

When the minority species is He^3 in a D plasma the fusion power generation can be large. In fact the largest fusion power so far generated in JET comes from this process. In recent experiments using Beryllium coated walls to reduce the dilution of deuterium by impurities this power has reached 100 kW, as shown in Fig. 12 which shows D-He^3 fusion power as a function of ICRH heating power. Also shown are the results for JET with carbon walls published previously (Boyd et al, 1989). The increased D-He^3 fusion power from 60 to 100 kW reflects the improvement of n_D/n_e due to be Be walls.

A comparison of plasma and α-particle (He^3) parameters measured in JET and those for the future D-T operation and for an ignited next step are given in Table II (Bickerton, 1988). The only major difference between the parameters in the α-particle simulation experiments in JET and those foreseen for the future lies in the large velocity space anisotropy of the high energy He^3 particles generated by the ICRF heating.

Slowing Down and Loss Behaviour of Fast Particles

Start et al (1990) describe a model calculation of the energy content of the fast ions in these minority heating experiments. The model includes classical slowing down of the fast ions

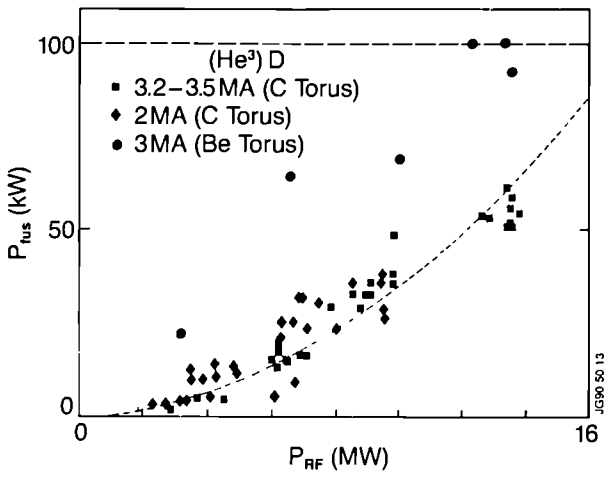

Fig. 12 The measured fusion production P_{fus} in a deuterium plasma with He^3 minority as function of the ICRH power P_{RF}. The solid symbols (■,◆) are the fusion yields in a carbon vacuum vessel. The higher points (•) are obtained after the introduction of Be and reflect the improvement of n_D/n_e from < 0.6 to > 0.8 and correspond to Q (D-He^3) ~ 7 x 10^{-3} at the highest powers.

Table II: Fast or Alpha-Particle Parameters

Parameter	Achieved on JET	Expected Values	
		JET Q=1	Ignited ITER
n_{fast}/n_{eo}	(1-3)%	0.1%	0.7%
$<E_{fast}>$	(1-5) MeV	2 MeV	2 MeV
$<\beta_{fast}>$	0.8%	0.6%	2%
$<p_\perp/p_{//}>$	10-50 (calculated) >7 (measured)	1	1
ρ_θ/a	0.3 (2MA)	0.3 (5MA)	0.07 (20MA)
v_{fast}/v_A	2 - $4_\perp$	2	2.8
τ_{so}/τ_E	≈1	≈1	0.2 - 1

JG90.1-96

on the plasma, taking into account the finite orbit size and the variation of slowing time over the orbit.

Fig. 13 compares the measured with the calculated fast particle energy, for various discharges, which were centrally heated with no sawteeth. Fig. 13(b) shows the results with finite orbit width included in the calculations, Fig. 13(a) has no orbit width included. It can be seen that the model gives a good fit to the observed fast ion content when orbit effects are included, without the need to introduce any extra fast ion loss term.

If nevertheless such a term is introduced into the model, Cottrell (1990) has shown that the fit becomes noticeably worse if τ_{loss} <2s (equivalent to D~ $a^2/4\tau$ > 0.1 m^2s^{-1}), as can be seen in Fig. 13(c). This is in good agreement with loss times deduced from Triton slowing down observations discussed above. Furthermore the loss time for the α particles corresponding to D_α ~ 0.1 m^2s^{-1} is comparable to typical plasma diffusion coefficients estimated in the core of similar JET plasmas which are in the range of 0.05 to 0.25 m^2s^{-1}. The loss times of about 2s are adequately long enough for the α-particles in a reactor plasma to give their energy to the plasma.

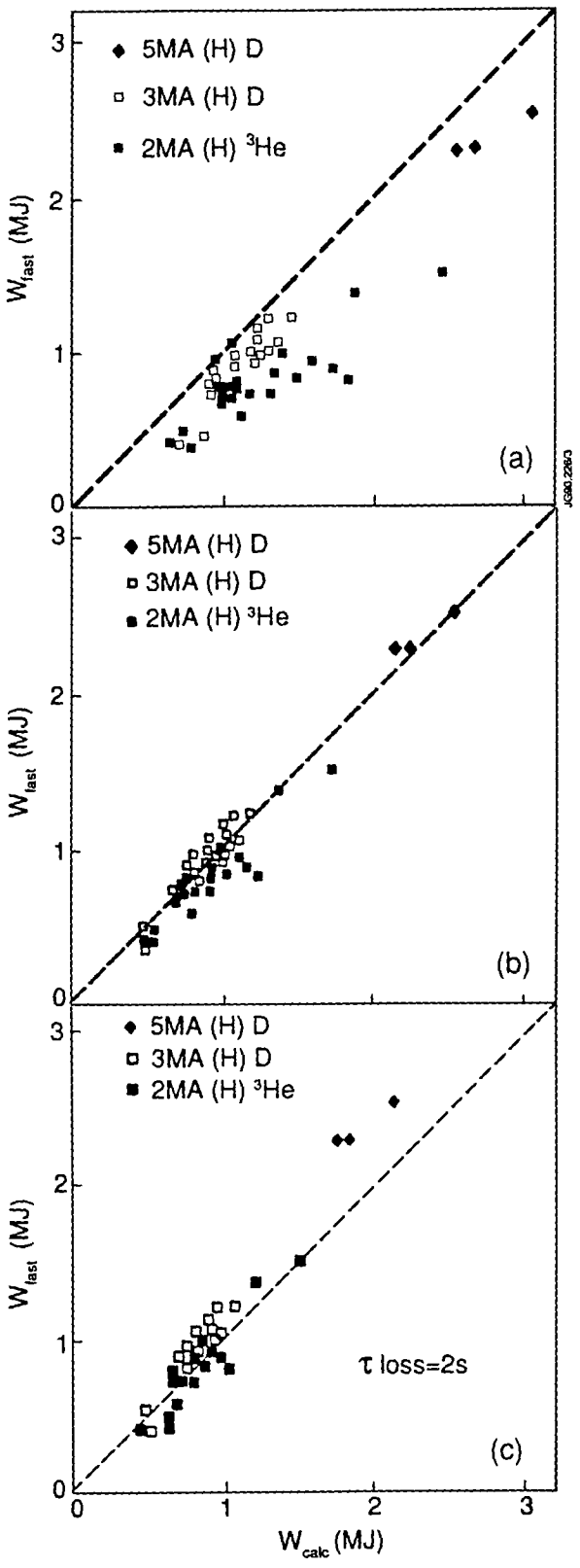

Fig. 13 Measured fast H-ion energy for D and He^3 plasmas versus calculated fast ion energy zero-orbit-width model (Fig. 13a) and for a finite orbit-width model (Fig. 13(b)), and wit inclusion of τ_{loss} = 2s (Fig. 13(c)). The fit in Fig. 13(c) is noticeably worse than in Fig. 13(b). 1 2 s implies that D_{fast} ($=a^2/4\tau_{loss}$) < 0.1 m^2/s.

8. FUSION PERFORMANCE IN JET

The fusion performance obtained in JET is shown in Fig. 14. The product $(n_D(0)T_i(0)\tau_E)$ is shown as a function of $T_i(0)$ for various plasma currents in H-modes, pellet and low density high $T_i(0)$ discharges. The points on the diagram are observed values in JET. The curves are values of P_α/P_{loss} for a thermal 50:50 D-T plasma. The shaded bands represent

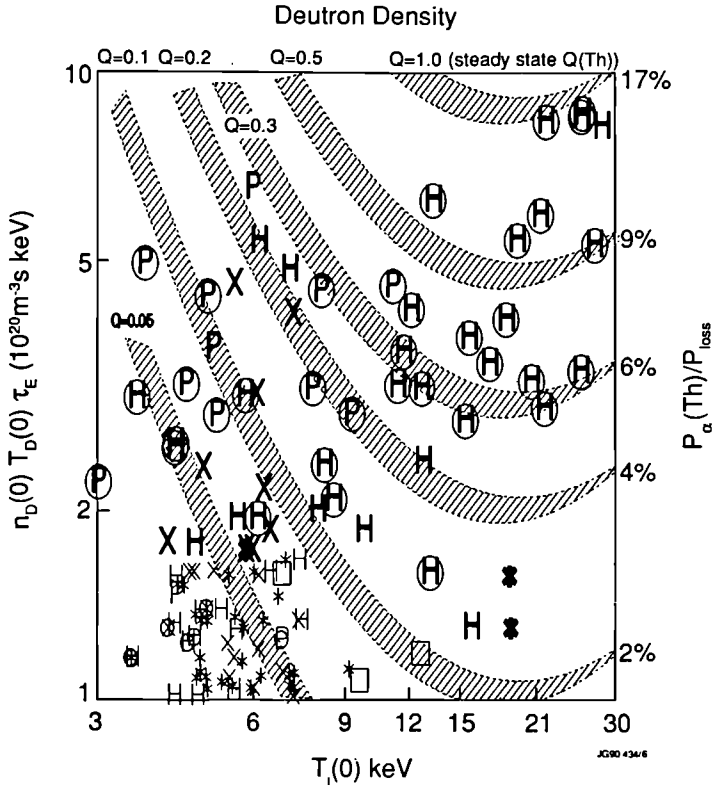

Fig. 14 The product of $(n_D T_i(0)\tau_E)$ as a function of $T_i(0)$ for I_p between 2 and 6.5 MA in H-modes (H), pellet (x), H-modes with pellets (P), and other discharges (*). The experimental points are averaged over 0.2s. Also indicated in the graph are shaded bands of constant P_α/P_{Loss} for a thermal 50:50 D-T plasma. In steady state these bands also correspond to the Q_{DT} shown. The width of the bands covers a range of profiles $\sim[1-(r/a)^2]^\alpha$ and dilutions in the case from $\alpha_n = 0.5$, $\alpha_T = 1.5$ with $n_D/n_e = 1$ to $\alpha_n = 0$, $\alpha_T = 1.3$ with $n_D/n_e = 0.8$ and the addition of a 20% temperature pedestal. It will be seen that the Q values especially at higher $T_i(0)$ are insensitive to these variations. The encircled points are in non-steady state with $(dW/dt)/P_t > 0.3$. For these points the shaded bands represent the thermal component of P_α/P_{Loss}, but not of course the thermal Q.

the effect of reasonable profile and Z_{eff} variation. The Q values[3] indicated are values which would apply to a steady-state thermal plasma (50:50 D-T) with same $(n_D T_i \tau_E)$, i.e. the value to be expected if P_t was reduced until $(dW/dt) = 0$. The actual Q for the highest JET points, which are not in steady state, is about half the value indicated by the curves.

Note that the $(n_D T_i \tau_E)$ values plotted include fast injected particles and thus show what $(n_D T_i \tau_E)$ the configuration could sustain. The thermal $((n_D T_i \tau_E), T)$ for the highest point is roughly 40% lower than the total value. Note also, that the best discharges are 4MA H-modes; (5MA H-mode discharges are not yet optimised). High current (<5 MA) limiter discharges with pellet peaking, sawtooth suppression and combined heating are also making substantial progress in the fusion product.

Other discharges e.g. ICRH H-modes and combined heating H-modes reach appreciable $((n_D T_i \tau_E), T)$ values : (2.5 x 10^{20}, 4 keV) and (3 x 10^{20}, 9 keV) respectively. The highest $(n_D T_i \tau_E)$ values of ~ 9 x 10^{20} m^{-3}keVs approach those,that are required for Q=1 in a steady-state 50 : 50 D-T plasma.

[3] Q is the ratio of the total fusion power (α-particles and neutrons) over the total power input for a plasma in steady state.

The actual fusion power measured in these D plasmas is shown in the form of the Q_{DD} versus volume averaged density in Fig. 15. The highest Q_{DD} values are obtained at moderate densities and high ion temperatures in H-modes. The highest H-mode values are twice those in L-mode. The highest Q_{DD} values have similar contributions from thermal and from beam-plasma processes.

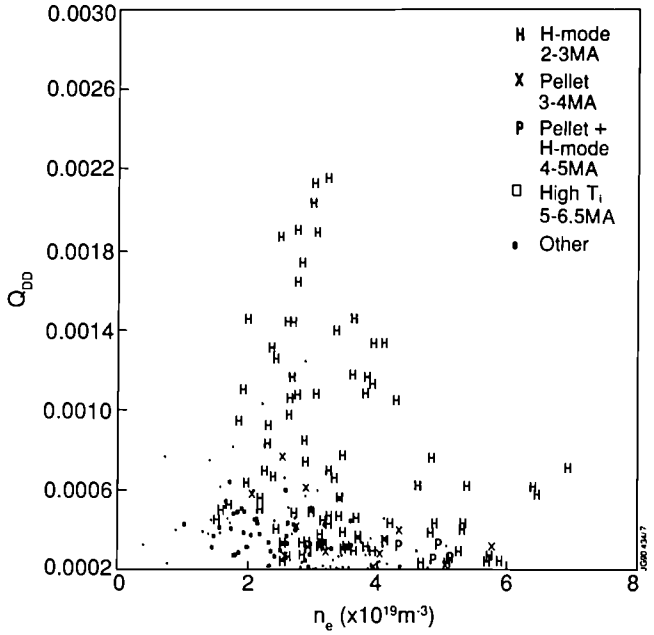

Fig. 15 Measured Q_{DD} values averaged over 0.2 s as function of the volume averaged electron density $<n_e>$ with the same designations as in Fig. 14.

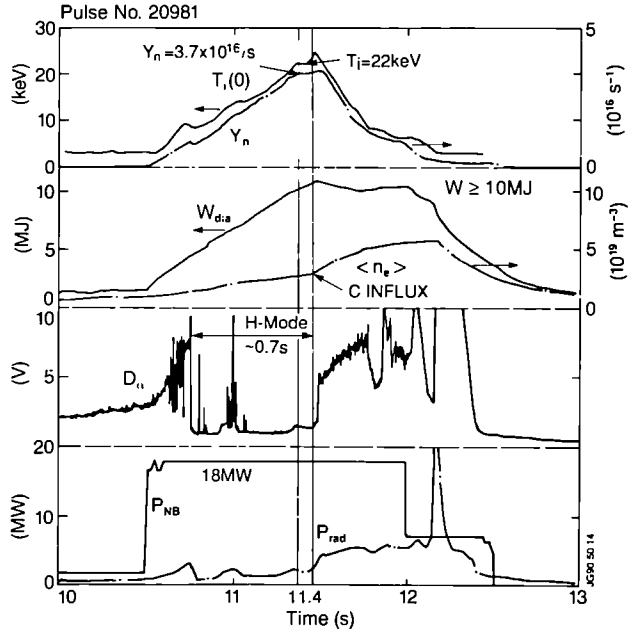

Fig. 16 Time evolution of high fusion yield H-mode Pulse No: 20981. From top to bottom are depicted the central ion temperature $T_i(0)$, the total neutron yield Y_n, the plasma diamagnetic energy W_{dia}, the volume averaged electron density $<n_e>$ and D_α intensity near the X-point, the neutral beam power P_{NB} and the radiated power losses P_{rad} as function of time. The large carbon influx at 11.5 s (marked by the second vertical line) is followed by a termination of the H-mode and an abrupt decrease in the high values of the fusion relevant parameters.

The time evolution of a discharge with such high Q_{DD} values is shown in Fig. 16. The top traces show the time development of a central ion temperature together with the neutron yield. Also shown are the total plasma energy as measured by the plasma diamagnetism and the volume averaged density. The break in the slopes of T_i, T_n, W_{dia}, $\langle n_e \rangle$ in time, mark the point where the carbon influx becomes important shortly before 11.5 s. The X-point discharge is in a H-mode state over nearly 1 s, as can be seen from the D_α signal. The bottom traces are the total NB power and the radiation losses measured in time. Despite the large carbon influx, radiation losses never become dominant in this discharge. The main fusion relevant parameters for this Pulse No: 20981 are summarised in Table III, at t=11.4s.

The relevant fusion parameters calculated by the TRANSP Code for 140 keV NBI of D beams into a T plasma are shown in Table IV. The data are calculated for a discharge otherwise similar to Pulse No: 20981 and are also in non-steady state.

Table III: Double Null H-mode
Pulse No:20981 (t=11.4s)

Plasma Parameters

$T_i(0) = 22keV$	$\overline{T}_i = 5.8keV$
$T_e(0) = 8.6keV$	$\overline{T}_e = 5.2keV$
$W_p = 10MJ$	$dW_p/dt = 8.9MW$
$n_0(0) = 3.7x10^{19}m^{-3}$	$\overline{n}_D = 3.2x10^{19}m^{-3}$
$n_D(0)/n_e(0) = 0.9$	$\overline{n}_D/\overline{n}_e = 0.8$
$Z_{eff}(0) = 1.4$	$\overline{Z}_{eff} = 1.9$
$P_{in} = 18MW$	$\tau_E = 1.1s$
$\beta = 1.8\%$	$\beta/\beta_{Troyon} = 0.5$
Neutron Rate $= 3.5x10^{16}ns^{-1}$	

D-D Observed Fusion Parameters

$Q_{DD} = 2.0x10^{-3}(>1.4x10^{-3}$ for $\sim 0.5s)$

$P_{fus} = 43kW\ (D-D)$

$n_D(0)T_D(0)\tau_E = 9x10^{20}m^{-3}keV\,s \quad (>3x10^{20}$ for $\sim 0.5s)$

Table IV: Double Null H-mode
Pulse No. 20981

Equivalent D-T Parameters

Calculated (TRANSP Code) for 140kV injection of D beams into a T target (leading to T:D=2:1)

Q_{DT}	= 0.7	(>0.5 for ~0.8s)
$Q_{thermal}$	= 0.13	
$Q_{beam\text{-}plasma}$	= 0.57	
P_{fuse}	= 12MW	(>8MW for ~0.8s)
P_α	= 2.4MW	(>1.6MW for ~0.8s)
P_α/P_{loss}	= 23%	(>15% for ~0.8s)

9. CONCLUSIONS

JET plasmas now display most of the characteristics to be expected from a reactor plasma:

- Densities up to $\bar{n}Rq_{cyl} / B_t = 33\ m^{-2}T^{-1}$ with $\bar{n} = 1.4 \times 10^{20}\ m^{-3}$ are obtained and appear to be limited by edge radiation loss processes.
- β values up to 5.5 % equal to the Troyon limit value at $B_t = 0.9$ T are obtained
- Strongly peaked ion temperatures > 28 keV with $T_i(0)/\bar{T}_i \sim 6$ are obtained in low density H-mode discharges.$T_i(0)$ and $T_e(0)$ are simultaneously in excess of 10 keV in higher density discharges
- Energetic (MeV) particles both with isotropic and with transverse velocities are contained for at least 2s while they slow down by apparently classical processes. This is adequately long enough for energy transfer in a reacting plasma, where even better confinement should be expected given the increased size and plasma current.
- The duration of fusion relevant conditions in JET H-mode discharges is at present limited to ≤ 1s by the influx of carbon impurities from localised plasma-target plate interaction. A new phase for JET is planned to develop a reactor relevant solution to this problem
- **100 kW** of fusion power in charged particles has been produced in D(He^3) plasmas. $n_D(0)T_i(0)\tau_E$ values of **7 to 9 x 10^{20} m^{-3}keVs** with $Q_{DD} > 2 \times 10^{-3}$ have been produced in D-D plasmas. For the same plasma parameters in a D-T plasma this is equivalent to $Q_{DT} \sim 0.7$, $P_\alpha \sim 2.4$ **MW**, $P_{fusion} \sim 12$ **MW** with $P_\alpha/P_{Loss} > 20\%$.

REFERENCES

Bickerton, RJ et al, (1988) Proc. 12th Int. Conf. on Plasma Phys. and Contr. Nucl. Fusion Research, Nice, Nuclear Fusion Supp 1989

Boyd, DA et al, (1989) Nuclear Fusion **29**(1989) 593

Campbell, DJ et al, (1986) Proc. 11th Int. Conf. or Plasma Physics and Contr. Nucl. Fusion Research, Kyoto, Nuclear Fusion Supp. 1987.

Conroy, S et al, (1990) Europhysics Conf. Abstracts **14B**, 98 (1990)

Ferron, J et al, (1990) Europhysics Conf. Abstracts **14B**, 371(1990)

Gibson, A, (1976) Nuclear Fusion, **16** (1976) 546

Goldston, RJ et al, (1984) Plasma Physics and Controlled Fusion **26**, 87 (1984)

Lomas, PJ et al, (1990) Europhysics Conf. Abstracts **14B**, 5 (1990)

Lowry, C. et al, (1990) Europhysics Conf. Abstracts **14B**, 338 (1990)

Pasini, D et al, (1989) "Observations on the Erosion of Carbon at High Temperatures in JET", Topical Meeting on High Temperature Erosion of Graphite in Plasmas, Princeton Plasma Physics Laboratory, July 25-27, 1989. To be published as a DOE report on Plasma Material Interaction and High Heat Flux Test Group.

Rebut, P-H, and Green, BJ Plasma (1976) Proc. 6th Int. Conf. on Plasma Phys. and Contr. Nucl. Fusion Research, Berchtesgaden, Nuclear Fusion Supp 1977

Ryter, F et al, (1990) Europhysics Conf. Abstracts **14B**, 94 (1990)

Smeulders, P et al, (1990) Europhysics Conf. Abstracts **14B**, 323 (1990)

Start, DF et al, (1990) Europhysics Conf. Abstracts **14B**, 1015 (1990)

Takahashi, H et al, (1990) Europhysics Conf. Abstracts **14B**, 367 (1990)

Troyon, F et al (1984), Plasma Physics and Controlled Fusion **26**, 209 (1984)

Wesson, JA et al, (1989) Nuclear Fusion, **29** (1989) 641

APPENDIX I

THE JET TEAM

JET Joint Undertaking, Abingdon, Oxon, OX14 3EA, U.K.

J.M. Adams[1], H.Altmann, A.Anderson[14], S.Attenberger[23], W.Bailey, P.Ballantyne, B.Balet, R.Barnsley[29], D.V.Bartlett, L.R.Baylor[23], A.C.Bell, P.Bertoldi, E.Bertolini, V.Bhatnagar, A.J.Bickley, H.Bindslev[14], J.Bizarro[21], S.Bliman[16], T.Bonicelli, S.J.Booth, G.Bosia, M.Botman, D.Boucher, H.Brelen, H.Brinkschulte, M.Brusati, T.Budd, M.Bures, T.Businaro, P.Butcher, H.Buttgereit, C.Caldwell-Nichols, D.J.Campbell, P.Card, G.Celentano, C.D.Challis, A.Cheetham, P.Chiron, J.Christiansen, C.Christodoulopoulos, P.Chuilon, R.Claesen, S.Clement[28], E.Clipsham, J.P.Coad, S.Conroy[12], M.Cooke, S.Cooper, J.G.Cordey, W.Core, G.Corrigan, S.Corti, A.E.Costley, G.Cottrell, J.Coulon[16], M.Cox[7], P.Cripwell[12], H.de Blank[15], G.Decker[32], H.de Esch, L.de Kock, E.Deksnis, G.B.Denne, G.Deschamps, G.Devillers, K.J.Dietz, J.Dobbing, N.Dolgetta, S.E.Dorling, P.G.Doyle, D.F.Düchs, H.Duquenoy, A.Edwards, J. Ehrenberg, T.Elevant[11], S.K.Erents[7], L.G.Eriksson[5], H.Fajemirokun[12], H.Falter, D.Flory, M.Forrest[7], J.Freiling[15], C.Froger, P.Froissard, K.Fullard, M.Gadeberg, A.Galetsas, M.Galley, M.Garribba, P.Gaze, X.Ge[25], R.Giannella, A.Gibson, R.D.Gill, A.Gondhalekar, C.Gormezano, N.A.Gottardi, C.Gowers, B.J.Green, W.K.Guo[25], R.Haange, G.Hammett[6], C.J.Hancock, P.J.Harbour, N.C.Hawkes[7], P.Haynes[7], J.L.Hemmerich, R.Hemsworth, F.B.Herzog, R.F.Herzog, J.Hoekzema, R.Hope, J.How, M.Huart, T.P.Hughes[30], M.Hugon, M.Huguet, A.Hwang[7], C.Idelon, B.Ingram, M.Irving, J.Jacquinot, H.Jaeckel, G.Janeschitz[13], O.N.Jarvis, F.Jensen, E.M.Jones, L.P.D.F.Jones, T.T.C.Jones, A.Kaye, B.E.Keen, M.Keilhacker, G.J.Kelly, W.Kerner, R.Konig, A.Konstantellos, M.Kovanen[20], P.Kupschus, P.Lallia, R.Lässer, J.R.Last, B.Laundy, L.Lauro-Taroni, K.Lawson[7], E.Lazzaro, M.Lennholm, P.Lomas, M.Lorentz-Gottardi[2], M.Loughlin, C.Lowry, B.Macklin, G.Maddison[7], G.Magyar, W.Mandl[13], V.Marchese, F.Marcus, J.Mart, E.Martin, R.Martin-Solis[31], P.Massmann, K.F.Mast[13], G.McCracken[7], P.Meriguet, S.F.Mills, P.Millward, S.L.Milora[23], E.Minardi[31], A.Moissonnier, F.Mompean, P.L.Mondino, F.Montvai[3], P.Morgan, H.Morsi, G.Murphy, M.Mynarends, C.Nardone, F.Nave[21], G.Newbert, M.Newman, P.Nielsen, P.Noll, W.Obert, D.O'Brien, J.O'Rourke, R.Ostrom, M.G.Pacco-Düchs, M.Pain, F.Paoletti, S.Papastergiou, D.Pasini, A.Peacock, N.Peacock[7], D.Pearson[12], C.Perry, V.Phillips[28], M.Pick, J.Plancoulaine, J-P.Poffé, F.Porcelli, L.Porte[19], R.Prentice, G.Radford[9], T.Raimondi, C.Raymond, P-H.Rebut, R.Reichle[13], J.Removille, G.Rey[16], F.Rimini, D.Robinson[7], A.Rolfe, R.Romain, R.T.Ross, L.Rossi, P.Rutter, H.C.Sack, G.Sadler, G.Saibene, N.Salmon[12], G.Sanazzaro, A.Santagiustina, R.Sartori, C.Sborchia, P.H.Schild, M.Schmid, G.Schmidt[6], S.M.Scott, A.Sibley, R.Simonini, A.Sips[15], P.Smeulders, S.Sommers, K.Sonnenberg, R.Stankiewicz[27], M.Stamp, P.Stangeby[18], D.F.Start, C.A.Steed, D.Stork, P.E.Stott, T.E.Stringer, D.Stubberfield, D.Summers, H.Summers[19], H.Tamnen, A.Tanga, A.Taroni, A.Tesini, P.R.Thomas, E.Thompson, K.Thomsen, J.M.Todd, P.Trevalion, B.Tubbing, F.Tibone, E.Usselmann, A.Vannucci, H.van der Beken, G.Vlases, M.von Hellermann, T.Wade, C.Walker, Z.Wang[26], D.Ward, M.L.Watkins, M.J.Watson, H.Weisen[10], J.Wesson, J.Wilks, U.Willen[11], D.Wilson, T.Winkel, S.Wolfe, B.Wolle[24], D.Wong, C.Woodward, M.Wykes, I.D.Young, L.Zannelli, Z.Zheng[25], Y.Zhu[26], M.Zouhar.

PERMANENT ADDRESS

1. UKAEA, Harwell, Didcot, Oxon. UK.
2. EUR-EB Association, LPP-ERM/KMS, B-1040 Brussels, Belgium.
3. Central Research Institute for Physics, Academy of Sciences, Budapest, Hungary.
4. ENEA-CENTRO Di Frascati, I-00044 Frascati, Roma, Italy.
5. Chalmers University of Technology, Göteborg, Sweden.
6. Princeton Plasma Physics Laboratory, New Jersey, USA.
7. UKAEA Culham Laboratory, Abingdon, Oxfordshire, UK.
8. Plasma Physics Laboratory, Space Research Institute, Sao José dos Campos, Brazil.
9. Institute of Mathematics, University of Oxford, UK
10. CRPP/EPFL, 21 Avenue des Bains, CH-1007 Lausanne, Switzerland.
11. Swedish Energy Research Commission, S-10072 Stockholm, Sweden.
12. Imperial College of Science and Technology, University of London, UK.
13. Max Planck Institut für Plasmaphysik, D-8046 Garching bei Munchen, FRG.
14. Risø National Laboratory, Denmark.
15. FOM Instituut voor Plasmafysica, 3430 Be Nieuwegein, The Netherlands.
16. Commissiariat à L'Énergie Atomique, Cadarache, F-13108 St Paul Lez Durance, France.
17. JAERI, Tokai Research Establishment, Tokai-Mura, Naka-Gun, Japan.
18. Institute for Aerospace Studies, University of Toronto, Downsview, Ontario, Canada.
19. University of Strathclyde, 107 Rottenrow, Glasgow, G4 0NG, UK.
20. Nuclear Engineering Laboratory, Lapeenranta University, Finland.
21. JNICT, Lisboa, Portugal.
22. CNP, Milan, Italy.
23. Oak Ridge National Laboratory, Oak Ridge, Tenn., USA.
24. University of Heidelberg, Heidelberg, FRG.
25. IPP, Academia Sinica, Beijing, P.R. China.
26. Southwestern Institute of Physics, Leshan, Sechuan, P.R. China.
27. RCC Cyfronet, Otwock Swierk, Poland.
28. Kernforschungsanlage, Jülich, FRG.
29. University of Leicester, Leicester, UK.
30. University of Essex, Colchester, UK.
31. Universidad Complutense de Madrid, Spain.
32. University of Dusseldorf, FRG.

J CR 88 156 5 (rev 18/1/90)

Confinement and Stability in JET: Recent Results

The JET Team
(presented by D.J.Campbell)

Invited Paper presented to the 17th European Conference on Controlled Fusion and Plasma Heating, Amsterdam, the Netherlands, 25th-29th June 1990

CONFINEMENT AND STABILITY IN JET: RECENT RESULTS

The JET Team*

presented by D.J.Campbell

JET Joint Undertaking, Abingdon, Oxfordshire, OX14 3EA, U K

ABSTRACT

The versatility of the JET device allows a wide range of tokamak operating regimes to be explored and plasmas bounded both by material limiters and by a magnetic separatrix have been investigated extensively. This has permitted the confinement and mhd stability properties of plasmas heated to temperatures above 10keV by neutral beam injection or ion cyclotron resonance heating to be studied in detail. Here the results of recent analyses of transport and confinement in the L– and H–mode regimes in JET are discussed and the properties of H–mode plasmas produced by both major forms of heating are compared. Several aspects of the mhd stability of such plasmas, particularly at high toroidal beta, β_φ, and at the density limit, are reviewed.

KEYWORDS

Fusion, Tokamak, JET, Magnetic Confinement, H–mode, Plasma Transport, Mhd Stability

1. INTRODUCTION

The study of the transport processes and mhd stability properties of tokamak plasmas in reactor–relevant regimes is one of the fundamental objectives of the JET project (Rebut *et al.*, 1985). In recent years, a graduated programme of enhancements to the JET device and developments in the accessible operating regime have permitted the study of plasmas with ion and electron temperatures simultaneously above 10keV in which energetic ions account for a significant fraction of the plasma pressure (Gibson *et al.*, 1988; Thomas *et al.*, 1989; Lomas *et al.*, 1989). These experiments have confirmed that the confinement and mhd stability properties of such high temperature, collisionless plasmas are broadly as expected, although in many areas the specific mechanisms underlying the observed behaviour are not understood.

In the course of these studies, the control of impurity generation and particle transport has emerged as the most important limitation to further improvements in the performance of JET plasmas. As a result, beryllium, whose properties as a potential plasma–facing material have been realized for some time (Rebut and Dietz, 1982), was introduced into the JET tokamak during the

* See paper by K J Dietz *et al.* in this issue for a list of the members of the JET Team

1989 experimental campaign. This has led to significant advances in several aspects of JET performance (Keilhacker *et al.*, 1989a; Thomas *et al.*, 1990; Dietz *et al.*, 1990; Gibson *et al.*, 1990). Here the results of detailed studies of mhd stability and of confinement and transport in plasmas bounded by carbon and beryllium surfaces are discussed and compared.

The paper is divided into three broad sections. The first deals with recent progress in the operating regimes of plasmas bounded both by a magnetic separatrix and by a material limiter. Specific consideration is given to the energy confinement properties of the various regimes and, in particular, to an analysis of the confinement properties of the ICRH–generated H–mode (Tubbing *et al.*, 1989a, Bhatnagar *et al.*, 1990). In the second section, the results of the most recent analyses of energy and particle transport are discussed. The third section is concerned with several aspects of mhd stability. Particular attention is given to mhd behaviour at high–β_φ and at the density limit and to recent progress in the understanding and stabilization of sawteeth.

2. PLASMA HEATING AND CONFINEMENT

2.1 H–mode Studies

Extensive investigations of the properties of H–mode plasmas in JET (e.g. Tanga *et al*, 1987; Keilhacker *et al.*, 1989b; Lomas *et al.*, 1989) have shown that the regime can be readily obtained in plasmas with an internal magnetic separatrix in both single (SNX) and double null (DNX) configurations in which the distance from the X–point to the target plates may be only a few cm. Indeed, recent analysis (O'Brien *et al.*, 1990) indicates that the X–point often lies several cm behind the target tiles during the H–mode. To date, experiments have been performed in the single null configuration at plasma currents of up to 5.3MA and, recently, DNX plasmas have been extended to 4.5MA.

While long ($\geq$ 3s) elm–free H–modes have been obtained at moderate power levels ($P_{tot} \leq$ 10–12MW) in which the H–mode was terminated by high levels of radiated power (bulk–P_{rad}/P_{tot} ~ 60%), at high power levels the regime is usually terminated prematurely by a rapid influx of carbon (the 'carbon bloom') resulting from excessive localized heating of the carbon target tiles. Recent experiments, therefore, have been designed to extend plasma performance in the H–mode by: (a) reducing the heat flux to the target by sweeping the X–point position and by strong gas puffing; (b) exploiting improved plasma purity and particle control resulting from the evaporation of beryllium; (c) improving the central plasma parameters by pellet injection and by making use of central heating due to higher energy neutral beams (6MW D^0 at 140keV/ 12MW D^0 at 80keV) and ion cyclotron resonance heating.

Development of these techniques has resulted in significant improvements in the parameters attainable in the H–mode. Sweeping (radial and vertical) of the X–point interaction region has extended the H–mode duration at high power by ~30% which, when combined with the enhanced particle pumping due to evaporated beryllium, has enabled 'hot ion H–modes' (Balet *et al*, 1989) to be sustained for periods ~ 1s with peak values of $T_i(0)$ ~ 28keV being achieved (Keilhacker *et al.*, 1989a; Gibson *et al*, 1990). In addition, it has been observed that the use of strong gas puffing (simultaneously in the X–point and plasma midplane) has significantly delayed the 'carbon bloom' and retarded impurity accumulation in the bulk plasma. Consequently long ($\leq$ 5.3s) virtually elm–free H–modes have been obtained, in which the stored energy and Z_{eff} reach steady–state (Stork *et al.*, 1989). Further aspects of improved H–mode performance are discussed by Tanga *et al* (1990).

It has been shown (Keilhacker *et al*, 1989b; Thomsen *et al*, 1989) that in H–mode plasmas, the plasma energy may be decomposed into a contribution from the plasma core, which exhibits an offset linear behaviour with increasing power, and a pedestal energy, resulting from the steep

temperature and density gradients at the separatrix, which is proportional to the power. Improvements in diagnostic capabilities have revealed edge gradients to be greater than previously realized. Figure 1 shows ion temperature profiles obtained by active charge exchange resonance spectroscopy (CXRS) from several phases of JET X–point discharges (von Hellermann *et al.*, 1990). Case (a), showing the peak ion temperature recorded during a 'hot ion H–mode', indicates that T_i ~ 5keV within 10cm of the last closed flux surface (LCFS). Cases (b) and (c) illustrate observations obtained during L and H–mode phases in which the plasma was swept radially to obtain a continuous profile. Although the nominal resolution of the diagnostic is ~ 12cm, a more detailed analysis of results in case (b) suggests that T_i ~ 3keV within several cm of the separatrix.

Figure 2 illustrates the edge density profile obtained by a swept multichannel reflectometer during an H–mode (Prentice *et al.*, 1990). This profile, deduced entirely self–consistently from reflectometer measurements, indicates the existence of an extremely steep gradient, although the minimum gradient consistent with these results is $\approx 4\times10^{20}m^{-4}$. The error bars are determined by the uncertainty in the determination of the time delay of the reflected signal (~ 0.3ns). Measurements obtained by density interferometry and from the LIDAR Thomson scattering system, which have poorer spatial resolution, are also shown.

Energy confinement in JET elm–free H–modes (Keilhacker *et al.*, 1989b; Watkins *et al.* 1989) can be described by either a power degradation scaling, with $\tau_E \propto P^{-0.7}$, in which τ_E is a factor of 2 to 3 above Goldston scaling (Goldston, 1984), or by an offset linear law in which $\tau_{inc}(s) \approx 0.14I_p(MA)$. The most recent experiments have extended the power range over which this behaviour has been confirmed by almost a factor of 2. As shown in Fig. 3., comparison of discharges before and after beryllium evaporation indicates no significant difference in confinement. Experiments at high–β_φ (section 4.1) have, furthermore, confirmed that no significant additional degradation of confinement occurs at β_φ values commensurate with the limit predicted by Troyon *et al.* (1984).

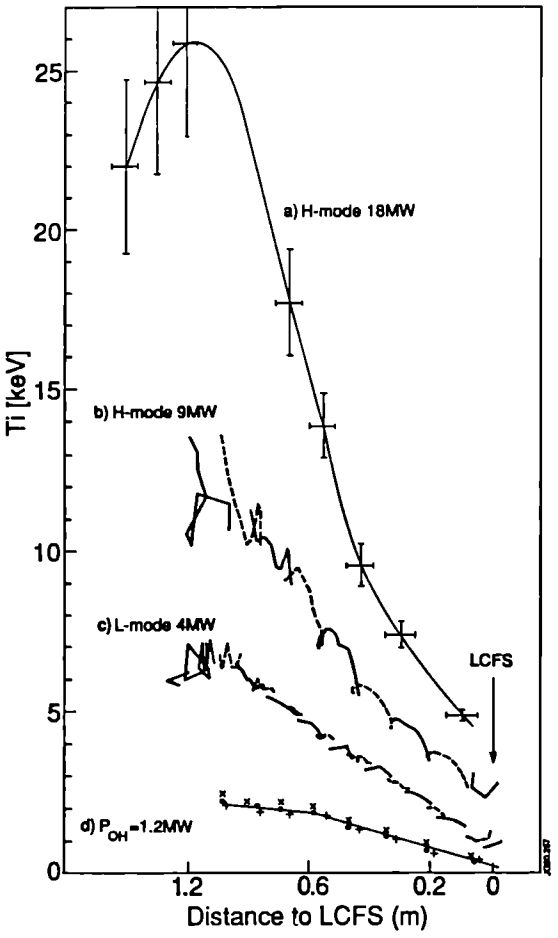

Fig. 1. Ion temperature profiles obtained from CXRS at different phases of X–point discharges. Cases (b) and (c) were obtained by sweeping the plasma position.

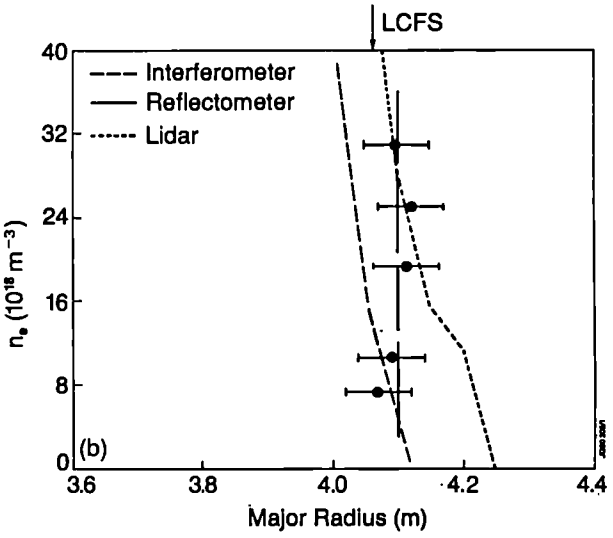

Fig. 2. Density profiles close to the separatrix of an H–mode plasma.

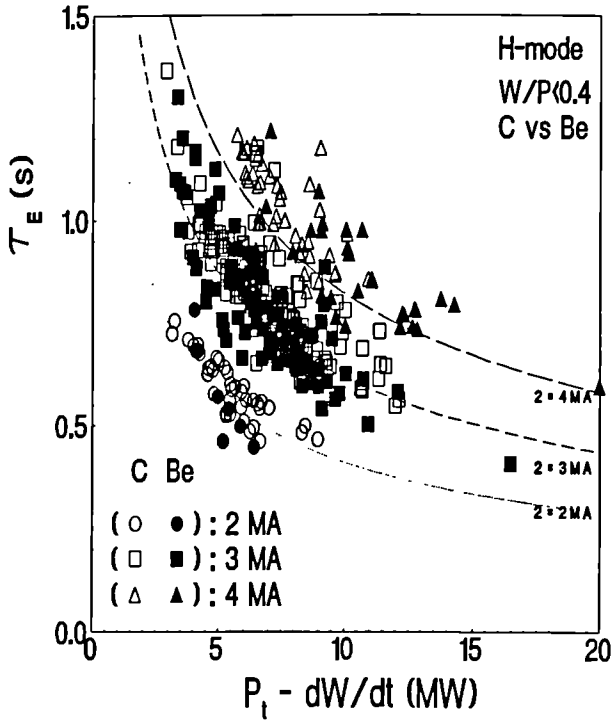

Fig. 3 Comparison of confinement time *vs* loss power in NBI heated elm–free H–modes with C and Be.

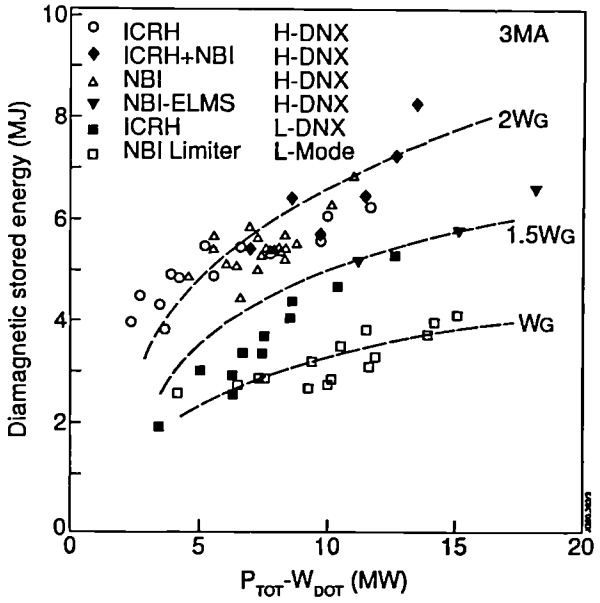

Fig. 4 Plot of diamagnetic stored energy *vs* loss power for various 3MA plasma regimes. W_G is Goldston L–mode prediction.

2.2 H–modes with ICRH

Attainment of H–modes using only ICRH (Tubbing *et al.*, 1989a; Bhatnagar *et al.*, 1990) represents one of the most significant consequences of the introduction of Be into the JET vacuum vessel. The introduction of a fast matching system to control the RF coupling during the L to H transition and the use of the dipole antenna configuration, which produces significantly less nickel impurity (Jacquinot *et al.*, 1988), also contributed to this advance. Previous attempts to produce H–modes in these conditions in JET had foundered on the high level of radiated power, produced mainly by nickel impurities sputtered from the Faraday screens of the RF antennas, but Be gettering has significantly reduced nickel sputtering, as well as reducing oxygen levels by an order of magnitude, virtually eliminating this problem.

ICRH H–modes were produced in 3MA DNX plasmas (which permit the curvature of the separatrix in the midplane to be matched to that of the RF antenna) in which the clearance between the separatrix and the RF antenna ranged from 1–3 cm. At the smallest separations, the characteristic drop in D_α light at the H–mode transition was not observed, though global energy confinement lay in the normal H–mode range. The plasmas were displaced slightly vertically ($\lesssim$ 3cm.) to favour the upper X–point, i.e. the direction of the ∇B drift. To date only the D(H) minority heating scheme has been exploited (though a few short–duration H–modes were produced at low toroidal field, ~ 1.2T, in the second harmonic majority hydrogen scheme). Although the threshold power for the H–mode was ~ 8MW at a toroidal field of 2.8T – similar to that for NBI in equivalent conditions – a hysteresis effect was observed which enabled the applied power to be reduced by as much as half while maintaining the H–mode for periods ~ 1s.

Plasma confinement in combined heating H–modes has also improved significantly as a result of the lower levels of radiation. In previous experiments (Tubbing *et al.*, 1989b), it was observed that the rate of rise of radiated power in combined heating H–modes was $\gtrsim$ 10MWs^{-1}, more than double that observed for NBI H–modes (~ 4MWs^{-1} in a carbonized torus), and was responsible for a

reduction in energy confinement in the former cases. The rate of increase in radiation in combined heating H–modes has now been reduced to ~ $3MWs^{-1}$ for similar powers and densities.

Figure 4 shows an overview of confinement in 3MA plasmas under different conditions, incorporating only data from Be gettered discharges, but from both C and Be belt limiter phases (Bhatnagar *et al.*, 1990). A small group of NBI heated belt limiter L–modes have been included for comparison purposes. Data from the ICRF heated DNX L–modes includes a contribution of 10–30% from fast ions and can be fitted by an offset linear behaviour with a $\tau_{inc} \approx 0.34s$. Data from ICRH, ICRH+NBI and NBI H–modes lie in the same range with $1.7W_G \leq W \leq 2.2W_G$, where W_G is the Goldston L–mode scaling prediction for these conditions.

2.3 Confinement in Limiter Plasmas

Experiments at plasma currents of up to 7MA using carbon limiters (e.g. Lomas *et al.*, 1989) found that global confinement was broadly described by either Rebut–Lallia (Rebut *et al.*, 1988) or Goldston L–mode scalings. However, at 3MA, confinement was generally better than predicted by both scalings, while at 6MA and above it was worse. Sawteeth, which broadened plasma profiles (Bhatnagar *et al.*, 1989; Jones *et al.*, 1989), poor density control and high fuel dilution were identified as the major problems. Recent experiments have, therefore, focussed on the use of Be gettering and Be limiters to improve plasma performance at high currents.

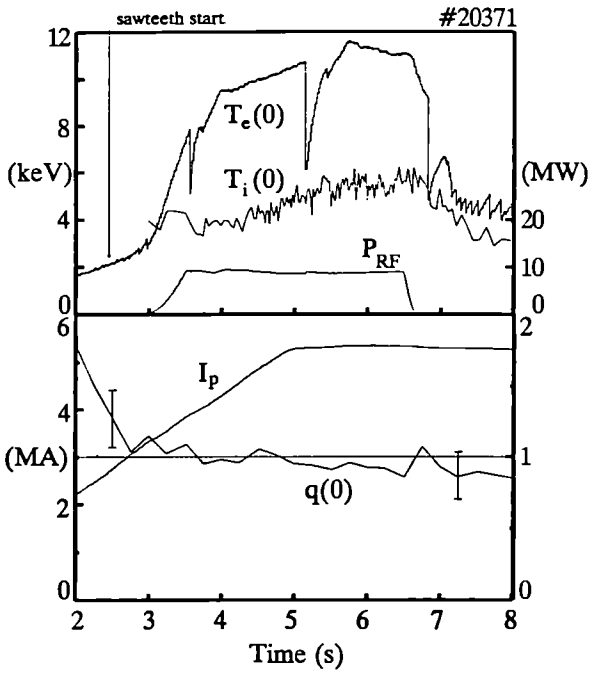

Fig. 5 Overview of 5MA limiter discharge in which sawtooth stabilization was obtained.

Restrictions on toroidal field operation (due to a faulty coil) limited experiments with beryllium plasma–facing surfaces to plasma currents of 5MA. While it has not yet been possible, therefore, to explore plasma performance at the highest currents, the use of Be has facilitated the development of a number of operating scenarios which can be extrapolated to 7MA at approximately constant q_ψ (> 3). By exploiting a fast current ramp ($1MAs^{-1}$) at constant q_ψ (~ 3.5) between 2.5 and 5MA, peaked temperature and density profiles have been established in several ways (Attenberger *et al.*, 1990). In particular, the density control provided by beryllium, combined with ICRH heating in the current rise phase, has extended sawtooth stabilization well into the flat–top at 5MA, as illustrated in Fig. 5. Peaked electron temperature profiles with $T_e(0) \sim 12keV$ have been maintained for several confinement periods. An alternative approach to sawtooth stabilization is the injection of a sequence of pellets during the current rise to establish a peaked density profile target for ICRF heating. This technique has established plasmas with central densities $n_e(0) \sim 2.3 \times 10^{20} m^{-3}$ in which sawteeth were suppressed by maintaining q(0) above unity and neutron emission was enhanced as in the pellet enhanced regime observed in 3MA experiments (Schmidt *et al.* 1989).

The most significant improvement in plasmas limited on the inner wall or belt limiters consequent on the introduction of Be can be ascribed to improvements in central parameters due to improved particle control, plasma purity and profile peaking (resulting from the suppression of sawteeth). Although a substantial reduction in radiation has led to significant increases in the density limit (see section 4.2), JET discharges are generally dominated by low–Z impurities which radiate

principally at the plasma edge. As a result, there is little difference in global energy confinement between discharges limited by carbon or beryllium surfaces. Figure 6 compares energy confinement times for a range of 5MA plasmas from all phases of operation. The majority of discharges cluster about the Goldston scaling prediction with no separation between plasmas with different limiter materials. The exceptions are discharges in which peaked profiles have been established either by ICRH sawtooth suppression, in which case there may be a significant fast ion population, or by pellet injection in which the pellet enhanced regime is achieved, which is associated with reduced ion heat transport. This is supported by Fig. 7, in which the total electron energy for these discharges is plotted against the predictions of Rebut–Lallia scaling. In this case, sawteeth–free and pellet shots lie in the same cluster as other plasmas.

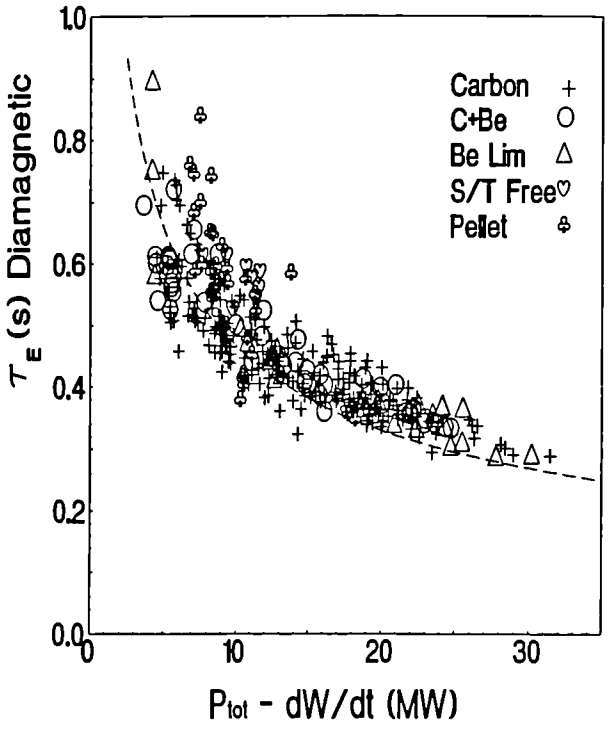

Fig. 6 Confinement time *vs* loss power for various plasma regimes at 5MA. Curve is Goldston L–mode prediction.

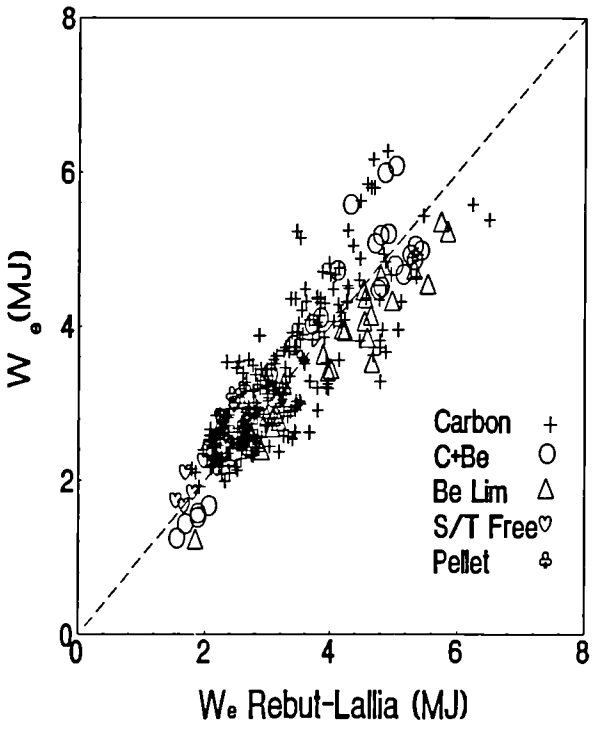

Fig. 7 Electron energy *vs* prediction of Rebut–Lallia model for 5MA limiter plasmas.

3. TRANSPORT STUDIES

3.1 Heat Flux Analysis

Heat flux analysis of local transport properties has been performed for a wide range of JET discharges using calculated heat and particle deposition profiles together with measured values of the plasma temperature and density profiles (e.g. Balet *et al.*, 1989; Taroni *et al.*, 1989; Watkins *et al.*, 1989). With appropriate allowance made for convective energy transport, effective heat diffusivities, χ_i^{eff} and χ_e^{eff}, may be deduced for ions and electrons from:

$$q_e = -n_e \chi_e^{eff} \nabla kT_e \qquad q_i = -n_i \chi_i^{eff} \nabla kT_i, \qquad (1)$$

where $q_{e,i}$ represents the conducted heat flux for electrons and ions. If experimental uncertainties do not allow ion and electron channels to be separated, an effective total diffusivity, χ_{eff}, may be defined using the total conducted heat flux, Q_{cond}:

$$\chi_{eff} = Q_{cond}/(n_e \nabla kT_e + n_i \nabla kT_i). \qquad (2)$$

Using the 1½–D transport code TRANSP (Goldston *et al.*, 1981), recent analysis has made use of enhancements in diagnostic capabilities to investigate the role of electron and ion conduction for several of the most important operating regimes in JET with a more systematic analysis of errors than has hitherto been possible (Balet *et al.*, 1990). Results for a hot ion H–mode with Be gettering are shown in Fig. 8. This discharge was formed by the injection of 17MW of neutral beams into a low density DNX target plasma (4MA/ 2.8T) to create peaked density and ion temperature profiles with $n_e(0) = 4.8\times10^{19}m^{-3}$ and $T_i(0) = 22keV$ at the analysis time (the fusion performance of this pulse, #20981, is discussed by Gibson *et al.* (1990)).

In this discharge, the ion power balance is dominated by ion heat conduction over the major part of the plasma, with equipartition energy the second largest loss channel. The input power to the electrons via equipartition is twice the direct input power from NBI. In the plasma centre, χ_i approaches the neoclassical value and is significantly lower than χ_e (although convection is also important). However, the two cross over at mid–radius, so that in the outer half of the plasma $\chi_i \geq \chi_e$, although the experimental uncertainties are large. The central value of χ_i in such discharges more closely resembles that deduced from hot ion L–modes than from previous hot ion H–modes (e.g. Balet *et al.*, 1989) and this may be related to the fact that the improved particle control following Be gettering allows a peaked density profile to be maintained into the H–mode phase of the more recent discharges.

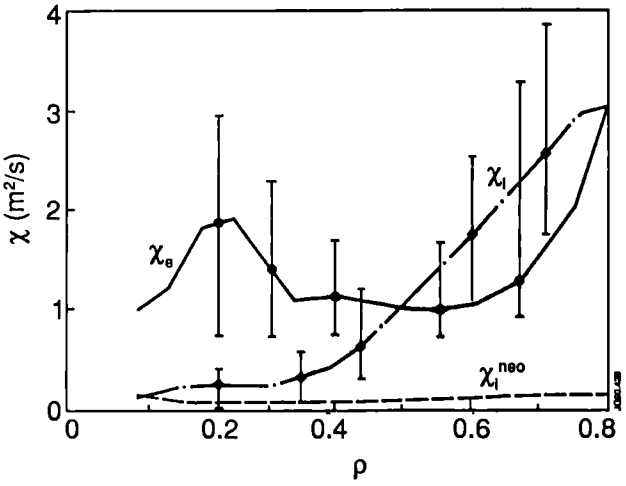

Fig. 8 Profiles of ion and electron heat diffusivities *vs* normalized minor radius for a hot ion H–mode.

The results of similar analyses for several standard JET discharge types are shown in Fig. 9. No ion temperature profile data is available for plasmas heated by ICRH alone, so the thermal diffusivity has been cast in the form of equation (2) to enable the effective diffusivity from the different regimes to be compared. In discharges with peaked density and ion temperature profiles ('pellet + ICRH' and 'hot ion H–mode') χ_{eff} falls to low values in the plasma centre and, in fact, $\chi_i \sim 1–3\times\chi_{i,neo}$ in these plasmas. In H–mode discharges, χ_{eff} falls at the plasma edge. In general, where χ_i and χ_e can be separated within experimental uncertainties, $\chi_e \geq \chi_i$ in the plasma centre and $\chi_i \geq \chi_e$ in the outer region. For such cases a detailed comparison has been made between local transport deduced from several variations of the ion temperature gradient driven turbulence (ITG) model, the Rebut–Lallia critical temperature gradient model and the experimentally derived values of χ_i. Briefly, it is found that the Rebut–Lallia model yields a good description of the observed variation of χ_i, though it predicts values that are somewhat too high in the centre for hot ion H–modes. For particular discharges, transport coefficients deduced from ITG theories are in error by two orders of magnitude. A detailed

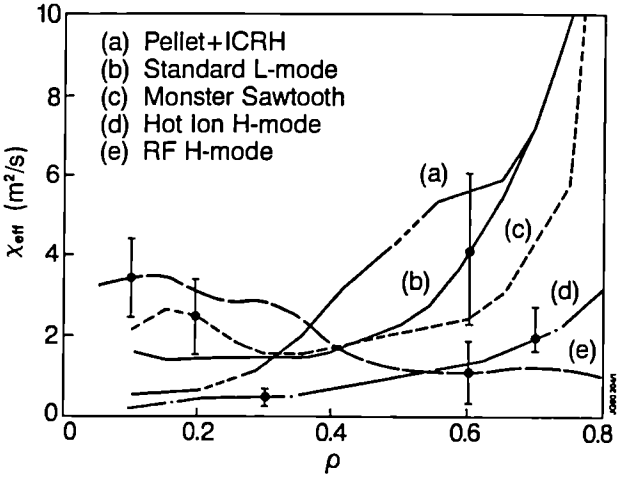

Fig. 9 Profiles of effective heat diffusivity for several types of plasma in JET ($\rho \equiv r/a$).

discussion is given in Balet *et al.* (1990).

A more systematic, quantitative assessment of the relevance of ITG models to the description of local transport in JET has been carried out using a database of 35 3MA L–mode plasmas for which spatially resolved ion and electron temperature profiles exist (Tibone *et al.*, 1990). For these discharges, which ranged from ICRH dominated plasmas with 'monster' sawteeth to NBI heated hot ion L–modes, the theoretically predicted heat fluxes from several ITG models have been compared with experimentally derived values of the total heat flux.

In the inner half of the plasma minor radius, the values of η_i for JET profiles are generally well above the theoretical threshold for all the models considered. However, the transport predicted for high T_i regimes is too large, as illustrated in Fig. 10 using the Romanelli (1989) theory as an example. On the other hand, because of the rapid decrease in the predicted transport with decreasing temperature, it is much less than the observed heat flux in the outer region. Thus, although regimes with peaked plasma profiles do exhibit enhanced confinement (Schmidt *et al.*, 1989; Balet *et al.*, 1989), ITG theories fail to account quantitatively for the observed variation of ion thermal conductivity with plasma parameters.

Toroidal plasma rotation and ion momentum transport have been studied in quasi–steady state conditions for a wide range of JET plasmas, including limiter and X–point plasmas and L and H–modes (de Esch *et al.*, 1990). Using measurements of ion temperature and rotation profiles deduced from a multichannel CXRS system (von Hellermann *et al.*, 1990), it is found that the central rotation velocity scales linearly with $T_i(0)$ for all types of beam–heated discharge, except in the presence of large amplitude mhd activity or ICRH, both of which are known to degrade toroidal momentum confinement (Snipes *et al.*, 1990; Stork *et al.*, 1987).

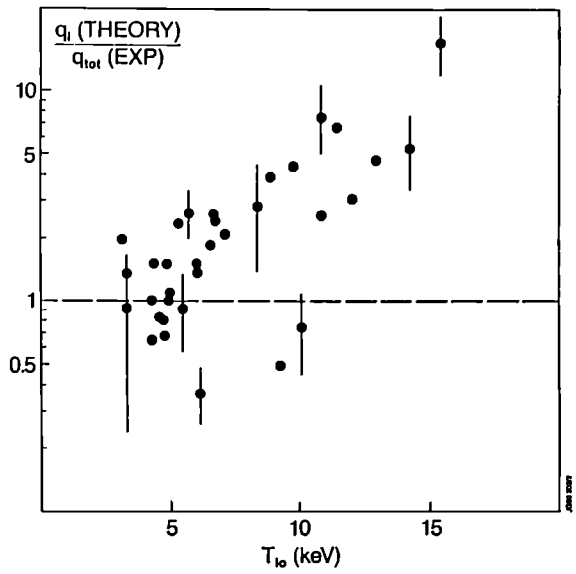

Fig. 10 Ratio of heat flux calculated from Romanelli (1989) ITG theory and that determined experimentally (at $r/a = 0.4$) *vs* central ion temperature. Data from a range of 3MA L–mode plasmas is included.

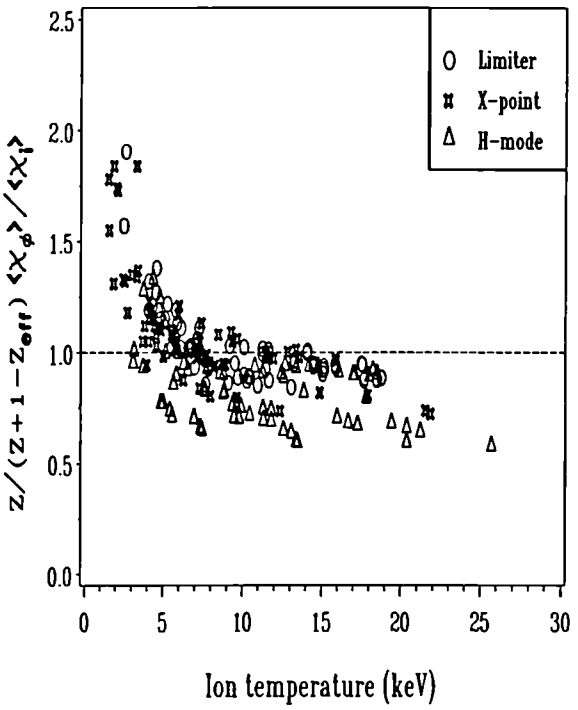

Fig. 11 Ratio of ion momentum and heat diffusivities *vs* central ion temperature. Data from a wide range of discharges is included.

The relationship between central values of χ_i and χ_φ, the toroidal momentum diffusivity, as a function of $T_i(0)$ is shown in Fig.11. This analysis uses a time–independent form of the ion heat and momentum transport equations, including a correction for the dominant impurity with normalized mass $Z = m_Z/m_D$ (for C or Be), but neglecting convection. It is found that $(Z/(Z+1-Z_{eff}))<\chi_\varphi>/<\chi_i> = 0.9 \pm 0.3$ for all plasmas with $T_i(0) > 4$keV, a result similar to that reported for TFTR (Scott *et al.*, 1989).

3.2 Perturbation Analysis of Heat and Particle Transport

Extensive analysis of heat pulse propagation (hpp) in JET using the temperature perturbation following the sawtooth collapse (e.g. Tubbing *et al.*, 1987) found that the deduced electron heat diffusivity χ_{hp} was generally a factor of 1–4 larger than the value deduced from conventional analysis of the electron power balance. This has stimulated the development of a description of χ_{hp} which identifies this quantity with an 'incremental' diffusivity, χ_{inc}, rather than the power balance diffusivity, χ_{pb}. A study of χ_{hp}, both in ohmic and auxiliary heated discharges (Lopes Cardozo and de Haas, 1990) found that, at mid–radius, $\chi_{hp} \propto Z_{eff}^{0.5} \langle T_e \rangle^{0.5}$, with essentially no dependence on density or power. This last result suggests an offset–linear formulation of the plasma stored energy. Moreover, for X–point plasmas, this study found no significant systematic difference between χ_{hp} in ohmic, L and H–phases of the discharge, in agreement with calculations of χ_{inc} deduced from analysis of global energy confinement.

Values of the particle diffusion coefficient D_e have also been derived by several perturbation techniques. Using measurements from a 12–channel microwave reflectometer, the density pulse following a sawtooth collapse has been exploited to obtain a value of the diffusion coefficient, D_{dp}, in the region $0.6 < r/a < 0.8$. For a series of 3MA limiter discharges with $3 \leq P_{tot} \leq 12$MW it was found that $0.2 < D_{dp} < 0.5$ m^2s^{-1} (±15%), with no systematic dependence on power. Similar values have been obtained by analysis of the density behaviour following shallow (Cheetham *et al.*, 1989) and deep (Baylor *et al.*, 1989) pellet penetration.

A more complete analysis of the sawtooth perturbation is required to include the possibility of direct coupling between heat and particle transport. For example, the heat pulse is observed to induce a local density dip, an effect which cannot be explained in terms of perturbations to the flux surfaces resulting from changes in the local pressure profile. The first results of such an analysis (Hogeweij *et al.*, 1990), using measurements obtained from 3MA, ICRF heated plasmas with $P_{tot} \leq 11$MW, show that, over the region $0.6 < r/a < 0.8$,

$$0.2 < D_{dp} < 0.8 \ m^2s^{-1} \ (\pm 25\%)$$

and

$$3 < \chi_{hp} < 9 \ m^2s^{-1} \ (\pm 25\%).$$

This confirms the results of earlier, independent, analyses. In addition, this analysis suggests that a term describing a ∇T_e–driven particle pinch (or a diffusion coefficient which is a decreasing function of ∇T_e) is required to model the response of the density to the temperature perturbation.

4. MHD STABILITY

4.1 High–β_φ Experiments

Although calculations have indicated that local pressure gradients in some discharges might lie close to the stability boundary for ideal ballooning modes, for example in the edge region of H–modes (O'Brien *et al.*, 1989) or the centre of pellet–fuelled discharges (Galvao *et al.*, 1989), global values of β_φ in JET have never previously exceeded 70% of the Troyon limit (Troyon *et al.*, 1984). Recent experiments have studied a regime of high β_φ in DNX H–mode plasmas heated by NBI and ICRH at power levels of up to 16MW (Smeulders *et al.*, 1990). These experiments used 80keV D^0 NBI into hydrogen target plasmas (for second harmonic ICRF heating) with a current of 2MA and toroidal field in the region $0.9 \leq B_\varphi \leq 1.4$T. As shown in Fig. 12, β_φ values of 5.5% have been achieved, which are commensurate with the Troyon limit,

$$\beta_T(\%) = 2.8 \ I_p(MA)/a(m)B_\varphi(T). \qquad (3)$$

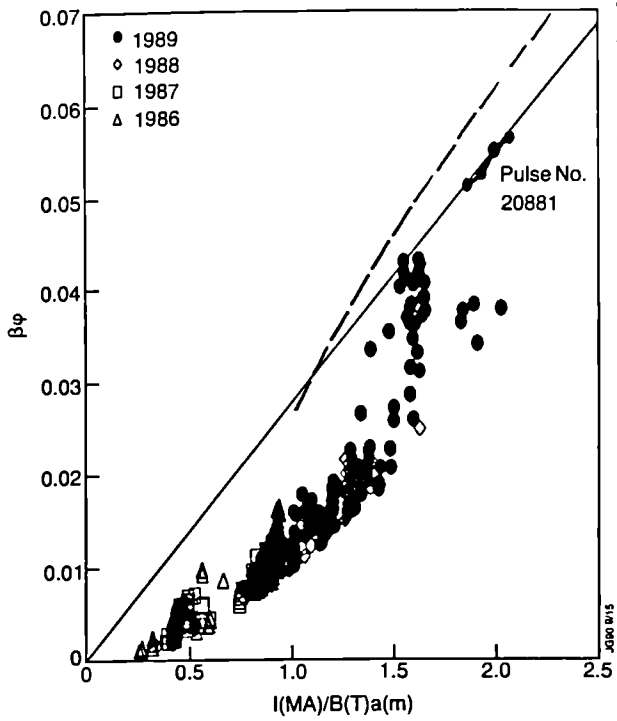

Fig. 12 Toroidal beta *vs* normalized current for high–beta discharges. The solid line represents the Troyon limit and the broken line a prediction derived from Stringer (1981).

The figure also shows that these values are close to limiting values originally predicted for JET (Stringer, 1981).

Virtually all high–β_φ discharges in JET are dominated by sawteeth, which are accompanied by substantial 'fishbone' activity. The sawteeth modulate the global β_φ by up to 15% and are responsible for significant reductions in the global (- 30%) and central (-70%) values of the neutron emission (Marcus *et al.* 1990). Detailed comparisons of sawteeth precursors and 'fishbone' activity using soft X–ray measurements show that both have a main m=n=1 component, though with larger amplitude higher–m components than is usual in low–β_φ plasmas. The displacement of the central plasma associated with the sawtooth collapse is approximately double that resulting from the 'fishbone' instability.

Magnetic activity at the plasma edge is generally dominated by n=1 modes, which are coupled to the central activity, and by 'elms'. However, continuous modes with higher n numbers can develop. In some cases, the mode, usually with n=2, grows to a large amplitude and locks. Although the dominant component has m=3, m=2 and m=4 components can be observed in the soft X–ray emission and an m=5 component can be identified in signals from the magnetic pickup coils at the plasma edge. The mode amplitude increases over a period of several hundred ms to a value of $\tilde{B}_\theta$ - 5G, following which β_φ decays, falling by 30% or more, as the mode continues to grow following locking, and finally reaches values of B_θ - 15G ($\tilde{B}_\theta/B_\theta$ - 1%).

Analysis of ideal ballooning stability in these discharges is complicated by the presence of a substantial fast ion population, which is included in experimental pressure profiles – determined by normalizing the electron pressure profile obtained from LIDAR Thomson scattering measurements to the total diamagnetic energy – and by uncertainties in the equilibria. Within these restrictions, it is found that in many cases the central region of the plasma is marginally stable to ballooning modes except near the magnetic axis, where the pressure gradient exceeds the ballooning limit (Hender *et al.*, 1990).

At the power levels explored to date, the β_φ values achieved appear to be limited by confinement and, in some cases, by large amplitude low–m,n mhd activity rather than by disruptive behaviour. As noted in 2.1, confinement at the highest values of β_φ is close to twice the Goldston L–mode value. However, the injected power is limited by the occurrence of the carbon 'bloom'. Further experiments are required, therefore, to investigate whether these values represent a real limit or are determined by experimental constraints.

4.2 Density Limits

Extensive experiments in carbon bounded plasmas (e.g. Wesson *et al.*, 1989) found that the density in JET was limited by disruptions. These occurred as the result of a well–defined sequence of events in which, as the density increased, the radiated power exceeded the input power, leading to thermal instability in the plasma edge. As a result, the electron temperature profile contracted,

driving the edge current inwards. This destabilized a sequence of mhd modes, principally the m=2,n=1 mode, which grew, locked and caused a major disruption.

The introduction of Be, firstly in the form of Be gettering and, subsequently, as a limiter material, has caused a fundamental change in the nature of the the density limit (Lowry *et al.*, 1990). This is illustrated in Fig. 13. As in the case of carbon, increasing density leads to increasing edge radiation, though at moderate densities ($<n_e>$ - $3\times10^{19}m^{-3}$) the steady–state level of radiation for Be bounded discharges may be only 50% of that for equivalent discharges bounded by carbon. Near to the limiting density, the radiated power increases rapidly. Bolometric and spectroscopic observations show that this phase is terminated by the formation of a MARFE (Lipschultz *et al.*, 1984) on the inner wall, at which time the radiated power may be transiently in excess of the input power. Detailed measurements of edge parameters at the limiter (Clement *et al.*, 1990) show that this occurs when T_e at the edge falls to 10 to 20eV.

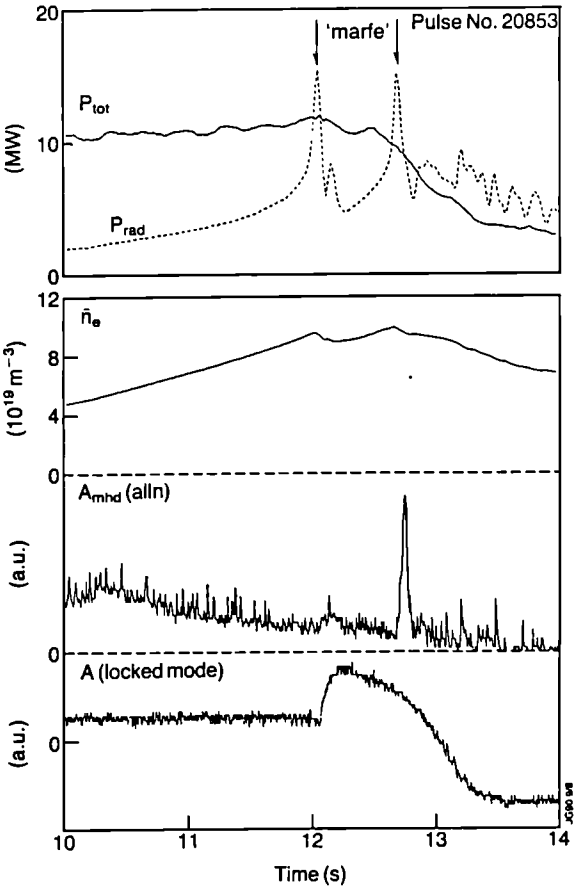

Fig. 13 Overview of plasma parameters for a density limit experiment in a 4MA/ 2.6T plasma with 11MW of input power. A_{mhd} indicates the level of rotating mhd activity and A(locked mode) the non–rotating activity. The signal after 12s in the latter is due to pick–up from the toroidal field decay.

Formation of the MARFE leads to a fall in edge electron density, though whether by changes in recycling (the limiter interaction is much reduced), screening, or a decrease in edge particle confinement is not yet clear. Nevertheless, the result is that the MARFE quenches, the plasma returns to a quiescent state and, if fuelling continues, the cycle can re–occur. Mhd activity plays little role in these events. The figure shows that there is no rotating or stationary mhd activity associated with the first MARFE, while at the second MARFE a small burst of mhd is observed which rapidly decays (the small signal apparent on the locked mode monitor is due to pickup from the decay of the toroidal field, which begins at 12s).

The result is that density limit disruptions are very infrequent in plasmas bounded by Be. In plasmas which do disrupt at the density limit, it is found that the MARFE decays and is replaced by a symmetric radiation shell which persists, radiating the total input power. The sequence of events leading to disruption is then as outlined for the carbon limiter. Understanding the balance between MARFE formation and the development of a symmetrically radiating layer is one of the major problems in explaining the different behaviour with carbon and beryllium limiters.

Analysis of density limit experiments in Be bounded plasmas shows that, while radiation determines the limit, the edge density is the key plasma parameter. In particular, comparison of similar discharges fuelled by gas puffing and pellet injection found that with deep pellet penetration, peaked density profiles could be sustained at substantially higher average density than with shallow penetration or gas fuelling. Nevertheless, the density limit occurred at the same edge densities in the three cases. In addition, the higher density limit obtained in helium discharges was explained by the differences in edge density profiles in helium leuterium

discharges (rather than, as had been suggested, the reduced oxygen content in the former case).

As a result of the reduced impurity radiation, the density limit in Be limiter discharges, both in ohmic and auxiliary heating phases, has been extended considerably (by a factor ~ 2) beyond that obtained with a graphite limiter. In addition, the density limit with ICRF heating, which had previously been limited by increased impurity levels and which barely exceeded the ohmic density limit, increased to that attained with NBI. At power levels of up to 20MW, the limiting density was found to scale with $P_{tot}^{0.5}$, the best fit being obtained by the use of the edge density (Lowry *et al.*, 1990). Values of $\bar{n}_e R q_c / B_\varphi$ ~ 35 were obtained with additional heating (compared to ~ 20 with graphite) and values above 40 were reached at high q_c. This exceeds the scaling proposed by Greenwald *et al.* (1988) by about 50%. At the highest powers, the fuelling rate became a significant consideration as hollow density profiles formed and, together with the results of pellet injection experiments, this suggests that the density limit should be considered as a *fuelling* limitation.

4.3 Sawteeth and their Stabilization

Elucidation of the instability underlying sawteeth has become a subject of considerable interest and extensive investigations have been undertaken at JET (e.g. Campbell *et al.*, 1989a). Analysis of the sawtooth collapse using tomographic reconstructions of soft X–ray emission measurements (Edwards *et al.*, 1986) revealed that the topology of the collapse in JET resembled the convective behaviour predicted by the 'quasi–interchange' model (Wesson, 1986), rather than that expected from full reconnection models (e.g. Kadomtsev, 1975) – a result confirmed by two–dimensional reconstructions of local T_e measurements obtained from ECE (Campbell *et al.*, 1989b).

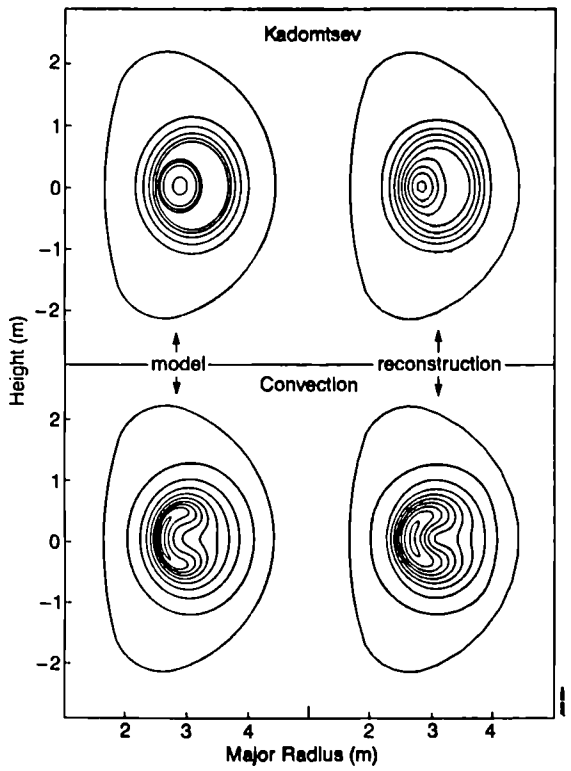

Fig. 14 Comparison of simulated soft X–ray analyses of two most common models for the sawtooth collapse: full–reconnection (Kadomtsev) and 'quasi–interchange' (convection).

Two–dimensional tomographic analysis based on two orthogonal cameras has inherent limitations on the poloidal resolution which can be achieved. To clarify the importance of these limitations, the accuracy of the soft X–ray reconstruction technique has recently been investigated using simulations of the topology associated with the two most common models of sawteeth. It is found (Wolfe *et al.*, 1990) that, for the case commonly studied in JET (in which the plasma core is displaced along the major radius) the analysis technique accurately reproduces the input emission profiles. As shown in Fig. 14, there are clear differences between the reconstructions which enabled the topologies associated with the two models (the full reconnection and the convective cell) to be unambiguously distinguished.

Much of the difficulty in understanding sawteeth is associated with uncertainties in the determination of the q–profile and, in particular, of the way in which q(0) is modulated by sawtooth activity. The accuracy of the polarimetric analysis used to derive q–profiles in JET has recently been investigated in some detail (O'Rourke and Lazzaro, 1990). In particular, Faraday rotation measurements have been incorporated self–consistently as additional

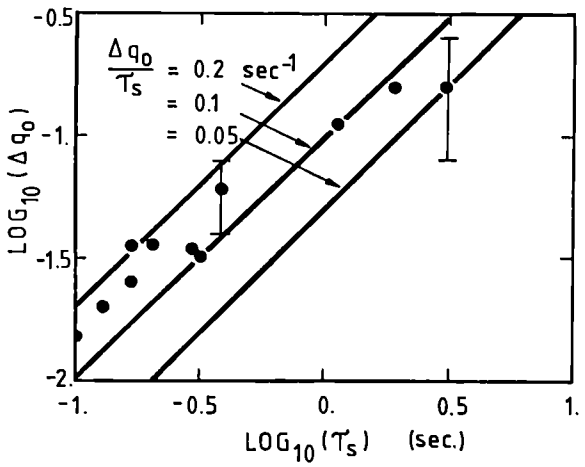

Fig. 15 Plot of change in central safety factor, Δq_0, *vs* sawtooth period, τ_s, derived from polarimetry.

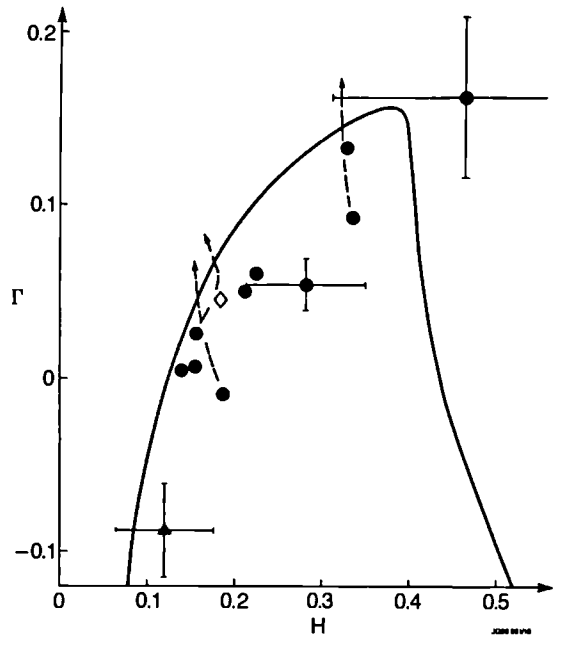

Fig. 16 Analysis of a range of discharges during sawtooth–free periods. Γ and H are defined in the text. The solid curve encloses the stable region and the dashed lines indicate the trajectories of discharges as the q=1 surface expands.

constraints in the equilibrium identification code IDENTC. A systematic check of the propagation of experimental uncertainties in the analysis has been performed which has confirmed the previously reported results (O'Rourke *et al.*, 1988) that q(0) - 0.7 (±20%) in normal sawtoothing discharges. In addition, by Abel–inverting the difference in polarimetric signals before and after a sawtooth collapse, it has been possible to study the variation of q(0) during the sawtooth period. Figure 15 shows that, for a range of ohmic and ICRF heated discharges, Δq(0) increases with the sawtooth period, τ_s, with a constant of proportionality lying in the range $0.05 - 0.2 s^{-1}$.

Sawteeth can be stabilized in JET either by the injection of pellets (Schmidt *et al.*, 1989), which broadens the current profile and raises q(0) above unity, or by on–axis heating (Campbell *et al.*, 1988), particularly with ICRH. In the latter case, polarimetric measurements show that q(0) < 1 (O'Rourke *et al.*, 1988) and it has been suggested (e.g. Pegoraro *et al.*, 1989) that energetic ions are responsible for the stabilization. Quantitative analysis of experimental results is difficult due to uncertainties in critical parameters, such as the q–profile and the distribution of the fast ions, both in space and in energy. However, by making certain simplifying assumptions, essentially that local quantities may be replaced by global parameters, a quantitative comparison between theory and experiment has been performed (Porcelli *et al.*, 1990).

The results of this analysis are shown in Fig. 16, in which data from a number of pulses with sawtooth–free periods are plotted in the (Γ, H) plane, where

$$\Gamma = \frac{\gamma_{mhd}}{\omega_{Dh}^{max}} \qquad (4a)$$

$$H = \frac{r_s}{s_0 R_0} \frac{\omega_A}{\omega_{Dh}^{max}} <\beta_{ph}>_a . \qquad (4b)$$

γ_{mhd} is the ideal mhd growth rate, ω_{Dh}^{max} the maximum fast ion precession frequency, ω_A the Alfvén frequency, s_0 the shear at the q=1 radius, r_s, and $<\beta_{ph}>_a$ the poloidal beta associated with the perpendicular fast ion energy (which, for central ICRH, is a reasonable measure of the fast ion energy within the q=1 radius). The area enclosed by the curve represents the stable region and the dashed lines indicate the trajectories followed by the discharges as the q=1 radius expands during the sawtooth–free period – it is predicted that, as the q=1 radius expands, the m=1 mode

should become increasingly unstable, leading to a sawtooth collapse. While the uncertainties in this analysis are large, further experimental observations lend support to this interpretation (e.g. Campbell *et al.*, 1989a). For example, the increasing difficulty in obtaining stabilization as the q=1 radius expands at high current ($\geq$ 5MA) and the fact that central ICRH is optimal for stabilization are consistent with the fast ion theory.

5. CONCLUSIONS

Recent experiments in JET using beryllium, both as a limiter material and for gettering, have resulted in a significant extension of JET operating regimes. The power range of elm–free H–mode experiments has been extended, by almost a factor of 2, and the previously observed confinement behaviour confirmed. In addition, an ICRH generated H–mode has been obtained. The confinement properties of both ICRH and combined heating H–modes are now equivalent to NBI H–modes. Improved control of particle recycling due to the use of Be has also improved the performance of limiter discharges. Sawtooth–free L–mode discharges with $T_e(0)$ - 12keV have been produced at 5MA and, at 3MA, a range of discharges with peaked density and temperature profiles have been obtained both on the inner wall and on the outside belt limiters.

Analysis of the local heat flux has confirmed that in many JET regimes ion transport dominates electron transport in the outer half of the plasma. In regimes with peaked density and temperature profiles, however, ion heat diffusivity falls to near neoclassical values in the plasma centre. Quantitative comparison of transport derived from theories of ion temperature gradient driven turbulence with that observed experimentally has found that the transport predicted was too strong. A study of ion heat and momentum diffusivities over many discharges from several JET regimes concluded that the values are strongly correlated. Investigation of electron transport by perturbative means has confirmed previous results and, in addition, obtained evidence of direct coupling between heat and particle transport.

Discharges with β_φ values close to the Troyon limit exhibit substantial mhd activity which can modulate or reduce β_φ, but further experiments are required to clarify whether the values of β_φ obtained are also limited by experimental constraints or whether a true limit has been reached. The change in the nature of the density limit – it is generally non–disruptive – and the considerable extension of the operating range observed are amongst the most significant consequences of the use of Be in JET. Moreover, these results indicate that densities in the range required for reactor operation can be achieved by development of appropriate fuelling techniques. Further studies of the sawtooth instability have confirmed the internal self–consistency of several of the critical diagnostic measurements. In addition, a quantitative assessment of sawtooth stabilization experiments supports the idea that energetic ions are central to the stabilization mechanism. Nevertheless, the internal contradictions of many of the observations remain and our understanding of sawteeth is still incomplete.

JET results indicate that, in spite of limits in our understanding of the phenomena which determine transport and mhd stability, many of the experimental techniques necessary for a study of reactor relevant plasmas are in place. Planned enhancements to JET in the near future will enable these techniques to be exploited fully.

6. ACKNOWLEDGEMENTS

It is a pleasure to acknowledge contributions from many colleagues. This paper has benefitted considerably from their critical appraisal and from their efforts in reducing large quantities of data to a comprehensible form. Pellet injection results were obtained as a result of work performed under a collaboration agreement between the JET Joint Undertaking and the US Dept. of Energy.

7. REFERENCES

Attenberger, S. *et al.* (1990). *Proc. 17th Euro. Conf. on Contr. Fusion and Plasma Phys.*, Amsterdam, 1990, 14B(1) 5–9.

Balet, B. *et al.* (1989). JET Preprint JET–P(89)81 (to be published in *Nuclear Fusion*).

Balet, B. *et al.* (1990). *Proc. 17th Euro. Conf. on Contr. Fusion and Plasma Phys.*, Amsterdam, 1990, 14B(1) 162–165.

Baylor, L. *et al.* (1989). *Bull. Am. Phys. Soc.* 34 2057 (see JET Preprint JET–P(89)80).

Bhatnagar, V.P. *et al.* (1990). *Proc. 17th Euro. Conf. on Contr. Fusion and Plasma Phys.*, Amsterdam, 1990, 14B(1) 255–258.

Bhatnagar, V.P. *et al.* (1989). *Plasma Phys. and Contr. Fusion* 31 333–344.

Campbell, D.J *et al.* (1988). *Phys. Rev. Lett.* 60 2148–2151.

Campbell, D.J *et al.* (1989a). In: *Plasma Physics and Controlled Nuclear Fusion Research 1988* (Proc. 12th Int. Conf., Nice), Vol. 1, pp 377–385 (IAEA, Vienna, 1989).

Campbell, D.J *et al.* (1989b). *Proc. 16th Euro. Conf. on Contr. Fusion and Plasma Phys.*, Venice, 1989, 13B(2) 509–512.

Cheetham, A.D. *et al.* (1989). In: *Plasma Physics and Controlled Nuclear Fusion Research 1988* (Proc. 12th Int. Conf., Nice), Vol. 1, pp 483–493 (IAEA, Vienna, 1989).

Clement, S. *et al.* (1990). *Proc. 17th Euro. Conf. on Contr. Fusion and Plasma Phys.*, Amsterdam, 1990, 14B(3) 1373–1376.

de Esch, H.P.L. *et al.* (1990). *Proc. 17th Euro. Conf. on Contr. Fusion and Plasma Phys.*, Amsterdam, 1990, 14B(1) 90–93.

Dietz, K.J. *et al.* (1990). *Plasma Phys. and Contr. Fusion.* This Issue.

Edwards, A.W. *et al.* (1986). *Phys. Rev. Lett.* 57 210–213.

Galvão, R.M.O. *et al.* (1989). *Proc. 16th Euro. Conf. on Contr. Fusion and Plasma Phys.*, Venice, 1989, 13B(2) 501–504.

Gibson, A. *et al.* (1988). *Plasma Phys. and Contr. Fusion* 30 1375–1390.

Gibson, A. *et al.* (1990). *Plasma Phys. and Contr. Fusion.* This Issue.

Goldston, R.J. *et al.* (1981). *J. Comput. Phys.* 43 61–78.

Goldston, R.J. (1984). *Plasma Phys. and Contr. Fusion* 26 87–103.

Greenwald, M. *et al.*(1988). *Nuclear Fusion* 28 2199–2207.

Hender, T.C. *et al.* (1990). *Proc. 17th Euro. Conf. on Contr. Fusion and Plasma Phys.*, Amsterdam, 1990, 14B(1) 399–402.

Hogeweij, G.M.D. *et al.* (1990). *Proc. 17th Euro. Conf. on Contr. Fusion and Plasma Phys.*, Amsterdam, 1990, 14B(1) 158–161.

Jacquinot, J. *et al.* (1988). *Plasma Phys. and Contr. Fusion* 30 1467–1478.

Jones, T.T.C. *et al.* (1989). *Proc. 16th Euro. Conf. on Contr. Fusion and Plasma Phys.*, Venice, 1989, 13B(1) 11–14.

Kadomtsev, B.B. (1975). *Fiz. Plazmy* 1 710–712.

Keilhacker, M. *et al.* (1989). In: *Plasma Physics and Controlled Nuclear Fusion Research 1988* (Proc. 12th Int. Conf., Nice), Vol. 1, pp 159–182 (IAEA, Vienna, 1989).

Keilhacker, M. *et al.* (1990). *Phys. Fluids B* 2 1291–1299.

Lipschultz, B. *et al.* (1984). *Nuclear Fusion* 24 977–988.

Lomas, P.J. *et al.* (1989). *Plasma Phys. and Contr. Fusion* 31 1481–1496.

Lopes Cardozo, N.J. and de Haas, J.C.M. (1990). *Nuclear Fusion* 30 521–532.

Lowry, C.G. *et al.* (1989). *Proc. 17th Euro. Conf. on Contr. Fusion and Plasma Phys.*, Amsterdam, 1990, 14B(1) 339–342.

Marcus, F.B. *et al.* (1990). *Proc. 17th Euro. Conf. on Contr. Fusion and Plasma Phys.*, Amsterdam, 1990, 14B(1) 331–334.

O'Brien, D.P. *et al.* (1990). *Proc. 16th Euro. Conf. on Contr. Fusion and Plasma Phys.*, Venice, 1989, 13B(1) 229–232.

O'Brien, D.P. *et al.* (1990). *Proc. 17th Euro. Conf. on Contr. Fusion and Plasma Phys.*, Amsterdam, 1990, 14B(1) 251–254.

O'Rourke, J. *et al.* (1988). *Proc. 15th Euro. Conf. on Contr. Fusion and Plasma Phys.*, Dubrovnik,

1988, 12B(1) 155–158.
O'Rourke, J. and Lazzaro, E. (1990). *Proc. 17th Euro. Conf. on Contr. Fusion and Plasma Phys.*, Amsterdam, 1990, 14B(1) 343–346.
Pegoraro, F. *et al.* (1989). In: *Plasma Physics and Controlled Nuclear Fusion Research 1988* (Proc. 12th Int. Conf., Nice), Vol. 2, pp 243–249 (IAEA, Vienna, 1989).
Porcelli, F. *et al.* (1990). *Proc. 17th Euro. Conf. on Contr. Fusion and Plasma Phys.*, Amsterdam, 1990, 14B(1) 327–330.
Prentice, R *et al.* (1990). *Proc. 17th Euro. Conf. on Contr. Fusion and Plasma Phys.*, Amsterdam, 1990, 14B(4) 1500–1503.
Rebut, P.H. and Dietz, K.J. (1982). In: *Fusion Technology 1982* (Proc. 12th Symp., Jülich, 1982), Vol 1, pp 85–100 (Pergamon Press, New York, 1983).
Rebut, P.H. *et al.* (1985). In: *Plasma Physics and Controlled Nuclear Fusion Research 1984* (Proc. 10th Int. Conf., London), Vol. 1, pp 11–27 (IAEA, Vienna, 1985).
Rebut, P.H. *et al.* (1989). In: *Plasma Physics and Controlled Nuclear Fusion Research 1988* (Proc. 12th Int. Conf., Nice), Vol. 2, pp 191–200 (IAEA, Vienna, 1989).
Romanelli, F. (1989). *Phys. Fluids B* 1 1018–1025.
Schmidt, G.L. *et al.* (1989). In: *Plasma Physics and Controlled Nuclear Fusion Research 1988* (Proc. 12th Int. Conf., Nice), Vol. 1, pp 215–228 (IAEA, Vienna, 1989).
Scott, S.D. *et al.* (1989). In: *Plasma Physics and Controlled Nuclear Fusion Research 1988* (Proc. 12th Int. Conf., Nice), Vol. 1, pp 655–667 (IAEA, Vienna, 1989).
Sips, A.C.C. *et al.* (1989). *Bull. Am. Phys. Soc.* 34 2055 (see JET Preprint JET–P(89)80).
Smeulders, P. *et al.*(1990). *Proc. 17th Euro. Conf. on Contr. Fusion and Plasma Phys.*, Amsterdam, 1990, 14B(1) 323–326.
Snipes, J.A. *et al.* (1990). *Nuclear Fusion* 30 205–218.
Stork, D. *et al.* (1987). *Proc. 14th Euro. Conf. on Contr. Fusion and Plasma Phys.*, Madrid, 1987, 11D(1) 306–309.
Stork, D. *et al.* (1989). *Bull. Am. Phys. Soc.* 34 2055 (see JET Preprint JET–P(89)80).
Stringer, T.E. (1981). *Comput. Phys. Commun.* 24 337–342.
Tanga, A. *et al.* (1987). *Nuclear Fusion* 27 1877–1895.
Tanga, A. *et al.* (1990). *Proc. 17th Euro. Conf. on Contr. Fusion and Plasma Phys.*, Amsterdam, 1990, 14B(1) 259–262.
Taroni, A. *et al.* (1989). In: *Plasma Physics and Controlled Nuclear Fusion Research 1988* (Proc. 12th Int. Conf., Nice), Vol. 1, pp 367–376 (IAEA, Vienna, 1989).
Thomas, P.R. *et al.* (1989). In: *Plasma Physics and Controlled Nuclear Fusion Research 1988* (Proc. 12th Int. Conf., London), Vol. 1, pp 247–255 (IAEA, Vienna, 1989).
Thomas, P.R. *et al.* (1990). In: *Proc. 9th International Conference on Plasma Surface Interactions*, Bournemouth (to be published in *J. Nucl. Mater.*).
Thomsen, K. *et al.* (1989). *Proc. 16th Euro. Conf. on Contr. Fusion and Plasma Phys.*, Venice, 1989, 13B(1) 233–236.
Tibone, F. *et al.* (1990). *Proc. 17th Euro. Conf. on Contr. Fusion and Plasma Phys.*, Amsterdam, 1990, 14B(1) 805–808.
Troyon, F. *et al.* (1984). *Plasma Phys. and Contr. Fusion* 26 209–215.
Tubbing, B.J.D. *et al.* (1987). *Nuclear Fusion* 27 1843–1855.
Tubbing, B.J.D. *et al.* (1989a). *Nuclear Fusion* 29 1953–57.
Tubbing, B.J.D. *et al.* (1989b). *Proc. 16th Euro. Conf. on Contr. Fusion and Plasma Phys.*, Venice, 1989, 13B(1) 237–240.
von Hellermann, M. *et al.* (1990). *Proceedings 8th APS Topical Conference on High Temperature Plasma Diagnostics*, Hyannis Port (to be published in *Rev. Sci. Instr.* – see JET Preprint JET–P(90)19).
Watkins, M.L. *et al.* (1989). *Plasma Phys. and Contr. Fusion* 31 1713–1724.
Wesson, J.A. (1986). *Plasma Phys. and Contr. Fusion* 28(1A) 243–248.
Wesson, J.A. *et al.* (1989). *Nuclear Fusion* 29 641–666.
Wolfe, S.W. *et al.* (1990). *Proc. 17th Euro. Conf. on Contr. Fusion and Plasma Phys.*, Amsterdam, 1990, 14B(1) 335–338.

Papers presented at the 9th International Conference on Controlled Fusion Devices

Many Authors

JET Papers presented at the 9th International Conference on Plasma Surface Interactions and Controlled Fusion Devices (Bournemouth, UK, 21-25 May 1990)
Volume I

	Title	Presenter
1)	Results of JET Operation with Beryllium (Invited Paper)	P.R.Thomas
2)	Evolution of Be - Containing Layers in JET Boundary Region (Oral Paper)	Dr. J.P.Coad
3)	Enhanced Carbon and Beryllium Influxes During High Power Operation in JET (Oral Paper)	D.Pasini
4)	Analysis of Deuterium Recycling in JET Under Beryllium First Wall Conditions (Oral Paper)	J.Ehrenberg
5)	Scrape-Off Layer Parameters in JET with Beryllium Limiters	S.K.Erents
6)	Impurity Coverage and Deuterium Inventory of Beryllium and Carbon First Wall Components after Beryllium Operation in JET	A.T.Peacock
7)	Carbon Yields and Influxes as a Function of Target Temperatures in JET X-Point Plasmas	R.Reichle
8)	Global Influx Impurity Behaviour During ICRF Heating in JET with Beryllium Limiters	M.Bures
9)	A Comparison of Global Modelling of Impurities in JET with Experimental Data Obtained Using Carbon and Beryllium Limiters	G.McCracken
10)	Systematics of Density Increase and Recycling Behaviour in JET H-Modes	D.Stork
11)	Edge Fuelling Scenarios and Scrape-Off Layer Parameters in JET with Beryllium Limiters	S.Clement
12)	Edge Measurements in JET During the H-L Mode Transition	S.K.Erents

JET Papers presented at the 9th International Conference on Plasma Surface Interactions and Controlled Fusion Devices (Bournemouth, UK, 21-25 May 1990) Volume II

	Title	Presenter
13)	Damage to JET Beryllium Tiles	E.Deksnis
14)	The Impurity Spatial Distributions, Sputtering Yields and Power Deposition at Beryllium and Carbon Belt Limiters in JET	Dr. A.Hwang
15)	Measurement of the Temperature Dependence of Carbon and Beryllium Fluxes in the JET Boundary Plasma using a High Heat-Flux Probe	D.D.R.Summers
16)	Impurity Control in JET using Fuelling	A.Gondhalekar
17)	Hydrogen Recycling Coefficient in Beryllium Experimental Determination and Test Simulation of the Density Evolution in a JET Plasma Discharge	G.Saibene
18)	Deuterium Release Measurements in the Be Phase of JET and Determination of Tritium Content in the Exhaust Gas.	R.Sartori
19)	Implantation and Re-emission of Hydrogen and Helium in the Beam Stopping Panels of a 10MW Ion Beam Line	H.D.Falter
20)	Modelling and Experimental Studies of Impurity Control in JET X-point Configurations	P.J.Harbour
21)	Deposition of Carbon and Beryllium Retention of Deuterium on Probes in the Scrape-off Layer of JET	H.Bergsaker
22)	Measurements of the Energy Distribution of Fast Tritons and Helium Atoms Escaping from the Plasma in JET	E.V.Carruthers
23)	Measurements of the Electron Temperature and Electron Density in the Edge Plasma of JET by ECE and Microwave Reflectometry	A.E.Costley
24)	The Characteristics of Neutral and Near Neutral Atom Emission at Plasma Boundaries and Their Diagnostic Exploitation - a Theoretical View	H.P.Summers

Effect of Beryllium on Plasma Performance in JET

K.J.Dietz

Invited Paper presented to the 17th European Conference on Controlled Fusion and Plasma Heating, Amsterdam, the Netherlands, 25th-29th June 1990

EFFECT OF BERYLLIUM ON PLASMA PERFORMANCE IN JET

K.J. DIETZ AND THE JET TEAM

JET Joint Undertaking, Abingdon, OX14 3EA, U.K.

ABSTRACT

JET is investigating beryllium as material for walls and limiters. Studies were carried out with initially a thin layer of beryllium evaporated onto the walls of the machine, later in addition the graphite material of the belt limiter was exchanged against beryllium. The use of this material was generally beneficial for the plasma behaviour. Combined with a reduction in the oxygen content, strong pumping of hydrogen isotopes was found which allowed JET to widen considerably the operational space with respect to ion temperatures, densities and plasma purity. In this paper a comparison of the plasma performance with graphite and beryllium will be presented. We will discuss especially the impurity behaviour with respect to fluxes, concentrations, effective charge and dilution, we will report on density limits, disruption behaviour, wall pumping, hydrogen isotope retention, and the power handling capability of the beryllium limiter in the present design. Examples of improved plasma performance will be given.

KEYWORDS

Beryllium; limiter; wall; impurities; wall pumping; hydrogen retention; density limit; disruptions.

INTRODUCTION

The use of beryllium in JET was proposed already during the design phase (Rebut, 1975). From the start of machine operation in 1983 studies were initiated by JET to assess beryllium as an alternative to graphite, the limiter material selected initially. These studies comprised of the investigation of beryllium limiters for the tokamaks ISX-B (Mioduszewski *et. al.*, 1986) and UNITOR (Hackmann and Uhlenbusch, 1984; Bessenrodt-Weberpals et. al., 1989), as well as the evaluation of single processes, i.e. measurements of sputtering yields (Bodhansky *et. al.*, 1985) and hydrogen retention (Möller *et. al.*, 1986; Causey *et. al.*, 1990).

In tokamak experiments it was found that beryllium is a well suited material for limiters which facilitates the conditioning of the respective machine, reduces the oxygen content of the plasma by gettering and allows for increased density limits. Thermal overloading of the beryllium limiters leads to surface melting which results in increased beryllium content of the plasma even then when the power to the limiters is reduced to values below the threshold for melting. This is due to hot spots at protrusions on the surface which were generated during the melting phase.

The investigation of single processes showed that beryllium has a sputtering yield comparable to that of graphite at ambient temperature, but which in contrast to graphite, is only moderately temperature dependent until evaporation becomes the main release process. At 600 K its long term hydrogen retention is by about a factor of three lower than the one for graphite. The mechanism for hydrogen pumping is comparable to that of a metal which dissolves hydrogen and does not form hydrides.

These results were analysed (Rebut *et. al.*, 1985; Hugon *et. al.*, 1989) and it was

expected that due to the lower nuclear charge of beryllium compared to graphite the plasma should contain more deuterons for a given impurity concentration. Unless hot spots become dominant, the beryllium concentration should be less than that for carbon because in contrast to graphite, beryllium does not show chemical erosion (hydride formation), radiation induced sputtering or for perpendicular incidence self-sputtering yields above unity. Beryllium is a getter for oxygen and therefore the oxygen content of the plasma and the sputtering by oxygen will be decreased. This will lead to reduced impurity contents and, based on the model which relates the maximum obtainable density to the radiation outside the q = 2 surface, to increased density limits.

Areas of concern remain the angular dependence of the self-sputtering rate for beryllium and the risk of thermally overloading the limiter surface. For the same surface temperature beryllium can take about 1.7 times the load of graphite but overloading, which never can be avoided, will inevitably result in surface melting whereas graphite only experiences increased erosion. On the other hand the maximum permitted surface temperatures for graphite and beryllium are similar. It was shown by theoretical analysis (Hugon *et. al.*, 1989) that 1300 K should not be exceeded for beryllium (evaporation limit) and for graphite the surface temperature should remain below 1500 K to avoid the carbon bloom by enhanced self-sputtering. That was confirmed for graphite surfaces during discharges in JET (Summers *et. al.*, 1990). The apparent sputtering yield of graphite rises from 5% for temperatures of 1300 K to unity for 1700 K. This can be understood in terms of self-sputtering and/or radiation enhanced sublimation. This result excludes graphite as a material for high heat flux components in case surface temperatures would exceed 1700 K.

EVALUATION OF BERYLLIUM AS WALL AND LIMITER MATERIAL

Preparation

In parallel to the experimental investigations into the properties of beryllium with respect to its behaviour in the presence of tokamak plasmas, designs were carried through to introduce into JET a beryllium limiter and at the same time to cover the internal surfaces by a thin evaporated beryllium layer.

The switch of the limiter material from graphite to beryllium was planned to be implemented in connection with the belt limiter which was designed to allow for an easy exchange of materials (Celentano *et. al.*, 1986). The limiter material is inserted in form of tiles between cooling fins which are welded to the water-cooled support structure. The tiles are 380 mm long and 75 mm deep, they have a width of 20 mm (beryllium) and 26 mm (graphite). They face the plasma with their narrow side. Any two plates are assembled into one unit. Each unit is held by disk springs which are located in slots in the fins. The tile pairs are aligned to each other to an accuracy better than 0.3 mm before more serious misalignment may have occurred

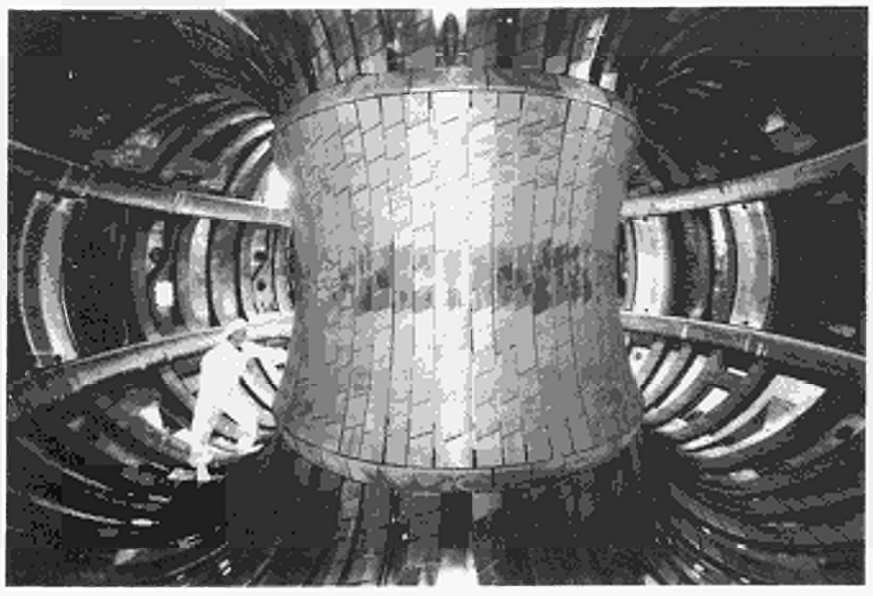

Fig. 1. The inside of the vacuum vessel

due to movements during pumping down of the vacuum vessel, during baking to the operation temperature of 300 C or during plasma operation. The plasma facing surface of the beryllium tiles is slotted every 20 mm to minimize the effect of thermal stresses.

The beryllium evaporators (Sonnenberg *et. al.*, 1986) consist of a hollow beryllium cylinder (mass 3 kg) which is closed at one end and supported by a carbon fibre tube. Inside there is a spirally wound carbon-fibre heater which can be electrically heated to 2400 C. Four such evaporators can be inserted into the vessel by 300 mm for evaporation and retracted again for pulse operation.

Operation with beryllium

Dilution of the JET plasma by low-Z impurities and the absence of proper density control were the main limitations to the performance during the use of graphite as limiter and wall material. The massive graphite elements in the vessel as shown in Fig. 1 were the tiles for the belt limiter, the inner wall protection, the X-point and the RF-antennae side protection. The rest of the vessel was carbonized including the screens for the RF-antennae.

Three phases were foreseen for the evaluation of beryllium. The carbon phase saw the operation of JET as a graphite machine in the configuration described above to establish reference discharges. The carbon/beryllium phase was characterized by beryllium evaporation. Twenty-six evaporations were made and 240 g of beryllium were deposited. Discharges on the inner wall, the X-point protection tiles and the belt limiter were carried out during this phase. The area in contact with the plasma was graphite covered with only a thin beryllium layer of about 100-300 Å thickness. The beryllium phase started after the exchange of the belt limiter material against beryllium. In addition evaporation was still carried out. Only the discharges run on the belt limiter can be considered to be made in a beryllium environment, the X-point discharges during the beryllium phase were still run on beryllium covered graphite.

Impurity behaviour

The impurity behaviour is discussed in detail by Hawkes *et. al.*, (1989) and by Thomas (1990). With carbon limiters and walls, after prolonged operation and glow discharge conditioning in helium, Zeff values between 2 and 3 can be obtained for

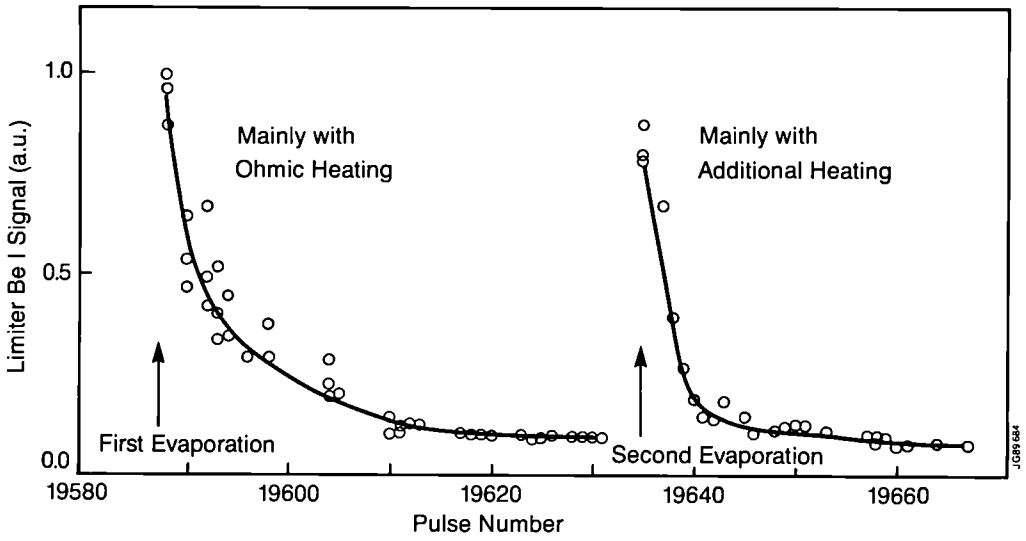

Fig. 2. Erosion of evaporated beryllium layers with pulse number

moderate plasma currents and low densities (3 MA, 1 - 2 x $10^{19}m^{-3}$). After tokamak discharge conditioning in helium slightly lower values can be achieved. The main impurities are carbon with typical concentrations of 5%, oxygen with 0.5 - 1%, and nickel with 0.01 - 0.1%.
With the start of the beryllium/carbon phase Z_{eff} decreased to 1.5 - 2, mainly due

to the reduction of carbon in the plasma to about 2%. The oxygen content is reduced by a factor of about ten and its contribution to Z_{eff} becomes negligible. This behaviour can be explained by oxygen gettering and the resulting decrease of carbon sputtering by oxygen. Nevertheless carbon remains the dominant impurity. Beryllium concentrations reach ~ 3% immediately after evaporation but fall rapidly to about 0.5% after a few discharges.

The apparent lifetime of the evaporated beryllium layer, derived from the decrease of the beryllium flux from the limiter, was short as shown in Fig. 2. This decrease is especially fast for discharges with additional heating were the beryllium flux is halved after about four discharges. The reduction in Z_{eff} together with the reduced content of oxygen and carbon do not depend on the surface coverage with beryllium of the components in contact with the plasma and remain unchanged over tens of discharges.

It was found that a small deuterium puff (~50 mbarl) during high power heating could reduce substantially the plasma contamination. Consequently Z_{eff} depends now to a large degree on the method of setting up the discharge and can be strongly influenced by gas influx. Figure 3 shows a comparison of discharges with and without that additional gas influx.

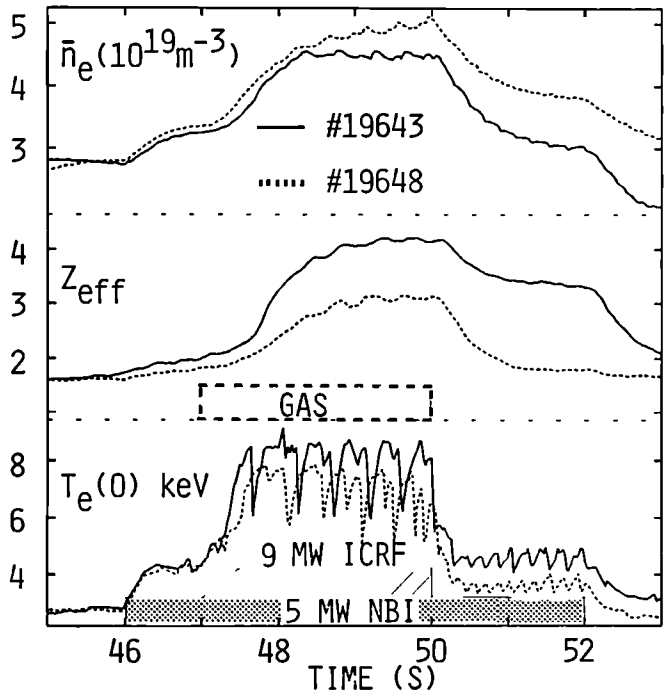

Fig. 3. Evolution of average electron density, effective charge and central electron temperature with and without additional gas injection

The impurity reduction could be achieved with affecting only marginally the central electron temperature or density and in addition the total neutron yield increases during the discharge with the additional gas feed. This behaviour is discussed in detail by Gondhalekar *et. al.*, (1990). It is observed that the additional gasflow into the edge increases the deuterium flux from the limiter into the plasma whereas the beryllium flux from the limiter remains unchanged. The concentration and accordingly the impurity content (mainly carbon) in the plasma is however reduced. This behaviour cannot be explained by the impurity screening model (G. M. McCracken *et.al.*, 1985). As an alternative it has to be assumed that the global particle confinement time has decreased. The central electron temperature did only change marginally with the gas puff indicating that the energy confinement time did not change substantially in contrast to the particle confinement time which is reduced by about 50%.

During the operation with the beryllium limiter beryllium became the dominant impurity, with carbon and oxygen both contributing negligibly to Z_{eff} or radiation. For low level additional heating (2 MW neutral beam, 2 MW RF) the radiated power

was below 20% with nickel from the RF-antennae screens radiating about half of this value. Discharges with more than 10 MW input power lead to hot spots on the limiter and to a severe increase of beryllium influxes. It was found, similar to the operation with beryllium gettering, that a gas puff of a few 100 mbarl during the additional heating period reduces Z_{eff} to values of about 1.5 and this even with heating powers of up to 30 MW for several seconds.

The Z_{eff} values of 1.5 achieved with an additional gas pulse at heating powers of up to 30 MW are comparable to the best ones ever obtained for a well conditioned graphite limiter for ohmic discharges. For the graphite limiter scenarios using high edge fuelling rates could not be employed due to the insufficient wall pumping and lower density limit.

The variation of the effective charge for ohmic discharges as function of density is shown in Fig. 4 for the different phases including the results obtained in 1988 with a well conditioned graphite machine.

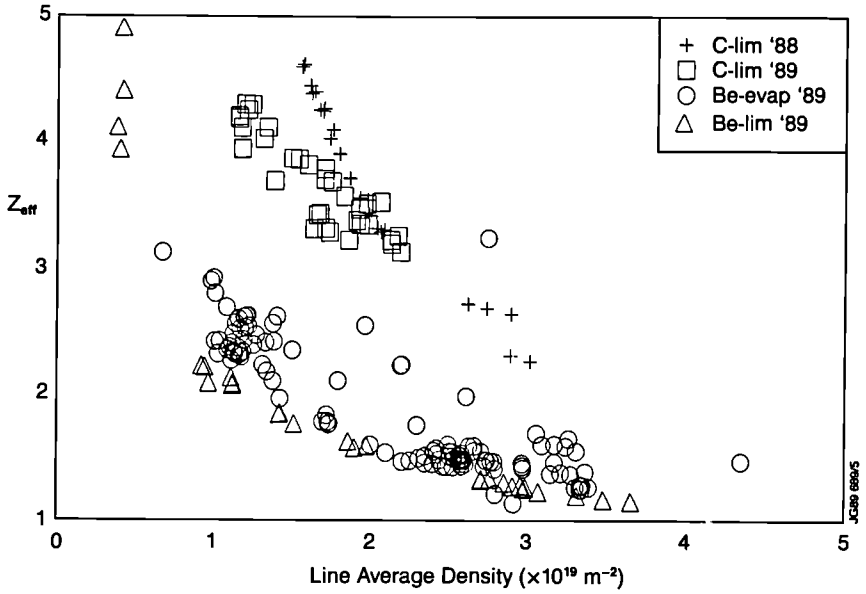

Fig. 4. Effective charge as function of density for ohmic discharges

With the reduction of the effective charge and the increased plasma purity the number of deuterons on the axis has increased for a given electron density. For $n_D(0)$ as the number of deuterons and $n_e(0)$ the number of electrons on the axis the dilution D becomes

$$D = n_{D}(0)/n_e(0) \qquad (1)$$

For additionally heated discharges the dilution changed from 0.5 - 0.6 during the carbon phase to 0.8 to 0.9 during the beryllium phase. Table 1 summarizes the main impurities and the corresponding dilution.

Table 1. Typical impurity content and dilution for the various operation phases in ohmic discharges

	C-Phase	C/Be-Phase		Be-Phase
		Limiter	X-Point	Limiter
Carbon (%)	5	3	1.5	0.5
Oxygen (%)	1	0.05	0.05	0.05
Beryllium (%)	-	1	1	3
Dilution	0.6	0.8	0.9	0.85

The dilution as well as the Z_{eff} values depend strongly on the power per particle. For heating powers in excess of 4 MW the Z_{eff} values and the dilution are given for the three operation phases in Fig. 5 and Fig. 6 as a function of the power per particle. For high power discharges the values were taken before the influx of impurities terminated high performance phases e.g. before the carbon bloom or high beryllium influx occurred. The points which are shown are points of existence which lie in three distinctive separate areas which represent the carbon, the C/Be and the Be phase. For the limiting cases, to stay e.g. below Z_{eff} = 1.5, the power per particle in the Be phase can be about a factor of 2.5 higher than in the C/Be phase and a factor 4 higher compared to the carbon phase. Similarly for the dilution, to stay above values of 0.8, the maximum tolerable power per particle relates as 1 : 1.5 : 2.5 with the Be phase again allowing for the highest powers.

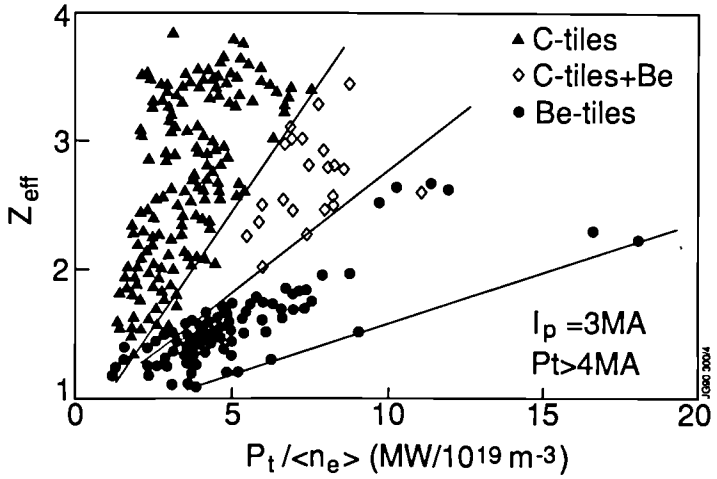

Fig. 5. Z_{eff} as function of power per particle

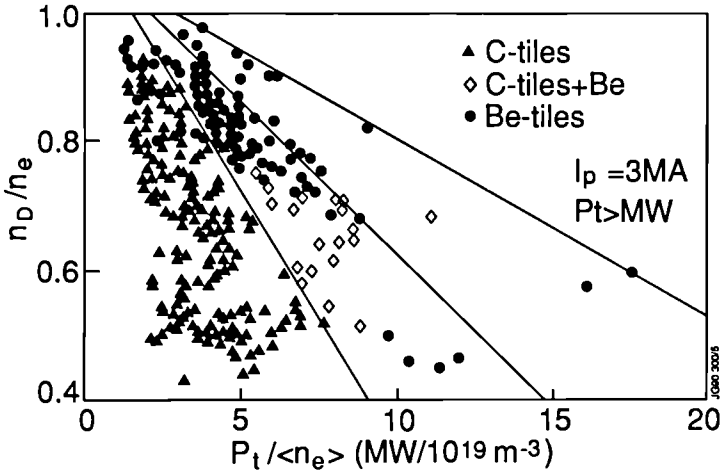

Fig. 6. Dilution as function of power per particle

Density limit and disruptions

In a carbon vessel the density limit occurs as a radiation limit. It is invariably a disruption limit. When during increasing the density the radiated power becomes comparable with the input power, the plasma edge cools and the plasma detaches itself from the limiter. An m = 2 instability grows which is destabilised by the radiative contraction of the temperature and current profiles (Wesson *et. al.*, 1986) and the plasma disrupts after times which can be as long as 1000 ms .This behaviour changed completely during the beryllium phase (Lowry *et. al.*,1990) as shown in Fig. 7 for an ohmic discharge for the beryllium limiter. As soon as the radiated power reaches about 50% of the input an asymmetric radiating structure, a Marfe, appears and after a short time time the radiated power increases well above

the ohmic input in form of a short spike. Excess density is simultaneously ejected and the plasma recovers. By continued fuelling this behaviour can be repeated several times. Instead of a disruptive density limit a soft 'Marfing' limit is obtained. The decrease in density at the end of the pulse coincidences with the ramping down of the plasma current which is normally accompanied with a density pump-out.

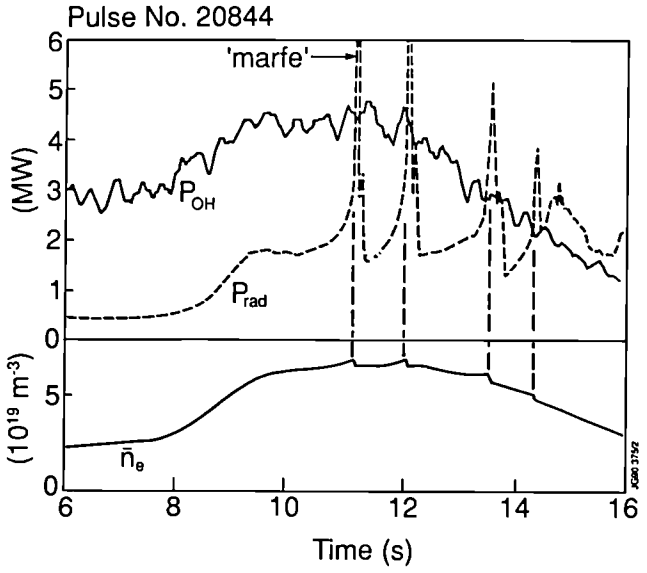

Fig. 7. Density development during an ohmic discharge with the beryllium limiter

The density limits in ohmic plasmas for a carbonized or beryllium gettered vessel are very similar despite lower impurity and radiation levels in the latter case. In ohmic plasmas with a beryllium limiter the density limit (marfing limit) inreased by a factor of about two and approached the density limit for neutral injection in a graphite vessel. The density limit for RF-heating was in the carbon phase only marginally larger than the ohmic limit. It is now identical with the neutral beam

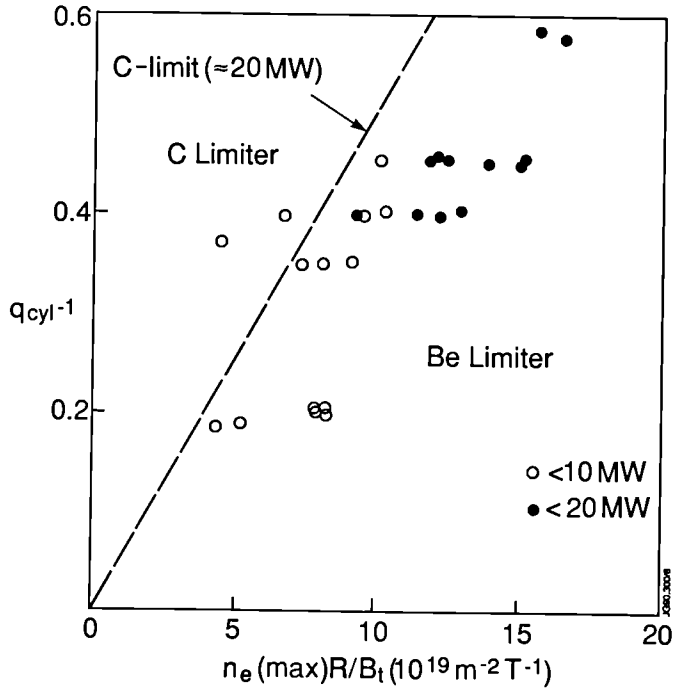

Fig. 8. Hugill diagram of operation with carbon and beryllium limiter

limit which is by about a factor of two higher. This behaviour is shown in Fig. 8 for discharges with the graphite and the beryllium limiter.

The density limit for the berylliated vessel or for the beryllium limiter depends on the power input and scales as the square root of the input power as shown in Fig. 9 for different heating methods. A better fit is obtained when for the Murakami parameter the edge density is used instead of the average density. For input powers of 10 - 20 MW a maximum value of about 33 x 10^{19} m^{-2} T^{-1} was obtained for the product of the Murakami parameter and the safety factor.

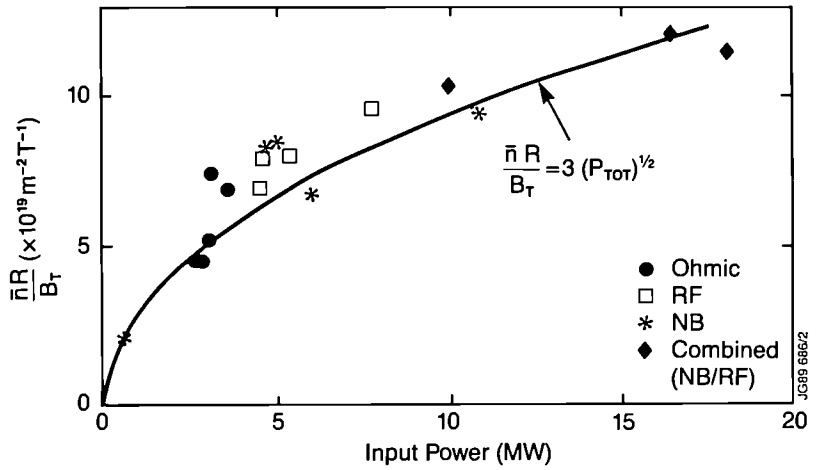

Fig. 9. Murakami parameter as function of input power during the beryllium phase for different heating methods at q_{cyl} = 2.5 and gas fuelling

The density profiles obtained during the experimental investigation of the density limit are generally flat or even hollow for high gas feed rates. Peaked profiles can be obtained for pellet fuelling, the highest central density which could be sustained was ne ~ 4 x 10^{20} m^{-3}.

Wall pumping and tritium retention

Graphite walls show hydrogen pumping during discharges (Sonnenberg *et. al.*, 1986; Ehrenberg *et. al.*, 1989). For a few seconds particle removal rates of up to a few $10^{20}s^{-1}$ can be obtained and even more after conditioning of the walls with tokamak discharges in helium. For beryllium the wall pumping can be more than one order of magnitude larger than for graphite. The mechanism appears to be the pumping of hydrogen atoms by metal walls (Ehrenberg *et. al.*, 1990; Saibene *et. al.*, 1990; Pick *et. al.*, 1985; Waelbroeck *et. al.*, 1979). With beryllium surfaces it is now possible for the first time to control the plasma density in such a way that starting from $10^{20}m^{-3}$ the density can be ramped down to $10^{19}m^{-3}$ within a few seconds.

Due to beryllium behaving as any metallic wall material, the vacuum vessel is no longer deconditioned after a high current disruption, therefore the number of useful discharges could be considerably increased.

One measure for the pumping capability of the wall is the characteristic time for deuterium pump out during a discharge after the gas supply is switched off. Typical times range from about 20 s for an unconditioned graphite machine to few seconds for a conditioned beryllium limiter. Figure 10 shows these times for the wall materials used and for different conditioning methods.

To obtain the same plasma density with beryllium as with graphite walls it is required to inject up to three times as many particles into the plasma. Therefore an area of concern is the retention of pumped hydrogen isotopes in the wall. Gas balance experiments (Sartori *et. al.*, 1990) indicate that for graphite limiters about 60% of the deuterium required to fuel the discharge is retained in the vessel, compared with about 10 - 20% for the beryllium limiter or beryllium

evaporation. Taking into account the larger amount of gas which has to be used to obtain similar densities for discharges with the graphite or the beryllium limiter, the total retention (number of particles) is about equal in both cases. From these measurements it can be concluded that for 100 high density, full power discharges during the D-T operation in JET up to 3 g of tritium can be trapped in the walls. This does not pose a problem with the tritium inventory.

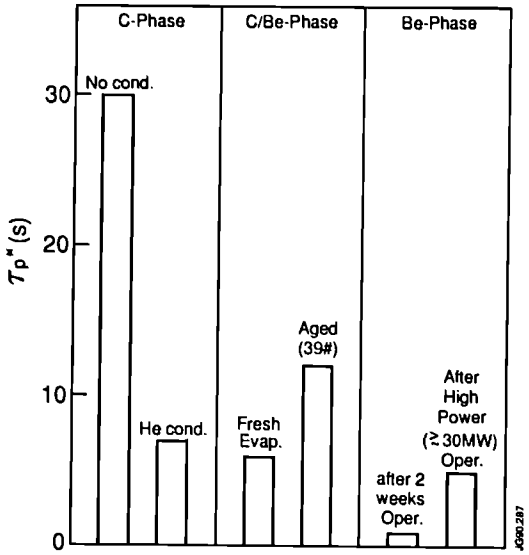

Fig. 10. Density pump out times for the different wall materials

Power handling capability

The maximum energy which can be accommodated by the high heat flux components in JET is higher than that corresponding to maximum heating power and typical maximum pulselength for which useful discharges can be sustained. The inner wall is able to survive loads of up to 400 MJ whereas useful plasmas could only be produced for a maximum of 17 MJ. At higher loads the plasma became contaminated by carbon to such an extent that with a dilution n_D/n_e of 0.7 at the start of the additional heating virtually no deuterium was retained in the plasma ($n_D/n_e \sim 0$) after about one second (carbon bloom). This happens as soon as the graphite reaches temperatures in excess of 1200 C when radiation induced sublimation and self sputtering become important.

The high surface temperatures result from misaligning of individual high heat flux components so that power loads are intercepted only by small surface areas. Reducing the deviation from circularity at the inner wall from about 20 mm to 4 mm did not suppress the carbon bloom; there was no substantial change neither in the loads nor in time delay between applying additional heating and the occurrence of the bloom. Operation with the graphite belt showed that for injected energies of 50 MJ the plasma dilution was already 0.5. The maximum injected energy applied was about 120 MJ. Localized surface damage was observed with small cracks developed perpendicular to the tile edges in highly loaded and consequently eroded areas.

The beryllium belt limiter was designed for a peak heat load of 4.8 MWm^{-2} under the assumption that 100% of the injected power is conducted and evenly shared between the upper and lower ring of the belt and that the scrape-off thickness lies in the range from 7.5 to 15 mm. The power handling capability is 40 MW for 10 s and the resulting surface temperature is 1000 C.

It was found during the operation with the belt limiter that even power sharing between the top and bottom ring could not be achieved. Under the best conditions the bottom ring received only 60% of the power conducted to the top one. The observed values for the scrape-off thickness (~ 5mm) were about a factor of two lower than those assumed for the design. That means that whereas for 40 MW of power flowing to the limiter the design value for the peak load is 4.8 MWm^{-2}, the actual loading could be as high as 15 MWm^{-2}.

Operation to date has been with smaller values than 40 MW conducted but the loads applied exceed the design value by a factor of two. Moreover, in contrast to the

graphite limiter, the edges of the beryllium tiles are further apart and chamfered. Due to fieldlines penetrating deeper between two adjacent tiles and their steep angle of incidence on the chamfers the beryllium tiles can receive loads of up to 100 MWm^{-2}. In addition misalignment of tiles due to mechanical inaccuracy leads as well to to increased heat loads as does the fieldripple which is about 2mm at the position of the belt limiter.

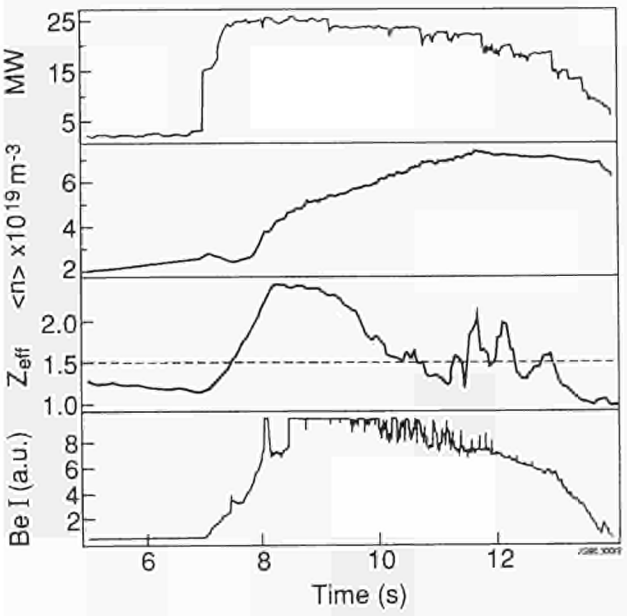

Fig. 11. Scenario for 180 MJ deposition into the torus

For the beryllium belt limiter during ohmic heating there was only moderate heating observed and no hot spots developed. The beryllium influx remained negligible. Discharges with additional heating, typically at I_p = 3 MA with heating powers from 10 MW onwards, led to the appearance of localized hot spots within 0.5 s after applying the power. This is consistent with the assessment of the power loads. Large beryllium influxes were observed. By tailoring the gas feed rates, a new operating regime was found which suppressed the build-up of the beryllium concentration in the plasma and allowed us to to apply up to 180 MJ to the plasma with Zeff values about 1.5 as shown in Fig. 11.

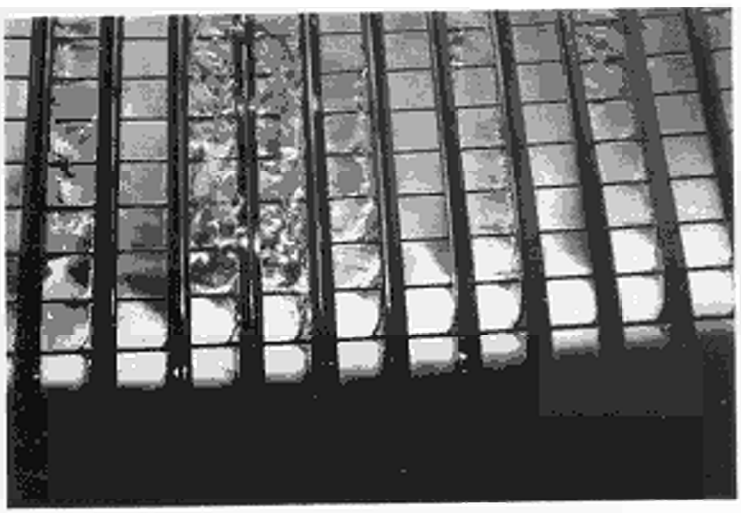

Fig. 12. Surface damage of the beryllium limiter

With increasing additional heating power hot spots were observed regularly and inspection of the tiles after opening of the vessel showed that about 5% of the surface had been melted as shown in Fig. 12, with the damaged areas centred around the minimum in the field ripple. A further 10-15% show signs of melting at the edges and additional 5% show damage due to localized abnormal loads (stress induced cracks). None of the tiles shows deep fissures, none lost substantial material from the surface or suffered any mechanical failure. A detailed description of the different types of defects is given by Deksnis *et. al.*, (1990).

Damage is localized with very severely affected tiles adjacent to those without any marks. There has been no gross mechanical failure on the more than 34000 castellations of the belt limiter. The observed failures relate more to the design features then to material problems. Therefore JET restarted operation in 1990 with essentially the same set of beryllium tiles which were used earlier. One of the aims of the present operation is to assess the behaviour of a surface damaged limiter under high power loads for long duration discharges at many repetitions.

PLASMA PERFORMANCE

The changes in the impurity and recycling behaviour resulted in improved plasma performance. Increased wall pumping allowed us to obtain the hot ion mode on the limiter, reduced radiation to investigate the beta limit, and reduced dilution to increase the fusion power from ^{3}He - D reactions to 100 kW and the fusion parameter for X-point discharges to 8 x 10^{20}m^{-3}keV s.

Hot ion plasmas for belt limiter discharges

For the operation with the carbon limiter the low density, high ion temperature regime is not accessible because of the low deuterium pumping of the limiter. Even tokamak discharge conditioning in helium was not effective to increase the pumping capability. Poor density control and the related difficulties in obtaining low density target plasmas were the consequence. For operation at higher densities, depending on conditioning, dilution ranges from 0.4 - 0.8, typical values are 0.5. Maximum Q_{DD} values of 5 x 10^{-4} were obtained.

With beryllium evaporated on the graphite belt limiter deuterium pumping becomes sufficiently strong for operation at low electron densities (~ 10^{19} m^{-3}). High power per particle was achieved and consequently high ion temperatures were obtained (T.T.C. Jones *et. al.*, 1990). The carbon influx from the belt limiter gives n_D/n_e of about 0.6, the Q_{DD} values increased to ~ 6.5 x 10^{-4}.

The plasmas using the beryllium limiter behaved similarly to those with beryllium evaporation with respect to power per particle, ion temperature and dilution. The density profiles were however, flat in contrast to those obtained earlier with the graphite limiter or beryllium evaporation. Pellet fuelled target plasmas resulted in peaked profile hot ion discharges. The maximum fusion yield in peaked discharges was Q_{DD}~ 9 x 10^{-4}. The neutron yield increased applying RF power. In many cases the neutron output was reduced after the influx of beryllium. Table 2 summarizes the maximum obtained power per particle and the resulting dilution and Q_{DD}-values for the operation with the belt limiter.

Table 2. Dilution and Q_{DD} for limiter discharges

	Power per particle (10^{-19}MW m^{-3})	Dilution	Q_{DD} (10^{-4})
Graphite	9	0.5	5.0
Graphite plus Be evaporation	14	0.6	6.5
Beryllium Gas or NI fuelled	20	0.6	7.7
Beryllium Pellet fuelled	20	0.6	9.0

Alpha particle simulation

For the full utilisation of α-particle heating in a reactor it is necessary that the slowing down time of the α-particles is shorter than their confinement time. To study their transport α-particles were simulated by using the nuclear reaction $^3He + D \rightarrow {}^4He(3.6\ MeV) + p(14.7\ MeV)$. That was made possible by heating ^3He minority ions with ICRH in a deuterium background (Start *et. al.*, 1990). The parameters for the energetic helium ions produced by the ICRH are very similar to those expected from DT fusion reactions in JET or NET. The main difference is the ratio of parallel to perpendicular pressure, which is very anisotropic for the RF driven minority.

The experiments were carried out during Monster sawtooth discharges with plasma currents ranging from 2 to 5 MA, toraidal fields from 2 to 3.4 T, densities on axis from 2 to 6 x 10^{19} m^{-3}, and central electron temperatures from 4 to 12 keV. On axis RF-heating at powers below 14 MW was used.

Previous experiments were carried out with carbon walls and limiters. The resulting maximum fusion power which could be obtained from the D - ^3He reaction was 60 kW. This power was limited by severe carbon influx. The dilution was 0.4. This problem could be eliminated by using beryllium evaporation. As a consequence of the higher plasma purity ($n_D/n_e \sim 0.7$) the reactivity increased and fusion powers of up to 100 kW were obtained. It was found that the α-particles slow down classically as predicted theoretically. Therefore it can be expected with confidence that efficient α-particle heating will occur in DT-burning tokamaks.

The beta limit

For thermal plasmas the maximum obtainable beta value is limited by MHD phenomena i.e. either by resistive kinks (Troyon-Gruber limit) or by ballooning modes. Under certain conditions the the ballooning limit may be higher by about 50%. Earlier experiments to investigate the beta limit in JET suffered from carbon influx and high dilution and the peaked density profiles became unstable at about 40% of the Troyon limit.

After beryllium evaporation the dilution was reduced and flat density profiles were obtained with neutral beam heating. The beta limit could be reached for double null X-point discharges with low toroidal fields (B ~ 1.2 T) during the H-mode phase (Smeulders *et. al.*, 1990). The required power to reach the beta limit was about 10 MW of neutral injection.

The beta limit in JET is a soft limit and follows the Troyon-Gruber relationship. It is characterised by beta-clipping, i.e. without becoming unstable a relaxation in mainly temperature occurs periodically whilst trying to exceed the limit. The maximum beta-values obtained were between 5 and 6% in good agreement with the prediction for JET performance.

H-mode with RF only

For a long time it appeared to be impossible to generate H-modes by ICRH alone, especially with the RF antennae at the low field side. With beryllium evaporation onto the nickel screen of the RF-antennae and dipole phasing it could finally be shown that it is possible to obtain H-modes with RF only (Bhatnagar *et. al.*,1990). That was a considerable change from the previous behaviour when for example the application of ICRH to neutral beam generated H-modes terminated them. This was caused by strong impurity influxes from the antenna screens. With advances in the antenna phasing the coupling could be improved and ICRH could be applied to neutral beam generated H-modes. There was however no improvement observed in the plasma behaviour. The radiated power was enhanced due to an increase of oxygen and nickel impurities with applying the RF power. The nickel was released from the antenna screens due to sputtering in the RF-rectified sheath in front of the antenna.

After beryllium gettering in the vessel and with an evaporated beryllium layer on the screens the impurity release during RF heating was considerably reduced due to decreased edge density. With this improvement and the simultaneous use of dipole phasing for the antennae, RF only H-modes of up to 1.5 s duration were obtained at power levels of up to 12 MW. Threshold power, edge behaviour and confinement is similar to H-modes obtained with neutral beams only. Energy confinement times are

similar to NBI cases and reach two times Goldston L-mode scaling. Figure 13 shows a time trace for a typical RF H-mode shot were the signature of the transition from L to H-mode can be clearly seen in the D_α and density traces.

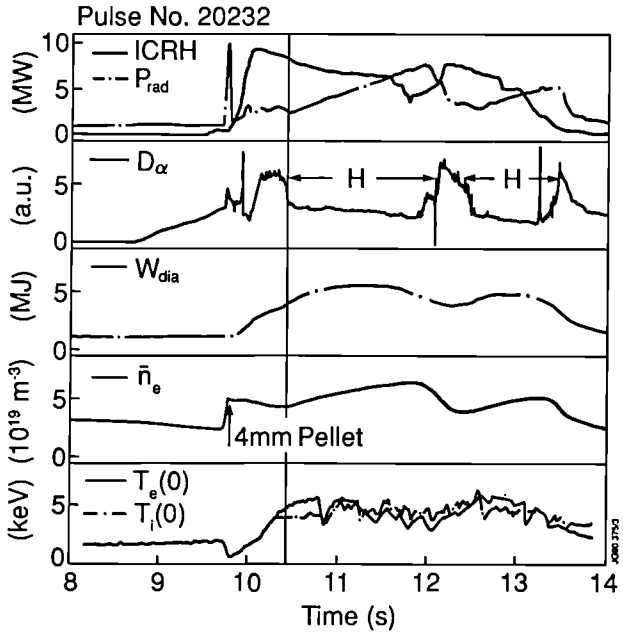

Fig. 13. Time traces for a RF only H-mode

Maximum fusion performance

Improvements in the fusion parameter $n_D \tau_E T_i$ were obtained in X-point discharges by using the techniques of beryllium evaporation to reduce the dilution, 140 keV beams (6 MW at 140 keV and 11 MW at 80 keV) to achieve deeper penetration and X-point radial and vertical sweeping to reduce the temperature of the target tiles and therefore to delay the carbon bloom.

For double null X-point discharges at 4 MA and a toroidal field of 2.8 Tesla the best conditions were obtained (Tanga *et. al.*, 1989; Harbour *et. al.*, 1989). The density on axis reached 4 x 10^{19} m^{-3}, the central electron temperature 8.6 keV at

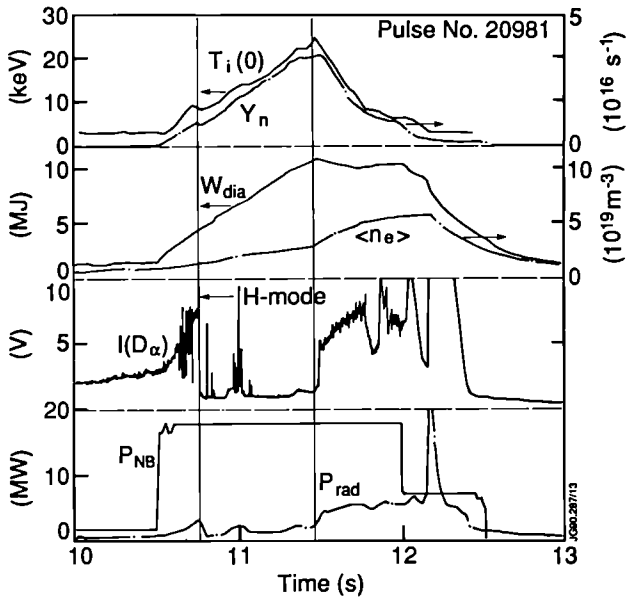

Fig. 14. Time trace for a maximum performance discharge

Zeff values of 1.4. The dilution at the maximum neutron output was ~ 0.9 and with the strong wall pumping in the resulting low density plasmas ion temperatures reached 22 keV. The confinement time (τ_E~ 1.1 s) did not change compared with previous operation with graphite. Neutron yields reached values of 3.5 x 10^{16} s^{-1} corresponding to Q_{DD} ~ 2 x 10^{-3}; the fusion parameter is increased to values exceeding 8 x 10^{20} m^{-3} keV s and the resulting equivalent fusion power would reach 12 MW for 18 MW of additional heating. The best conditions were only obtained transiently (~ 0.1 s), the carbon influx terminated the good performance. An example for a high performance H-mode discharge is given in Fig. 14.

SUMMARY AND CONCLUSIONS

From the experiments carried out during the beryllium assessment we can conclude that both, higher plasma purity levels and higher density operation can be achieved with beryllium limiters in comparison with graphite ones. These improvements result mainly from the elimination of oxygen and the strong wall pumping capability of beryllium. Good use was made of the widened operation regime: low density high ion temperature discharges on the limiter were possible, beta limits could be explored and RF only H-modes were obtained.

Despite very accurate alignment of the belt limiter hot spots and local melting of the limiter surface was found. Consequently plasma facing components have to be designed in such a way that alignment is not critical and that the heat load is distributed evenly.

The H-mode performance was considerably improved compared to earlier experiments, however this mode of operation was prevented from reaching its full potential by a strong influx of carbon after one second after the commencement of the high power heating. Calculations show that an equivalent Q_{DT}-value above unity would have been achieved by delaying the carbon bloom by another second. Steps are being undertaken to improve the performance. For the 1990 operation the carbon tiles on the lower X-point target plates and the nickel antenna screens are replaced with beryllium. Later the X-point target plates will be watercooled and better aligned than presently and disruption feedback coils will be installed to stabilize m=2, n=1 modes. Furthermore it is proposed to install early in 1992 a pumped divertor with the aim to study particle and power exhaust and impurity transport with power and particle loads similar to those expected in the next generation of tokamaks.

REFERENCES

Bessenrodt-Weberpals, M., J. Hackmann, C. Nieswand and J.Uhlenbusch (1989). The effect of beryllium limiters on the tokamak plasma of UNITOR. *J. Nucl. Mat.* 162-164, 435-438

Bhatnagar, V. P., M. Bures, D. Campbell, S. Clement, A. Hatayama, J. Jaquinot, D. F. H. Start, D. Stork, A. Tanga, F. Tibone and B. J. D. Tubbing (1990). ICRH produced H-modes in the JET tokamak. *Proc. 17th EPS Conference on Contr. Fusion and Plasma Heating in Europhysics Conference Abstracts* (K Bethge, ed.) 14 B, 255 - 258

Bohdansky J., J. Roth and W. Ottenberger (1985). Sputtering measurements of beryllium. *IPP-JET* Report No. 31

Causey, R. A., J. M. Beeston, G. R. Longhurst and L. G. Miller (1990). Tritium retention and migration in beryllium. Proc. 9th Int. Conf. Plasma Surface *Interactions in Contr. Fusion Devices, Bournemouth, UK.* In publication

Celentano, G., E. Deksnis, R. Shaw, K. Sonnenberg and J. Booth (1986). The JET belt limiter. *Proc. 14th Symp. Fusion Technology* 1, 581-587

Deksnis E., A. Cheetham, A. Hwang, P. Lomas, M. Pick and D. D. R. Summers (1990). Damage to JET beryllium tiles. Proc. 9th Int. Conf. on Plasma Surface *Interactions in Contr. Fusion Devices, Bournemouth, UK.* In publication

Ehrenberg, J., P. Coad, L. de Kock, S. K. Erents, A. Gondhalekar, D. Godall, J. Hancock, P. Harbour, T. T. C. Jones, G. McCracken, P. Morgan, C. Nicholsen, G. Neil, J. O'Rourke, J. Partridge, M. Pick, J. Simpson, K. Sonnenberg, A. Stevens, M. Stamp, P. Stott, D. Summers, T. Tagle and J. Vince (1989). Hydrogen and helium recycling in tokamaks with carbon walls. *J.Nucl. Mat.* 162-164, 63-79

Ehrenberg, J., V. Philipps, L. de Kock, R. Causey and W. Hsu (1990). Analysis of deuterium recycling in JET under beryllium first wall conditions. *Proc. 9th Int. Conf. Plasma Surface Interactions in Contr. Fusion Devices, Bournemouth, UK.* In publication

Gondhalekar, A., A. Cheetham, S. K. Erents, N. Gottardi, P. D. Morgan, J. O'Rourke,

D. Pasini, M. F. Stamp, P. R. Thomas and M. von Hellermann (1990). Impurity control in JET using fuelling. *Proc. 9th Int. Conf. Plasma Surface Interactions in Contr. Fusion Devices, Bournemouth, UK* . In publication

Hackmann, J. and J. Uhlenbusch (1984). Experimental study of the compatibility of beryllium limiters with a tokamak plasma. *Nuclear Fusion* 24, 640-642

Harbour, P. J., K. D. Lawson, P. D. Morgan, R. Reichle, M. F. Stamp, D. D. R. Summers, J. Ehrenberg, S. K. Erents, N. Gottardi, G. Haas, M. von Hellermann, M. F. Johnson, M. Keilhacker, L. de Kock, E. Lazzaro, K. Mast, D. Stork, J. A. Tagle, A. Tanga and B. Tubbing (1989). Analysis of the effect of beryllium gettering on X-point plasmas. *JET-P(89)80,* 57-70

Hawkes, N., R. Barnsley, R. Gianella, M. von Hellermann, K. Lawson, F. Mompean, P. Morgan, N. Peacock, M. Stamp, P. Thomas and H. Weisen (1989). Impurity behaviour in JET following beryllium evaporation. *JET-P((89)80,* 23-28

Hugon, M., P. P. Lallia and P. H. Rebut (1989). A comparison between beryllium and graphite as materials for JET limiters and walls. *JET-R(89)14*

Jones, T. T. C., P. J. Lomas, S. Attenberger, J. P. Christiansen, G. A. Cottrell, R. Gianella, L. de Kock, P. Kupschus, G. McCracken, C. G. Lowry, P. Nielsen, D. Pasini, R. Prentice, G. Sadler, M. F. Stamp, D. D. R. Summers and M. von Hellermann (1990). The fusion performance of JET limiter plasmas using Be coated graphite and solid Be surfaces. *Proc. 17th EPS Conference on Contr. Fusion and Plasma Heating in Europhysics Conference Abstracts* (K Bethge, ed.) 14 B, 9 - 12

Lowry, C. G., D. J. Campbell, N. Gottardi, K. Lawson, and G. Vlases (1990). Density limits in JET with beryllium. *Proc. 17th EPS Conference on Contr. Fusion and Plasma Heating in Europhysics Conference Abstracts* (K Bethge, ed.) 14 B, 339 - 342

McCracken, G. M. and P. C. Stangeby (1985). The interpretation of plasma edge conditions in tokamaks. P*lasma Phys. Contr. Fusion* 27, 1411-1425

Mioduszewski, P. K., P. H. Edmonds, C. E. Bush, A. Carnevali, R. E. Clausing, T. B. Cook, L. C. Emerson, A. C. England, W. A. Gabbard, L. Heatherly, D. P. Hutchinson, R. C. Isler, R. R. Kindsfather, P.W. King, R. A. Langley, E. A. Lazarus, C. H. Ma, M. Murakami, G. H. Neilson, J. B. Roberto, J. E. Simpkins, C. E. Thomas, A. J. Wootton, K. Yokoyama, R. A. Zuhr, K. H. Behringer, K. J. Dietz, E. Källne, P. J. Lomas, P. D. Morgan, P.E. Stott, A. Tanga, K. H. Sonnenberg, M. F. Smith, J. Watkins, R. D. Watson, J. B. Whitley, D. H. J. Goodall, N. J. Peacock, R. Clayton, J. von Seggern and K. G. Tschersich (1986). The beryllium limiter experiment in ISX-B. *Nuclear fusion,* 26, 1171-1192

Möller, W., B. M. U. Scherzer and J. Bohdanski (1986). Retention and release of deuterium implanted into beryllium. *IPP-JET Report No. 26*

Pick, M. A. and K. Sonnenberg (1985). A model for atomic hydrogen-metal interaction and application to recycling,recombination and permeation. *J. Nucl. Mat* 131, 208-220

Rebut, P. H. (1975). The JET Project, *EUR-JET-R5*

Rebut, P. H., M. Hugon, S. J. Booth, J. R. Dean, K. J. Dietz, K. Sonnenberg and M. L. Watkins (1985). Low-Z material for limiters and wall surfaces in JET: Beryllium and carbon. *JET-R(85)03*

Saibene, G., R. Sartori, A. Tanga, A. Peacock and M. Pick 1990. Hydrogen recycling coefficient in beryllium: experimental determination and test simulation of the density evolution in a JET plasma discharge. *Proc. 9th Int. Conf. Plasma Surface Interactions in Contr. Fusion Devices, Bournemouth, UK.* In publication

Sartori, R., G. Saibene, D. J. H. Godall, E. Usselmann and P. Coad (1990). Deuterium release measurements in the beryllium phase of JET and determination of the tritium content in the exhaust gas. *Proc. 9th Int. Conf. Plasma Surface Interactions in Contr. Fusion Devices, Bournemouth, UK,* in publication

Smeulders P., J. M. Adams, B. Balet, D. Campbell, A. Cheetham, S. Corti, A. Edwards, N. Gottardi, C. Gowers, T. C. Hender, G. Huysmans, J. Jaquinot, E. Joffrin, O. Kwon, E. Lazzaro, F. B. Marcus, P. Morgan, F. Nave, P. Nielsen, D. O'Brien, J. O'Rourke, F. Porcelli, L. Porte, G. Sadler, G. Sips, D. Start, A. Tanga, D. Ward and H. Weisen (1990). High beta regimes in JET. *Proc. 17th EPS Conference on Contr.Fusion and Plasma Heating in Europhysics Conference Abstracts* (K Bethge, ed.) 14 B, 323 - 326

Sonnenberg, K., K. J. Dietz and P. Kupschus (1986). Wall concepts and density control in JET. *Proc.14th Symp. Fusion Technology* 1, 273-285

Start, D. F. H., V. P. Bhatnagar, M. Bures, D. J. Campbell, J. P. Christiansen, J. G. Cordey, W. G. F. Core, G. A. Cottrell, L. G. Eriksson, T. Hellsten, J. Jaquinot, O. N. Jarvis, P. Lallia, P. J. Lomas, C. G. Lowry, P. Nielsen, J. O'Rourke, F. Rimini, G. Sadler, A. Tanga, P. R. Thomas, K. Thomsen, B. Tubbing, P. van Belle and J. A. Wesson (1990). 3He-D fusion studies and a-particle simulations using MeV ions created by ICRH in the JET tokamak. *Proc. 17th EPS Conference on Contr.Fusion and Plasma Heating in Europhysics Conference*

Abstracts (K Bethge, ed.) 14 B, 1015 - 1018

Summers, D. D. R., S. K. Erents, M. Hugon, A. Hwang, R. Reichle, M. F. Stamp and P. C. Stangeby (1990). Measurements of the temperature dependence of carbon and beryllium fluxes in the JET boundary using a high heat flux probe. *Proc. 9th Int. Conf. Plasma Surface Interactions in Contr. Fusion Devices, Bournemouth. UK. In publication*

Tanga, A., D. V. Bartlett, R. Gianella, C. Gowers, N. A. Gottardi, J. Jaquinot, P. J. Harbour, M. F. Johnson, E. Lazzaro, K. Lawson, P. Morgan, D. Stork, K. Thomson, B. Tubbing and M. von Hellermann (1989). Plasma characteristics of H-mode in JET with beryllium gettering. *JET-(89)80,* 53-55

Thomas, P. R. (1990). Results of JET operation with beryllium. *Proc. 9th Int. Conf. Plasma Surface Interactions in Contr. Fusion Devices, Bournemouth, UK. In publication*

Waelbroeck, F., I. Ali-Khan, K. J. Dietz and P. Wienhold (1979). Hydrogen solubilisation into and permeation through wall materials. *J. Nucl. Mat.* 85 & 86, 345-349

Wesson, J. A., R. G. Gill, M. Hugon, F. C. Schüller, J. A. Snipes, D. J. Ward, D. V. Bartlett, D. J. Campbell, P. A. Duperrex, A. W. Edwards, R. S. Granetz, N. A. O. Gottardi, T. C. Hender, E. Lazzaro, P. J. Lomas, N. Lopes Cardozo, K. F. Mast, M. F. F. Nave, N. A. Salmon, P. Smeulders, P. R. Thomas, B. J. D. Tubbing, M. F. Turner and A. Weller (1989). Disruptions in JET. *Nucl. Fusion,* 29, 641-665

Papers presented to 16th Symposium on Fusion Technology

London, UK., 3rd-7th September 1990

Many Authors

JET Papers presented at the 16th Symposium on Fusion Technology (London, UK, 3-7 September 1990) Volume I

	Title	Presenter
1)	Supplying JET from the UK 400kV Supergrid: A Major Engineering Achievement Relevant to the NEXT Step	E Bertolini
2)	The JET High-Speed Pellet Launcher Prototype - Development, Implementation and Operational Experience	P Kupschus
3)	Pumping of ^{3}He and ^{4}He Gas using Argon Frosted Liquid Helium Cryopumps at Sub-Condensation Temperatures	P Massmann
4)	Operational Experience with the JET Beryllium Evaporators	A Peacock
5)	Development of Interface for Remote Mass Spectrometer	T Winkel
6)	Design of High Heat Flux Components for the JET Pumped Divertor	E Deksnis
7)	Power Loading Tests of the JET Pumped Divertor Plates	H Falter
8)	JET Pumped Divertor Cryopump	W Obert
9)	Reionised Power Deposition in the JET Neutral Beam Duct and Plasma Facing Components	H de Esch
10)	An Optical Scanning Diagnostic for Neutral	A Bickley
11)	Some Key Technical Developments for the Fast Ion and Alpha Particle Diagnostic System on JET	J Hoekzema
12)	Automatic VSWR Control in JET ICRH Transmitters	G Bosia
13)	ICRF Antenna for the JET Pumped Divertor Configuration	R Lobel
14)	Tokamak Stray Field Compensation System for JET Neutral Beam	D Cooper
15)	An Analytic Procedure for Currents and Forces Calculation in JET	S Bobbio
16)	High Power Tests of the JET Prototype LHCD Launcher	H Brinkschulte
17)	Real Time Diagnostic Data Acquisition and Plasma Control using Transputers	E van der Goot

JET Papers presented at the 16th Symposium on Fusion Technology (London, UK, 3-7 September 1990) Volume II

	Title	Presenter
18)	Specific Features of the Control and Data Acquisition for the JET Pellet Injector	M Gadeberg
19)	The JET In-Vessel Inspection Man-Machine Interface	T Businaro
20)	JET Gas Economy with C and Be First Wall and Implications for the Gas Introduction System	J How
21)	A Numerical Model for the Gas Dynamics of a Fast Pellet Injector	D Flory
22)	The Design and Construction of the TARM - A Crane-Mounted Remotely-Controlled Transporter for JET	L Jones
23)	Beryllium Related Maintenance on JET	S Booth
24)	Safety Analysis of Potential Graphite Oxidation Effects in JET	M Wykes
25)	Methodology of Tritium and Radiation Compatibility Assessments for JET Diagnostic and Other Systems and the Preliminary Results	C Caldwell-Nichols
26)	Risk Assessment Methodology for the JET Active Gas Handling System (AGHS) and the Significance of the Exhaust Detritiation System in Meeting Design Safety Targets	A Bell
27)	The JET Quality Assurance Programme and its Associated System of Technical Documents	P Meriguet
28)	The Independent Assessment of Planned Tritium Operations at JET	H Campbell
29)	Octant Removal at JET for a Toroidal Field Coil Exchange	G Celentano
30)	JET TF Coil Fault - Detection, Diagnosis and Prevention	J Last
31)	The JET Divertor Magnetic Configuration and Coil Design	J Last
32)	The Conversion and Operation of the Neutral Beam Power Supplies up to 160KV	R Claesen
33)	The High Power, Wide Bandwidth Disruption Feedback Amplifiers for JET	P Mondino

Papers presented to 13th IAEA Conference on Plasma Physics and Controlled Nuclear Fusion Research

Washington, USA., 1st-5th October 1990

Many Authors

Recent JET Results and Future Prospects

Abstract

The latest results of JET plasmas in transient and steady states are presented. Substantial improvements in plasma purity and corresponding reductions in plasma dilution have resulted from the use of beryllium as the first wall material facing the hot plasma. As a consequence, plasmas with a fusion triple product ($n_D(0)\tau_E T_i(0)$) in the range 8-9x10^{20}m^{-3}skeV have been achieved (within a factor of 8 of that required in a fusion reactor), albeit under transient conditions. The general JET performance has also improved, allowing the parameters of a reactor plasma to be individually achieved in JET. In view of their importance for reactors, the JET results are presented with particular emphasis on their significance for the formulation of a plasma model for the Next Step. However, impurity influxes limit the attainment of better parameters and prevent the realisation of steady state conditions at high heating powers. To address this problem of impurity control, and those of plasma fuelling and helium ash exhaust, a New Phase is planned for JET with an axi-symmetric pumped divertor configuration that will allow operating conditions close to those of a reactor. The divertor configuration should demonstrate a concept of impurity control and determine the size and geometry needed to fulfil this concept in a reactor. It should identify appropriate materials for plasma facing components and define the operational domain for the Next Step.

1. INTRODUCTION

The objective of JET is to obtain and study plasmas in conditions and dimensions approaching those needed in a thermonuclear reactor [1,2]. The present paper concentrates on progress towards this objective during the last two years of JET operation, since the 1988 IAEA Conference [3]. The transient and steady state behaviour of JET plasmas are presented in view of their importance for reactor plasmas. JET operation and the consequences of using a beryllium "first wall" are discussed and the best fusion performance and general plasma behaviour in JET are reported. The underlying results are presented with particular emphasis on their significance for the formulation of a plasma model for a Next Step tokamak. In view of the importance of dilution and exhaust for ignition [4] and the need for adequate impurity control and understanding of the scrape-off layer plasma, a New Phase is planned for JET with a divertor configuration and this is also discussed.

2. JET OPERATION

Since 1988, further additions and technical enhancements to JET have been made:

- reinforcement of the vacuum vessel to withstand radial and vertical instabilities and permit operation at full power up to 7MA in the material limiter configuration and up to 6MA in the X-point configuration (inconel rings fitted above and below the mid-plane at the in-board walls to stiffen and strengthen the vessel);
- belt limiter tiles, ion cyclotron resonance heating (ICRH) antennae screens and lower X-point dump plates were changed to beryllium and beryllium evaporation has also been used;
- one neutral beam injection (NBI) box was modified to operate at 140kV to provide better penetration at higher density. The other NBI box remained at 80kV. This gave a total power of 18MW (instead of 21MW with both boxes at 80kV);
- each ICRH generator power unit was upgraded to 2MW, offering the potential of 32MW total power source and ~24MW coupled to the plasma through eight antennae;
- a prototype lower hybrid current drive (LHCD) system has been installed, offering the potential of 4MW at 3.7GHz;

In addition, a faulty toroidal field coil has been removed and replaced successfully with a spare coil.

JET is now about midway through its experimental programme. The technical design specification of JET has been achieved in all parameters and exceeded in several cases (see Table I). The plasma current of 7MA in the limiter configuration [5] and the current duration of up to 30s at 3MA are world records and are over twice the values achieved in any other fusion experiment. 5.1MA and 4.5MA are also world records in the single-null and double-null divertor configurations, respectively [6]. NBI heating has been brought up to full power (~21MW) and ICRH power has been increased to ~22MW in the plasma. In combination, these systems have delivered 35MW to the plasma.

3. THE USE OF BERYLLIUM IN JET

Over the last two years impurities and density control have been the main obstacles to the improvement of JET performance. Carbon first-wall components had been developed so that they were mechanically able to withstand the power loads encountered. However, the interaction of the plasma with these components, even under quiescent conditions, caused unacceptable dilution of the plasma fuel. In addition, imperfections in the positioning of the components led to localised heating at high power, and the following problems occurred:

- the production of impurities increased with the input power to the plasma;
- at high power, the heat load on the tiles caused a plasma evolution which exhibited a catastrophic behaviour - the so-called "carbon catastrophe". Increased plasma dilution, increased power radiated, reduced neutral beam penetration and a threefold fall of fusion yield resulted from the carbon influx;
- for lower input power with long duration, problems were also encountered. Without fuelling, deuterium was pumped by the carbon and replaced by impurities, resulting in severe dilution of the plasma;
- the maximum density achieved without the occurrence of plasma disruptions appeared to be limited by edge radiation.

The situation has been redressed by the progressive introduction of beryllium "first-wall" components since 1989 [7]. First, beryllium was evaporated as a thin layer on the carbon walls and limiters; then, as the material for the limiter tiles; and finally, as the material for the lower X-point target tiles and the open screens of the ICRH antennae.

With a carbon first-wall, the main impurities were carbon (2-10%) and oxygen (1-2%). With beryllium evaporated inside the vessel, oxygen was reduced by factors >20, and carbon by >2. Although beryllium increased, carbon remained the dominant impurity for this phase. With beryllium limiters, the carbon concentration was reduced by a further factor of 10, but beryllium levels increased by ~10, and became the dominant impurity. Due to the virtual elimination of oxygen and replacement of carbon by beryllium, impurity influxes were reduced significantly, in line with model calculations [8] which take account of impurity self-sputtering. In addition, nickel was eliminated from the plasma when the nickel screens for the ICRH antennae were replaced by beryllium.

During 1989, plasma dilution and the effective plasma charge, Z_{eff}, were reduced significantly in ohmic plasmas and with strong additional heating. Fig. 1(a) shows the dilution factor, n_D/n_e, as a function of input power per particle, $P_i/\langle n_e \rangle$. The corresponding values of Z_{eff} are shown in Fig. 1(b). With moderate power, it was not possible to maintain n_D/n_e much above 0.6 with carbon, but values greater than 0.8 were routinely achieved with beryllium. Furthermore, high power operation was possible only with beryllium.

Impurity radiation was also reduced and operation with beryllium gettering allowed improved density control (due to high wall pumping of both deuterium and helium). On the longer timescale (minutes to hours), very little deuterium was retained compared with a carbon first-wall; >80% of the neutral gas admitted to JET is recovered, compared with ~50% with a carbon first-wall. This has important advantages for the tritium phase of JET operation.

4. JET PERFORMANCE

4.1. Fusion performance

With carbon X-point target plates, the length of the H-mode has been extended (up to 5.3s) either by sweeping the X-point (both in the radial and vertical directions) to reduce the X-point tile temperature, or by using strong gas puffing in the divertor region. This, together with the better plasma purity achieved with a beryllium first-wall, resulted in increased ion temperatures ($T_i(0)$ in the range 20-30keV) and improved plasma performance, with the fusion triple product ($n_D(0)\tau_E T_i(0)$) increasing significantly. Such improved fusion performance could otherwise have been achieved only with a substantial increase in energy confinement.

In a particular case, the central ion temperature reached 22keV, the energy confinement time, τ_E, was 1.1s, with a record fusion triple product ($n_D(0)\tau_E T_i(0)$) of 8–9x10^{20}m^{-3}skeV. The neutron yield for this discharge was also amongst the highest achieved on JET at 3.5x10^{16}ns^{-1}, with Q_{DD}= 2.4x10^{-3}. A full D-T simulation of the pulse showed that 12MW of fusion power would have been obtained transiently with 16MW of NBI power, giving an equivalent fusion amplification factor Q_{DT} ~ 0.8, reaching near breakeven conditions and within a factor of 8 of that required by a reactor. Similar results were also obtained at medium temperatures, with T_e~T_i~10keV.

The overall fusion triple product as a function of central ion temperature is shown in Fig. 2 for a number of tokamaks.

4.2. General behaviour

Reduced impurity levels allowed prolonged operation at higher densities and improved the general JET performance, as follows:

- the pumping of deuterium with a beryllium first-wall was more efficient than with a carbon first-wall and provided improved density control. This permitted low density and high temperature (up to 30keV) operation for times >1s;
- the density limit increased [9], and a peak density of 4x10^{20}m^{-3} was achieved with pellet fuelling. The density is limited principally by fuelling and not by disruptions, as was found with carbon limiters;
- sawtooth free periods exceeding 5s were achieved, but the stabilisation mechanism is still not yet clear [10]. The central electron temperature appears to saturate at about 12keV, even though the central heating power to the electrons can be higher than that to the ions;
- H-modes were established with ICRH alone and for periods >1s. With beryllium antennae screens, H-modes were established with either monopole or dipole phasing [11]. The confinement characteristics of ICRH H-modes were similar to those with NBI alone;
- β-values up to the Troyon limit were obtained in double-null X-point plasmas [9].

Thus, the parameters of a reactor plasma have been achieved individually in JET.

However, the best fusion performance was obtained in a transient state and could not be sustained in steady state. Ultimately, the influx of impurities caused a degradation in plasma parameters. Furthermore, a severe carbon influx ("carbon catastrophe") was still a problem for inner wall and X-point operation, and is a serious limitation in H-mode studies.

5. UNDERLYING RESULTS AND THEIR SIGNIFICANCE

The underlying JET results are presented with particular emphasis on their significance for the formulation of a plasma model for the Next Step.

5.1. Density limit

With a carbon first-wall, the plasma density was limited, in general, when the radiated power reached 100% of the input power. This led to the growth of MHD instabilities and ended in a major disruption. The density limit was dependent on plasma purity and power to the plasma.

With a beryllium first-wall, the maximum operating density increased significantly by a factor of 1.6-2. A record central density of 4x10^{20}m^{-3} was achieved by strongly peaking the density profile using a sequence of 4mm solid deuterium pellets injected at intervals throughout the current rise phase of an X-point discharge. Furthermore, the nature of the density limit changed and the

frequency of disruptions at the density limit were much reduced. Disruptions did not usually occur, and the limit was associated rather with the formation of a poloidally asymmetric, but toroidally symmetric radiating structure (a "MARFE"), which limits the plasma density to within the stable operating domain. These results constitute a substantial enhancement of JET's operating capability.

Heating and fuelling were varied systematically, using both gas and pellet fuelling. With deep pellet fuelling and either NBI or ICRH, peaked profiles were obtained (Fig. 3). Just before a density limit MARFE occurred, pellet fuelled discharges reached the same edge density as gas fuelled discharges, but the central densities were considerably higher. The central density depends, therefore, on the fuelling method used. The profiles are similar near the edge, but are remarkably flat with gas fuelling.

These observations suggest that the edge density may be correlated with the density limit and is found to increase approximately as the square root of power (Fig. 4). This endorses the view that the density limit is determined by a power balance at the plasma edge and the cause of disruptions is related to radiation near the q=2 surface. Thus, under beryllium conditions, when the radiation is low, or confined to the outermost edge, there are no density limit disruptions.

5.2. Density profiles and transport

Of significance also are the density profiles obtained with edge fuelling, which tend to be flatter with the lower Z_{eff} achieved with beryllium, in contrast to those obtained with carbon, which tended to be more peaked, even with edge fuelling. The occurrence of flat density profiles suggest that there is no need for an anomalous inward particle pinch, except perhaps on impurities. This observation poses important questions related to particle transport, and in particular, the transport and exhaust of helium ash products.

The relaxation of the peaked density profiles achieved with pellet injection allows an estimate of particle transport. For a 4mm pellet injected into 3MA/3.1T plasma, the decay of the central electron density is shown in Fig. 5. Following injection, the decay constants are 1.8s for the ohmically heated discharge and 1s when ~8MW ICRH is applied. The global energy confinement times are in a similar ratio. It is therefore reasonable to assume that particle and energy transport are linked. Furthermore, modelling studies of similar discharges suggest that the diffusion coefficient is lower in the central plasma than further out and that there is no need for a large anomalous inward particle pinch in the central plasma [12].

Impurity transport studies have been possible from the measurement of emissivity profiles by the soft X-ray cameras following the injection of laser-ablated, high-Z impurities. The evolution of the nickel density profile has been determined (Fig. 6(a)) and so the particle fluxes can be plotted as a function of the density gradient at different radii. Fig. 6(b) shows that fluxes and gradients are linearly related through a diffusion coefficient which increases with radius. There is no evidence of a significant pinch term for the impurities.

This measurement also provides evidence of better confinement in H-modes. The temporal evolution of NiXXVI emission is shown in Fig. 7 for the L- and H-phases of two similar discharges with ~9MW of additional heating. In contrast to the decaying signal of the L-phase, the signal rises rapidly to a steady value which persists to the end of the H-phase. This shows that impurities have considerably longer confinement times in the H-phase and endorses the view that an edge transport barrier exists, which could be destroyed (for example, by ELMs) on transition from the H- to the L-phase.

5.3. Temperature

High ion temperatures have been obtained at the low densities possible with a beryllium first-wall and with the better penetration afforded by NBI at 140kV. Record ion temperatures were achieved of up to 18keV in limiter plasmas and up to 30keV in X-point plasmas (with powers up to 17MW). In this mode, the ion temperature profile is sharply peaked and the electron temperature is significantly lower than the ion temperature, by a factor of 2-3. The central ion temperature (as shown in Fig. 8) increases approximately linearly with power per particle up to the highest temperatures, indicating that ion thermal losses are anomalous, but ion confinement degrades little with input power. On the other hand, the central electron temperature saturates at ~12keV, even though with ICRH the central heating power to the electrons can be higher than that to the ions. Electron thermal transport is also anomalous and electron confinement degrades strongly with increased heating power. This suggests that electrons are primarily responsible for confinement degradation.

At higher densities with combined NBI and ICRH, central ion and electron temperatures were both above 11keV in a 3MA plasma for power input of 33MW (21 MW NBI and 12MW ICRH).

Extensive studies have also been performed in the 'monster-sawtooth' regime [10] in which sawteeth oscillations have been suppressed for up to 5s by central ICRH. Peaked temperature profiles (with both central ion and electron temperatures above 10keV) were maintained for several seconds. In an equivalent D-T mixture, this would result in a significant enhancement in the time-averaged neutron rate compared with a sawtoothing discharge. This does not mean, however, that ion losses are necessarily small.

5.4. Electron heat pulse propagation

The propagation of temperature perturbations (determined from the electron cyclotron polychromator) and density perturbations (determined from the multichannel reflectometer) following the collapse of a sawtooth provide good measurements of energy and particle transport. The decay of the temperature perturbation at different radii in a 3MA/3.1T ohmically heated discharge is shown in Fig. 9(a). This decay can be modelled with an heat pulse diffusivity, χ_{HP}~$3.2m^2s^{-1}$, which should be compared with χ_e~$1m^2s^{-1}$, obtained from power balance considerations. The results in an L-mode plasma, heated with 9.5MW of ICRH, are shown in Fig.9(b) and indicate that, although χ_e~$2m^2s^{-1}$, the same χ_{HP}~$3.2m^2s^{-1}$ can be used in the simulation to fit the data. It is also found that, within experimental uncertainties, the same χ_{HP} can be used also for H-regime plasmas and does not depend on heating power.

The propagation characteristics of the density perturbation indicate that the density pulse is slower than the temperature pulse and that the density pulse is comprised of both an outward and inward propagating perturbation (the latter resulting from the earlier interaction of the temperature pulse with the limiters) [12].

Furthermore, simultaneous measurements of the temperature and density perturbations indicate that the particle pulse diffusion coefficient, D_{DP}~D_e«χ_{HP}.

5.5. Global energy confinement

With a carbon first-wall, the energy confinement time improves with increasing current and degrades with increasing heating power, independent of the heating method. With a beryllium first-wall, energy confinement times and their dependences are effectively unchanged: energy confinement does not appear to be affected by the impurity mix (carbon or beryllium in deuterium plasmas).

In the X-point configuration, high power H-modes (up to 25MW) have been studied. In comparison with limiter plasmas, confinement is a factor ~2 better, but the dependences with current and heating power are similar (Fig. 10).

With a carbon first-wall, H-modes with ICRH alone were not obtained. Beryllium evaporation on the nickel antennae screens led to lower impurity production and H-modes were successfully obtained with ICRH alone. With beryllium antennae screens, the threshold for the H-mode was reduced somewhat for dipole phasing, and ICRH H-modes were also obtained with monopole phasing. However, this required feedback control of the plasma position to allow for the movement of the plasma boundary during the L-H transition. In all cases, H-mode confinement with ICRH alone was similar to that with NBI, that is independent of the heating method.

A particular discharge (Fig. 11) exhibited an H-mode and pellet enhanced performance [11]. A 4mm pellet was injected into a 3MA/2.8T double null X-point plasma, heated with 9MW of ICRH and 2.5MW of NBI (which served primarily as a diagnostic for the measurement of the ion temperature). The stored plasma energy increased to 8MJ (still increasing at a rate ~4MW when the period of pellet enhanced confinement ceased). The energy confinement time reached ~1.0s and with central electron density ~$8x10^{19}m^{-3}$, Z_{eff}~1 and central electron and ion temperatures ~10keV, the fusion triple product was ~$8x10^{20}m^{-3}skeV$. The neutron yield was $10^{16}s^{-1}$. This phase terminated as the central density decayed, although the stored energy remained high (again favouring the existence of an edge confinement barrier) until the end of the H-mode. Subsequently, plasma temperatures recovered, with the bulk deuterium ions being effectively heated in this ICRH scheme which used a high concentration of hydrogen minority ions.

5.6. Beta limits

Experiments have explored the plasma pressure (indicated by the β-value) that can be sustained in JET and investigated the plasma behaviour near the expected β-limit in a double-null H-mode configuration, at high density and temperature and low magnetic field (B_t = 1T). β_t values up to ~ 5.5% were obtained, close to the Troyon limit $\beta_t(\%) = 2.8I_p(MA)/B_t(T)a(m)$, where I_p is the plasma current and a is the plasma minor radius [9]. Significantly, the JET limit does not appear to be disruptive at present power levels. Rather, a range of MHD instabilities occur, limiting the maximum β-value without causing a disruption. The behaviour near both the density and β-limits may be interpreted in terms of resonant instabilities which have the magnetic topology of an island.

5.7. Alpha-particle simulations

The behaviour of alpha-particles has been simulated in JET by studying energetic particles such as 1MeV tritons, and ^{3}He and H minority ions accelerated to a few MeV by ICRH [11]. The energetic population has up to 50% of the stored energy of the plasma and possesses all the characteristics of alpha-particles in an ignited plasma, except that in the JET experiments, the ratio of the perpendicular to parallel pressure was above three, while in a reactor plasma the distribution will be approximately isotropic. The mean energy of the minority species was about 1MeV, and the relative concentration of the ^{3}He ions to the electron density was 1-2%, which is comparable to the relative concentration of alpha-particles in a reactor (7%). Under conditions with little MHD activity, no evidence of non-classical loss or deleterious behaviour of minority ions was observed, even though the ratio of the fast ion slowing down time to the energy confinement time in JET is greater than that expected in a reactor.

Fusion reactivity measurements were undertaken on the D-^{3}He reaction when minority ^{3}He ions were accelerated to energies in the MeV range using ICRH. During a 5s monster sawtooth produced by 10MW of ICRH, a reaction rate of $4x10^{16}s^{-1}$ was achieved, which corresponded to 100kW of fusion power and Q=1% was reached. This was carried out with a beryllium first-wall and benefitted from an improved fuel concentration n_D/n_e of up to 0.7. Comparison of the measurements with theoretical predictions suggest nearly classical trapping and thermalisation of the energetic particles.

6. PLASMA MODELLING

6.1. Formulation of a plasma model

Any model used to predict the performance of a Next Step tokamak must be consistent with the foregoing data. In particular, it must explain:

- the resilience of the electron temperature to heating;
- the heat and density pulse propagation studies;
- no intrinsic degradation of ion confinement with ion heating;
- the density decay after pellet injection; and
- the similar behaviour of particle and heat transport.

It is possible to formulate a transport model, based on one phenomenon and consistent with JET data and with physics constraints. Specifically, above a critical threshold, $(\nabla T_e)_c$, in the electron temperature gradient, the transport is anomalous and greater than the underlying neoclassical transport. The electrons are primarily responsible for the anomalous transport, but ion heat and particle transport are also anomalous. The general expressions for the conductive heat fluxes and the anomalous transport coefficients are:

$$Q_e \equiv -n_e\chi_e\nabla T_e = -n_e\chi_{an,e}(\nabla T_e - (\nabla T_e)_c)$$

$$Q_i \equiv -n_i\chi_i\nabla T_i \text{ and } \chi_i = 2\chi_e\frac{Z_i}{\sqrt{1+Z_{eff}}}\sqrt{\frac{T_e}{T_i}}$$

$$D_i \approx (0.3\text{+}0.5)\,\chi_i$$

The critical electron temperature gradient model of Rebut et al [13] specifies possible dependences for χ and D and this is explored further in [12].

6.2. To model a Next Step tokamak

The fuelling, impurity control and exhaust capability of a Next Step tokamak will be dependent on whether deuterium and impurities (including helium) accumulate in the plasma centre. The production and transport of helium ash towards the plasma edge (where it must be exhausted) will depend on the relative importance of energy and particle confinement, the effect of sawteeth, the effect of the edge transport barrier in the H-mode and the behaviour of the scrape-off layer plasma.

Although the transport model of Section 6.1 applies in both L- and H-regimes, and ensures that particle and energy transport will follow each other in the transition from the L- to H-regime (since χ and D are linked in the model), it is necessary to include several additional elements in order to complete the model for a Next Step tokamak. For example, the spontaneous improvement in edge confinement has yet to be modelled. The reduction in MHD activity observed experimentally suggests the presence of some other instability at the edge of L-mode plasmas, where the effect of atomic physics on MHD might be important. This is apparently easier to suppress in an X-point configuration with high edge magnetic or rotational shear. Furthermore, an understanding of the scrape-off-layer (SOL) plasma is also needed.

7. IMPURITY CONTROL AND THE NEW PHASE PLANNED FOR JET

Achieving control of the impurity influx into the plasma is a pre-requisite to the construction of a tokamak reactor. In the case of high Z impurities, radiation losses may prevent reaching ignition. The presence of low Z impurities, in addition to helium produced by nuclear reactions, dilutes the concentration of reacting ions and therefore reduces the alpha-particle power. Under present conditions, the lifetime of the plasma facing components would be severely limited. Understanding the SOL plasma is needed because of the importance of dilution and exhaust for ignition.

So far, JET has concentrated on **passive** methods of impurity control. Studies of **active** methods of impurity control are a natural development of the JET programme and accordingly, a New Phase for JET is planned to start in 1992 [4], with first results becoming available in 1993 and continuing to the end of 1996.

The aim of the New Phase is to demonstrate, prior to the introduction of tritium, effective methods of impurity control in operating conditions close to those of the Next Step, with a stationary plasma of 'thermonuclear grade' in an axisymmetric pumped divertor configuration. Successful impurity control would lead also to an increase in alpha-particle power by more than a factor of two.

Specifically, the New Phase should demonstrate:

- control of impurities generated at the divertor target plates;
- decrease of the heat load on the target plates;
- control of plasma density;
- the exhaust capability;
- a realistic model of particle transport.

7.1. Key concepts of the JET pumped divertor

Since sputtering of the target plates cannot be suppressed, the impurities produced must be retained close to the target plates for effective impurity control. This can be achieved by friction with a strong plasma flow, directed along the divertor channel plasma (DCP) towards the target plates. If large enough, the frictional force between the plasma and the impurities should prevent impurity migration towards the X-point. The plasma flow will be generated by a combination of gas puffing, the injection of low speed pellets and the recycling and recirculation of some of the flow at the target plates towards the X-point. The connection length along the magnetic field line between the X-point and the target plates should be sufficiently long to achieve effective screening of impurities.

Rapid sweeping of the target plates to limit the localised heat load, to limit erosion and to affect redeposition is an important feature. Methods of ensuring that a substantial fraction of input power can be radiated in a controlled way in the DCP remain key elements.

7.2. Modelling the edge plasma

The plasma behaviour in the SOL and the DCP can be qualitatively understood. Impurity retention in the divertor is determined from the steady state momentum equation for impurity ions, which for the simplest, realistic case gives the impurity density, n_z, decaying exponentially with distance from the target on a scale length, λ_z, given by:

$$\lambda_z^{-1} = \lambda_F^{-1} - \lambda_e^{-1}, \quad \text{with} \quad \lambda_F^{-1} = \frac{m_z v_z}{T\tau_z} \quad \text{and} \quad \lambda_e^{-1} = \alpha_z \frac{1}{T}\frac{dT}{dx}$$

The temperature gradient scale length is given by the heat transport equation with electron heat conductivity parallel to the magnetic field ($\kappa=\kappa_0 T^{5/2}$) being dominant and dependent primarily on the input power. To ensure impurity control, the frictional force must exceed the sum of the pressure and thermal forces, that is:

$$\lambda_F^{-1} > \lambda_e^{-1}.$$

To increase the hydrogen-impurity friction and radiated power in front of the target plates, a low temperature, high density plasma is needed. This will also limit erosion and therefore increase the lifetime of the target plates.

To solve the full set of classical fluid equations for the conservation of particles, momentum and energy in the SOL and DCP, a numerical 1-½ D transport model has been developed [14]. Monte Carlo methods are used for neutral deuterium and impurities in the flux surface geometry of the pumped divertor. Erosion at the target plates is determined by a model of sputtering tested against JET experimental data [8]. The calculations show that impurities can be retained near the target plates for plasma flows, typically ~$10^{23}s^{-1}$ near the X-point. The steady state distributions of Z_{eff} (with beryllium impurities), for conditions in the SOL and DCP, with and without flow, are shown in Fig. 12(a). These results are obtained for an electron density ~$10^{20}m^{-3}$ at the target plates. At target densities approaching $10^{21}m^{-3}$, the reduction of erosion and the plasma flow associated with high recycling at the target plates ensures impurity control. Furthermore, the calculations show that the ion temperature in the SOL can be substantially larger than the electron temperature (Fig. 12(b)). In present JET discharges, probe measurements indicate, that at low density, the electron temperature at the target plates is lower than the ion temperature, determined from broadening of the H_α emission and power balance considerations [7].

7.3. The pumped divertor configuration

The aims of the New Phase can be realised with the internal multi-coil configuration shown in Fig. 13. The design allows a large plasma volume at 6MA and the operational flexibility to modify the magnetic configuration in the vicinity of the X-point independent of the plasma current and separately on the high and low field sides. In contrast to the normal configuration for a divertor, all divertor coils carry current flowing in the same direction as the plasma current.

Water-cooled, hypervapotron elements, made of copper and covered by beryllium, will be used for the high heat flux components of the target plates, and these are expected to accommodate power fluxes up to $15MWm^{-2}$ at the copper-beryllium interface. A pumping chamber is introduced in the vicinity of the target plates to provide control of the main plasma density. Pumping is achieved by a cryo-pump to avoid excessive hydrogen retention and to be compatible with the tritium phase.

With this configuration, single null X-point operation should be possible for performance and impurity control studies. Plasmas should be obtained at 6MA for 10s, a volume ~$93m^3$ and a connection length from the X-point to the target plates of 3m, and at 5MA for 10s, a volume ~$80m^3$ and a connection length ~10m should be achieved. In addition, it should be possible to run 3MA double null X-point plasmas for up to 20s at 3.4T and for up to 1 minute at 2.1T.

7.4. JET programme in the New Phase

A schedule for the JET programme incorporating the New Phase is shown in Table II. The earliest date to have a pumped divertor in JET is 1992. Further optimisation would likely be necessary about 18 months later, in the light of new experimental results.

By the end of 1994, all information on particle transport, exhaust and fuelling, first wall requirements and enhanced confinement regimes needed to construct a Next Step tokamak, should be available. Final tests with tritium, including alpha-particle heating studies could be performed in the two years following, leading to completion of the JET programme by the end of 1996. During the tritium phase of operation, and even later, tests on prototype elements for a Next Step tokamak could be undertaken on the JET site, using the test facilities, tritium plant and power supplies.

8. CONCLUSIONS

In summary, the paper sets out the main JET results and future prospects. JET has successfully achieved and contained plasmas of thermonuclear grade. **Individually**, parameters required for a fusion reactor have been obtained, and **simultaneously**, the fusion product $(n_D(0)\tau_E T_i(0))$ has reached 8-$9\times10^{20}m^{-3}skeV$, for both medium (~10keV) and high (>20keV) central temperatures, and is within a factor of 8 of that required in a fusion reactor; neutron yield has increased to ~$3.5\times10^{16}ns^{-1}$, corresponding to an equivalent Q_{DT}~0.8. However, these values were in a **transient** state and could not be sustained in steady state.

A clearer picture of energy and particle transport also starts to emerge. The resilience of the electron temperature suggests that the electrons are primarily responsible for confinement degradation. The occurrence of flat density profiles suggests that there is no need for an inward pinch term, except perhaps for impurities. Particle and energy transport exhibit similar behaviour. The critical electron temperature gradient model is one such model consistent with these observations.

In a reactor, the density limit should not be a problem; high densities and flat profiles are likely; an advanced divertor concept for impurity control is required. These conditions of high plasma density at the separatrix are unfavourable for the methods of non-inductive current drive envisaged at present.

A New Phase is planned for JET with an axi-symmetric pumped divertor configuration to operate with a stationary plasma (10s-1minute) of thermonuclear grade. In this New Phase, JET should be able to:

- demonstrate a concept of impurity control;
- determine the geometry needed to fulfil this concept in a reactor;
- identify appropriate materials for plasma facing components;
- define the operational domain for the Next Step.

To ensure the success of a Next Step ignition device, it is imperative that all aspects of plasma behaviour, impurity control and plasma exhaust be included in the model used to define the size of the device and its toroidal field, plasma current and operating conditions.

9. REFERENCES

[1] The JET Project - Design Proposal: EUR-JET-R5.

[2] Rebut, P-H., et al, Fusion Technology, **11**, (1987), 13-281.

[3] The JET Team, Proc. of 12th Int. Conf. on Plasma Phys. and Contr. Nucl. Fus. Res., (Nice, France, 1988), Nuclear Fusion Supplement, **1**, 41.

[4] Rebut, P-H., Lallia, P.P., and Keen, B.E., Proc. of the 13th Symposium on Fusion Engineering, (Knoxville, USA, 1989), **1**, 227.

[5] Lomas, P.J. and The JET Team, Proc. of 13th Int. Conf. on Plasma Phys. and Contr. Nucl. Fus. Res., (Washington, USA, 1990), Paper IAEA-CN-53/A-6-2.

[6] Tanga, A. and The JET Team, Proc. of 13th Int. Conf. on Plasma Phys. and Contr. Nucl. Fus. Res., (Washington, USA, 1990), Paper IAEA-CN-53/A-4-1.

[7] Thomas, P.R. and The JET Team, Proc. of 13th Int. Conf. on Plasma Phys. and Contr. Nucl. Fus. Res., (Washington, USA, 1990), Paper IAEA-CN-53/A-5-3.

[8] Summers, D.D.R., et al, J. Nuclear Mater., to be published (1990).

[9] Smeulders, P. and The JET Team, Proc. of 13th Int. Conf. on Plasma Phys. and Contr. Nucl. Fus. Res., (Washington, USA, 1990), Paper IAEA-CN-53/A-3-4.

[10] Campbell, D.J. and The JET Team, Proc. of 13th Int. Conf. on Plasma Phys. and Contr. Nucl. Fus. Res., (Washington, USA, 1990), Paper IAEA-CN-53/A-6-3.

[11] Start, D.F.H. and The JET Team, Proc. of 13th Int. Conf. on Plasma Phys. and Contr. Nucl. Fus. Res., (Washington, USA, 1990), Paper IAEA-CN-53/E-2-1.

[12] Taroni, A., et al, Proc. of 13th Int. Conf. on Plasma Phys. and Contr. Nucl. Fus. Res., (Washington, USA, 1990), Paper IAEA-CN-53/A-2-1.

[13] Rebut, P-H., Lallia, P.P., and Watkins, M.L., Proc. of 12th Int. Conf. on Plasma Phys. and Contr. Nucl. Fus. Res., (Nice, France, 1988) Nuclear Fusion Supplement, 2, 191.

[14] Keilhacker, M., et al, Proc. of 13th Int. Conf. on Plasma Phys. and Contr. Nucl. Fus. Res., (Washington, USA, 1990), Paper IAEA-CN-53/A-5-1.

Table I

JET Parameters

Parameters	Design Values	Achieved values
Plasma Major Radius (R_O)	2.96m	2.5-3.4m
Plasma Minor Radius horizontal (a)	1.25m	0.8-1.2m
Plasma Minor Radius vertical (b)	2.1m	0.8-2.1m
Toroidal Field at R_O	3.45T	3.45T
Plasma Current:		
Limiter mode	4.8MA	7.1MA
Single null X-point	not foreseen	5.1MA
Double null X-point	not foreseen	4.5MA
Neutral Beam (NB) Power		
(80kV, D)	20MW	21MW
(140kV, D)	15MW	8MW (one box converted, so far)
Ion Cyclotron Resonance Heating (ICRH) Power to Plasma	15MW	22MW

Table II : JET Development Programme

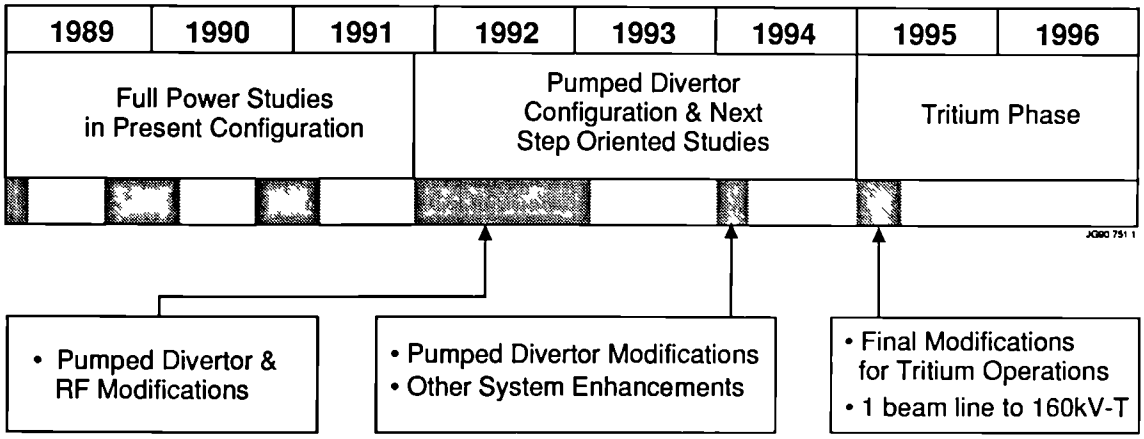

Appendix I

THE JET TEAM

JET Joint Undertaking, Abingdon, Oxon, OX14 3EA, U.K.

J.M. Adams[1], H. Altmann, A. Andersen[14], S. Attenberger[23], W. Bailey, P. Ballantyne, B. Balet, R. Barnsley[2], M. Baronian, D.V. Bartlett, L.R. Baylor[23], A.C. Bell, H. Bergsaker[11], P. Bertoldi, E. Bertolini, V. Bhatnagar, A.J. Bickley, H. Bindslev[14], T. Bonicelli, S.J. Booth, G. Bosia, M. Botman, D. Boucher, H. Brelen, H. Brinkschulte, T. Brown, M. Brusati, T. Budd, M. Bures, T. Businaro, P. Butcher, H. Buttgereit, C. Caldwell-Nichols, D.J. Campbell, P. Card, G. Celentano, C.D. Challis, D. Chiron, J. Christiansen, C. Christodoulopoulos, P. Chuilon, R. Claesen, S. Clement[21], E. Clipsham, J.P. Coad, M. Comiskey, S. Conroy[12], M. Cooke, S. Cooper, J.G. Cordey, W. Core, G. Corrigan, S. Corti, A.E. Costley, G. Cottrell, J-P. Coulon[16], M. Cox[7], P. Cripwell, H. de Blank[15], G. Decker[17], H. de Esch, L. de Kock, E. Deksnis, G.B. Denne-Hinnov, G. Deschamps, G. Devillers, K.J. Dietz, S.L. Dmitrenko, J. Dobbing, N. Dolgetta, S.E. Dorling, P.G. Doyle, D.F. Düchs, H. Duquenoy, A. Edwards, J. Ehrenberg, A. Ekedahl, T. Elevant[11], S.K. Erents[7], L.G. Eriksson, H. Fajemirokun[12], H. Falter, D. Flory, M. Forrest[7], J. Freiling[15], C. Froger, P. Froissard, K. Fullard, M. Gadeberg, A. Galetsas, D. Gambier, M. Garribba, P. Gaze, X. Ge[25], R. Giannella, A. Gibson, R.D. Gill, A. Gondhalekar, C. Gormezano, N.A. Gottardi, C. Gowers, B.J. Green, K. Guenther[26], R. Haange, G Haas, G. Hammett[6], C.J. Hancock, P.J. Harbour, N.C. Hawkes[7], P. Haynes[7], J.L. Hemmerich, R. Hemsworth, F.B. Herzog, R.F. Herzog, J. Hockzema, G Hogeweij[15], J. How, M. Huart, T.P. Hughes[4], M. Hugon, M. Huguet, A. Hwang[7], B. Ingram, M. Irving, J. Jacquinot, H. Jaeckel, J.F. Jaeger, G. Janeschitz[13], O.N. Jarvis, F. Jensen, E.M. Jones, L.P.D.F. Jones, T.T.C. Jones, J. Junique, A. Kaye, B.E. Keen, M. Keilhacker, G.J. Kelly, W. Kerner, R. Konig, A. Konstantellos, M. Kovanen[20], P. Kupschus, R. Lässer, J.R. Last, B. Laundy, L. Lauro-Taroni, K. Lawson[7], M. Lennholm, A. Loarte, R. Lobel, P. Lomas, M. Loughlin, C. Lowry, B. Macklin, G. Maddison[7], G. Magyar, W. Mandl[13], V. Marchese, F. Marcus, J. Mart, E. Martin, R. Martin-Solis[8], P. Massmann, G. McCracken[7], P. Meriguet, S.F. Mills, P. Millward, S.L. Milora[23], E. Minardi[22], P.L. Mondino, F. Montvai[3], P. Morgan, H. Morsi, G. Murphy, M. Mynarends, O. Naito[11], C. Nardone, F. Nave[21], G. Newbert, M. Newman, P. Nielsen, P. Noll, W. Obert, D. O'Brien, J. O'Rourke, R. Ostrom, M. Pain, F. Paoletti, S. Papastergiou, D. Pasini, A. Peacock, N. Peacock[7], D. Pearson[12], C. Perry, V. Phillips[28], M. Pick, R. Pitts[7], J. Plancoulaine, J-P. Poffé, F. Porcelli, L. Porte[19], R. Prentice, G. Radford[9], T. Raimondi, P-H. Rebut, R. Reichle[13], G. Rey[16], F. Rimini, D. Robinson[7], A. Rolfe, R.T. Ross, L. Rossi, P. Rutter, H.C. Sack, G. Sadler, G. Saibene, G. Sanazzaro, A. Santagiustina, R. Sartori, C. Sborchia, P.H. Schild, M. Schmid, G. Schmidt[6], B. Schunke, S.M. Scott, A. Sibley, R. Simonini, A. Sips[15], P. Smeulders, S. Sommers, R. Stankiewicz[27], M. Stamp, P. Stangeby[18], D.F. Start, C.A. Steed, D. Stork, P.E. Stott, T.E. Stringer, P. Stubberfield, D. Summers, H. Summers[19], L. Svensson, J.A. Tagle[21], H. Tamnen, A. Tanga, A. Taroni, A. Tesini, P.R. Thomas, E. Thompson, K. Thomsen, J.M. Todd, P. Trevalion, B. Tubbing, F. Tibone, E. Usselmann, H. van der Beken, G. Vlases, M. von Hellermann, T. Wade, C. Walker, R. Walton[6], D. Ward, M.L. Watkins, M.J. Watson, H. Weisen[10], J. Wesson, J. Wilks, U. Willen[5], D. Wilson, T. Winkel, S. Wolfe, B. Wolle[24], D. Wong, C. Woodward, M. Wykes, I.D. Young, L. Zannelli, Z. Zheng[25], Y. Zhu[26], W. Zwingmann.

PERMANENT ADDRESSES

1. UKAEA, Harwell, Didcot, Oxon, UK.
2. University of Leicester, Leicester, UK.
3. Central Research Institute for Physics, Academy of Sciences, Budapest, Hungary.
4. University of Essex, Colchester, UK.
5. Chalmers University of Technology, Göteborg, Sweden.
6. Princeton Plasma Physics Laboratory, New Jersey, USA.
7. UKAEA Culham Laboratory, Abingdon, Oxon, UK.
8. Universidad Complutense de Madrid, Spain.
9. Institute of Mathematics, University of Oxford, UK.
10. CRPP/EPFL, 21 Avenue des Bains, CH-1007 Lausanne, Switzerland.
11. Swedish Energy Research Commission, S-10072 Stockholm, Sweden.
12. Imperial College of Science and Technology, University of London, UK.
13. Max Planck Institut für Plasmaphysik, D-8046 Garching bei München, FRG.
14. Risø National Laboratory, Denmark.
15. FOM Instituut voor Plasmafysica, 3430 Be Nieuwegein, The Netherlands.
16. Commissariat à L'Énergie Atomique, Cadarache, F-13108 St. Paul Lez Durance, France.
17. University of Dusseldorf, FRG.
18. Institute for Aerospace Studies, University of Toronto, Downsview, Ontario, Canada.
19. University of Strathclyde, 107 Rottenrow, Glasgow, G4 0NG, UK.
20. Nuclear Engineering Laboratory, Lapeenranta University, Finland.
21. CIEMAT, Madrid, Spain.
22. ENEA-CNR, Milano, Italy.
23. Oak Ridge National Laboratory, Oak Ridge, Tenn., USA.
24. University of Heidelberg, Heidelberg, FRG.
25. Institute for Mechanics, Academia Sinica, Beijing, P.R. China.
26. Akademie der Wissenschaften der DDR, Berlin, DDR.
27. RCC Cyfronet, Otwock Swierk, Poland.

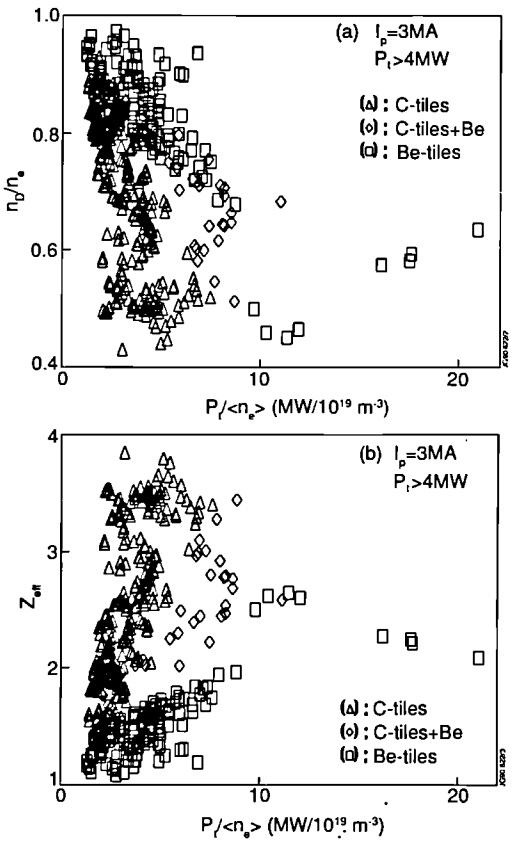

Fig. 1 (a) Dilution factor, n_D/n_e, and (b) the effective charge, Z_{eff}, as functions of power per particle ($P_t/<n_e>$) for carbon limiter tiles, beryllium gettering and beryllium limiter tiles.

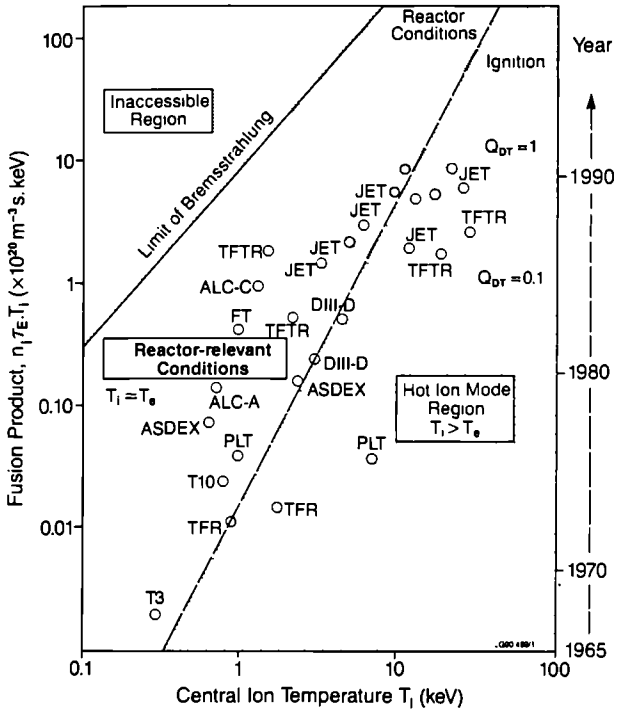

Fig. 2 Overall performance of the fusion product ($n_D(0)\tau_E T_i(0)$) as a function of central ion temperature ($T_i(0)$), for a number of tokamak devices.

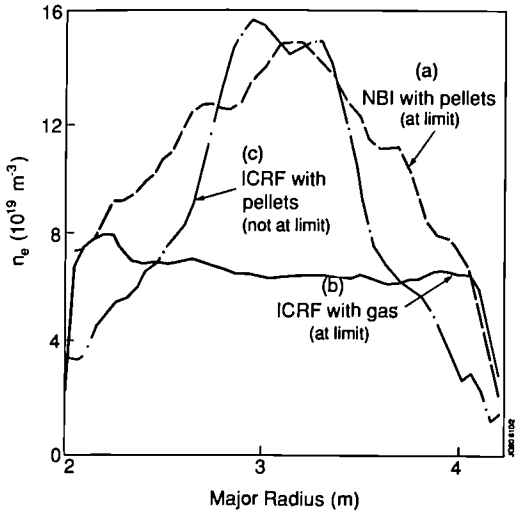

Fig. 3 Electron density profiles for different fuelling and heating methods.

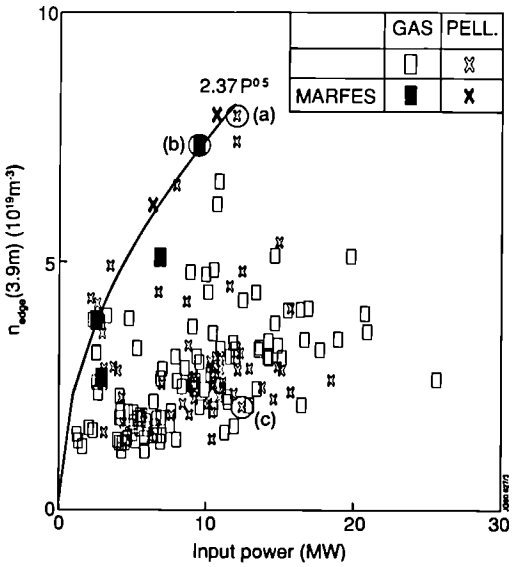

Fig. 4 The edge electron density (n_{edge}) versus input power (P) showing that the density limit occurs at the boundary of the operational domain close to the curve n_{edge} (x10^{19}m^{-3}) = 2.37 $P^{1/2}$(MW). The profiles shown in Fig. 3 correspond to the three data points circled.

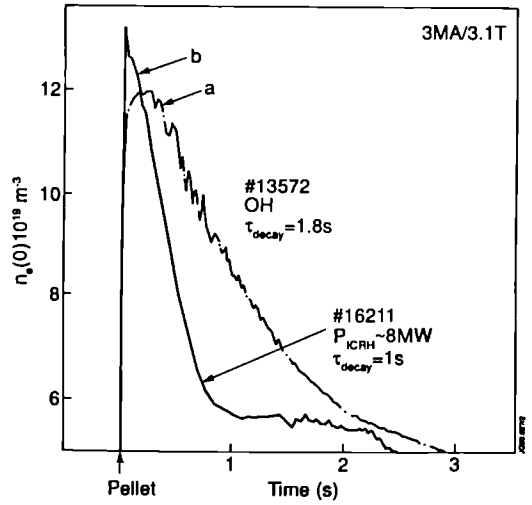

. 5 Decay of central density following pellet injection into discharges with (a) ohmic heating only and (b) ~8MW ICRH.

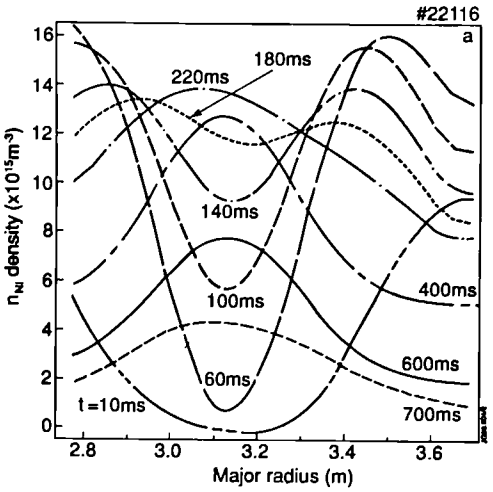

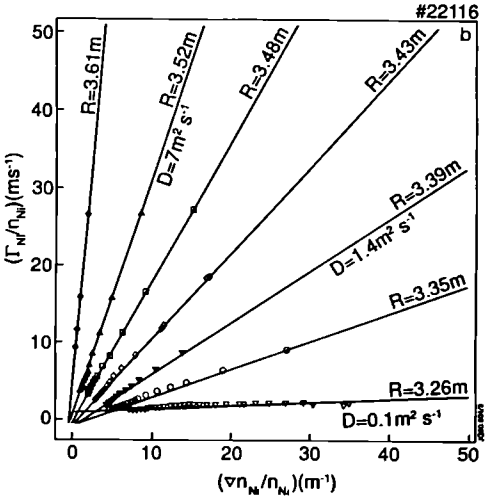

Fig. 6 (a) Nickel density profiles from X-ray tomography at times following laser ablation and (b) normalised particle fluxes versus normalised density gradients for nickel impurities at different plasma radii.

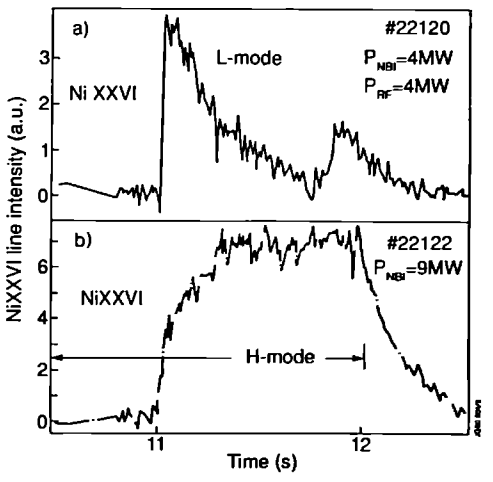

Fig. 7 (a) Temporal evolution of NiXXVI emission in (a) the L-phase and (b) the H-phase of two similar discharges with ~9MW of additional heating.

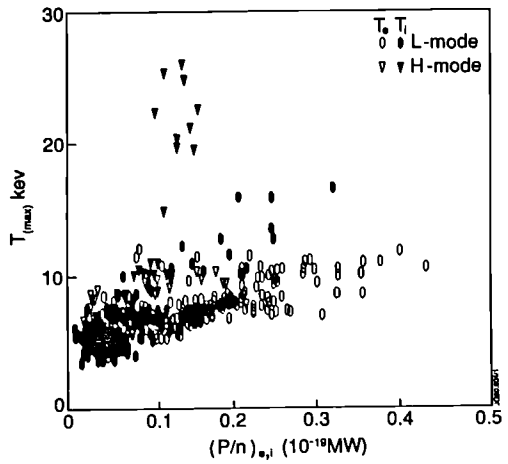

Fig. 8 Central ion (T_i) and electron (T_e) temperatures as functions of power per particle $(P/n)_{e,i}$ to either species.

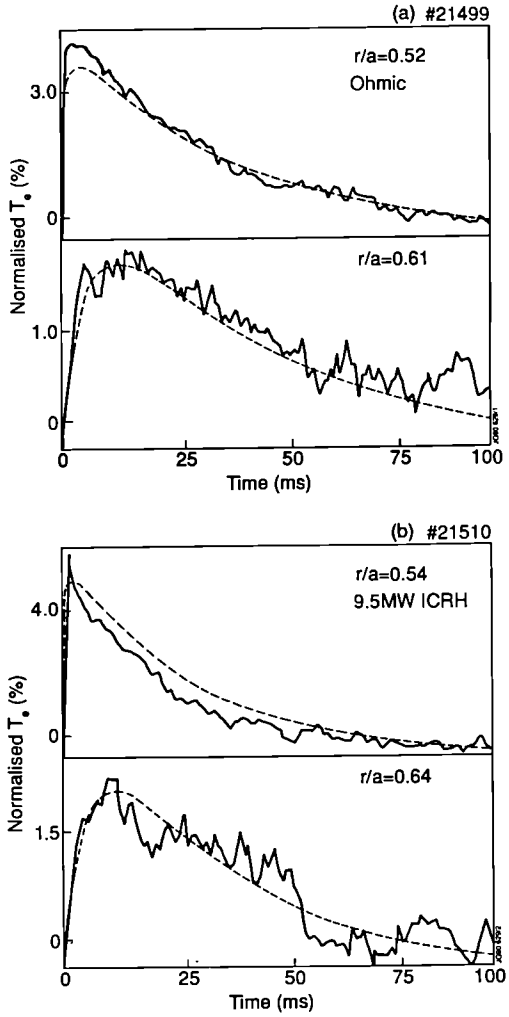

Fig. 9 Temporal evolution of electron temperature perturbations (normalised to the central electron temperature prior to the collapse of a sawtooth) at different radii for 3MA/2.8T discharges with (a) ohmic heating only and (b) 9.5MW ICRH. Dashed lines are from model calculations using $\chi_{HP}=3.2m^2s^{-1}$.

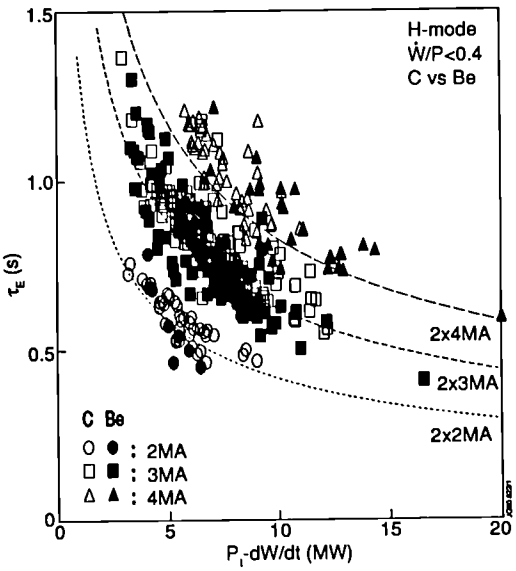

Fig. 10 Global energy confinement time (τ_E) during the H-mode as a function of input power for different currents and first wall materials.

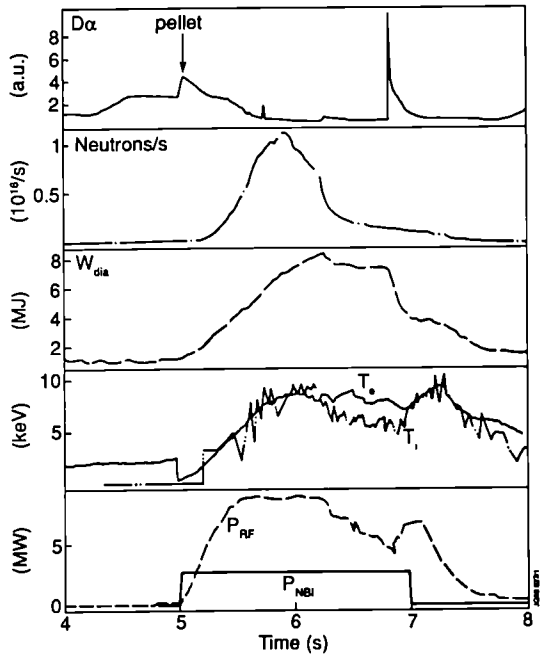

Fig. 11 Characteristics of JET Pulse 22490 in which the good confinement properties of the H-mode and central pellet injection are combined.

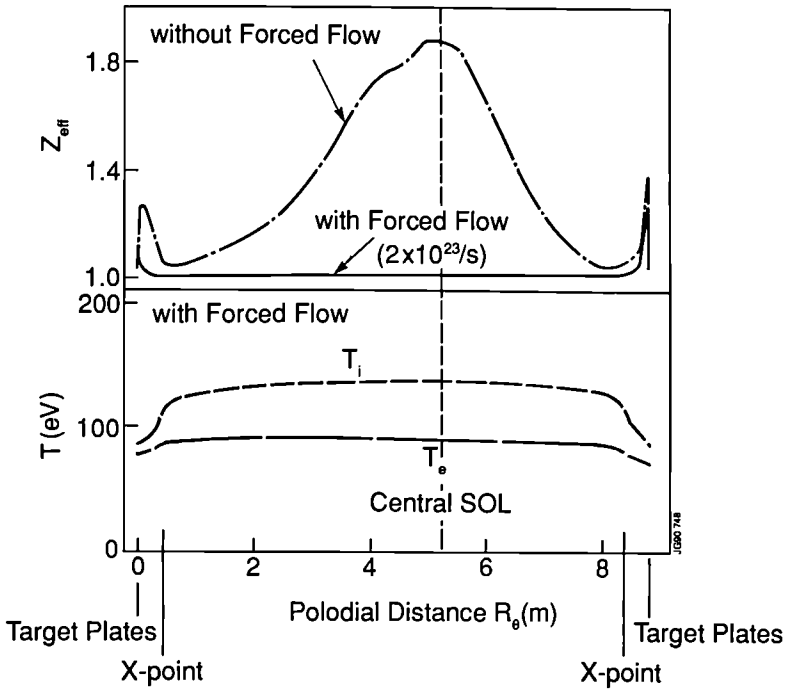

Fig. 12 Poloidal distribution in the SOL and DCP between target plates of (a) the effective ionic charge, Z_{eff}, for cases with and without flow and (b) the electron and ion temperatures for the case with flow.

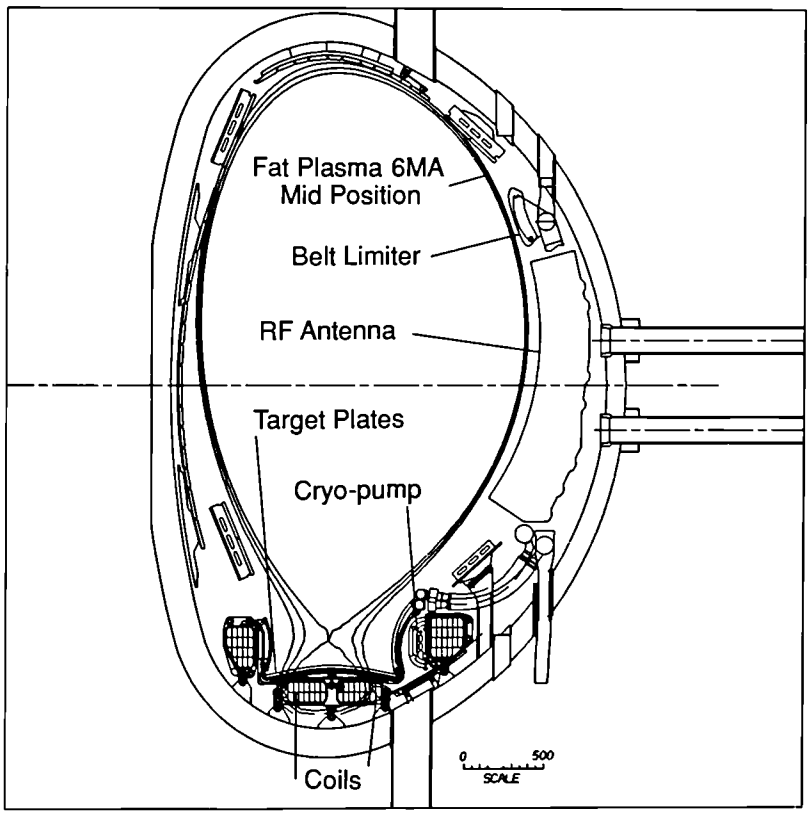

Fig. 13 Cross-section of JET showing the plasma and main elements of the pumped divertor planned for the New Phase of JET.

OPTIMISATION OF PERFORMANCE IN JET LIMITER PLASMAS

Abstract

Improvements to the performance of JET limiter plasmas have been made by increasing the plasma current, by suppressing sawteeth, by peaking the density profile and by using Beryllium evaporation and employing Beryllium limiters. Central electron temperatures $T_e \sim 12keV$, ion temperatures $T_i \sim 18keV$, central electron densities $n_{e0} \sim 2.3 \times 10^{20} m^{-3}$ have been demonstrated in limiter plasmas with currents 3-5MA. A 7MA discharge with $q_\psi \sim 3.2$ has been demonstrated and heating experiments have just begun.

1. Introduction

It has already been shown [1] that the confinement of high current low q limiter plasmas in JET is in line with the expectations of Goldston or Rebut-Lallia scalings [2,3], but that the profiles of density and temperature are rather flat. Projections of the D-T fusion performance of such L mode plasmas in JET [4] suggest that $Q_{DT} \sim 0.5 - 0.8$ might be obtained at 7MA (including the beam driven yield). A more direct extrapolation to DT operation of 4.5MA H mode plasmas already run in Deuterium suggests [5] that higher fusion performance will be obtained using such divertor configurations rather than a limiter configuration despite the higher plasma current. In order to enhance the fusion performance of limiter plasmas without employing a regime of enhanced confinement, it is necessary to make the profiles of density and temperature more peaked as has already been demonstrated at low current in the pellet enhanced plasma [6]. In order to obtain peaked profiles it is necessary to suppress sawteeth as for example in the monster sawtooth regime [7]. Furthermore, in sawtoothing discharges with centrally deposited power, it appears that the incremental confinement time no longer scales favourably with plasma current for $q_{CYL} \lesssim 3$ [8]. With the broad density profiles characteristic of high current sawtoothing discharges neutral beam penetration is poor. This reduces the central ion temperature, reduces beam refuelling of the core and reduces the beam driven fusion yield.

Thus to optimise the fusion yield in JET limiter plasmas requires more than a simple increase of plasma current. It is clearly necessary to suppress sawteeth, produce a high central density, maintain a low edge density and keep the influx of impurities to a minimum. The following sections describe experiments addressing these issues for plasma currents of 3-5MA. The progess of experiments at 7MA currently underway is briefly described.

2. Sawtooth suppression at 5MA

Sawtooth stabilisation during the current rise phase has already been demonstrated [9]. By using a faster current ramp at constant $q_\psi \sim 3.5$ and employing Beryllium evaporation to control the density it has been possible to extend the sawtooth free periods well into the flat top at 5MA [10] as shown in fig 1. An axial electron temperature $T_{e0} \sim 12kev$ has been obtained with a strongly peaked profile as shown in fig 2. The ion temperature is only $T_{i0} \sim 5keV$ so the fusion performance is modest. Note that there are a few sawtooth crashes during the ICRH and during this time the soft X ray inversion radius grows from a small value to $r/a \sim 0.3$. Faraday rotation measurements indicate $q_0 = 0.95 \pm 0.15$ and constant in time during the sawtooth free periods. Since the inversion radius is large we infer that the q profile is rather flat. The fast ion slowing down time is long because the density is low and the electron temperature is high and therefore the fast ion energy content is large (35-50% of total). Normal sawteeth resume shortly after the ICRH is switched off. It is probable that the sawtooth is being transiently stabilised by the fast ions in manner similar to that of the normal monster. However since monster sawteeth do not normally occur during flat top heating at 5MA the detailed q profile shape must be important or it must be necessary to build up a high fast ion pressure to stabilise the sawtooth at high current. It is expected that a continuation of the current ramp will permit sawtooth stabilisation at higher current. The confinement time is plotted against power input for these plasmas and 5MA sawtoothing plasmas in fig 3. It can be seen that the confinement is very close to the Goldston prediction when allowance is made for the fast ion energy content.

3. Peaked density profiles at 5MA

The injection of a string of pellets during the current rise, as shown in fig 4, leads to high central densities $n_{e0} \sim 2.3 \times 10^{20} m^{-3}$ at 5MA. In order to obtain the strongly peaked density profile shown in fig 5 it is necessary that the pellets penetrate deeply and this is achieved by careful choice of pellet timing. The small inversion radius sawteeth present before the first sawteeth are suppressed by the pellets and indeed polarimetric measurements show that q_0 is raised above unity. It is important to keep q_ψ roughly constant during the current ramp and pellet injection since disruptions invariably occur at $q_\psi \sim 4$ if q_ψ is allowed to fall. 6MW of ICRF heating were applied at 5MA after the last pellet and, as shown in fig 4, a transiently enhanced D-D rate is observed. 1.5 sec after the start of ICRH, and after the peak D-D rate, the central density has decayed to $n_{e0} \sim 6 \times 10^{19} m^{-3}$. T_{e0} is much lower than in the experiment of section 2, but $T_{i0} \sim T_{e0} \sim 5keV$ and $Q_{DD} \sim 5 \times 10^{-4}$. The global confinement time is enhanced transiently by $\sim 30\%$ compared with gas fuelled discharges as shown in fig 3.

4. Density profile control in plasmas with strong ion heating

The use of Beryllium limiters has permitted operation with low $Z_{eff} \lesssim 1.5$ at moderate density [11]. However at low density, $P_{TOT}/\langle n_e \rangle \gtrsim 5 \times 10^{-19} MWm^{-3}$, the deuterium concentration n_D/n_e is typically ~ 0.6 similar to Carbon limiters conditioned by Beryllium evaporation or by extensive pulsing in Helium. The main effect of Beryllium (either limiters or evaporation) is improved density control which extends the range of P_{NB}/n_{e0} and, as shown in fig 6, this has resulted in higher ion temperatures in 3MA belt limiter plasmas.

For the case of Carbon limiters and Beryllium evaporation a density profile peaking factor $n_{e0}/\langle n_e \rangle \sim 3$ was obtained as a result of central beam fuelling and low edge recylcling compared to $n_{e0}/\langle n_e \rangle \sim 1.5$ for bare carbon belt limiter plasmas [12]. Unexpectedly, for low density plasmas with Beryllium limiters the density profiles were flat even with central beam fuelling. In order to produce peaked density profiles in this case it was necessary to fuel the target plasma with deeply penetrating pellets. Fig 7 shows the time history of the density profile reconstructed from a series of similar shots. It can be seen that the initial central density is $n_{e0} \sim 7 \times 10^{19} m^{-3}$ with a peaking factor $n_{e0}/\langle n_e \rangle \sim 4$, but that the central density decays during the heating though the profile shape remains peaked. The ion temperature reaches $T_{i0} \sim 18kev$ with a strongly peaked profile $T_{i0}/\langle T_i \rangle \sim 7$. This profile peaking enhances the thermonuclear performance by a factor 3 compared with 'normal' flat profiles in L mode, even though the global confinement is unchanged. In these discharges the ICRH suppresses sawteeth which otherwise would flatten the profiles. In addition ICRF acceleration of injected deuterons increases the driven D-D reactivity by 30-40% in such discharges [13]. The broadening of the neutron spectum due to the ICRF is clearly visible in fig 8. In this case the D-D fusion gain was $Q_{DD} \sim 9 \times 10^{-4}$ which was slightly improved over previous inner wall plasmas at 3MA. Recently yet higher gains, $Q_{DD} \sim 1 \times 10^{-3}$, were obtained in inner wall plasmas at 4.7MA.

5. 7MA plasmas

Plasma currents of 7MA were demonstrated in 1988 [1]. These plasmas were obtained using a simultaneous ramp of toroidal field and plasma current with $q_\psi \sim 2.5$. The flat top was only 2 seconds limited by volts seconds. In order to pass $q_\psi = 3$ early in the current rise without disruption it was necessary to establish early sawteeth by strong gas puffing. This discharge is not suitable for current rise heating because of the variation in toroidal field. Recently, the fast current rise developed for the experiments described in sections 2 and 3 has been extended to 7MA. The flat top was 3 seconds long but 8 Volt-sec remain to extend this further. By making the plasma more D shaped q_ψ was held at ~ 3.2 at 7MA. Sawtooth have been suppressed well into the flat top of a 6MA discharge and suppressed during the rise to 7MA by applying ICRF in the current rise. An electon temperature $T_{e0} \sim 9keV$ was obtained in both cases. Ion heating experiments, using NBI, have begun in these high current discharges.

6. Conclusions

It has been shown that sawtooth can be suppressed and peaked density profiles formed at high current low q belt limiter plasmas. The former produces very high electron temperatures $T_{e0} \sim 12kev$, the latter high densities $n_{e0} \sim 2.3 \times 10^{20} m^{-3}$. The use of Beryllium to control recycling together with central fuelling by pellets has allowed peaked density profiles in 3MA beam heated plasmas with ion temperatures up to 18keV enhancing the thermonuclear reactivity over normal flat profiles. Here ICRF suppresses sawteeth and enhances the beam plasma reactivity by the acceleration of injected deuterons. The highest values of D-D fusion gain yet obtained in a limiter plasma on JET is $Q_{DD} \sim 1 \times 10^{-3}$.

Thus the foundations have been laid for performance optimisation at the highest plasma currents in JET (up to 7MA). These promising results suggest that the performance projections for 7MA D-T operation in JET [4] might indeed be pessimistic.

Acknowledgements

It is a pleasure to acknowledge the other members of the Task Forces who carried out this work- D.Bartlett, M.Brusati, J.P.Christiansen, H.D'Esch, R.Giannella, A.Gondhalekar, G.Cottrell, T.T.C.Jones, P.Kupschus, G.Magyar, F.Marcus, P.Nielsen, D.Pasini, R.Prentice, G.Sadler, M.Stamp, A.Tanga, A.Taroni, and H.Weisen.

References

[1] Bickerton R.J and the JET Team, Plasma Physics and Controlled Nuclear Fusion Research, Proceedings 12th IAEA Conference, Nice, Vol 1 (1988) p41

[2] Goldston R.J. Plasma Physics and Controlled Nuclear Fusion, **26** p87 1984

[3] Rebut P-H, Lallia P, Watkins ML, Plasma Physics and Controlled Nuclear Fusion Research, Proceedings 12th IAEA Conference, Nice, Vol **2** (1988) p191.

[4] Gibson A and the JET Team Plasma Physics and Controlled Nuclear Fusion, 30 p1390 1988.

[5] Tanga A and the JET Team, This conference

[6] G.L.Schmidt and the JET Team, Plasma Physics and Controlled Nuclear Fusion Research, Proceedings 12th IAEA Conference, Nice, Vol 1 (1988) p215.

[7] Campbell D.J et al, Phys. Rev. Lett. 60 p2148 1988

[8] Bhatnagar V.P et al, Plasma Physics and Controlled Fusion 31 (1989) p333 and JET-P(88)51.
[9] Bures M et al, Plasma Physics and Controlled Fusion 31 (1989) p1843 and JET-P(89)03 p77.
[10] Lomas P.J et al, Proc 17 European Conference on Controlled Fusion and Plasma Heating 1 p5 (Amsterdam) 1990.
[11] Keilhacker M and the JET Team, Phys. Fluids B 2 p1291 1990.
[12] Jones T.T.C et al, Proc 17 European Conference on Controlled Fusion and Plasma Heating 1 p9 (Amsterdam) 1990.
[13] Sadler G et al, Proc 17 European Conference on Controlled Fusion and Plasma Heating 1 p1 (Amsterdam) 1990.

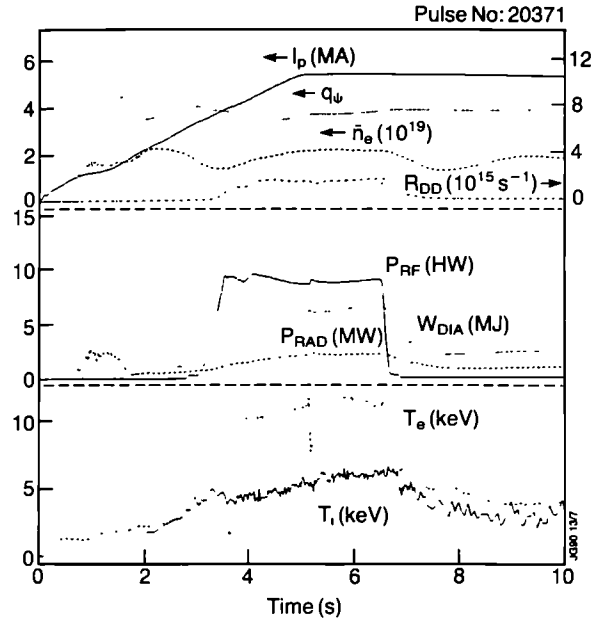

Fig 1. Various time traces for a 5MA plasma where ICRF is applied during the current rise and showing sawtooth stabilisation.

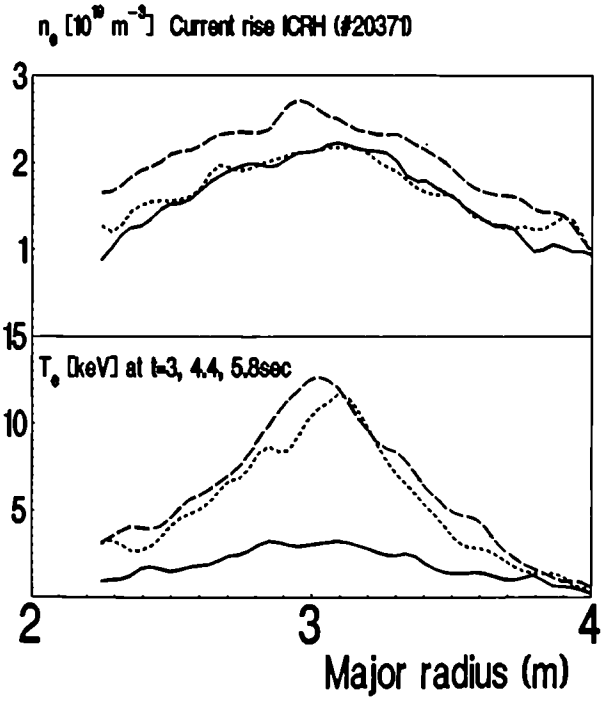

Fig 2. Density and temperature profiles for the pulse illustrated in fig 1.

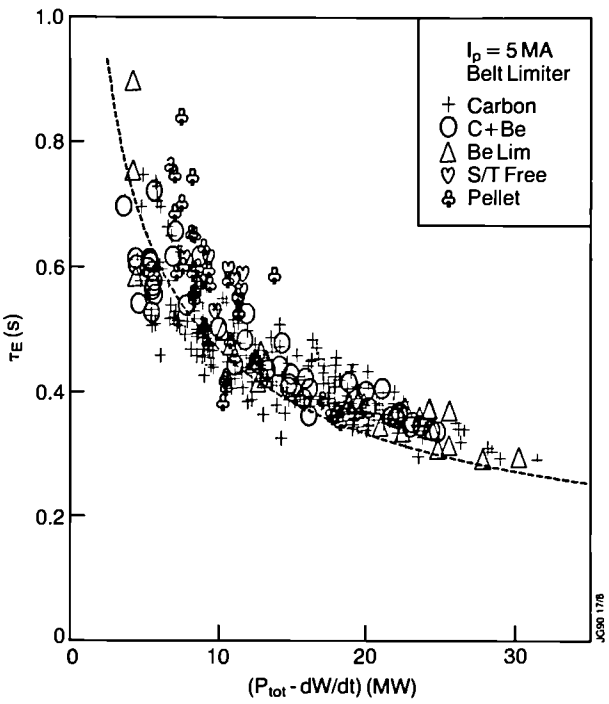

Fig 3. Confinement time plotted against loss power for 5MA belt limiter plasmas. The various symbols indicate the limiter material and distinguish the sawtooth free cases described in section 2 and the pellet cases of section 3.

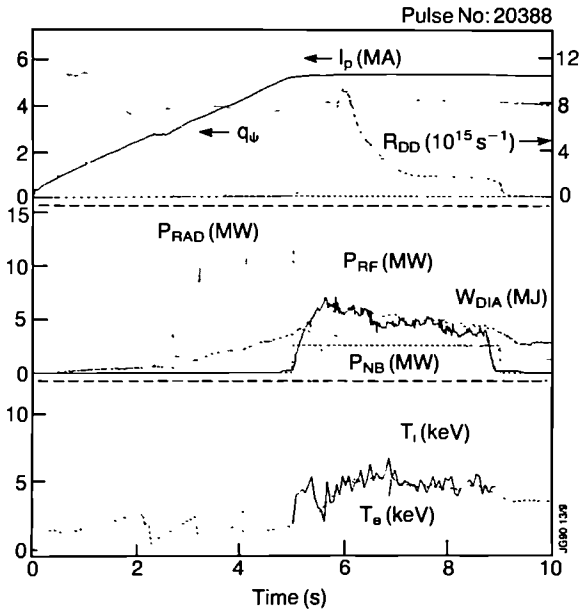

Fig 4. Various time traces for a 5MA plasma with pellet injection during the current rise followed by ICRF heating in the flat top.

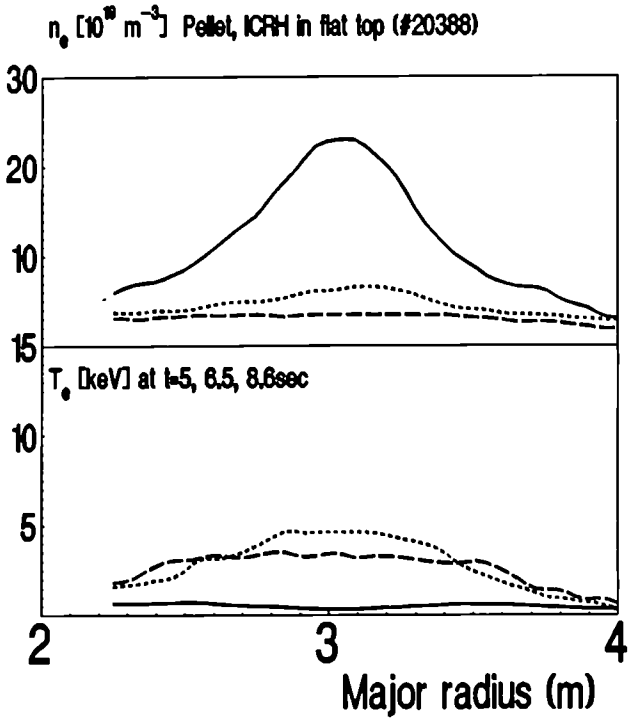

Fig 5. Density and temperature profiles for the pulse illustrated in fig 4.

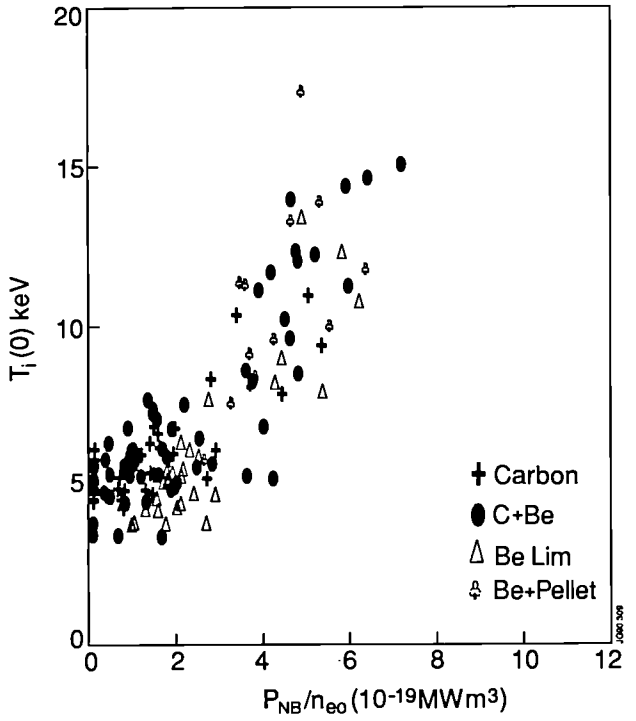

Fig 6 Axial ion temperature plotted against Neutral Beam power normalised to the axial density for 3MA belt limiter plasmas. The symbols indicate the limiter material and distinguish pellet fuelled target plasmas.

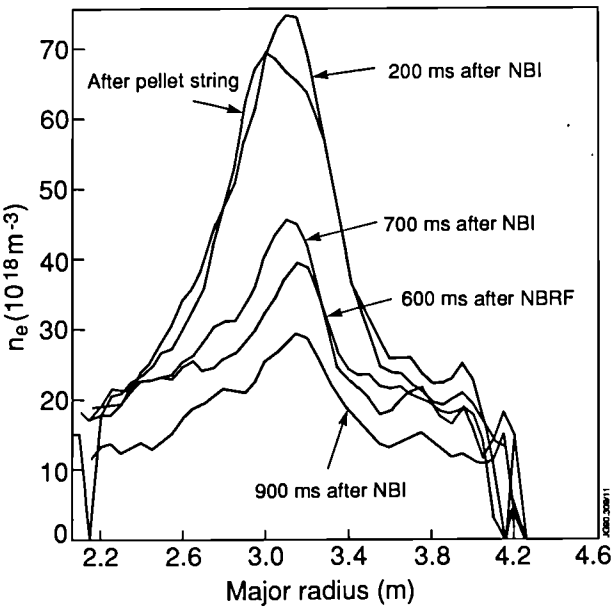

Fig 7. Density profile evolution reconstructed using LIDAR data for several similar discharges where heating was applied to pellet fuelled target plasmas.

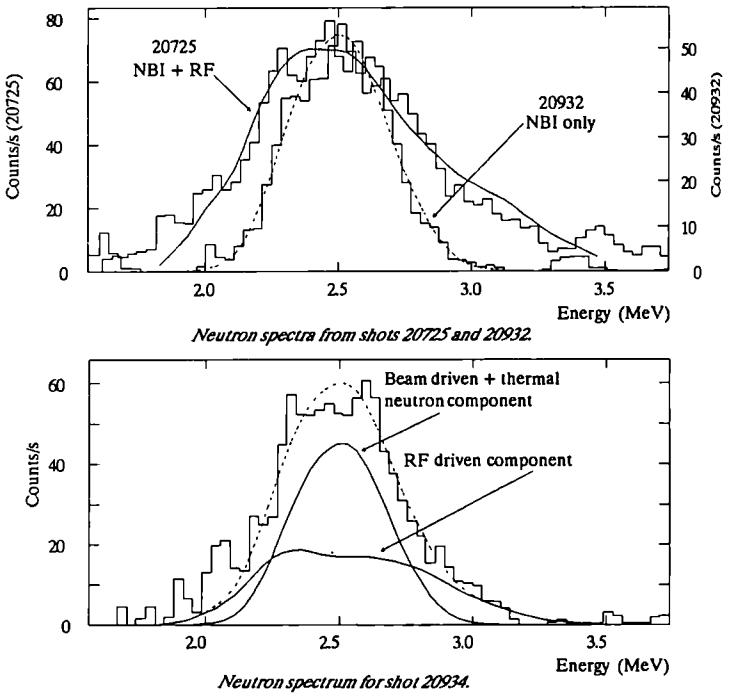

Fig 8 Neutron energy spectra illustrating ICRF enhanced reactivity. Top compares two discharges with similar neutral beam power with and without ICRF and shows the broadening of the spectrum. The bottom shows an unfolding of the spectrum to illustrate the ICRF driven component.

High performance H modes in JET

The JET Team

(presented by A.Tanga)

JET Joint Undertaking, Abingdon, Oxon OX14 3EA, UK.

Abstract

In JET the scientific properties and technical basis of good confinement regimes have been evaluated in the light of the potential extrapolation of such regimes to reactor requirements. In this paper the main experimental H-mode results are discussed highlighting global confinement scaling, low q regimes, the role of the target plate material, the density limit, and finally sawtooth suppression and hot-ion mode.

1. Introduction

The H-mode in JET has been demonstrated with single and double null x-point configurations, which in general are marginally limiting at the x-point target tiles. H-modes have been achieved with NB heating, ICRF heating and with combined NB and ICRF heating. The power threshold for the H-mode and the global energy confinement time does not depend on the heating method. In the ELM free H-mode there is an improvement of about a factor of two in the global confinement time compared to JET limiter L-modes, up to the total additional power of 25MW.

The development of the JET H-mode, towards steady state conditions, depends on wall conditioning and on the material of the divertor target plates, which determines the amount and type of impurity released, and affect the time evolution of plasma density. The substantial reduction of Z_{eff} ($\simeq$ 2.) and improvement of n_D/n_e to 0.8-0.9, produced by routine Beryllium gettering of the graphite tiles was probably mainly due to the nearly complete removal of Oxygen and Oxygen generated Carbon sputtering. The reduction of Nickel was mainly due to the Beryllium gettering of the ICRF antennae screens. As a consequence of lower radiation losses and improved density control longer ELM free H-mode phases have been achieved ($\lesssim$ 5.4s) .

The transport of impurities in the JET H-mode is characterized by a balance between neoclassical effects and anomalous transport leading to a build up of impurities in the plasma ($\tau_{imp}/\tau_E > 1$) [1]. Further local analysis of energy transport in high power H modes confirms the reduction in thermal conductivity (energy flux/gradT) across the whole plasma cross section reported earlier [2] .

In the JET H-mode the density limit corresponds to the radiative collapse which ends the H phase.

With additional power well above the threshold, the H-mode can occur simultaneously with other plasma regimes such as the monster sawtooth or the hot-ion mode.

In the hot-ion H-mode, with NB(D)injection, at moderate plasma densities ($< n > 1 \div 4.10^{19}$ m^{-3}) T_i is 2 or 3 times larger than T_e ($T_i \gtrsim$ 22keV, $Q_{dd} \simeq 2.5x10^{-3}$). The values of Q_{DT} for D-T simulated versions of the same discharges are above 0.5 for times of the order of one energy confinement time.

2. Operational regimes

The H-mode in JET has been demonstrated in single null (I_p < 5MA) and double null (I_p <4.5MA) configurations , generally with the plasma limiting on the x-point target tiles , but also with the plasma in contact with the inner wall. In single null configuration the H-mode has been achieved with NB at 80keV and at 140keV both in deuterium and hydrogen target plasmas. In double null configuration, where it has been possible to obtain good RF coupling, the H-mode has been achieved with ICRF alone in dipole with Hydrogen minority, and in combination with NB(D) in Deuterium plasmas. The JET H-mode is characterized by a transition to an ELM free period lasting several seconds. The duration of the H-mode is considerably shorter for power in excess of 10MW due to a strong carbon influx from overheated graphite dump tiles [3] .

The threshold power for the H-mode was similar for double and single null configurations, with ICRF and NB heating. The H-mode power threshold was lower with a well conditioned vessel. The power threshold, while scaling approximately linearly with the applied toroidal field as reported earlier [4], does not show a clear dependence on plasma current or plasma density. Scans of the plasma radial position show a minimum power threshold if the gap between the plasma and limiter, or between the plasma and the inner wall is above 5-8cm. For shorter distances the threshold power increases. H-mode was achieved even with the plasma in contact with the inner wall protection tiles, which required a threshold power of 10 MW at B_T =2.2T. Plasma recycling and power load were distributed on the inner wall. We think that this regime is similar to the inner wall H-mode achieved in DIII-D [5] . Fig 1. shows the plot of additional heating power versus the gap between the plasma and the inner wall. L marks the discharges which had not undergone an H transition, while H marks the H modes. The H-mode power threshold is a function also of the position of the x-point as determined from magnetic diagnostics [6] . The threshold for H-mode has only a weak dependece on the location of the x-point within 10 cm outside the surface of the dump plate, with the plasma in a marginal limiter configuration or 10 cm inside, with plasma in x-point configuration.

3. Global confinement

The main properties of global confinement time of the JET H-mode have been extended to higher additional power. The general trend of the global energy confinement time, as a function of the total loss power, is shown in fig 2. The two main trends of increase with plasma current and degradation with heating power continue at high powers the trend reported earlier [4] . The scaling of the global confinement time is similar in single null and double null configuration. From the analysis the data it appears that the global confinement time has only a weak dependence on the toroidal field (as $B_T^{0.3 \div 0.07}$). In operation at low values q_{cyl} it appeared that there was not an abroupt deterioration of confinement in the approach to q_{cyl} of 2, as shown in fig 3. [7]. The scaling of the global confinement time observed in the JET H-mode is similar to that observed in other tokamaks. A size scaling has been derived by combining data from JET and DIII-D [8]. A large database with data from JET, DIII-D, ASDEX, JFT2-M, PDX and PBX has been created, the scaling obtained by the analysis of the data of all these tokamak is $\tau_E = 0.07 A^{0.5} I^{0.94} P^{-0.68} R^{1.72} k^{0.68} (R/a)^{-0.13}$, when the toroidal field and density dependence are suppressed [9]. As an example a plot of the JET data versus the combined H-mode scaling, is shown in fig. 4. A detailed analysis of the local transport of JET H-mode will also be presented at this conferece [10].

4 Approach to steady state conditions

The ELM free H-mode is a transient effect which is terminated either by radiative collapse, for additional input power below 10MW, [11]; or by carbon influx, for power in excess of 10MW.

4.1 Carbon Influx

A strong carbon influx, which terminates the H-mode, enter the plasma when the surface temperature of the dump plates exceeds the temperature of 2500 C. The onset of the carbon influx can be delayed by radial sweeping of the x-point position or, and by a strong gas puff. With strong puff long ELM free H-modes phases have been obtained, exceeding 5 seconds as shown in fig 5(a,b) The main effect of strong gas puff is a reduction of the surface temperature of the x-point tiles (fig 5 c,d) in the heated zone where the power is deposited by fast ions on drift orbits. [3,6] . The reduction in temperature is probably caused by reduced ion temperature and/or increased ion collisionality. The reduction in temperature leads to a significant drop in carbon sublimation and radiation enhanced sputtering. The gas puff causes increased divertor radiation losses with general reduction in conduction losses.

4.2 Radiative collapse.

The impurity confinement time, as determined by laser blow off measurements and impurities transport computer simulation [12] is much longer than the energy confinement time, with typical values up to 4s. [1,12] As an example the time evolution of the concentration of NickelXXV and NickelXXVI, obtained by laser blow-off of a Nickel coated target, are shown in fig 6. the result of transport analysis show that there is an outward flow of impurities, [1,12] . The plasma behaves as a " leaky " integrator. For intrinsic impurities, in the H-mode, the outward flow is an order of magnitude smaller than the inward flow, which is generated by the plasma interaction with the dump plates. Consequently, during the ELM free H-mode the concentration of the intrinsic impurities increases continously as a function of time, until the total radiated power becomes excessive [11] . However if the inflow of intrinsic impurities could be reduced by at least a facor of 5, by for example the use of a pump divertor, the simulations show that a balance could be reached after a few impurity confinement times at levels of radiation compatible with the input power.

5. Effects of dump plate material on the H-mode.

The comparative properties of graphite and Beryllium gettered graphite have been studied.

With graphite tiles Oxygen and Carbon were the dominant impurities , radiative losses by Oxygen were dominant at high densities. Among other impurities Nickel, mainly generated by the ICFR antennae screens, accounted for a 10% fraction of the radiated power. With Beryllium gettered graphite tiles the concentration of Oxygen was reduced to a negligible amount. The reducion of Carbon concentration can be explained as due to the absence of Oxygen sputtering generated Carbon impurities as in the case of Beryllium gettered graphite limiter [13] .

In fig 7 the trend of Z_{eff} , as measured by visible bremsstrahlung, versus the total loss power (total input power minus the time derivative of the plasma energy) is shown. Fig 7 shows an average reduction of 1-2 units, at all levels of power. Consequently charge exchange spectroscopy measurements show that with Beryllium gettred graphite dump plates the ratio of electron to deuteron density was 0.8-0.9, whilst without Beryllium gettering it was 0.5-0.6.

6 Density limits

During the H-mode generally the plasma density increases continuosly until a radiative collapse of the H-mode occurs, [11] , precipitating an H to L transition and sometimes a full plasma disruption. For the H-mode the density limit coincides with the high density prior to the H to L transition. The limit on the plasma density is caused by the fact that the power which is radiated by the bulk of the plasma approaches the input power. It is therefore natural to expect the density limit to scale with the square root of the total input power with a scaling similar to that observed in in recent JET limiter discharges [14] . The values of the maximum volume average electron density prior to the H to L mode transition have been plotted versus the total input power in fig 8, for a series of 3MA H-mode discharges. the experimental points with Z_{eff} smaller than 3 (crosses) have a higer density than those with Z_{eff} larger than 3. For reference a Hugill plot of the non disrupting H-mode pulses is shown in fig 9 for discharges with Beryllium gettering.The line $qnR\,B_t = 20x10^{19}$ $m^{-2}T^{-1}$ encompasses the values for the dicharges with moderate additional heating (< 10MW) and fuelled by gas puffing. The lower limit $qnR\,B_t = 12x10^{19}$ $m^{-2}T^{-1}$ refers to Ohmic x-point

discharges. Preliminary results have been achieved with central pellet fuelling which have produced more peaked density profiles. The values of the pellet fuelled discharges are not shown in fig 9.

7. Sawtooth stabilization

Sawtooth suppression has been observed in H-mode discharges with NB and ICRF heating. The time evolution of a series of discharges showing sawtooth suppression during H-mode is presented in fig.10.

With NB heating in excess of 8MW, at least twice the power threshold for H-mode transition, injected into a relatively low density ohmic deuterium target, the H-mode is accompained by a period of sawtooth stabilization of the duration of.6 -.8 s. In this phase a modest enhancement (10-15%) of central ion and electron temperatures is observed.

With ICRF heating during the H-mode [15] sawtooth suppression occurs routinely with ICRF input powers in excess of 7MW. The maximum duration of the monster sowtooth has been 2.5s. The start and end time of sawtooth suppression was not correlated with the H-mode phase, but sometimes the monster crash caused an H to L transition. The temperature peaking factor obtained in sawtooth suppressed H-modes is enhanced by approximately 50% . A series of electron temperature profile shapes with sawtooth suppressed H-modes is shown in fig 11. Here the peaking factor ranges between 3 and 4 (with electron pressure peaking factors between 4 and 5) with values of cylindrical $q = 3.2$ and averages densities in in the range $2 - 4 \times 10^{19} m^{-3}$. It should be noted that in this case the shape of the electron temperature profiles are similar to those obtained in the case of limiter monsters [16] and that the value of the edge plasma temperature is not very high.

With combined ICRF/NB heating sawtooth suppresion in H-mode has also been achieved, as shown by one of the traces in fig 12. In this pulse, ($P_{RF} = 2$MW and $P_{NB} = 6$MW, $< n > = 2.5$E19m-3). Polarimetric analysis of the safety factor radial profile indicate that the central value of q is driven below unity in a way similar to other monster sawtooth, while estimates of the content of fast particles confirm the agreement with the theoretical expectations of sawtooth stabilization.

8. Hot-ion H-mode

In x-point configuration with NB injection in a low density ohmic target it has been possible to produce simultaneously a hot-ion plasma and an H-mode transition. This regime is characterzed by very high ion temperatures in excess of 20keV, while the electron temperature vas 8-10keV. For large values of NB power and low densities the ion temperature profile is very peaked : The ratio of central to volume average ion temperature reaches values of 4-5 .

The D-T performances of these pulses ara examined by considering the standard $n_D \tau_E T_i$ diagram, shown in fig 13. Here the Q curves are for parabolic profiles of density and temperature raised to the power 1 2 and 3/2 respectively. The Q curves are rather insensitive to the form of the profiles. The time evolution of plasma parameters for pulse 20981 are shown in fig 14.

The time behaviour of the pulse was simulated by the 1 1/2-d TRANSP code for the actual conditions of NB injection and background plasma. A good check on the consistency of this data is that of the predicted and measured neutron yeld. The D-T simulations are completed by rerunning the code with the same measured profiles and replacing the background deuterium plasma with a tritium or with a 50-50 D-T mixture. The results are shown in fig 15. Here the time evolution of the fusion power is shown in its components for the case of deuterium injection in a Tritium plasma. The NB power was 17MW, the time derivative of plasma stored energy was 8MW. With Q defined as follow $Q = P_{th-\alpha}/(P - dW/dt) + (P_{b-th} + P_{\alpha b})/P$, the peak value corresponds to Q=0.77 [17].

9. Conclusions

a) The experiments at JET have shown that the ELM free H-mode is a transient plasma regime. The analysis of the results of impurities injection experiment and of the spectroscopical data suggests that if one could control the plasma density and drastically reduce the influx of impurities the H-mode could reach a steady state transport equilibrium.

b) The H-mode is achieved in a configuration with a magnetic separatrix, which can be marginally limiting on the x-point dump plates or on the inner wall protection plates. A parameter related to the shear at the plasma edge, for this marginally limiting configurations, could be the ratio between q_ψ and q_{cyl}. H-mode has been achieved with q_ψ larger or equal to 7-8 while q_{cyl} was 2-3.

c) In the H-mode the global energy confinement time shows an improvement of approximately a factor of two over the limiter L-mode independently of the heating method and in the range of additional power up to 25MW.

d)The radiation collapse, which terminates the H-mode, determines the values of the density limit, which scales with square root of the input power.

e) An improvement in plasma purity and reduction of fuel dilution has been achieved with Beryllium gettering of graphite tiles.

f) In low density ohmic target, and largely with ICRF heating it as been possible to achieve transient stabilization of sawteeth during the H-mode

g) With NB injection in low density deuterium plasmas a hot-ion plasma has been created during the H-mode. In these discharges the highest plasma thermonuclear reactivities have been obtained.

References :

1) Giannella R. et al. in Proc. of 16th European Conference on Contr. Fusion and Plasma Phys., Venice, 1989 Vol. I p.209.

2) Watkins M.L. et al. Plasma Phys. and Contr. Fusion Vol 31, p. 1713, (1989).

3) Stork D., et al. Proceedings of 9th International Conference on Plasma Surface Interactions, 21-25 May 1990, Bournemouth,UK paper P 25.

4) Keilhaker M. for the JET Team, Proc. 12th Conference on Plasma Physics and Controlled Nuclear Fusion, 12-19 October 1988, Nice, France, Vol I p. 159.

5) Jackson G.L., et al., Bull. Am. Soc. Vol 33 p. 1963 (1988)

6) O'Brien D.P., et al., Proc. 17th EPS Conference on Controlled Fusion and Plasma Physics, 25-29 June 1990, Amsterdam, The Netherlands, Vol I p.251.

7) Lazzaro E., et al., "H-mode confinement at low q and high beta in JET " to be published in Nuclear Fusion.

8) Shissel D.P., De Boo J.C., et al., Tubbing B.J.D., et al. "H-mode Energy Confinement scaling from DII-D and JET Tokamaks" to be published in Nuclear Fusion

9) Cordey J.G., et al., at this conference paper IAEA-CN-53/F/3-19

10) Taroni A., Tibone F., et al., at this conference paper IAEA-CN-53/A/2-1

11) Tanga A., et al., Nucl. Fus. Vol 27, p. 1877 (1987).

12) Lauro-Taroni L., et al., in Proc. 17th EPS Conference on Controlled Fusion and Plasma Physics, 25-29 June 1990, Amsterdam, The Netherlands, Vol I p.247.

13) Thomas P.R. for the JET Team, "Results of JET operation with Beryllium", Proceedings of 9th International Conference on Plasma Surface Interactions, 21-25 May 1990, Bournemouth,UK paper I:01.

14) Gibson A. for the JET Team " Fusion relevant performances in JET ", invited paper 17th EPS Conference on Controlled Fusion and Plasma Physics, 25-29 June 1990, Amsterdam, The Netherlands, to be published on Plasma Physics and Controlled Fusion
and Smeulders P. for the JET Team, at this conference, paper IAEA-CN53/A-3-4.

15) Tubbing B.J.D., et al., Nucl. Fus. vol 29, p. 1953 (1989)

16) Campbell D.J., et al., Proc. 11th Conference on Plasma Physics and Controlled Nuclear Fusion, 13-20 November 1986, Kyoto, Japan, Vol I p. 441.

17) Stubberfield P.M., Balet B. and Cordey J.G., "Extrapolation of the high performances JET plasmas to D-T operation " to be publlished on Plasma Physics and Controlled Fusion.

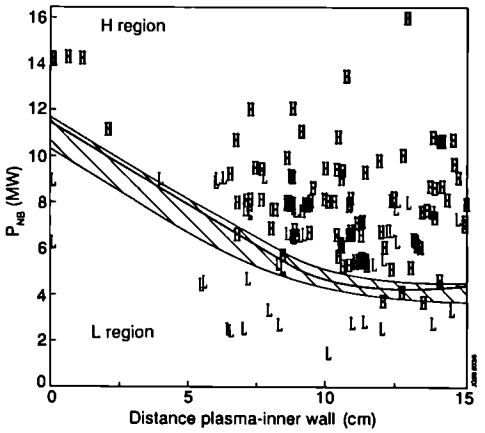

1) Plot of power threshold for H-mode transition as a function of the gap between the plasma and the inner wall protection tiles, for a series of NB heated disharges. Plasma current was 3MA, Toroidal field 2.2T. The symbol H represents the discharges which made the transition, the symbol L represents those discharges which stayed in L-mode. In the H area there are some discharges which did not make the transition.

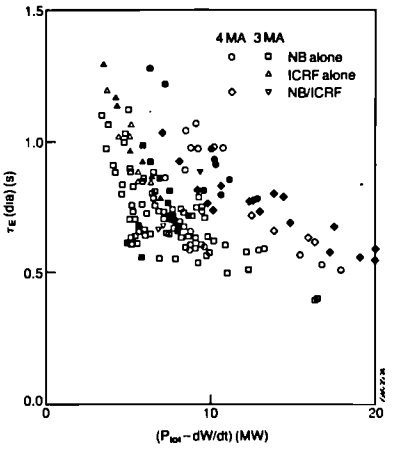

2) Global energy confinement time versus total loss power for all the 3MA and 4MA discharges with $(dW/dt)/P < 0.3$. The solid points refer to pellet fuelled discharges.

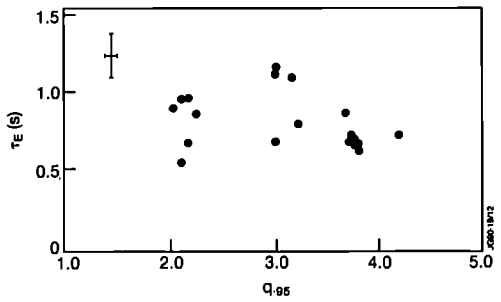

3) Global energy confinement time as a function of the safety factor at 95% of the flux surfaces. The data refer to a set of 3MA discharges in deuterium with NB heating in a narrow power range around 9MW. The range of toroidal field is betwwen 1.2 and 2.4T.

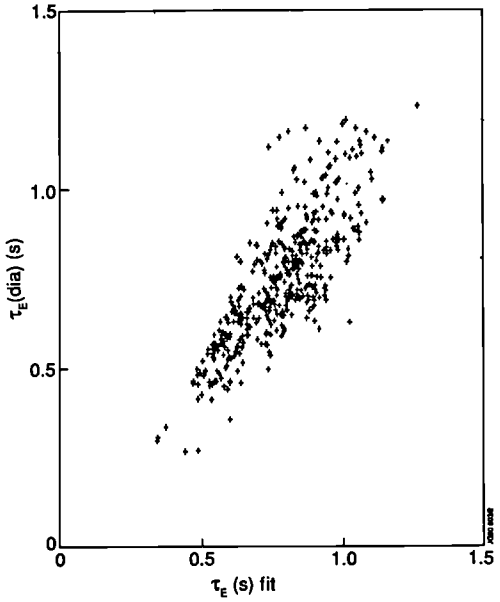

4) Global energy confinement time as measured, versus H-mode scaling derived by combining data from JET, DIII-D, PDX, PBX, JFT2-M.

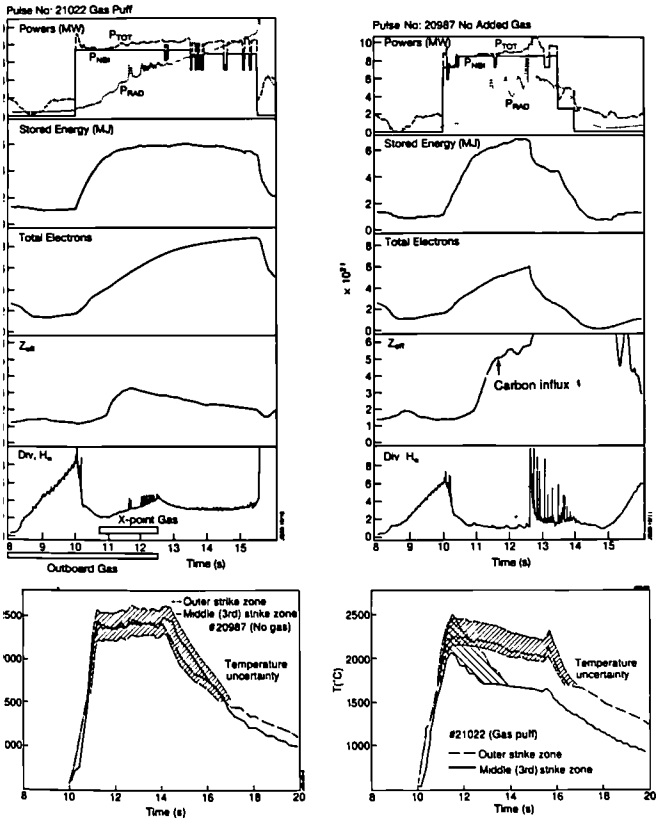

5) Comparison of long pulse H-mode (pulse 21022) with (a) added gas, and (b) a discharge with same plasma and similar NB power with no added gas. The early carbon influx in the no gas shot can be clearly seen.in (c) and (d) the measured surface maximum temperature of the dump plate carbon tiles for the discharges in (a) and (b) respectively.

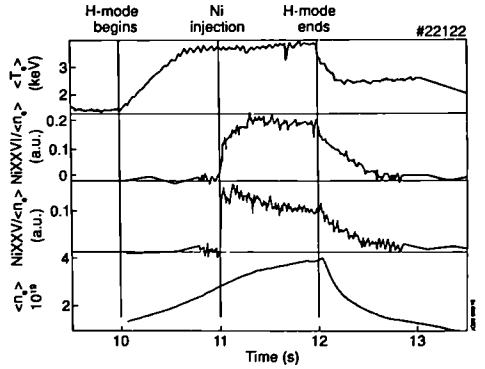

6) Time evolution of the ratio of the Nickel intensities during an H-mode. the Nickel is injected with laser blow-off tecnique at t = 11 s. Form top to bottom Volume average electron temperature, traces of density normalised NickelXXVI and NickelXXV, volume average plasma density.

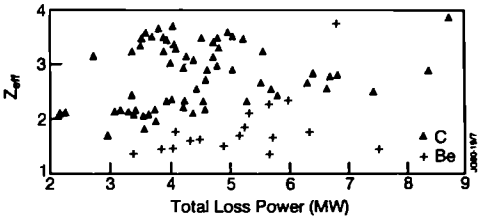

7) Comparison of the values of Z_{eff} from horizontal bremsstrahlung between Carbon and Beryllium gettering for 3MA H-modes.

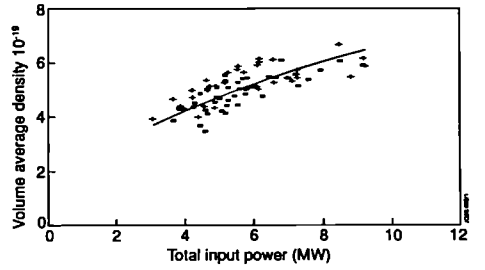

8) Volume average electron density at the end of 3MA H-mode pulses versus total input pover. The crosses refer to pulses with Z_{eff} less than 3.0 , while the squares refer to pulses with Z larger than 3.0. The line is $n_e(10^{19}m^{-3}) = 2.12 \times P^{0.5}(MW)$

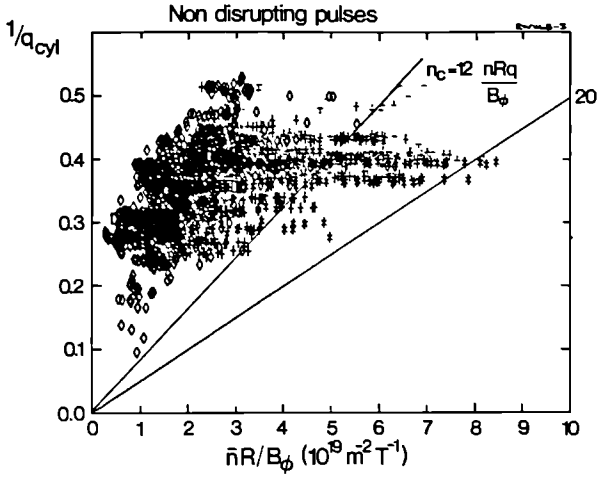

9) Hugill plot for ohmic and additionally heated x-point discharges. Symbols: diamonds represent ohmically heated plasmas, crosses represent Neutral Beam heated plasmas, asterisks represent combined ICRF and NB heated plasmas.

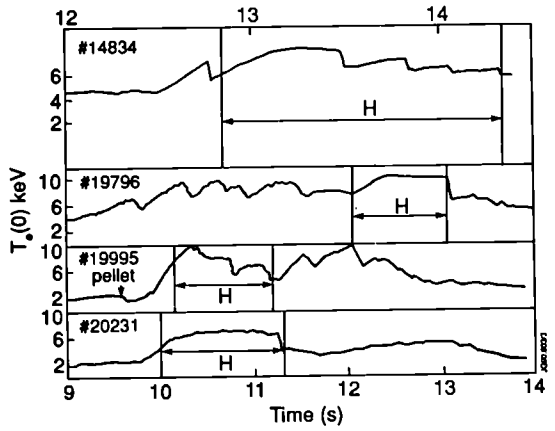

10) Time evolution of central electron temperature in H-modes with suppressed sawtooth: pulse no.14834 NB heating, pulse no. 19796 NB/ICRF, pulses no.19995 and no.20231 ICRF heating.

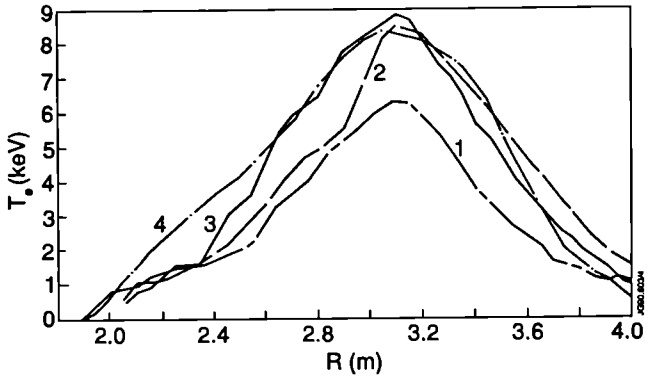

11) LIDAR electron temperature profiles of H-mode with suppressed sawtooth, 1. pulse no. 20231, 3. pulse no. 19995, 4. pulse no. 19796, 2. limiter comparison case pulse no. 12924

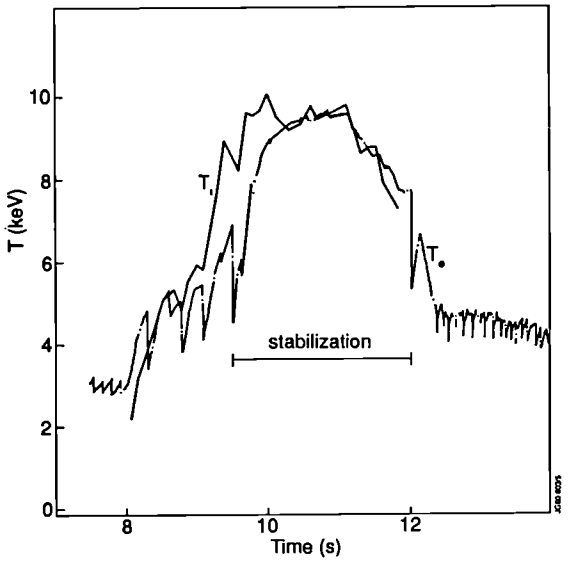

12) Time evolution of ion and electron temperature for a sawtooth suppressed H-mode with combined ICRF and NB heating

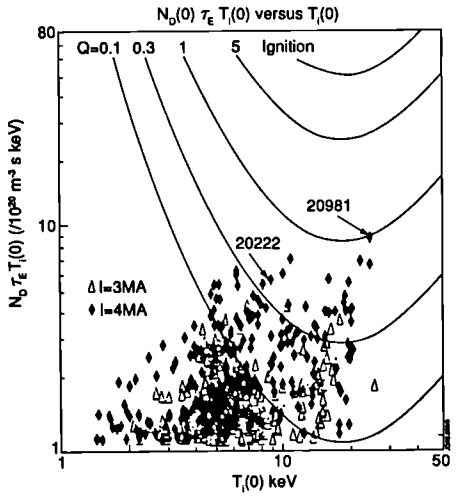

13) $n_D\tau_E T_i$ versus T_i (0)

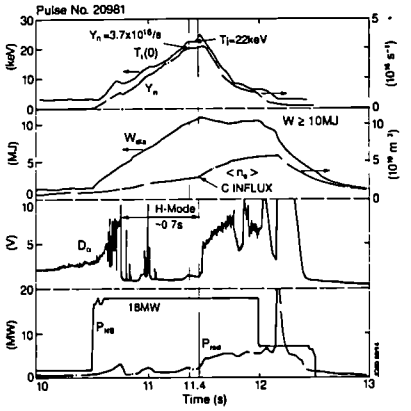

14) Time evolution of high fusion yeld pulse no 20981. from top to bottom are depicted the central ion temperature T_i , the total neutron yeld Y_n the plasma diamagnetic energy W_{dia} , the volume average electron density n_e , and D_α intensity near the x-point, the neutral beam power and the radiated power loss as a function of time. The carbon influx at 11.5 s is followed by the loss of the H-mode.

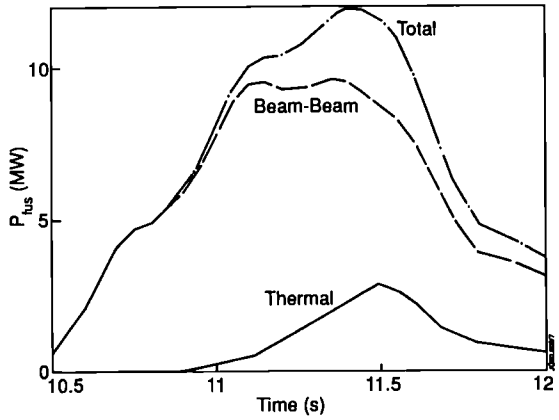

15) TRANSP code simulation of a D-T version of pulse no. 20981 obtained by using the same set of the experimental measurements which are a good representation of the D-D case . The only changes are the species mix and the injection energy. This figure shows total fusion power, thermal and beam-thermal contributions, assuming 15MW of D (at 140keV) injection on a target Tritium plasma. Only D-T reactions have been considered.

INTERPRETATION AND MODELLING OF ENERGY AND PARTICLE TRANSPORT IN JET

Abstract

The study of energy and particle confinement in JET plasmas has been performed by means of various interpretive and predictive techniques. This paper deals with the most recent and relevant results obtained, concentrating on local rather than on global analysis. Electron and ion energy transport and particle transport are studied and their relationship is examined. Comparisons with the predictions of theoretical models are presented, with special attention to transport coefficients derived from the theory of ion temperature gradient driven turbulence and to the critical electron temperature transport model of Rebut et al. [1].

1. Introduction

In this paper we report on the results of studies carried out to assess the local energy and particle transport properties on the basis of JET experimental data. The important issue of global confinement and its relationship to local transport models is discussed extensively in another contribution to this conference [2] where JET data are analysed together with data from other tokamaks collected in the so-called ITER data base. The global confinement of JET plasmas can also be found in other contributions to this conference [3-5].

A proper understanding of plasma transport requires the derivation of a complete transport model applicable in all relevant regimes. It must be capable of predicting the evolution of plasma profiles in the present and next step generation of tokamak devices. We have not reached this goal, but we have made much progress in:

— identifying the most important phenomena to be explained, pointing out correlations between the transport of electron and ion energy and the transport of particles;

— assessing various models proposed to explain and predict the plasma performance in tokamak devices.

In Section 2 we address the problem of electron and ion energy transport. We quantify the absolute and relative magnitudes of the electron and ion heat transport coefficients. A comparison with the predictions of models based on the theory of the ion temperature gradient driven turbulence is presented. We summarise the results obtained and assess the validity of the critical electron temperature gradient model of Rebut et al. (R-L-W in the following) [1].

The evolution of electron density profiles is analysed in Section 3, and it refers mainly to full transport code simulations based on an extension of the R-L-W model to include particle transport.

Section 4 presents the results of an integrated analysis of the propagation of the electron temperature and density perturbation following a sawtooth crash and their implications for transport models. An impurity transport analysis which implies a departure from simple conventional modelling assumptions and the relevance of neoclassical transport theory, is discussed in Section 5. Some concluding remarks are given in Section 6.

2. Electron and Ion Heat Transport

There are regimes in JET where the electron and ion contributions to heat transport can be separated with the aid of interpretive codes. Among these regimes are the hot ion L and H-modes, sawtooth free discharges with strong RF heating (a "diagnostic" low power NBI is used to determine T_i by charge exchange recombination spectroscopy) and pellet fuelled discharges with combined heating [6,7]. Figure 1 illustrates results for two typical cases. The first is a hot ion H-mode discharge with plasma current I_p = 4MA, toroidal field B_T = 2.8T, neutral beam injected power P_{NBI} = 17.9MW, peak electron density $n_e(o)$ = $4.8\times10^{19}m^{-3}$ and peak electron and ion temperatures $T_e(o)$ = 8.8keV and $T_i(o)$ = 22.3keV. The second is a monster sawtooth discharge with I_p = 3MA, B_T = 3T, P_{NBI} = 2.6MW, ICRH power 8.9MW, $n_e(o) = 4.5\times10^{19}m^{-3}$, $T_e(o)$ = 8.8keV and $T_i(o)$ = 6.1keV. The figure illustrates the spatial dependence of the electron and ion heat diffusivities χ_e and χ_i, evaluated using the interpretive code TRANSP under the assumption of a diagonal transport matrix with no heat pinch term. The ion transport is clearly anomalous, except perhaps in the central region of the hot ion H-mode. (See also [6-9] for pellet fuelled cases). We also find as a general trend that $\chi_i \geq \chi_e$ in the outer region of the plasma while χ_e becomes comparable or more important in the central region. Plots of the temperature increase in the central region as a function of the power input per particle to electrons and ions (fig. 2) illustrate in a crude, but rather general way, that as T_{eo} increases, χ_e must become larger in the central plasma region; this is not so for T_{io} and χ_i.

Several attempts to relate the observed heat transport to predictions of models derived from the theory of electrostatic microinstabilities have failed to reproduce JET results [7-10]. The most recent study [8] has considered models of the anomalous ion energy transport derived from the theory of ∇T_i-driven turbulence [11-13]. The analysis shows that, while there is some qualitative agreement (e.g. in pellet fuelled auxiliary heated discharges [14]) between theoretical predictions and experimental findings, there is a serious quantitative disagreement, namely:

— all models predict too low ion energy transport in the region $\rho \geq 0.7$ ($\rho \leq 1$ is a normalised radius) even when fully developed turbulence is taken into account.

— all models predict a large χ_i in the central and intermediate plasma region. Hence one expects T_i to be determined by $\eta_i = n_i\nabla T_i / T_i \nabla n_i$ close to the instability threshold η_i^{cr}. Thus to reconcile theory with JET results a substantial increase of η_i^{cr} is required (Fig. 3).

An extensive campaign of simulations using predictive transport codes has allowed the assessment of heat transport models [15]. Ohmic and L-mode discharges have been considered, covering the following range of parameters: I = 3-5MA, average electron density $\bar{n}_e$ =1.5-7.$10^{19}m^{-3}$, B_T = 2.2-3.4T, auxiliary power (ICRH, NBI or combined) up to 25MW. These computations show that among the theory-based models adapted empirically to simulate experimental results, the R-L-W model emerges as rather good and complete; it covers electron and ion heat and particle transport (see also Section 3). These results confirm previous findings, carried out on a more restricted set of discharges which also included the H-mode regime [9], [16].

We recall that the R-L-W model predicts the existence of a critical electron temperature gradient ∇T_e^{cr} such that the electron heat flow is given by:

$$q_e = -n_e\chi_e^{RLW}\nabla T_e\left(1-\left|\frac{\nabla T_e^{cr}}{\nabla T_e}\right|\right) \qquad (1)$$

when $|\nabla T_e| > |\nabla T_e^{cr}|$. The expressions for ∇T_e^{cr} and χ_e^{RLW} can be found in ref. [1]. Transport is assumed to be neoclassical when $|\nabla T_e| < |\nabla T_e^{cr}|$ or $\nabla q < 0$, q being the safety factor. Moreover:

$$\chi_i \propto \frac{Z_i}{\sqrt{1+Z_{eff}}}\sqrt{\frac{T_e}{T_i}}\chi_e^b, \qquad D_e \propto \chi_e^b, \qquad \chi_e^b = \chi_e^{RL}\left(1-\left|\frac{\nabla T_e^{cr}}{\nabla T_e}\right|\right) \qquad (2)$$

D_e is the electron diffusion coefficient, Z_i and Z_{eff} the ion charge and the plasma effective charge.

If, in an interpretive analysis, the ∇T_e^{cr} term in Eq. (1) is not taken into account explicitly, the resulting χ_e must be compared to χ_e^b. On the other hand χ_e^{RLW} applies to the analysis of heat pulse propagation (see Section 4). It should be noted that no critical ion temperature gradient is predicted for ion energy transport, consistent with the results shown in Figs 1 and 2. Similarly no inward particle pinch is predicted for a pure plasma.

The main deficiencies with the R-L-W model have been found in the outer region of the plasma, especially at low density, where $|\nabla T_e^{cr}|$ tends to exceed the observed $|\nabla T_e|$. It is expected that the model, based on a single phenomenon [1], has to be modified here. Atomic physics processes may affect the model [17] and phenomena related to MHD instabilities might be important. An empirical solution to this problem, adopted in the predictive $1^1/_2$-D code JETTO, is to reduce the anomalous transport gradually when $|\nabla T_e|$ approaches and becomes smaller than $|\nabla T_e^{cr}|$. We also remark that a quantitative validation of the R-L-W model in the central region of the plasma is subject to large uncertainties owing to the dependence of χ_e^{RLW} on the local shear and the practical difficulty of measuring ∇q in this region. A similar remark applies to other models and in particular to η_i related transport coefficients which depend sensitively on the local shear length.

3. Simulation of the Plasma Density Evolution

JETTO code simulations have been used to study simultaneously the evolution of density and temperature profiles in the ohmic and L-mode plasmas described in Section 2. The following expression (based on the R-L-W model) have been used for the flux of the hydrogenic species:

$$\Gamma_i = -D\nabla n_i + n_i(v_{an} + v_w) \qquad (3)$$

$$D = \alpha\chi_e^b, \quad v_{an} = -\alpha_{in}\frac{2Dr}{a^2}.$$

v_w and v_{an} are the neoclassical (Ware) [18] and anomalous inward pinch velocities; α and α_{in} are constants to be determined; a is the minor radius.

The impurity ion density profiles needed to compute the electron density n_e are not modelled but evaluated from Z_{eff} (from visible bremsstrahlung or charge exchange recombination spectroscopy) and the concentrations of the most relevant impurities (from UV spectroscopy). It is assumed that the impurity ions are fully ionised and this is valid for most of the plasma, when dominated by relatively low Z impurities ($Z \leq 8$).

We find that the time scale of the evolution of n_e requires $\alpha \approx 0.3$-0.5. There are cases, in particular with RF heating alone and $Z_{eff} \geq 2.5$, where an anomalous inward term seems to be required in the region $\rho \geq 0.3$-0.4, and $v_{an}/v_{ware} \geq 10$. Figure 4a illustrates such a case. Various regimes however, do not need an anomalous inward velocity, as first pointed out in [19] for discharges with pellet injection. Other cases are found in ohmic low Z_{eff} discharges and with NBI heated discharges where a high density is reached, developing a flat or even hollow density profile. An example, corresponding to a relatively clean plasma ($Z_{eff} \leq 1.5$) is illustrated in fig. 4b, where for comparison we also show the peaked profile of n_e that would be obtained with the same inward pinch as in the previous case.

4. Analysis of Heat and Density Pulse Propagation Measurements

The analysis of fast transients provides a method for determining a linearised matrix of transport coefficients from measured data and complements interpretive and predictive studies. Recent work at JET has been based on an analysis of the heat and density pulses following sawtooth crashes which takes into account the coupling between heat and particle transport [20]. The main result of the analysis is the determination of the 2 x 2 diffusion matrix in a system of linearised diffusion/convection equations simulating the propagation of the perturbations. Figure 5 shows the measured and simulated temperature and density perturbations evolving at various radii in a typical case. Values of the linearised particle and thermal diffusion coefficients D^P and χ_e^P with $D^P/\chi_e^P \leq 0.1$ are derived in the outer plasma region $\rho \geq 0.65$ from this kind of analysis. These values are consistent with the values of D and χ_e^{RLW} found in the simulation of the same pulse (fig. 6). In fact a linearisation of such a model shows that D and χ_e^{RLW} are dominant diagonal terms and can be compared to D^P and χ_e^P.

The pulse propagation analysis shows that there is a linear coupling between particle inward pinch and negative temperature gradient. The sign and magnitude of the coupling are correlated to the initial density decrease (see fig. 5b at r/a = 0.69) coinciding with the location of the maximum temperature perturbation. Such a term is not found linearising the R-L-W model for a pure plasma. It is possible that it is due to an anomalous inward flux of impurities

proportional to ∇T_e, related to a thermoelectric force in the direction parallel to the magnetic field. This has not been considered in the model so far.

5. Transport of Impurities

The study of impurity transport has largely been based on the calculated evolution of impurity density profiles in prescribed experimental plasma profiles. Computed and experimental emissivities from individual lines [21,22] and soft X-ray profiles [23] and radiation profiles are compared. The conventional approach assumes the impurity flux Γ_I to be given by:

$$\Gamma_I = -D_I \nabla n_I + n_I v_I$$
$$v_I = -\alpha_I D_I r / a^2. \qquad (4)$$

where n_I is the impurity density. The diffusion coefficient D_I and the convective velocity v_I are to be determined from the simulations and are assumed to be the same for all ionisation states.

In many cases the simple approach with D_I and α_I radially constant, fails. For example impurity transport appears to be reduced to a level close to neoclassical in the central region of "good confinement" in pellet fuelled discharges [21] and also in the central region of ohmic and RF heated discharges [23].

The simple approach (4) with constant coefficients also fails for the analysis of H-mode discharges: a rather low diffusion coefficient $D_I \approx 0.1 m^2/s$, and a spatial variation of v_I which depends on the plasma temperature and density profiles [22] is needed. Figure 7 shows the empirically determined spatial profile of v_I during the H-phase of a high density pulse ($\bar{n}_e \geq 7 \times 10^{19} m^{-3}$, developing a hollow profile, $Z_{eff} \approx 2$, decreasing with time, $I_p = 3.1MA$, $B_T = 2.2T$, $P_{NBI} = 8MW$). Before density steady state, in a phase lasting 3.5 seconds, the velocity v_I has to be outward in the region $\rho \leq .8$ in order to explain the nickel emissivity lines and radiated power; the empirical convective velocity v_I is consistent, within the large uncertainties of the analysis, with neoclassical theory [24]. This situation is reminiscent of the absence of an anomalous inward pinch term in the modelling of the electron density evolution in L-mode plasmas as shown in fig. 4b.

6. Conclusions

The analysis carried out at JET shows that no pure theoretical model is sufficiently correct or complete enough to explain all features exhibited by the wide variety of plasma regimes found in JET. We underline the problems associated with a quantitative assessment of such models using the theory of instabilities driven by ∇T_i as an example. Time dependent simulations of a variety of phenomena evolving on different time scales indicate a correlation between energy and particle transport. In particular, we find that D/χ_e as normally defined in interpretive codes is larger than D^p/χ_e^p from pulse propagation analysis. We also find that neoclassical theory may be relevant for impurity transport under various circumstances. These results are generally consistent with the picture of the energy and particle transport assumed by the critical electron temperature model of Rebut et al. [1]. This model, which has been successfully tested in a variety of JET plasma conditions, is a good candidate for predicting tokamak plasma performance.

Acknowledgements

We are indebted to the entire JET team and in particular to the diagnostics and data management groups for providing the basic data for this study.

References

[1] REBUT, P.H. et al., Plasma Physics and Controlled Nuclear Fusion Research, 1988, (Proc. 12th Int. Conf., Nice 1988) 2, 191.
[2] CORDEY, J.G. et al. IAEA - CN-53/F-3-19, these Proceedings.
[3] REBUT, P.H. and the JET Team, IAEA - CN-53/A-1-2, these Proceedings.
[4] LOMAS, P.J. et al., IAEA - CN-53/A-6-2, these Proceedings.
[5] TANGA, A. and the JET Team, IAEA - CN-53/A-4-1, these Proceedings.
[6] WATKINS, M.L. et al., Plasma Physics and Controlled Fusion 31, 1713 (1989).
[7] BALET, B. et al., Proc. of 17th EPS Conference on Controlled Fusion and Plasma Heating, Amsterdam 1990, 1, 162.
[8] TIBONE, F. et al., as Ref. [7], 2, 805.
[9] TARONI, A. et al., as Ref. [5], 1, 367.
[10] DÜCHS, D.F. et al., Plasma Physics and Controlled-Nuclear Fusion Research, 1986 (Proc. 11th Int. Conf., Kyoto 1986) 1, 325.
[11] LEE, G.S. and DIAMOND, P.H., Physics of Fluids 29, 3291 (1986).
[12] ROMANELLI, F., Physics of Fluids B 1, 1018 (1989).
[13] MATTOR, N., Culham Laboratory Report CLM-P872(1990).
[14] SCHMIDT, G.L. et al., as Ref. [5], 1, 215.
[15] SACK, C., et.al., as Ref. [7], 2, 801.
[16] WATKINS, M.L. et al., Proc. of 15th EPS Conference on Controlled Fusion and Plasma Heating, Dubrovnik, 1988, 1, 247.
[17] REBUT, P.H. and HUGON, M., Plasma Physics and Controlled Nuclear Fusion Research 1984 (Proc. 10th Int. Conf., London 1984) 2, 197.
[18] HIRSHMAN, S.P. and SIGMAR, D.J., Physics of Fluids, 20, 418 (1977).
[19] BAYLOR, L.R. et al. Bull. Am. Phys. Soc. 34 (9), 2057 (1989) and JET Report JET-P(90)01.
[20] HOGEWEIJ, G.M.D., as Ref. [6], 1, 158.
[21] BEHRINGER, K. et al., IAEA-TEC DOC-534, 167, IAEA, Vienna (1989).
[22] LAURO-TARONI, L. et al., as Ref. [6], 1, 247.
[23] PASINI, D. et al., JET Report JET-P(90)01, acccepted for publication in Nuclear Fusion.
[24] FUSSMANN, G. et al., Journal of Nuclear Materials 162-164, 14 (1989).

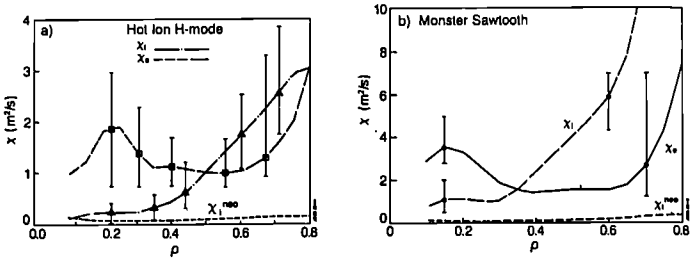

Fig. 1 Radial dependence of χ_e and χ_i for a hot ion H-mode (case a, pulse 20981) and a RF heated non-sawtoothing discharge (case b, pulse 19739).

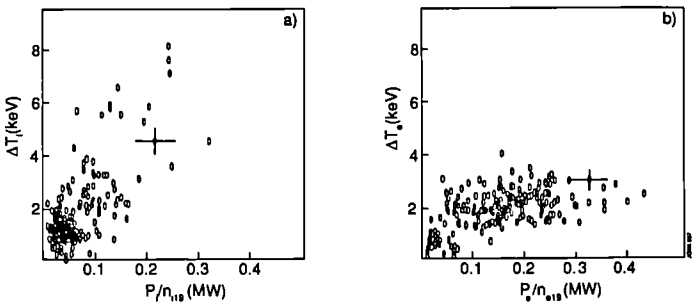

Fig. 2 Increase of the ion (case a) and electron temperature (case b) as a function of P/n; ΔT, P and n refer to $\rho < 1/3$. Sawtooth-free L and H-mode plasmas with $2 \leq P_{tot} \leq 25MW$, $1 \leq n_e \leq 5 \times 10^{19} m^{-3}$ and various combinations of ICRF and NBI are considered.

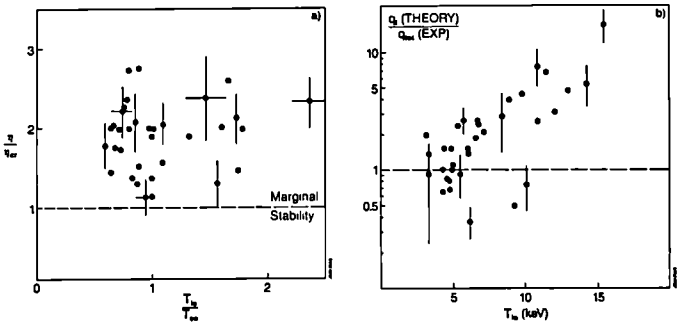

Fig. 3 JET data (referring to sawtooth-free, L-mode, 3MA pulses) compared with the predictions of one of the published versions of η_i-mode theory [13]: a) ratio of the measured $\eta = L_{n_e}/L_{T_i}$ to the theoryetical threshold value as a function of T_{io}/T_{eo}; b) ratio of the predicted ion heat flux to the total measured heat flux at $\rho = 0.4$, as a function of peak ion temperature.

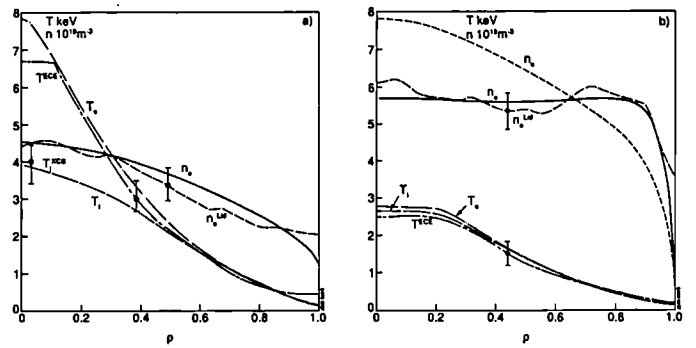

Fig. 4 Comparison of computed and experimental T_e and n_e profiles for a sawtoothing RF discharge (case a, pulse 19617, $B_T = 3.1T$, $I = 3MA$, $P_{RF} = 8MW$) and a sawtoothing NBI discharge (case b, pulse 20334, $B_T = 3.1T$, $I = 3MA$, $P_{NBI} = 8MW$). In case b, the peaked density profile was computed with the same v_{an} as in case a, the flat one was computed with $v_{an} = 0$.

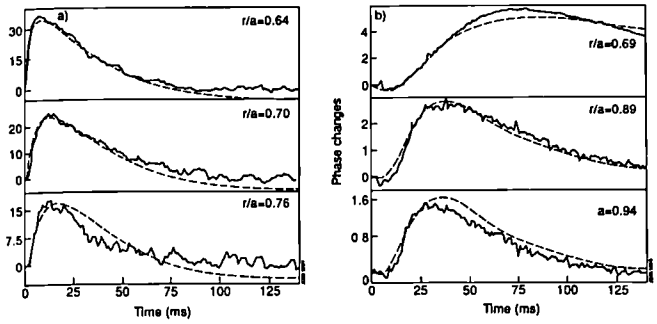

Fig. 5 Measurements and simulations of the propagating perturbation of T_e (case a) and n_e (case b); ΔT_e is normalised to the central temperature before the sawtooth crash, Δn_e is given by the phase changes of the reflectometer. Pulse 19617 is considered, as in fig. 4a.

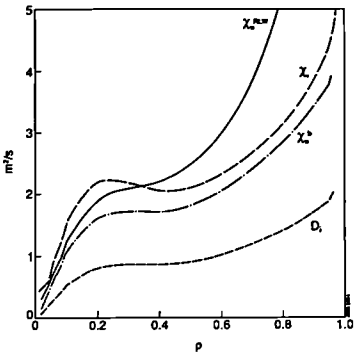

Fig. 6 Radial variation of χ_e^{RL}, χ_e^b, χ_i and D_i obtained from the simulation of pulse 19617 (see figs. 4a and 5).

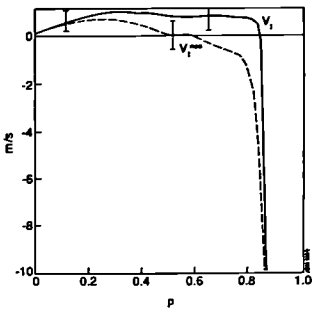

Fig. 7 Radial dependence of the empirical and neoclassical v_I found by simulating the impurity behaviour in an H-mode with a hollow density profile (pulse 21022).

High Density Regimes and Beta Limits in JET

Abstract

Results are first presented on the density limit in JET discharges with graphite (C), Be gettered graphite and Be limiters. There is a clear improvement in the case of Be limiters. The Be gettered phase showed no increase in the gas fuelled density limit, except with Ion Cyclotron Resonance Heating (ICRH), but, the limit changed character. During MARFE-formation, any further increase in density was prevented, leading to a soft density limit. The soft density limit was a function of input power and impurity content with a weak dependence on q. Helium and pellet fuelled discharges exceeded the gas-fuelled global density limits, but essentially had the same edge limit. In the second part, results are presented of high β operation in low-B Double-Null (DN) X-point configurations with Be-gettered carbon target plates. The Troyon limit was reached during H-mode discharges and toroidal β values of 5.5% were obtained. At high beta, the sawteeth were modified and characterised by very rapid heat-waves and fishbone-like pre- and post-cursors with strongly ballooning character.

1. OPERATION NEAR THE DENSITY LIMIT

Operation near the density limit has been systematically studied in JET for limiter discharges, with C limiters, with evaporated Be layers and with Be limiters [1]. The operating density in tokamaks is usually presented in the form given in Fig.1. Each point represents the maximum obtained normalised density during a discharge with either Ohmic (OH), Neutral Beam (NBI), ICRH or combined heating. The broken lines marked by OH (C) and NBI(C) are the highest limits obtained in the previous campaigns with C walls and limiters [2] ($nRq_c/B_t = 12$ for OH and $20 \times 10^{19} m^{-2}T^{-1}$ with NBI). There are clear improvements due to the Be limiters and Be coated walls. After conditioning of the Be limiter, which led to a strong reduction of Cl, the limit was substantially extended beyond that with Be gettering, so that $nRq_c/B_t \approx 33$ was reached with combined heating, ICRH and NBI heating. Furthermore the limiting density increases with the applied power as we shall see shortly. Pellet fuelled and He discharges have exceeded the deuterium gas fuelled limits. There is strong evidence that the edge density determines the limit. The limit at low q (q~2), however, is unchanged and is still set by major current disruptions.

There has not yet been such a systematic study for X-point discharges, but the behaviour is similar, with somewhat lower density limits. The highest densities so far in X-point discharges are obtained in H-modes with $nRq_c/B_t \approx 20 \times 10^{19} m^{-2}T^{-1}$. At higher densities, typically when $P_{rad}/P_t \approx 60\%$, an H to L- mode transition occurs and the density falls without causing a disruption. In limiter discharges the nature of the limit is different for C and Be limiters. With C, the limit is marked by an asymmetrical edge radiation (MARFE) that leads to a symmetric radiative collapse and ends in a hard disruption. With Be limiters the limit is generally marked by the appearance of a MARFE which, in gas fuelled discharges, is accompanied by a fall in recycling and reduction in density. This typically leads to a soft density limit with a relaxation oscillation of density, radiation and MARFE near the limit. The internal inductance of the plasma during the MARFE generally did not increase, indicating that the plasma was not contracting significantly, as in the pure C limiter during the radiation collapse. This is consistent with the absence of strong MHD fluctuations and disruptions in the Be-gettered and limiter plasmas.

The line-averaged density could be substantially increased with pellet fuelling, providing the pellets penetrated deeply. The limit for both pellet and gas fuelled discharges can be unified by considering the edge density and the input power (Fig. 2). The dependence of the density limit on the total power P_t and in particular on the radiation power balance in the edge region of the discharge has been suggested in a number of papers [2-5]. These models suggest that the limit should increase approximately as $P_t^{1/2}$. The MARFE limit for pellet and gas fuelled discharges does lie at the boundary of the existence region.

2. CONCLUSIONS: DENSITY LIMIT

Operation near the density limit in JET can be summarised as follows :

- The density limit for additionally heated discharges in JET is now independent of the heating method and exceeds $nRq_c/B_t = 33 \times 10^{19} m^{-2}T^{-1}$ for Be limiters and $20 \times 10^{19} m^{-2}T^{-1}$ for the H-mode;
- The density limit has a different MARFE behaviour for Be limiters compared with C limiters and leads to a density pump-out returning the discharge to a stable operation region;
- The density limit in gas and pellet fuelled discharges increases with input power approximately as $P_t^{1/2}$ and is determined by edge parameters, particularly the edge density;
- The high limit obtained in JET means that acceptable densities should be reached in next step devices provided that sufficient degree of impurity exclusion can be obtained.

3. BETA LIMITS

High β operation has been achieved at low toroidal fields ($B < 1.2$ T) where the Troyon limit [6] is reached with additional heating at power levels ~10MW below that at which carbon self-sputtering becomes important [7]. It has not yet been possible to surpass the Troyon limit as has been done in DIII-D [8].

Fig.3 shows the maximum toroidal β_φ as a function of q_c^{-1} obtained for all discharges between 1986 and 1989. A steady state β_φ of 5.5% has been reached for DN H-modes in a hydrogen plasma. In these discharges with Be coated walls, β saturation is generally observed without disruptions. The saturation is related to MHD-modes, ELM's and n=1 activity. Sawtooth and fishbone events occur and sometimes continuous n=1, 2, or 3 modes appear, which can lead to a β decline. A peaked and roughly triangular p(r) profile develops from an initially broad profile. The internal inductance decreases from ~ 1 to 0.7, which indicates a broadening of j(r) towards those profiles used in the β-optimisation by Troyon [6]. The decrease of the inductance is calculated to be due to the bootstrap current, which is approximately 25% of the total current.

4. BETA SATURATION

The evolution of β for the discharge with the highest β obtained so far is shown in Fig.4. Also shown is the MHD activity, central ion temperature and volume-averaged density as a function of time. The main β-limiting mechanism in this discharge is the high-β sawtooth. Increased MHD (n=1 and n=3) activity (around t=15 s) leads to a diminished rate of rise in β after the crash and to a decline in the central ion temperature and so contributes to the β saturation.

The high-β sawteeth differ from those at low β in two ways :

1. The associated heat pulse is very rapid with $\tau_{HP} \sim 100\mu s$ instead of ~10 ms.
2. Dominant (1,1), (2,1) and higher m pre- and postcursors are seen, similar to high-β fishbones but of twice the amplitude. The modes have a ballooning character near the outer edge with a ratio in amplitude from the low to high B-side of ~10 as seen by the X-rays. Similar to a normal sawtooth, a high-β sawtooth causes a flattening of the pressure profile within the q=1 radius.

5. HEAT LOSSES

Like other H-mode discharges in JET the high-β discharge has a confinement time twice that of the Goldston L-mode [9]. The observed plasma energy W_{DIA} lies close to the energy W_G calculated from the effective power input and $\tau_E = 2 \times \tau_G$ [10]. The fraction of the losses due to high β sawteeth is 10 to 15% and that due to the intermittently appearing MHD-modes 20 to 30% of the total energy losses. This is sufficient to prevent further β increase since the heating power P is close to the critical power required to reach the Troyon limit. The fishbones and especially the sawtooth events strongly affect the fast particle distribution as measured by the neutron emission with consequences for future α-particle heating.

The central neutron emission drops by 70 % (Fig.5) and its total rate by 30 % during a sawtooth [11]. Fishbones are observed which individually cause up to 10% drop in the global neutron emission. However they occur about 10 times more frequently than sawteeth and may contribute appreciably to the central loss of fast particles and energy. Relatively large heat losses (150 kW) have also been measured by the neutral particle analyser with losses that are proportional to the MHD mode amplitude. Measurements with a multi-channel O-mode reflectometer indicate that high frequency density fluctuations grow exponentially with β_N. The measurements are carried out between 3.9 and 4.1 m with frequencies ~130 kHz well above the n=1 MHD modes present; perhaps, indicating high-n ballooning-mode activity.

6. BETA COLLAPSE

In a few JET cases, high β collapses occur triggered or preceded by large n=2 (or sometimes n=1 or 3) MHD activity with δB~15 G at the edge, and differ from β-saturation in various ways [7]:

- a dominant (3,2) and other coupled n=2 modes are responsible as seen from SXR analysis,
- there is a drop in the electron density in contrast to the saturation due to the high β-sawteeth,
- the central ion temperature and the fast ions are not affected at first.

7. PLASMA STABILITY

The stability of the high-β discharges has been examined with various stability codes : ERATO [12], HBT [13], BALLOON [14] and FAR code [15]. These stability studies are discussed more fully in [16]. It is found that before a high-β sawtooth the central plasma over more than half its radius is close to or even above the marginal ideal ballooning stability threshold. The ideal n=1 internal kink is also found to be strongly unstable for $\beta_N \approx 1$ when $q_0 \leq 1$. This instability may be linked to the observed (1,1) instabilities which seem to cause the β-saturation. We have calculated the fast particle effects on the internal kink. It is found that at the β values reached, the fast particles can no longer stabilise the internal kink. The operation is outside the Porcelli-Pegoraro stable region in the $(\gamma_{MHD}, \omega_*, \beta_{ph})$ space with experimental values of (1.0, 0.5, 1.5) [17]. In addition, severe fishbone activity is expected in this regime, resulting from the coupling with high energetic beam ions above 40 keV. It is further found that in the cases where the β-collapse occurs internal modes of either n=2 or n=1 structure, appear to be responsible for the enhanced plasma losses. These modes have been simulated by the FAR code where the q-profile has been tuned to match the measured X-ray fluctuations over the plasma cross-section [16]. In the case where n=1 modes are dominant, the q-profile had to be relatively flat in the centre with $q(0) \approx 1.1$, supported by Faraday-rotation measurements.

8. CONCLUSIONS: BETA LIMIT

In low q discharges at high β, saturation of the plasma energy is observed without disruptions. Global n=1 modes in the form of high-β sawteeth and fishbones are generally responsible for this saturation. Occasionally, β-collapses occur which seem to be related to large n=2 (some- times n=1 or 3) MHD modes. Triangular temperature profiles exist at the limit, which together with the rather flat density profiles lead to constant ∇p across the plasma. Such peaked pressure profiles are favourable for a fusion reactor. Both the fishbones and sawteeth strongly affect the fast particle distribution. This has important consequences for future α-particle heating, burn control and wall loading. The role of the ballooning limit in the inner part of the plasma is not yet clear. Generally good agreement between theoretically predicted internal modes and observations at the beta limit, has been obtained. The role of the fast particles on the beta limit needs further study both theoretically and experimentally. Further experiments in JET are required to see if the beta limit remains a soft limit even at much higher input powers.

9. REFERENCES

[1] C.Lowry et al, Proc.17th Eur.Conf.on Contr.Fusion & Plasma Phys., Amsterdam (1990)
[2] J.Wesson et al. Nuclear Fusion **29**, 641 (1989)
[3] D.Campbell et al, Proc. 11th Int.Conf. on Plasma Physics and Contr. Nucl. Fusion Research, Kyoto, Nuclear Fusion Supp. (1987)
[4] A.Gibson, Nuclear Fusion,**16** (1976) 546.
[5] P-H.Rebut amd B.Green, Proc. 6th Int.Conf. on Plasma Physics and Contr.Nucl. Fusion Research, Berchtesgaden, Nuclear Fusion Supp. 1977
[6] F.Troyon, R.Gruber et al, Plasma Phys.& Contr. Fusion **26**(1984)209
[7] P.Smeulders et al, Proc.17th Eur.Conf.on Contr.Fusion & Plasma Phys., Amsterdam (1990)
[8] J.Ferron et al, Proc.17th Eur.Conf.on Contr.Fusion & Plasma Phys., Amsterdam (1990)
[9] R.Goldston, Proc.11th Eur.Conf.on Contr.Fusion & Plasma Phys., Aachen (1984)
[10] A.Gibson et al, Proc. 17th Eur.Conf.on Contr.Fusion & Plasma Phys., Amsterdam (1990), to be published in Plasma Phys. & Contr.Nucl.Fusion.
[11] F.Marcus et al, Proc.17th Eur.Conf.on Contr.Fusion & Plasma Phys., Amsterdam (1990)
[12] R.Gruber et al, Computer Phys. Commun. **21** (1981) 323
[13] J.P.Goedbloed,G.M.D.Hogewey et al, Proc.10th Int.Conf. on Plasma Phys.and Contr. Fusion, London 1984, IAEA (1985)165
[14] D.P.O'Brien, C.M.Bishop et al, Proc. 16th Eur. Conf. on Contr.Fusion and Plasma Phys., Venice (1989)
[15] L.A.Charlton et al, Journal Comp. Phys. **86**, 270 (1990)
[16] T.C.Hender et al, Proc.17th Eur. Conf. on Contr. Fusion & Plasma Phys., Amsterdam (1990)
[17] F.Porcelli et al, Proc.17th Eur.Conf.on Contr.Fusion & Plasma Phys., Amsterdam (1990)

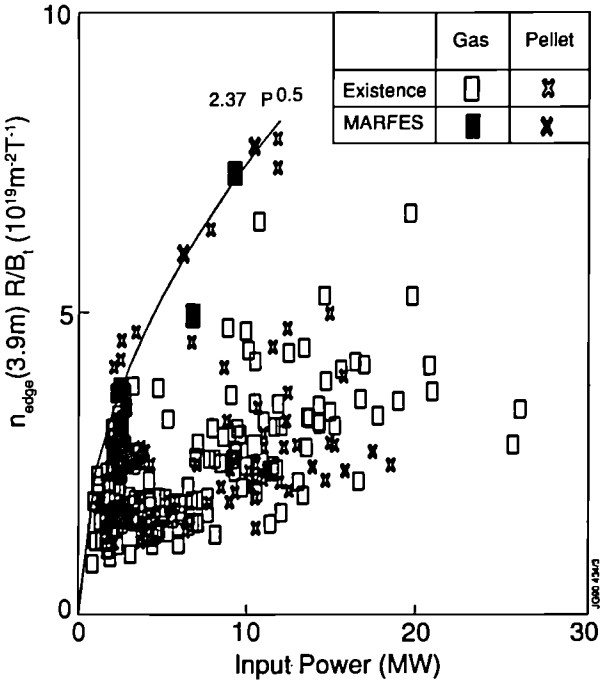

Fig.2. The normalised edge density versus input power showing that the MARFE density limit occurs at the boundary of the existence region close to the curve $n_{edge}R/B_\phi = 2.37\ P_t^{1/2}$ [10^{19}m^{-3}, m, T, MW]. B_ϕ varies in the range 1.4 to 2.6 T.

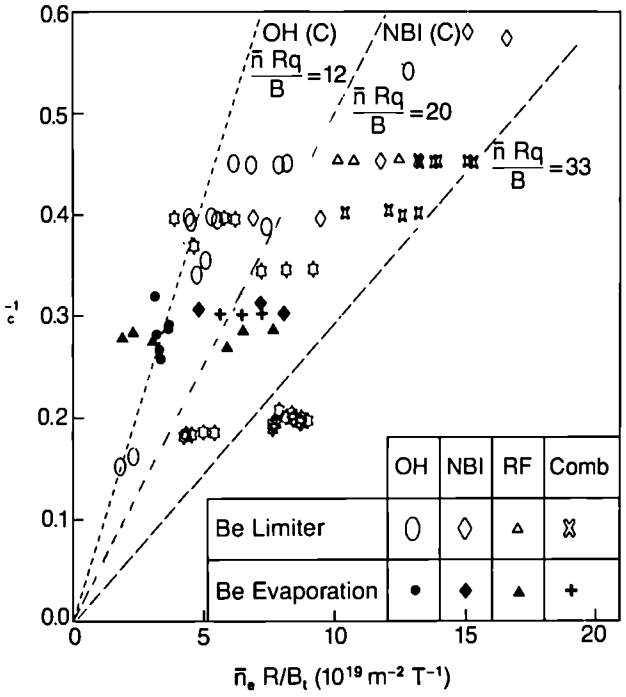

g.1 The operating density range for JET shown as normalised current $q_c^{-1} = \pi R I_p / 5 A B_\phi$ ı,MA,m²,T] versus normalised density $n_e R/B$ [10^{19}m^{-3},m,T]. Comparison is made between rbon disruptions (two broken lines at left) and MARFES with Be evaporation (solid symbols) d Be limiter (open symbols)

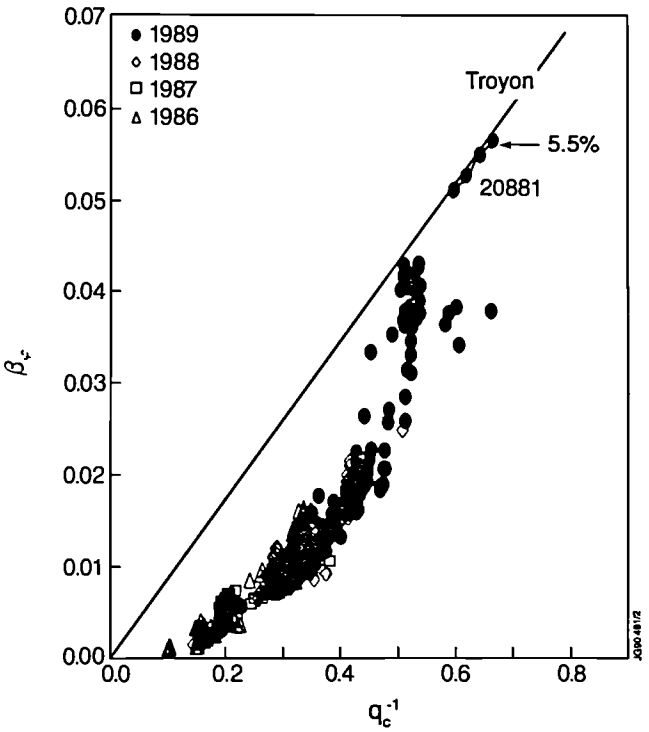

Fig.3. The maximum toroidal beta ($\beta_\phi = 2\mu_0 \langle p \rangle / B_\phi^2$) as a function of q_c^{-1} (proportional to normalised current $I_p/B_\phi a$[MA,T,m]), for all JET discharges with the poloidal beta $\beta_\theta > 0.4$. The line is the Troyon limit $\beta_{Troyon} = 0.028\ I_p/B_\phi a$ [MA,T,m]. The highest β is 5.5%.

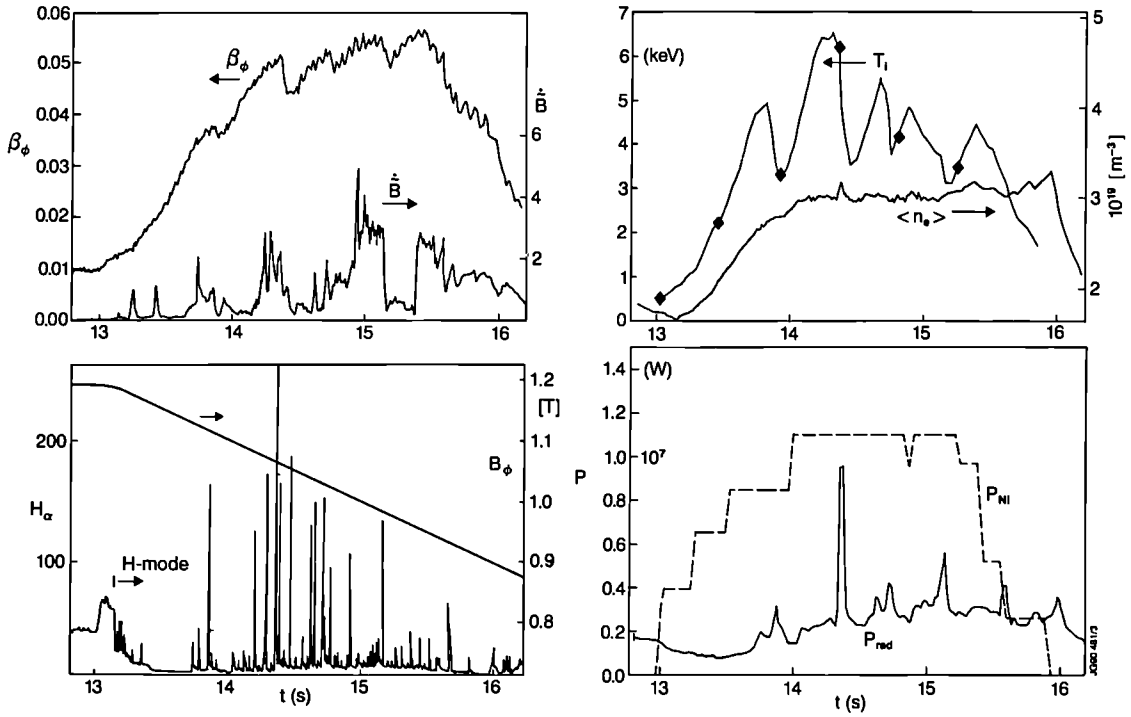

Fig.4. Evolution of β_ϕ, MHD-mode amplitude $\tilde{B}_\phi$ (top-left); H_α and magnetic field B_ϕ (bottom-left); ion temperature T_i, volume average density $<n>$ (top-right); and injected power P_{NI}, radiated power P_{rad} for the 5.5 % β discharge, a 2MA Double-Null H-mode at 0.9T with 11MW 80 kV D-injection into a H plasma. $T_e(0)$ and $T_i(0)$ of 3.5 and 6 keV were obtained in these low q discharges ($q_{95} \approx 2.2$ or $q_c \approx 1.6$) and κ of 1.8. Z_{eff} slowly increases in time from 1.3 and levels off at ~2.5. The confinement time $\tau_E = 0.35$ s.

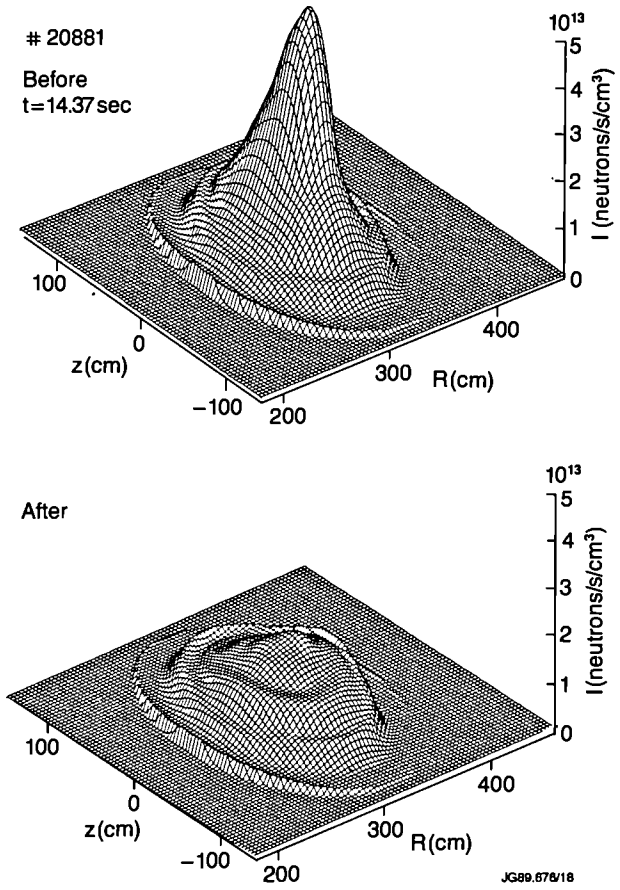

Fig.5. Cross-sections of the plasma neutron emissivity before and after a beta crash. The central emission drops by 70%. The integration time is 100ms.

Modelling Impurity Control by Plasma Flows in the JET Pumped Divertor

M. Keilhacker, E. Deksnis, P. Harbour, P. H. Rebut, R. Simonini, A. Taroni, G.C. Vlases, M.L. Watkins

Abstract

A pumped divertor is planned for the extension phase of JET (1993 - 96) in order to control impurities during long pulse, high power operation. Target-produced impurities tend to migrate along the field lines, out of the divertor, due to temperature gradient forces. This is opposed by the friction forces arising from the streaming of hydrogen into the divertor. This problem is studied using both analytic and numerical methods. For the highest power anticipated, impurities will be trapped by "natural divertor recycling" only at high scrape-off layer (SOL) densities approaching $10^{20}m^{-3}$. At lower densities, a forced flow or "external recirculation" must be induced, e.g. by shallow pellet injection or gas puffing, to insure impurity retention. Steady state then requires removal of an equal amount of neutral flow from the divertor, which imposes fairly severe pumping requirements. Less flow is needed, for a given SOL density, as the ion power flow is reduced.

I. Introduction

The aim of the planned extension of JET (1993 - 1996) is to demonstrate effective methods of impurity control in operating conditions relevant to a Next Step Tokamak. The central task of this phase will be to investigate impurity control in a new divertor configuration, the primary functions of which are to remove the principal source of impurities as far from the main plasma as possible, and to retain the impurities produced at the divertor target plates. The production of impurities will be minimized by reducing the divertor plasma temperature as far as possible, and by proper selection of target plate materials. Retention of the impurities in the divertor region will be enhanced by inducing a strong flow of deuterium towards the target plates.

The general features of the proposed divertor are illustrated in Fig. 1. It is of the "open" type, with Beryllium-clad, water-cooled (Hypervapotron) copper target plates. The in-vessel four-coil system allows both for horizontal sweeping of the plasma along the target to spread the heat load, and for vertical motion of the X-point to vary the connection length and plasma volume. The possible divertor configurations span the range from a "slim" 6 MA plasma (total divertor coil current of 1.8 MA) with a connection length in the divertor region, corresponding to a field line 1 cm away from the separatrix in the equatorial plane, of about 6.7 m, to a "fat" 6 MA plasma (divertor current of 0.74 MA) with a connection length 3.5 m.

Impurities produced at the target plates are subject to several forces, the most important of which, in steady state, are the ion thermal force, directed away from the target plates, the deuterium-impurity friction force towards the target, and the impurity pressure gradient force which arises to establish a force balance. The ion thermal force is determined principally by the ion heat flow in the scrape-off layer (SOL), while the counter-acting friction force depends on the magnitude and spatial distribution along the field (coordinate s) of the deuterium particle flux, $\Gamma(s)$, and is inversely proportional to the ion temperature to the 3/2 power. Thus the friction force can in principle be set at a level sufficient to overcome the thermal force. From global balance considerations of the SOL and the divertor channel plasma (DCP), the magnitude of the flux at the divertor target plate, Γ_t, is determined by the mid-plane SOL plasma density and the power flow in the SOL. The form of $\Gamma(s)$, denoted $\hat{\Gamma}(s) \equiv \Gamma(s)/\Gamma_t$, is controlled by the hydrogen particle source distribution in the SOL and the DCP as sketched in Fig. 2. In the "local recycling" zone, which extends approximately one effective ionization length normal to the target, $\hat{\Gamma}(s)$ increases rapidly going towards the plate, due to ionization of neutrals emanating from the target plates. Some of the neutrals, however, are not locally recycled, but escape and then may re-enter the DCP further up the flux tube via reflection from the side walls, or transmission across the private flux region. We refer to this as "distant recycling". It extends the region of significant hydrogen flux further from the target plates, thus enhancing the effectiveness of the friction force term. Case a of Fig. 2 corresponds to purely local recycling at the target plates, while Case b corresponds to roughly half of the target plate flux being uniformly "distantly recycled" between the local recycling zone and the X-point. The relative amount and distribution of the distantly recycled particles depend both on divertor plasma conditions and on divertor geometry.

It is also possible, in principle, to extract some of the incident neutralized ion flux from the targets and directly "recirculate" it, e.g. by baffles, into the X-point region, as was suggested in Ref. [1]. This would produce a $\hat{\Gamma}(s)$ distribution as shown in Case c, Fig. 2. Finally it may be necessary in some cases, for impurity retention, to induce a moderate $\hat{\Gamma}(s)$ in the SOL, in excess of the natural flow from the main plasma, by strong gas puffing or shallow pellet injection. This imposed flow, which we term "external recirculation", would require pumping of an equivalent neutral flux from the divertor chamber to maintain a steady state. The resulting flux distribution is shown as Case d.

The purpose of this paper is to determine the conditions under which the recycling (local plus distant) is sufficient to retain target-produced impurities in the divertor, and to calculate the amount of additional "recirculation" flow required when the "natural" flow is insufficient. We begin (Section 2) with a simple analytic model which elucidates the most important physical processes. This is followed by a discussion of the full 1-1/2 code and its results (Sect. 3). Conclusions are drawn in Section 4.

II. Impurity Retention Overview

Impurity retention in the divertor may be estimated by examining the magnitude of the different forces on the impurity ions as given by the steady state momentum equation

$$m_z n_z v_z \frac{dv_z}{ds} = -\frac{dp_z}{ds} + n_z ZeE + \frac{m_z n_z (v_i - v_z)}{\tau_{zi}} + n_z \alpha_z \frac{dT_e}{ds} + n_z \beta_z \frac{dT_i}{ds}. \quad (1)$$

Here we have considered a single impurity species of charge state Z, mass m_z, density n_z, temperature T_z, pressure p_z, and flow speed v_z. The simplification to a single charge state is well justified, because the most important forces acting on the impurity all scale approximately as Z^2, and thus their ratio is independent of Z. The subscripts e and i refer to the electrons and the hydrogenic ions, and τ_{zi} is the hydrogenic ion-impurity collision time. The forces on the right hand side of Eq. (1) are due to the impurity pressure gradient, where $p_z = n_z T_z$, the electric field E, the frictional force, and the thermal forces with coefficients α_z for electrons and β_z for ions.

This equation, along with the other appropriate conservation equations, are solved in detail using a 1-1/2 code, as discussed in Section 3. To gain insight into those results, however, we begin with a simplified analytic description of the impurity distribution, as deduced from Eq. (1) in the trace approximation, where the hydrogenic flow is specified *a priori*, and is not affected by the impurities.

The electric field may be eliminated from Eq. (1) by using the electron momentum equation and taking the electron pressure to be nearly constant along s. In addition, we take $\frac{dv_z}{ds} = 0$ and $T_z \cong T_i$, so that Eq. (1) becomes.

$$\frac{T_i}{n_z}\frac{dn_z}{ds} = \frac{m_z(v_i - v_z)}{\tau_{zi}} + (\alpha_z - 0.71\,Z)\frac{dT_e}{ds} + (\beta_z - 1)\frac{dT_i}{ds} \qquad (2)$$

with $\alpha_z = 0.71Z^2$, and $\beta_z = 1.76Z^2$ for the case of Beryllium with Z = 3 [2].

For most cases of interest $\nabla T_e \ll \nabla T_i$, since they are both determined by classical heat conduction and $\kappa_{\|e} \gg \kappa_{\|i}$, so that we can neglect the ∇T_e term in Eq (2). In addition, we take $v_z = f_v v_i$ as a further simplification, where $f_v = 0$ everywhere except in a thin impurity ionization zone near the target. Integrating the resulting equation gives

$$\frac{n_z(s)}{n_z(o)} = \exp\left\{-\int_o^s F_{fi}ds + \int_o^s F_{Ti}ds\right\} \qquad (3)$$

with $$F_{fi}(s) = C_f \cdot Z^2 \frac{\Gamma(s)}{T_i(s)^{5/2}} \quad m^{-1}, \qquad (4)$$

and $$F_{Ti}(s) = (\beta_z - 1)\frac{1}{T_i}\frac{dT_i}{ds} \quad m^{-1}. \qquad (5)$$

Note that F_{fi} and F_{Ti} are inverse local scale lengths associated with the friction and thermal forces, respectively. Here and in the following, the units are MKS, except for T_i, which is expressed in eV. The value of C_f is then 1.2×10^{-20}.

For a large enough deuterium flux, Γ, the impurity density decreases going towards the X-point until the point where $\Gamma(s)$, determined by the distribution of recirculated neutrals, becomes small enough that $F_{fi} < F_{Ti}$. Beyond that point, $n_z(s)$ begins to increase. Fig. 2b shows qualitatively the behaviour of the solution for the four source distributions of Fig. 2a. If we adopt the criterion that $n_z(L)/n_z(0)$ be less than a certain value, say e^{-3}, the criterion for retention of impurities becomes

$$\int_o^L F_{fi}(s)ds \geq \int_o^L F_{Ti}(s)ds + 3. \qquad (6)$$

In order to carry out the integrals, the hydrogenic ion temperature and particle flux distributions along s must be specified. The latter is postulated, and then checked by a Monte-Carlo calculation, as described in section 3. The temperature is governed by both conduction and convection, and is given, to close approximation, by

$$T_i(s)^{7/2} = \frac{7}{2}\left(\frac{q_{eff}}{K_{o,i}}\right)s + T_{di}{}^{7/2} \qquad (7)$$

where $q_{eff} \cong .6\ q_i$, the ion heat flow per unit area, for values of recirculated Γ near the minimum required to entrench the impurities [3], T_{di} is the divertor ion temperature, and $K_{o,i}$ is a constant.

Combining equations (4), (5), and (7), shows that the ratio of the ion friction and thermo-electric terms scales approximately as

$$\frac{F_{fi}(s)}{F_{Ti}(s)} \sim \Gamma(s)\cdot(s + s_o)^{2/7}, \qquad (8)$$

$$\text{where } s_o = \frac{2}{7}\left(\frac{K_{o,i}}{q_{eff}}\right)T_{di}{}^{7/2}.$$

Consider the case $\Gamma(s) \sim$ constant over some interval,for example Case c of Fig. 2. Because of the relatively weak variation of F_{fi}/F_{Ti} with s, it can be shifted from less than one to greater than one over most of the interval by a small change in Γ. Thus, one can go from a case of very poor impurity retention to good retention with small changes in Γ which extend over long distances, e.g. by distant recycling and/or external recirculation.

Incorporating equations (4), (5) and (7) into (6) yields, as the criterion for retention of impurities,

$$\frac{C_f(1-f_v)Z^2\Gamma_t}{\left(\frac{7}{2}\frac{q_{eff}}{K_{o,i}}\right)^{5/7}}\int_o^L \frac{\hat{\Gamma}(s)ds}{(s+s_o)^{5/7}} \geq \left(\frac{2}{7}\right)(\beta_z - 1)\ln\left(\frac{L}{s_o}+1\right) + 3. \qquad (9)$$

The target flux, Γ_t, is determined by specifying the mid-plane or, more generally, the stagnation point separatrix plasma density n_b, and the parallel heat fluxes, $q_{\|e}$ and $q_{\|i}$, using a model similar to that of Ref. [4]. For given power into the divertor and very high values of n_b, Γ_t is sufficiently high that local plus distant recycling alone is sufficient to satisfy relation (9) for the proposed divertor geometry. As n_b is decreased for a given power, Γ_t decreases and T_{di} increases, which tends to reduce the left hand side of relation (9). In order to retain impurities, $\hat{\Gamma}(s)$ must be "extended" further up the field line, either by (single point) recirculation, e.g. at the X-point (Case c), or by injection of particles uniformly into the SOL (Case d).

For X-point injection, the flux required for impurity retention is

$$\Gamma_x \geq \frac{\frac{2}{7}\left(\frac{7q_{eff}}{2K_{o,i}}\right)^{5/7}}{C_f Z^2}\frac{\left[\frac{2}{7}(\beta_z - 1)\ln\left(1+\frac{L}{s_o}\right)+3\right]}{\left[(s_x+s_o)^{2/7} - s_o{}^{2/7}\right]}. \qquad (10)$$

The relation (10) assumes Γ_x is constant along s, and thus does not include the contribution of the local high recycling region, which is small for Γ_x non-negligible compared with Γ_t.

Relation (10) implies that the minimum required flux can be written

$$\Gamma_x \sim q_{eff}{}^{5/7} f(q_{eff}, T_{di}, s_x, L) \qquad (11)$$

where the variation of f with its arguments is small. For example, a change of q_{eff} by a factor of 10 changes f by only 5 %. Furthermore, a factor of 4 variation in T_{di} changes f by 20%, while doubling the distance to the injection point, s_x, from 4m to 8m reduces f by ~25%.

Thus, as the main result, this simple analysis predicts that for the case of single point recirculation at the X-point, the required Γ_x depends primarily on the ion heat flow and somewhat less strongly on the connection length. Γ_x scales as $P_i{}^{5/7} \cdot s_x{}^{-2/7}$ for $s_x{}^{2/7} >> s_o{}^{2/7}$.

We note that the electron temperature does not enter this analysis directly, since the dominant forces are associated with the ions. However, the electron temperature and density in the divertor are important in that they determine the fraction of neutrals that is distantly recycled, rather than locally, and thus they control the amount of "recirculation", which must be added to retain impurities.

The integrals in Eq. (3) can be evaluated for simple $\hat{\Gamma}(s)$ other than the step function form corresponding to relation (10), without changing the basic scaling appreciably. For example, for uniform injection into the DCP between s=0 and s_x, corresponding approximately to the expected distant recycling pattern at low SOL densities, the required flow is increased by 35% relative to X-point injection, while uniform injection into the SOL between s_x and L (external recirculation) reduces Γ_x by about 23%.

III. Code Calculations of Impurity Retention

a) The Model

To study the requirements for effective impurity control in more detail a 1-1/2D model (EDGE1D) of the plasma boundary in the proposed pumped divertor configuration has been developed. (For a detailed description of the model see Ref. [5].). The model is based on the plasma model of the JET 2D boundary code EDGE2D [6] and the impurity model of Ref. [7]. The latter is valid for arbitrarily high impurity concentrations.

Fluid equations for the conservation of particles, momentum and energy along the magnetic field are solved for electrons,

hydrogenic ions and impurity ions. Transport coefficients, friction, thermal forces and electric fields (not necessarily ambipolar) are classical [8] and allow for arbitrarily high impurity concentrations [7]. In general, the full non-coronal distribution of impurity charge states and the corresponding radiated energy losses are determined. A single impurity temperature, set equal to the hydrogen temperature, is assumed. The electron density is evaluated from quasi-neutrality.

For the boundary conditions at the target plates the Bohm condition is adopted, i.e. it is assumed that hydrogenic and impurity ions reach their sound speed at the plates. The heat fluxes at the plates are prescribed with the appropriate energy transmission coefficients for a two component plasma.

Transport transverse to the magnetic field is replaced by specified temperature and density profiles assumed to decay exponentially outwards from the separatrix with decay lengths, λ_T = 1.5 cm and λ_n = 1 cm, respectively. The width, $\delta = 3\,\lambda_T$, of the SOL plasma is chosen such that the residual fluxes are negligible.

A full 2-D Monte Carlo code (NIMBUS) [9] is retained for the sources of neutral particles. Deuterium particles are recycled at the target plates as neutrals. The Monte Carlo code defines the spatial distribution of the ionisation sources in the vicinity of the target plates. To enhance the plasma flow in the divertor region, some of the recycled neutrals are removed and recirculated into the scrape-off layer as plasma ions, with prescribed spatial distribution along the separatrix.

The Monte Carlo code defines also the spatial distribution of the impurity sources due to erosion at the target plates. Impurity atoms are generated by sputtering due to plasma ions and neutrals of any species. An effective sputtering coefficient is taken into account following Ref. [10]. However, it is also possible to normalise the source of impurities to their outgoing flux onto the target plates, thus implying a prescribed impurity content.

Work is currently in progress to implement a full 2-D version of the plasma flow, including impurities at arbitrary concentrations.

b) Numerical Results

As an example, we now discuss results of calculations based on the "slim" divertor configuration. Figure 3 shows the corresponding computational mesh and the most important input parameters. As a "reference" case we choose a total input power of 40 MW, corresponding to the maximum available power in JET. This power is shared equally between the ions and electrons ($P_e = P_i$) and is input uniformly along the separatrix into the SOL. The calculations are for beryllium impurities which are produced self-consistently by sputtering from the target plates. The magnitude of the externally recirculated flux is varied parametrically and, in most cases, is injected uniformly along the separatrix from the main plasma into the SOL. For given n_b, P_i, P_e and external recirculation fraction f_R of the target flux, all other SOL and DCP parameters are determined.

Figure 4 shows calculated profiles of the deuterium and total impurity densities, the ion and electron temperatures, and the principal forces acting on the impurity ions as functions of the distance along the field line from the outside target for runs typical of poor (run 724) and good (run 712) impurity retention. It can be seen that for run 724, a large fraction of the impurities accumulate in the SOL adjacent to the main plasma. To quantify the degree of impurity retention we use the ratio of the number of beryllium ions retained in the two divertor regions to the total number in the SOL and DCP; we call this ratio η(%). The two cases displayed in Fig. 4 differ mainly in the level of external recirculation, and only slightly in the separatrix stagnation point density (n_b = 8.3 and 9.1 x $10^{19}m^{-3}$, respectively). For run 724 there was no external recirculation while for run 712 10% of the target flux was extracted and reinjected uniformly into the SOL. It can be seen that this relatively small external recirculation makes a major change in the retention, increasing η from 16% to 92%.

The second set of frames for Fig. 4 shows the electron and ion temperatures. In all our simulations the ion temperature in the SOL is higher than that of the electrons, mainly due to the lower ion thermal conductivity along field lines. The increased ion temperature near the stagnation point in run 724 arises from the high impurity density there, and the dependence of thermal conductivity on the effective charge state. The prediction that the ion temperature in the SOL should exceed the electron temperature is in agreement with experimental observations in JET [11]. Also the temperatures near the target plates are in the 10 - 20 eV range at higher edge densities and correspondingly larger hydrogen fluxes to the targets.

The third frame of Fig. 4 shows the force balance. For $f_R = 0$, the distribution of Γ, which arises from recycling alone, does not provide a large enough integrated friction force to retain the impurities, and they accumulate near the point of maximum temperature, with the impurity pressure gradient force balancing the ion thermal force. For $f_R = 0.1$, the external recirculation extends the range of the friction force sufficiently to enable it to overcome the thermal force all the way to the SOL, and the impurities are effectively retained in the DCP. The fourth frame shows the distribution of fluxes, on an enlarged scale, for the two cases. It can be seen that the change in the level of the flux is small compared to the target fluxes (which are off scale, and correspond to 7.0 and 6.0 x $10^{24}m^{-2}s^{-1}$, respectively), but nevertheless the impurity distribution is completely altered.

Relation (9), which gives the criterion for impurity retention, can be satisfied in either of two ways. One can increase the target flux Γ_t to a large value, which occurs automatically at very high SOL densities. Alternatively, when operating at moderate SOL densities, and hence moderate target fluxes, the integral can be increased by extending the range of $\hat{\Gamma}$ by the combined effects of distant recycling and, when necessary, external recirculation. Figure 5 shows the distribution of flux for four different code runs, corresponding to different target fluxes and distributions. Each of these runs produced retention greater than 90%, achieved by different combinations of target flux and external recirculation, as indicated on the figure. Figure 5b displays the normalized flux, $\hat{\Gamma} = \Gamma(s)/\Gamma_t$, which shows its "extension", and hence the extension of the friction force, to larger values of s by the use of uniform external recirculation in the SOL. Figure 5a shows the non-normalized flux, $\Gamma(s)$, and indicates that the values of the actual local $\Gamma(s)$ over much of the divertor plasma (0 to 8m) are roughly similar, in agreement with the predictions of the analytic model.

Figure 6 summarizes the results of an extensive set of runs. Fig. 6a shows the fraction, f_R, of the target flux Γ_t which must be externally recirculated in order to retain 90% of the impurities in the DCP versus SOL density , n_b, for three values of the total (to both targets) ion heat flow, 20 MW, 10 MW and 5 MW. A simple SOL model (e.g. that of Ref. [4]) shows that $\Gamma_t \sim n_b^2$ for $T_d > 15$ ev. Thus, at high values of n_b, Γ_t is very large and the friction force integral arising from the natural recycling which occurs is sufficient to retain impurities. As the edge density is decreased, Γ_t decreases and an increasingly large flow fraction f_R must be externally recirculated. The required recirculated flow itself, however, becomes relatively independent of density for low and medium n_b (Fig. 6b), consistent with Equs. (10) and (11). Under these conditions the required externally recirculated flow is fairly large and is probably not compatible with achievable steady state pumping rates.

The solid curves of Fig. 6 are results obtained by using a self-consistent beryllium sputtering model. In those simulations, the ratio of the total number of beryllium ions to deuterium ions in the edge plasma decreases from 1,5% at the lower densities to 0.1% at $n_b \equiv 1 \times 10^{20}m^{-3}$. Since these values are somewhat lower than those which have been observed in JET experiments with beryllium to date, we have repeated the simulations with a fixed relative impurity content of 1.5% and the results are shown as dashed lines

in Fig. 6a. In this case, the required fractions f_R are increased slightly.

The situation is somewhat improved for reduced power flows, as can be seen from the graphs in Fig. 6. Lower values of f_R are required for a given SOL density, n_b. This arises in part because the divertor density falls substantially. This increases the distant recycling in the divertor and reduces the flow which must be provided by external recirculation. This effect is illustrated in Fig. 7, which shows the fraction of neutrals, which emanate from the plate and are reionized in the DCP, as a function of computational mesh point (as shown in Fig. 3). For high power, most of the ionization occurs very near the target, whereas at lower power, the effective range of ionization extends much further along the DCP. The increased effective ionization range also increases the fraction of neutrals which are pumped by the cryopump.

Preliminary results from the code indicate that the flow requirements for the "fat" magnetic configuration are relatively unchanged from those of the "slim" magnetic configuration described above.

IV. Conclusions

The entrenchment of impurities in a forced flow of plasma towards the target plates is a candidate concept for impurity control in Next Step Tokamaks, and is the focus of the Pumped Divertor planned for JET. Analysis shows that the effectiveness of the friction force in overcoming the ion thermal force is strongly reduced at high ion temperature in the SOL, which occurs at high ion power flows (P_i). The hydrogenic flow required for effective impurity retention increases approximately as $P_i^{5/7}$. At high SOL densities, recycling at the target plates is very high, and this "natural" recycling flux is sufficient to retain the impurities effectively. At moderate and low SOL densities, however, the "natural" recycling flux must be augmented by "external recirculation" to retain impurities. The fraction of the target flux needed for impurity retention increases as density decreases, but decreases with decreasing ion power flow. Pumping the required external recirculation flows is likely to be possible only at rather high edge densities, approaching $n_b \sim 10^{20} m^{-3}$. The situation improves at lower P_i. Operation with clean plasmas is likely, therefore, only at high densities. This may have severe consequences, e.g. for current drive.

First steps towards validating these complex SOL models have been taken by establishing consistency with observed edge data in JET X-point operation [11]. In particular, the predicted conditions $T_i > T_e$ in the SOL, and divertor temperatures T_{ed} in the range 10 - 20 eV at high n_b, have been observed.

Acknowledgements:

The authors wish to thank G. Radford, D. Reiter (KFA, Jülich) and J. Spence for their help with the numerical analysis.

References

[1] Workshop on the New Phase of JET, Report No: JET-R(89)16.

[2] NEUHAUSER, J., SCHNEIDER, W., WUNDERLICH, R., LACKNER, K., Nucl. Fus. 24 (1984) 39.

[3] VLASES, G.C., JET Report (to be published, 1990).

[4] LACKNER, K., Plasma Phys. and Contr. Fus. 26 (1984) 105.

[5] KEILHACKER, M., SIMONINI, R., TARONI, A. and WATKINS, M.L., Nucl. Fus. (to be published)

[6] SIMONINI, R., KEILHACKER, M., TARONI, A. and WATKINS, M.L., 17th EPS Conf. on Contr. Fusion and Plasma Heating, Amsterdam, 1990, Vol. III, p. 1369.

[7] IGITKHANOV, Y.u.L., Contributions to Plasma Physics 28 (1988) 477.

[8] BRAGINSKII, S.I., Review of Plasma Physics 1, Consultants Bureau, New York (1965), p. 205.

[9] CUPINI, E., DeMATTEIS, A., SIMONINI, R. NET Report EUR XII-324/9 (1984).

[10] HUGON, M., LALLIA, P.P. and REBUT, P.H., Report No: JET-R(89)14.

[11] HARBOUR, P.J., SIMONINI, R., TAGLE, J.A., GOTTARDI, N., VON HELLERMANN, M., et al., 9th Int. Conf. on Plasma Surface Interactions in Contr. Fusion Devices, Bournemouth, 21-25 May 1990 (to be published in J. Nucl. Mat.).

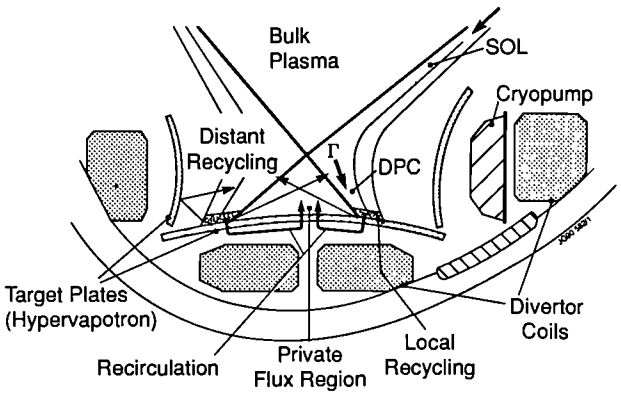

FIG. 1. *Schematic Diagram of the JET Pumped Divertor*

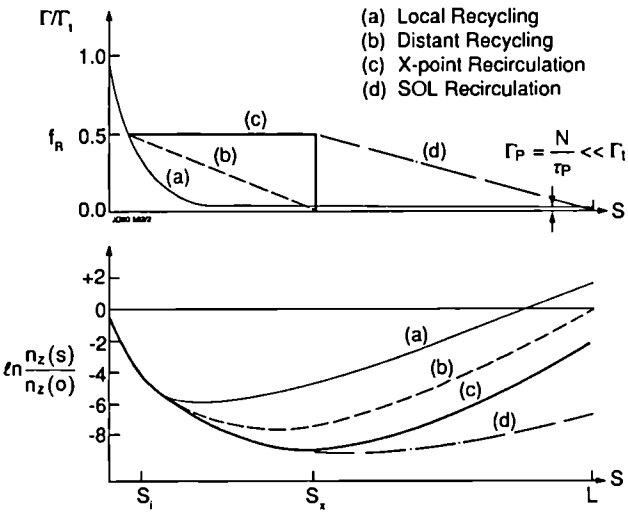

FIG. 2. *Sketch of the Behaviour of the Hydrogenic Flux to the Target (above) and the Resulting Impurity Distribution (below) for Various Recirculation Patterns. s is the distance along a field line from the target, while s_i, s_x, and L refer to the effective ionization length, connection length, and stagnation point locations.*

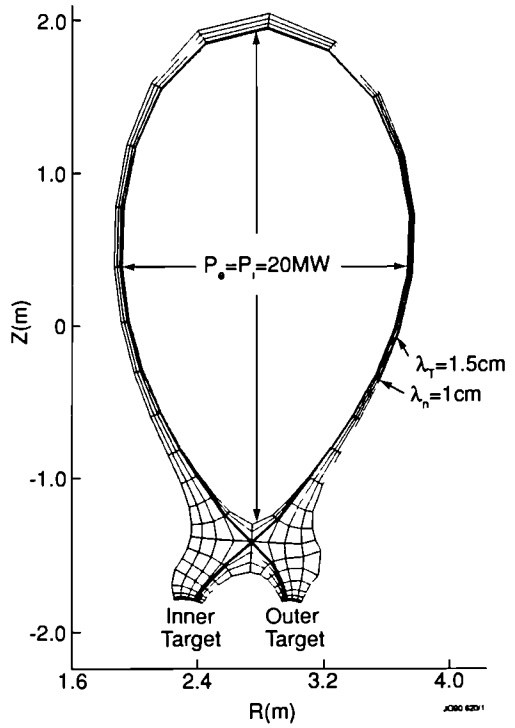

FIG. 3. *The Computational Mesh and some Input Parameters used for the EDGE1D Code Calculations.*

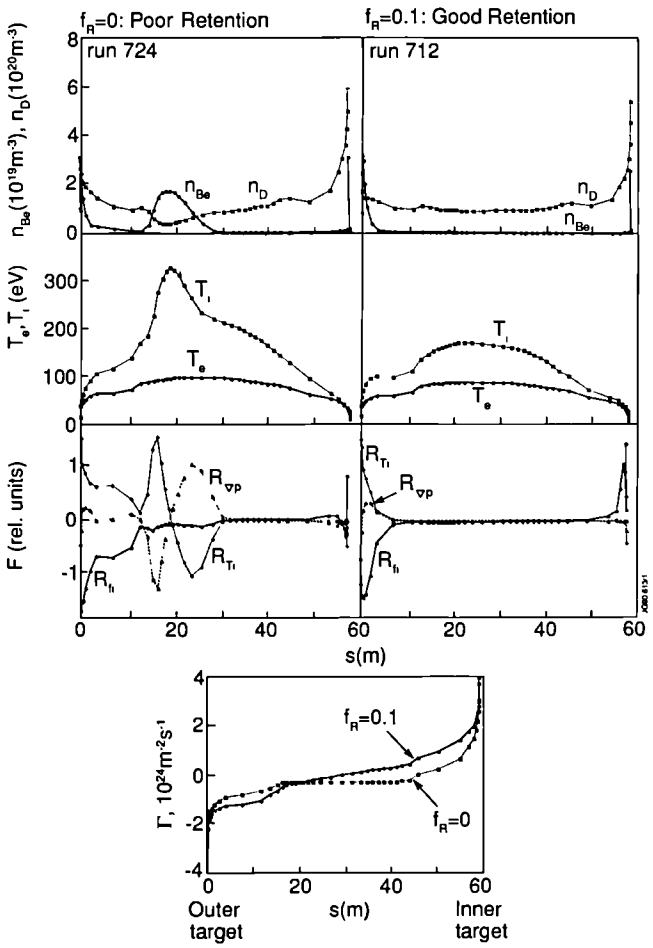

FIG. 4. *Behaviour of Various Plasma Parameters versus s, for a Case of Poor Impurity Retention (left) and Good Impurity Retention (right). f_R is the Fraction of Target Flux which is Externally Recirculated.*

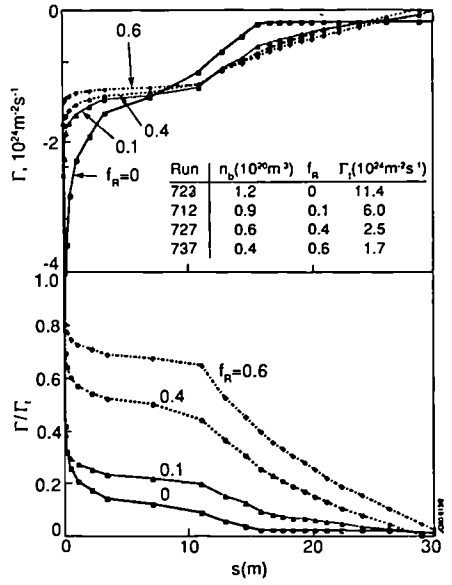

FIG. 5. *Distribution of Hydrogenic Flux (above), and Normalized Hydrogenic Flux $\hat{\Gamma}(s) = \Gamma(s)/\Gamma_t$ (below) for four High Retention Runs with Varying Recirculation Fractions.*

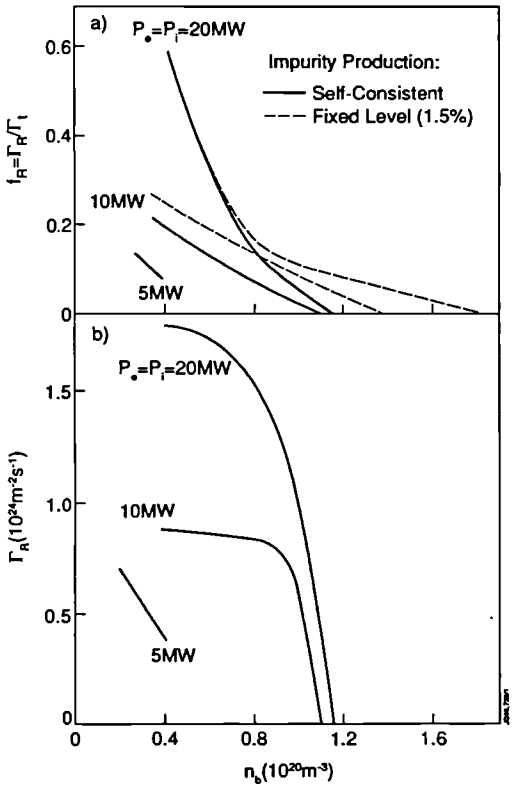

FIG. 6. (a) External Recirculation Particle Flux Fraction f_R, and (b) Particle Flux Γ_R required for 90% Impurity Retention versus SOL Density, for Three Values of Ion Power Flow in the SOL.

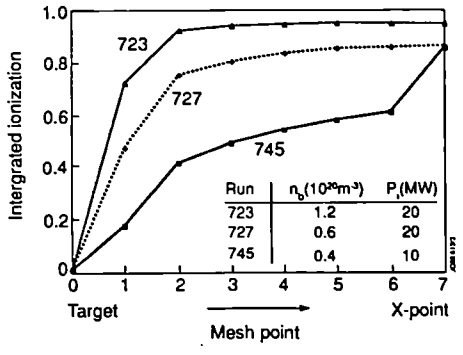

FIG. 7. *Integral of Ionization versus Computational Mesh Point. The distant recycling fraction increases as SOL power decreases.*

COMPARISON OF BERYLLIUM AND GRAPHITE FIRST-WALLS IN JET

Abstract

JET has operated with beryllium as a first-wall material in 1989 and 1990. An initial period with beryllium evaporation onto the original graphite surfaces was followed by operation with beryllium belt-limiter tiles. Beryllium Faraday shields for the ICRH antennae and lower X-point target tiles were installed for experiments in 1990. The use of beryllium has increased the density limit, significantly reduced deconditioning following disruptions, allowed heavy gas fuelling for impurity control, reduced the impurity influx from the ICRH antennae so that ICRH-only H modes were possible for the first time and permitted hot-ion plasmas on the outer limiters. This paper describes the primary effects of beryllium which led to these improvements in performance.

1. INTRODUCTION

JET has used graphite limiters, X-point target plates and vessel protection tiles since the start of operation. Although high performance plasmas have been obtained, it has become apparent that the lack of density control, the fuel dilution, radiative density limit and the "carbon bloom" all present serious obstacles to the development of the JET programme. Beryllium was proposed [1] for JET as an alternative to graphite in order to circumvent some of the these difficulties. It has the obvious advantage that its nuclear charge (and so radiative cooling rate) is lower than carbon whilst having physical sputtering yields which are similar to graphite. Although beryllium melts at a very much lower temperature than graphite sublimes, this disadvantage is offset by its higher thermal conductivity and the phenomenon of "radiation enhanced sublimation" in graphite. Pilot experiments with beryllium limiters were conducted on the UNITOR [2] and ISX-B [3] tokamaks. The results of these experiments were sufficiently encouraging that the decision was made early in 1989 to conduct the beryllium experiment on JET.

There have been four experimental phases of the beryllium experiment:

(i) **A graphite only** phase which was used to bring the machine back into operation following the 1988/89 shut-down. Since the machine was poorly conditioned in this phase, data representative of graphite operation is taken from 1988 experiments.

(ii) The **beryllium evaporation** phase was intended to separate the gettering effect of beryllium from its use as a material limiter. Four evaporators, equispaced in the mid-plane of the machine, were used to deposit a layer about 150 Å thick on the inside wall and about ten times that on surfaces near to the evaporators. The evaporations were performed overnight in order not to interrupt tokamak operation.

(iii) The **beryllium limiter** phase saw the replacement of the graphite tiles in the two outer belt-limiters by beryllium components. Evaporation continued to be used to coat the ICRH antennae, the X-point target tiles and the inner-wall.

iv) In **1990** the nickel Faraday shields of the ICRH antennae were replaced by beryllium components and a trial set of lower x-point targets were constructed out of tiles originally intended for the protective frame around the ICRH antennae.

This paper describes the primary effects of the use of beryllium and compares them with observations from the graphite only phase. The resulting high performance plasmas are described in greater detail in the other JET papers which are presented at this conference [4,5,6,7,8].

2. IMPURITY SOURCES

2.1 Graphite Only Phase

Although there was some variability, according to the kind of operation and its timing relative to vessel vents, the sources of carbon and nickel during operation with graphite surfaces were consistent with expectations based on laboratory sputtering data. The effective yield of carbon (which is defined as the ratio of the carbon to deuterium source rates) falls from about 8% at low density to 4% near the high density limit, as shown in Fig. 1. As the input power is increased, the effective yield curve moves to higher density. Calculations of the effective yield, which take account of self sputtering and use Langmuir probe data for the boundary plasma conditions, give a satisfactory account of the experimental data [9]. Measurements of the amount of erosion found at the wettest part of the limiters are in general agreement with this picture. For the main part, the nickel source emanated from the ICRH Faraday shields. Again, when use was made of a model for the plasma in front of the antenna and the circuit formed between it and the Faraday shields, the data could be described by sputtering [10]. Sputtering of nickel by carbon is an important component of the ICRH induced nickel source.

Oxygen and chlorine behave quite differently from carbon and nickel. Both depend on the conditioning history of the machine. The sources are strongest close to the density limit. An interesting result, which became apparent after the beryllium gettering, is that a significant proportion of the carbon source is due to sputtering by oxygen, (which has a yield close to unity). Thus, periods close to major vents, such as that early in 1989, are characterised by larger effective sputtering yields for *carbon* than when the surfaces are well conditioned.

2.2 Beryllium Evaporation

The most obvious effect of the beryllium evaporation was the almost total disappearance of the oxygen source due to gettering. For otherwise similar plasma conditions, the OII signal fell by a factor of more than 20, the carbon source was also reduced; a factor of two being typical. Whilst this could be due to the coverage of graphite surfaces with beryllium, modelling of this and the variability in the graphite phase suggests that it is the elimination of oxygen sputtering which is responsible. Once beryllium had been introduced in the vacuum vessel, chlorine became the next most important impurity instead of oxygen.

Following an evaporation, the beryllium film would be removed from the region of the limiters in contact with the plasma in a few pulses. In the course of these pulses, the carbon source increased with the exposed graphite surface area. Subsequently there would be very little development in any of the impurity sources over periods of at least 40 pulses. The coating of the ICRH Faraday shields by beryllium reduced the nickel source and would gradually deteriorate over 10-20 pulses.

2.3 Beryllium Limiter Phase

The installation of the beryllium limiters had the obvious effect, for limiter plasmas at least, of replacing the carbon source by beryllium. This further reduction in the carbon source and its consequent effect on the ICRH antennae brought about the virtual elimination of the nickel influx from the Faraday shields. As will be described later, the improvement in the operating range with ICRH was dramatic.

The beryllium effective yield behaves in a similar fashion with density and power to that of carbon, as shown in Fig. 2. However, the yield is as much as 2-3 times greater at the low density end of the curve than that anticipated from normal incidence physical sputtering. The boundary ion temperature is inferred from measurements to be much greater than that of the electrons in these plasmas. A possible result of this is that the ions arrive at the limiter surface at grazing incidence so that the effective yield is enhanced, particularly by self-sputtering.

Both carbon and beryllium limiters had hot spots at which sublimation or evaporation took place. The effective yields described above pertain to power levels and regions of the limiters which are not significantly affected by hot spots. The impurity source from the hot spots causes the "carbon (or beryllium) bloom" which has a severe effect on high performance plasmas [11].

The beryllium X-point targets have been used for plasma experiments but, at the time of writing, the results have not yet been evaluated.

3. IMPURITY CONCENTRATIONS AND PLASMA RADIATION

The impurity concentrations observed in the different phases of operation can be broadly summarised by remarking that the effective yield for all the impurity species is nearly identical with the ratio of the core density of that species to the deuteron density. This is a somewhat surprising result because the ionization lengths for each of the species involved are quite different. Nevertheless, the relationship holds for the spectroscopically derived particle sources and the density ratios n_C/n_D and n_{Be}/n_D as shown in the lower halves of Figs. 1 and 2.

The deuterium pumping conferred by the beryllium limiter allows heavy gas fuelling to be used to reduce impurity concentrations during high power heating. This gas fuelling has little effect on the density of the core plasma but does raise the density at the boundary. The discharges used in Fig. 2 had just enough fuelling to sustain the line density by feedback. However it should be noted that the effective yield and the Z_{eff} value can by multi-valued at a given density. Interestingly, the relationship between the effective yield and n_{Be}/n_D is maintained during the heavy fuelling. This shows that its effect must be to reduce the overall particle confinement time. The mechanism behind this is not understood and is being investigated.

The radiated power is measured with bolometers and VUV/XUV survey spectrometers. The sum of radiation components from each species, calculated from selected line strengths, give good agreement with the bolometric total radiated power.

With graphite limiters the radiated power accounted for 30-100% of the input power even with beryllium evaporation. Carbon and oxygen contributed the bulk of the radiation prior to the introduction of beryllium. In the evaporation phase, chlorine became an important radiator, particularly near the density limit, and carbon provided the rest.

Plasmas on the beryllium limiters radiate 15-60% of the input power with the lower end of the range being typical. Only chlorine and beryllium contribute significantly. During operation, the chlorine was gradually eliminated and thus led to a considerable improvement in the density limit, which is described in the next section. Thus the lower charge of beryllium, compared with that of carbon, has conferred a definite advantage by reducing the radiated power and increasing the operating range.

4. THE DENSITY LIMIT

The density limit is determined by the loss of thermal stability when the radiated power becomes a substantial fraction of the input power. A MARFE forms, whereupon the plasma column either contracts radially until it becomes MHD unstable and disrupts or the MARFE ejects which ejects a sufficient number of particles that thermal stability and poloidal symmetry are restored without a plasma disruption. In JET the former behaviour is associated with graphite limiters and the radial contraction occurs when the radiated power is 100% of the input. The softer limit is observed with beryllium limiters and is triggered when 50-60% of the power is radiated. During the MARFEing phase the radiation can exceed 100% of the input.

The Ohmic heating density limit on the beryllium limiters at $q_\psi \approx 3.8$ and $I_p = 3MA$, was improved by 50% over the best value achieved with the graphite limiters. Reducing the field to (1.55) T, so that $q_\psi \approx 2.6$ was obtained, increased the density limit by a further 20%. The line average density was $0.6 \times 10^{20} m^{-3}$.

In the graphite phase, NBH could be used to increase the density limit. As expected from simple power balance arguments, the density increases as the square root of the total input power. On the other hand, with ICRH the

limit remained close to the Ohmic value because of the impurity influx from the antennae. However, the beryllium evaporation coated the Faraday shields sufficiently that the performance with ICRH became identical to that with NBH. When the beryllium limiter was introduced the impurity influx was so reduced that ICRH only H-modes became possible for the first time.

5. PLASMA PUMPING

Density control with graphite surfaces had always been a problem in JET because the recycling coefficient was close to unity. As shown in Fig. 3, the characteristic decay time for the deuteron density, when the gas feed was switched off, was typically 30 seconds. The density control could be improved for a few pulses by conditioning the limiter with helium plasmas.

Beryllium evaporation caused a long term change in this behaviour and the density decay time dropped to about 5-12 seconds. It can be seen in Fig. 3 that the pumping was still effective after one days operation, although the decay time would approximately double. The beryllium limiters brought about a further improvement and the pumping time fell to 1-2 seconds. Some temporary deconditioning would occur after very high power (>30MW) heating. Helium plasmas are also pumped by the beryllium limiters but not at all by the graphite (even with beryllium evaporation). The density decay rates are fairly similar to those of deuterium.

In respect of the deuterium pumping, JET with beryllium is very similar to other all metal tokamaks. This pumping brings about the following improvements in plasma operation:

(i) Effective density control is possible,
(ii) as noted earlier, large influxes of deuterium can be used to control impurities during additional heating without a consequent density rise and
(iii) the deconditioning effect of MARFE's or disruptions has been significantly reduced.

With graphite limiters, gas desorption in pulses subsequent to a major disruption would often be sufficient to prevent plasma start-up. It often proved necessary to recondition the chamber by GDC in helium for a few hours. This loss of experimental time has largely been eliminated by the used of beryllium, either because the gas load following a disruption is reduced or because of the pumping of the following start-up. Many more high performance pulses can be obtained in a session as a result.

The pressure in the torus falls off as ~ $t^{-0.75\pm0.1}$ following a plasma shot with beryllium surfaces. At least 80% of the deuterium used is recovered in the pumps. From the time dependence of the D_2 and DH fractions, it is concluded that the gas release is recombination dominated.

6. CONCLUSIONS

JET has been successfully operated with beryllium evaporation onto graphite surfaces and with beryllium limiters, ICRH Faraday shields and X-point target tiles. Although hot spots and surface melting have been observed on the beryllium components, the plasmas can be optimised so that improved performance over the graphite phase is obtained.

Beryllium has shown itself to be a viable replacement for graphite as a plasma facing material. Applications can be seen for both in the first wall of a next step tokamak. However neither material can satisfactorily match the requirements for divertor target tiles, because of the problem of blooms, unless most of the power is radiated from the target plasma. The demonstration of a divertor configuration consistent with the requirements of next step tokamaks is the goal of the proposed pumped divertor phase of JET.

7. REFERENCES

[1] REBUT, P.H., et al., JET Report (85) 03.
[2] HACKMAN, J., UHLENBUSCH, J.,J. Nucl. Mater., 128-129 (1984) 418.
[3] ISLER, R.C., et. al., Nuclear Fusion 25 (1985) 1635.
[4] REBUT, P.H., et al., IAEA-CN-53/A-1-2, these Proceedings.
[5] LOMAS, P.J., et al., IAEA-CN-53/A-6-2, these Proceedings.
[6] TANGA, A., et al., IAEA-CN-53/A-4-1, these Proceedings
[7] START, D., et. al., IAEA-CN-53/E-2-1, these Proceedings.
[8] SMEULDERS, P., et al., IAEA-CN-53/A-3-4, these Proceedings.
[9] KEILHACKER M., et. al., Phys. Fluids B2 (1990) 1291.
[10] BURES, M , et. al., Fusion Engineering and Design 12 (1990) 209.
[11] ULRICKSON, M., et. al., to be published in J. Nucl. Mater., (1990)

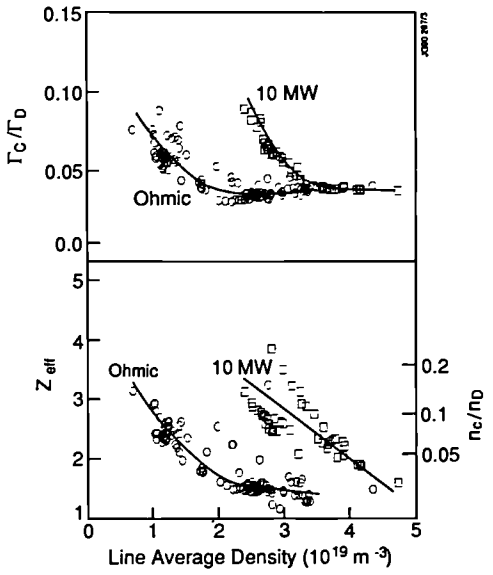

Fig 1: The effective yield (Γ_c/Γ_D), Z_{eff} from visible Bremsstrahlung and central ionic concentration ratio (n_c/n_D) against line average density for Ohmic and additionally heated (10MW) discharges during the graphite phase of operation.

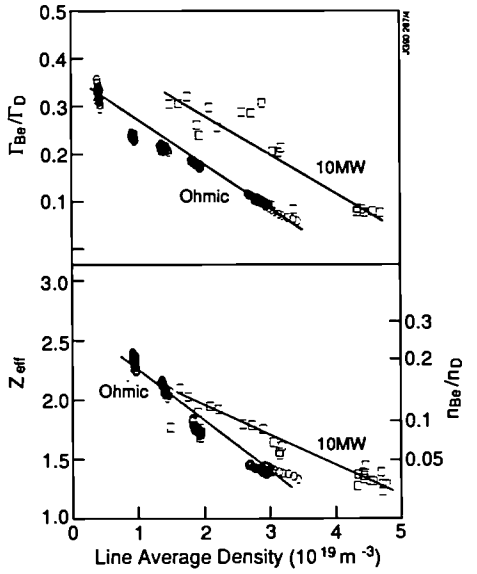

Fig 2: The effective yield (Γ_{Be}/Γ_D), Z_{eff} from visible Bremsstrahlung and central ionic concentration ratio ($n_{Be}n_D$) against line average density for Ohmic and additionally heated (10MW) discharges during the beryllium limiter phase of operation.

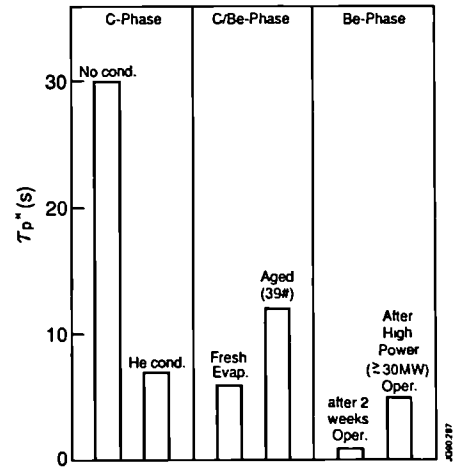

Fig 3: The characteristic decay time for the electron density after switching the gas feed off for different phases of recent JET operation.

ICRF HEATING IN REACTOR GRADE PLASMAS.

Abstract

Impurity influxes in JET discharges due to ICRH have been reduced to insignificant levels. This has allowed high quality H–modes to be produced with ICRH alone and has enhanced the density limit which is now the same as the NBI limit. Improvement in the deuterium fuel fraction has led to the generation of 100kW of non thermal ^{3}He–D fusion power. Alpha–particle simulations using MeV ions created by ICRH show classical energy loss and suggest that α–heating in a reactor will be highly efficient. A clear demonstration of TTMP damping of the fast wave in high beta plasmas has been achieved. A broadband ICRH system is proposed for NET/ITER which will allow fast wave current drive and central ion heating for burn control and ignition.

1. Introduction

During JET operation in late 1989 and 1990 the impurity problems associated directly with ICRF heating have been eliminated for all practical purposes. This has been due mainly to beryllium gettering of the nickel RF antenna screens and their subsequent replacement by screens with Be elements. Other important measures to reduce sputtering from the screens have been dipole antenna phasing and alignment of the screen elements with the magnetic field. These improvements have enabled ICRH on JET to make substantial advances in several important areas of plasma performance and these are described in the present paper. For the first time, long 'elm'–free H–modes have been created by minority ICRH alone and have identical characteristics with those produced by neutral beam injection. Similarly, the density limit no longer depends on the type of additional heating. Fast ions created by ICRH have been used to produce 100kW of fusion power from non–thermal ^{3}He–D fusion reactions and to simulate the behaviour of α–particles in a reactor. Section 5 shows the results of Be influx measurements and section 6 describes a demonstration of TTMP absorbtion of 48MHz fast magnetosonic waves in high beta plasmas. The final section describes a proposal for NET/ITER of a broadband ICRH system operating between 17MHz to 40MHz to give fast wave current drive, central bulk ion heating and non–thermal D–T fusion.

2. H–modes produced by ICRH alone

An example of an H–mode created by RF alone in a double–null X–point plasma with I_p=3MA, B_t=2.8T is shown in fig.1. The RF power was 7MW and dipole phasing was used. The Dα signal shows the H–mode to extend for 1.3s during which time the energy content given by the diamagnetic loop reaches 6MJ. Comparison with the energy obtained from magnetic analysis suggests that 1.3MJ of this is due to fast ions. The confinement time of the thermal component alone is 0.7s which is twice the Goldstone L–mode value and is similar to values obtained with neutral beam injection (NBI) for the same power level. In fig 1 the central electron temperature reached 9.5keV at the end of the H–mode when the central density had risen to 3.7×10^{19}m^{-3}. Monopole phasing ($P_{rf}\approx$10MW) also produces H–modes and, in some of these, Monster sawteeth occur.

These experiments were assisted by a new feedback system which keeps the coupling restance (R_c) constant by controlling the separation (X_s in fig. 1) of the last closed flux surface from the antenna. In pulse 21906 the requested 3.5 ohm coupling was maintained across the L–H transition and throughout the H–mode phase by plasma movements of the order of 0.01m. Without feedback control R_c is reduced by a factor of three during the H–mode causing generator trips and RF power loss[1].

3. ^{3}He–D non–thermal fusion experiments

The fusion reaction $^3He + D \rightarrow {}^4He(3.6MeV) + p(14.7MeV)$ has been studied in JET using ^{3}He minority ICRH. The first experiments with carbon coating of the vessel achieved 60kW of fusion power [2]. Recently, experiments with Be coating have reached 100kW as shown in fig 2a. The maximum value of Q ($=P_{fus}/P_{rf}$) was 1% (fig 2b). The later results were obtained with I_p = 3MA, B_t = (3.0–3.4)T, ne(0)$\approx4\times10^{19}$m^{-3} and $P_{rf}\leq$14MW. As previously, the reaction rate was measured by detecting the 16.6MeV γ–rays from the weak branch $^3He + D \rightarrow {}^5Li + \gamma$. In most discharges the ICRF resonance was on axis. Some data were taken with off–axis heating to reduce the power density and test for heating of the ^{3}He ions beyond the energy for maximum fusion rate ($\simeq$0.5MeV). The yields were similar with on and off–axis heating implying that the ^{3}He energy was about optimum. A Stix code [2] agrees well with the yields in the carbon vessel for a fuelling ratio $n_d/n_e \simeq 0.4$. To fit the data with Be gettering this model requires $n_d/n_e\simeq0.7$ which is consistent with $Z_{eff} \simeq 2.5$ compared with $Z_{eff} \simeq 3.5$ previously.

4. Alpha–particle simulation studies

Minority ions created by ICRH in JET can reach MeV energies. The anisotropic distribution allows their energy content to be deduced from diamagnetic loop and Shafranov shift measurements. The energy content can then be compared with theory to test for non–classical loss processes which might reduce the α–particle heating in a reactor. Such comparisons have been made for near steady state Monster sawtooth data which avoids fast ion redistribution by sawteeth. Results are shown in figs 3a and 3b for H–minority ions. Values of W_{fast} are plotted against model calculations which assume a) an RF power density of Gaussian form with a width of 0.3m, b) that 65% of P_{rf} is absorbed by the minority (as deduced from modulation experiments) and c) that the fast ions form a Stix[3] distribution on each flux surface. This basic model is supplemented by corrections for the effect of the fast ion orbits on the slowing down time. The slowing down time is averaged over both the orbit and the energy distribution. Fig 3a shows W_{fast} compared with the results of the basic model only which generally overestimates W_{fast}. However, including orbit effects gives excellent agreement (fig. 3b). A lower limit of 2s is placed on any anomalous loss time which implies that α–particles in a reactor will yield all their energy to the plasma, at least in the absence of mhd.

5. Beryllium influx from the antenna screens

It is well known that impurity fluxes are released from the screens of powered ICRF antennae on JET. The flux depends on antenna voltage, the plasma density near the screen, the angle of the screen bars to the magnetic field, the phasing and the screen material. The sensitivity to voltage and phasing are illustrated in fig 4 for Be coated screens. Note the threefold reduction with dipole phasing. Beryllium coating of the screens and its use as a first wall material, together with dipole phasing and alignment of the screen bars with the field, have reduced the influxes to insignificant levels. The behaviour can largely be understood in terms of sputtering due to RF field rectification in the sheaths formed where the magnetic field intercepts the screen bars[4]. With the present antenna the field can connect a) adjacent bars and b) different points on the front face of the same bar by virtue of its V–shape. The latter effect is sensitive to phasing and disappears for dipole operation. Beryllium gettering is beneficial partly because of the low sputtering coefficient (especially for self sputtering) and partly because it strongly pumps oxygen and other impurities. The influx contribution to Z_{eff} is $\Delta Z_{eff} \simeq 0.05$ –0.1

6. TTMP damping of the fast wave

Directed fast waves are a strong candidate for non–inductive current drive in reactor plasmas where TTMP is the predominant direct electron damping process. So far, fast wave current drive experiments have been made in low β plasmas and with high RF frequency[5] such that the absorption was mainly by electron Landau damping (ELD). The present experiments were carried out in I_p=2MA, B_t=1.3T, double–null X–point hydrogen plasmas with the ICRF (48MHz) tuned to $2\omega_{ch}$ on the high field side of the magnetic axis. No mode conversion layers existed in the plasma centre where direct electron heating could only occur through damping of the fast wave by combined TTMP and ELD. The electron β was 1.5% so that TTMP was expected to contribute significantly. The electron heating power density was obtained from the T_e (ECE) response to RF power modulation. The profile is peaked on axis as shown in fig 5a and accounts for 22±5% of the input power, the rest being absorbed at $2\omega_{ch}$. Full wave and ray tracing calculations predict more peaked profiles (fig. 5a) but agree with the fraction of the total power absorbed. Data were also obtained from soft X–ray cameras which viewed more of the minor radius than the ECE measurements. Note that the damping is almost zero near the q=1 surface (see fig 5b). A recent Hamiltonian treatment of the wave–particle interaction [6] predicts that quasilinear theory is most likely to break down at q = 1 resulting in just such a reduced absorption.

7. A broadband ICRH system for NET/ITER

An ICRH system operating between frequencies of 17MHz and 40MHz has been proposed for the NET and ITER tokamaks. At 40MHz deuterium minority heating takes place in the centre of the machine. The 'minority' fraction, $n_d/(n_d + n_t)$, is about 30% for which more than 50% of P_{rf} is damped on the deuterium ions. This high minority density also restricts the fast ion tail temperature ($T_t\simeq$150keV for $P_{rf}\simeq$50MW) with the essential effect of providing an intense ion heating source near the magnetic axis. This ion heating is the most important aspect in achieving ignition or burn control according to simulations using the transport code JETTO[7,8]. For Kaye–Goldston scaling[9] the fusion reaction rate is typically 40% higher than that achieved using electron heating methods (ECRH or NBI at MeV energies)[see ref 8]. The advantage of ion heating depends on the confinement scaling assumed and is greatest for Rebut–Lallia[9] and smallest for H–modes ($\tau_h\simeq2\tau_{kg}$) which are predicted to readily achieve ignition. The Kaye–Goldston case almost ignites so that the ICRH could be used for burn control [9] in this situation.

17MHz is chosen for fast wave current drive by TTMP + ELD since there is no competing cyclotron damping at this frequency. Current drive calculations have been made using 3–D ray tracing and analytic fits to current drive efficiencies[10]. The current achieved is found to depend on the antenna position (on or above the midplane) and on the poloidal field; different geometries give different shifts in the parallel wave vector as each ray propagates. The maximum value of γ ($= \langle n_e \rangle I_p R/P_{rf}$) is 0.3×10^{20}A/W/m^2 for antennae in the midplane as shown in fig 6. The largest value of γ for antennae above the midplane is 0.2×10^{20}A/W/m^2.

8. Summary

Substantially reduced impurity influx has allowed ICRH on JET to produce high quality H–modes, an enhanced density limit and 100kW of non–thermal ^{3}He–D fusion power. Alpha particle simulations using ICRF accelerated minority ions imply efficient α–heating in reactors. TTMP damping of the fast wave has been demonstrated in high β plasmas. The dual purpose ICRH system proposed for NET/ITER allows both central bulk ion heating at 40 MHz for burn control, and fast wave current drive at 17MHz with $\gamma \simeq 0.3\times10^{20}$A/W/m^2.

9. References

1) Tubbing B J D et al. Nuclear Fusion 29(1989)1953.
2) Boyd D A et al., Nuclear Fusion 29(1989)593.
3) Stix T H, Nuclear Fusion 15(1975)737.
4) D'Ippolito D and Myra J, Proc. IAEA Tech. Comm. Meeting on Fusion Engineering and Design, Garching, FRG(1989).
5) Moreau D, O'Brien M R, Cox M, and Start D F H, in Controlled Fusion and Plasma Physics (Proc. 14th Eur. Conf., Madrid, 1987) Vol III, European Physical Society (1987) 1007.
6) Becoulet A et al., paper IAEA–CN–53 E–3–10, this Conference.
7) Cenacchi G and Taroni A, JET Report JET–IR88/03 (1988).
8) Koch R et al paper IAEA–CN–53 G–2–9 this conference.
9) Corrigan G et al, Proc 17th European Conf. on Controlled Fusion and Plasma Heating, Amsterdam,1990, Vol II p 801.
10) Bhatnagar V P et al., Proc. Joint Varenna–Lausanne Int. Workshop on Theory of Fusion Plasmas, 1990, to be published.

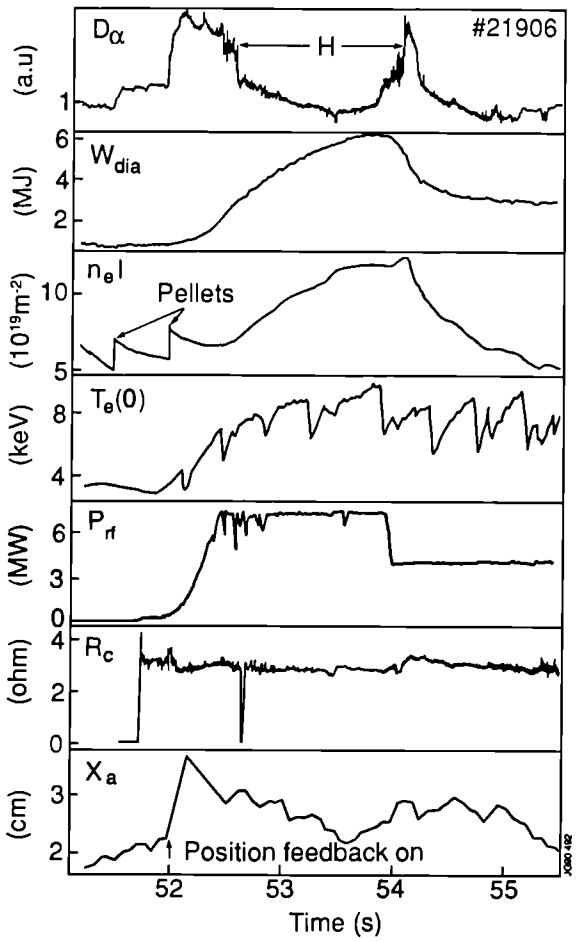

Fig. 1 Plasma parameters during ICRF only H–mode. Note the plasma position control to keep the coupling resistance constant.

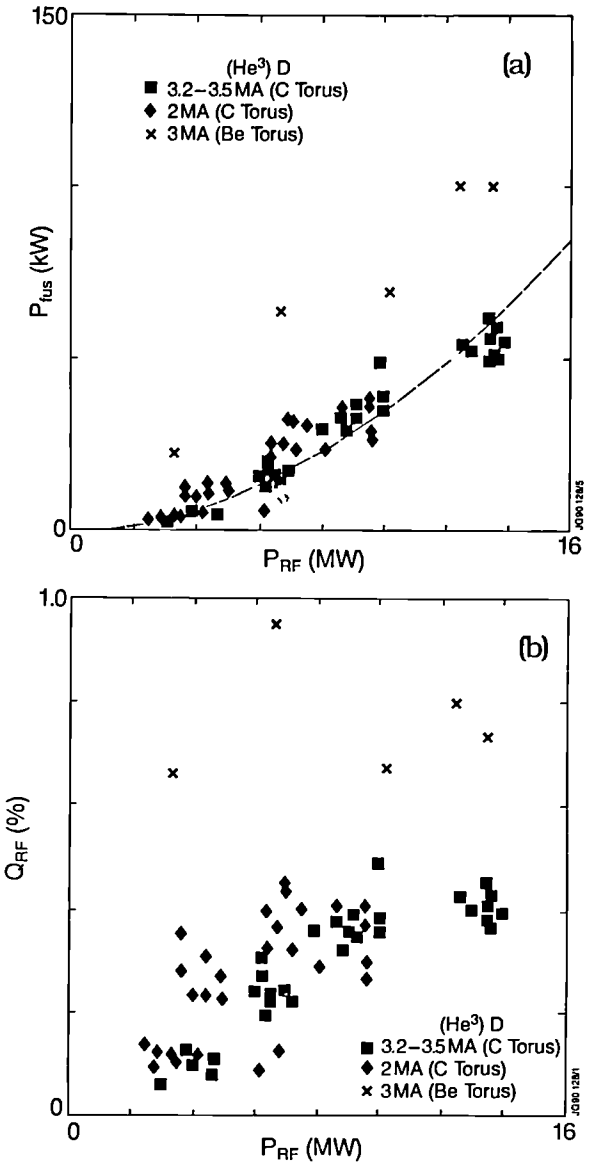

Fig. 2 a) ^{3}He–D fusion yield versus P_{rf} and b) Q–value versus P_{rf}.

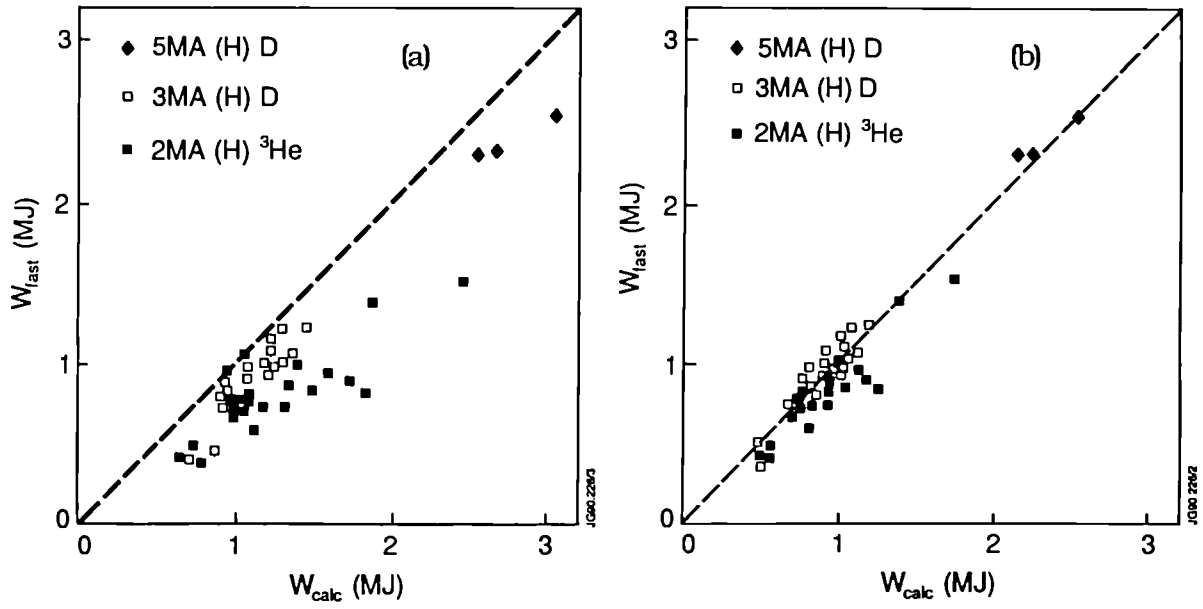

Fig. 3 W_{fast} versus theoretical values for a) no orbit corrections and b) with orbit corrections.

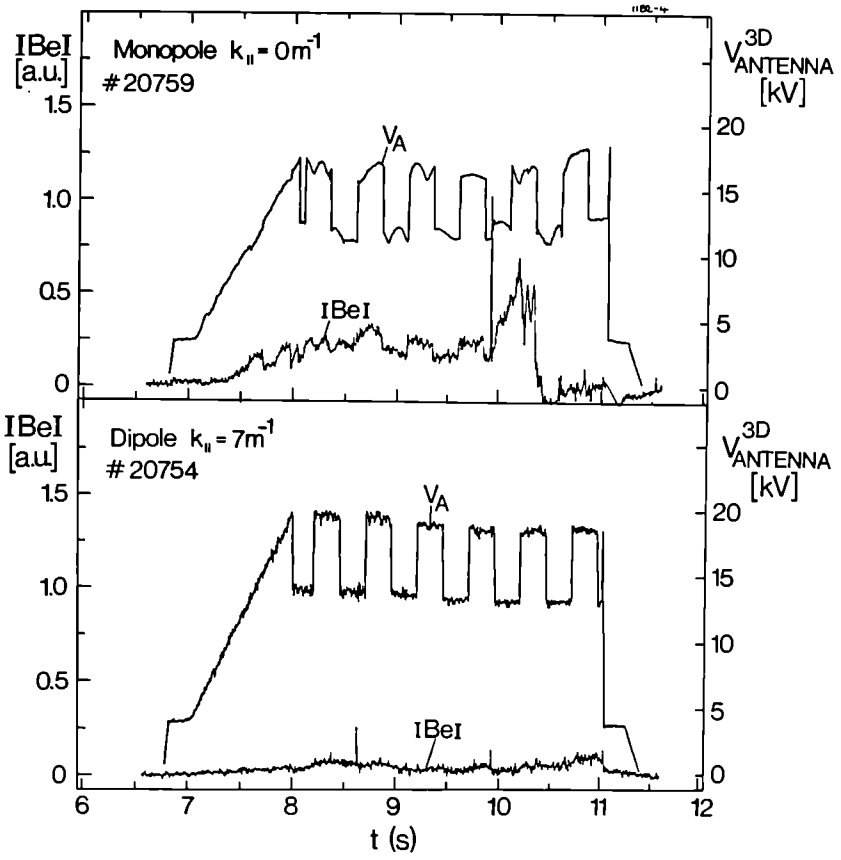

Fig. 4 Be influx sensitivity to antenna voltage and phasing.

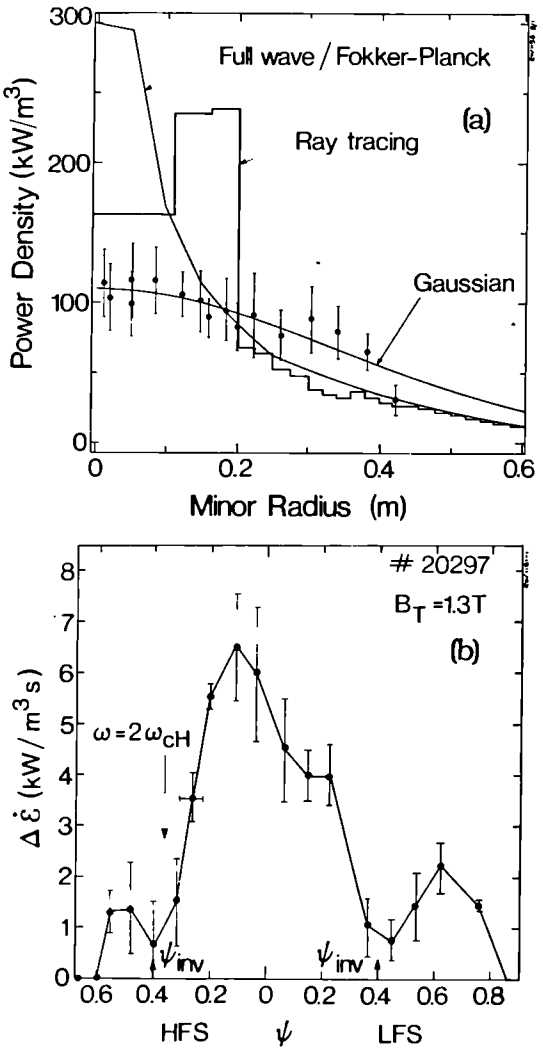

Fig. 5 TTMP + ELD power density profiles from a) theory and ECE measurements and b) soft X-ray emission. ψ is the magnetic flux normalised to unity at the boundary.

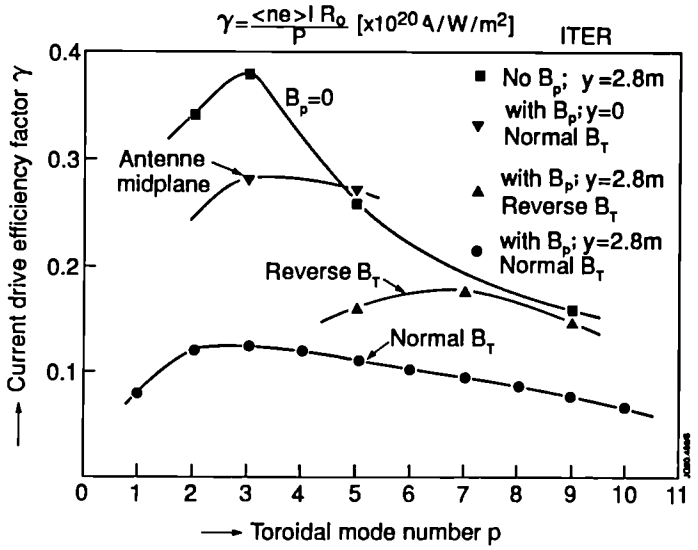

Fig. 6 FWCD current drive efficiency for various antennae and magnetic field configurations. The distance y is the height of the antenna centre above the midplane.

SAWTEETH AND THEIR STABILIZATION IN JET

Abstract

Sawtooth relaxations control the central plasma parameters in most JET discharges and, as a result, have a significant influence on fusion performance. Several techniques have, therefore, been developed for the stabilization of sawteeth in various JET operating regimes. Under some circumstances, sawtooth suppression appears to be associated with the central safety factor, q_0, rising above unity. However, in other cases, q_0 remains significantly below unity and it is thought that stabilization is due to the influence of a population of energetic particles. Detailed measurements of the evolution of the current profile in JET during sawteeth have confirmed that q_0 remains below unity throughout the sawtooth cycle and thus the trigger for the sawtooth collapse remains problematic. Further diagnostic investigations of the sawtooth collapse have shown that the collapse takes the form of a convective plasma flow, but the cause of the resultant energy transport is not understood.

1. Introduction

Sawteeth are one of the fundamental mhd instabilities of tokamak plasmas. They play a key role in limiting central plasma parameters, and thereby fusion reactivity, in the near–ignition regime. Nevertheless, in spite of considerable experimental and theoretical investigations, both at JET (see e.g. [1]) and elsewhere, no consistent picture of the instability has emerged. Furthermore, while several techniques for sawtooth stabilization exist [2–4], their extension to reactor relevant plasmas is not assured in view of the limited understanding of the mechanisms involved.

Recent experiments at JET have focussed on a number of aspects of the sawtooth problem: the development of a detailed description of the sawtooth instability and its relationship to the the q–profile; the attainment of sawtooth stabilization at the highest plasma parameters; and, finally, the investigation of the interaction between the sawtooth instability and energetic particles, both in relation to fusion performance and to the stability of the m=1 mode.

2. The Sawtooth Instability

In JET, sawteeth are accompanied by a variety of mhd activity [1] which may give rise to island–like structures with poloidal and toroidal mode numbers m=n=1. However, these do not appear to play a role in the sawtooth instability, which occurs as a rapidly growing helical deformation of the plasma core, also with m=n=1, followed by a flattening of temperature and density profiles across the central plasma, the entire event having a timescale of ~100μs. The topology of the sawtooth collapse in JET, as first elucidated by tomographic analysis of soft X–ray (SXR)

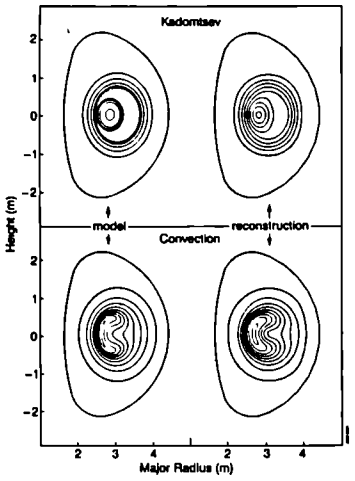

FIG 1: *Comparison of simulated soft X–ray analyses of the two most common models for the sawtooth collapse: full–reconnection (Kadomtsev) and 'quasi–interchange' (convection).*

emission measurements made with orthogonal cameras [5], resembles the convective flow of plasma suggested by the 'quasi–interchange' model [6] rather than the behaviour proposed by full–reconnection models (e.g. [7]).

Recently, possible limitations of the SXR analysis, particularly in relation to its poloidal resolution, have been explored by simulation of the behaviour expected from different models of the collapse [8]. In these investigations, flow patterns predicted by the 'quasi–interchange' and full reconnection models were used to generate SXR emission profiles and the line–integrated measurements which would be obtained from the X–ray cameras. The 'observations' were analyzed to produce tomographically inverted profiles such as those derived experimentally. The results are illustrated in figure 1, which shows the input and output flow patterns. There are clear differences between the reconstructions which enable the topologies associated with the two models to be unambiguously distinguished. More generally, it was found that, for the case commonly studied in JET (in which the plasma core is displaced along the major radius), the analysis technique accurately reproduced the emission profiles.

Further confirmation of the topology of the sawtooth collapse was obtained from two–dimensional reconstructions of local temperatures derived from electron cyclotron emission (ECE) measurements obtained with a 12–channel grating polychromator [9]. The method exploits the rotation of mhd structures using assumptions about their helical symmetry (for sawteeth, it is assumed that reconstructed modes have m=n) [10]. Application of the technique is, therefore, restricted to cases where the structure changes on a timescale somewhat greater than its rotational

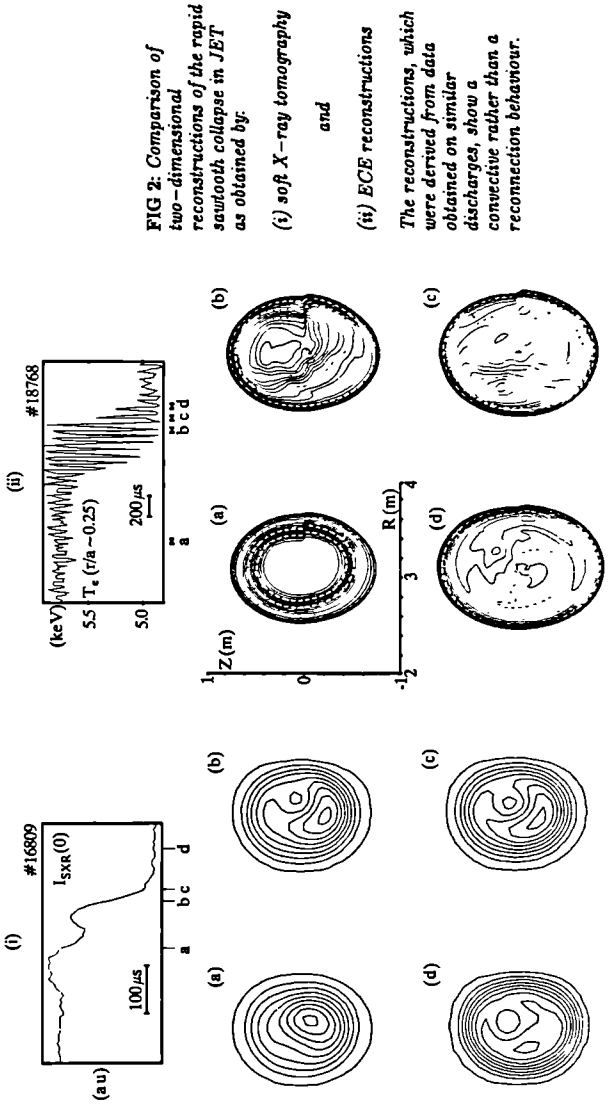

FIG 2: *Comparison of two–dimensional reconstructions of the rapid sawtooth collapse in JET as obtained by: (i) soft X–ray tomography and (ii) ECE reconstructions. The reconstructions, which were derived from data obtained on similar discharges, show a convective rather than a reconnection behaviour.*

period. For example, analysis of the sawtooth collapse requires rotational frequencies of ~10–20kHz and is limited to discharges with high power NBI. Figure 2 compares an ECE reconstruction of a sawtooth collapse with a SXR tomographic reconstruction from a similar discharge. Both show the formation of a crescent–shaped, or 'convective', structure.

It has been recognized for some time (e.g. [6]) that the rapid timescale of the sawtooth collapse presents a significant challenge to theoretical models. More fundamentally, it is found that the rapid growth of the m=1 arises spontaneously and cannot be explained by the increase of a linear growth rate arising from the evolution of the plasma equilibrium [11]. Figure 3 shows the growth of the instability, as deduced from the displacement of the peak of tomographically inverted SXR profiles, for three sawtooth collapses in different discharges. The initial noise level is ~1cm and the displacement rises out of this noise with a growth rate ~$(25\mu s)^{-1}$. Extrapolation of this growth backwards in time yields a displacement equal to the Debye length, perhaps the smallest realistic scale for the instability, on a timescale of order ~100μs. In contrast, existing models of

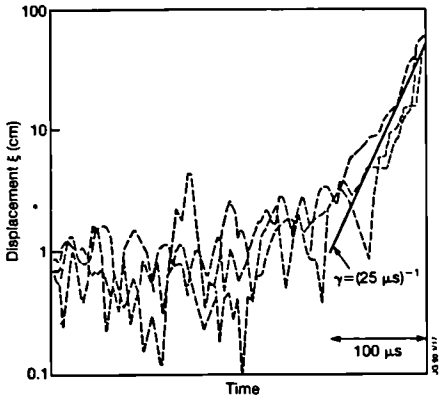

FIG 3: *The displacement of the peak of the soft X–ray emission, derived from two–dimensional tomographic reconstructions, during the fast sawtooth collapse. Experimental results for three cases are illustrated. The data shows that a growth rate of $(25\mu s)^{-1}$ is achieved even before the displacement is large enough to be detected above the experimental noise.*

the instability involve changes in quantities such as q or β which would require timescales ~100ms to generate such large growth rates.

3. Current and Safety Factor Profiles

The determination of the q–profile or, perhaps more precisely, the way in which the q–profile is modulated by sawtooth activity, is one of the central problems in understanding sawteeth. On JET, the principal diagnostic of the q–profile is a multichannel far–infrared interferometer/ polarimeter. A new analysis of the polarimetric signals [12], which combines the constraints imposed by polarimetric measurements of the internal poloidal fields with external magnetic measurements in a self–consistent equilibrium calculation, has confirmed earlier conclusions that q_0 remains well below unity (0.75 ± 0.15) during normal sawteeth.

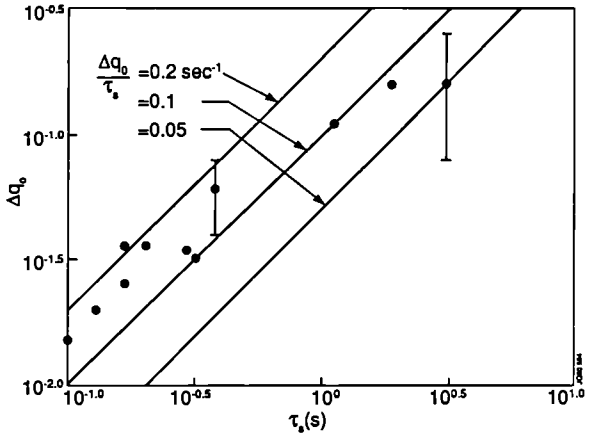

FIG 4: *Plot of the change in the central safety factor, Δq_0, vs the time between sawtooth collapses, τ_s, derived from polarimetric measurements.*

By Abel–inverting the difference in polarimetric signals before and after a sawtooth collapse, it has been possible to study the variation of q_0 during both sawteeth and sawtooth–free periods. As the sawtooth period is significantly longer than the integration time of the diagnostic electronics, sawteeth are visible in the raw data, so that coherent averaging over many sawteeth is unnecessary. Results of this analysis for a series of discharges with ohmic and ICRF heating are shown in Figure 4. It is found that Δq_0 increases with τ_s, the time between sawtooth collapses, at a rate of $0.05 - 0.2 s^{-1}$. Further confirmation of such modulation of the central q–profile has been obtained by analysis of the expansion of the sawtooth inversion radius with increasing sawtooth duration. The difference in the inversion radii, Δr_i, of successive sawtooth collapses was deduced from tomographically inverted SXR emission profiles and a relationship $\Delta r_i / \Delta \tau_s = 0.06 ms^{-1}$ obtained.

A major inconsistency remains, however, in our understanding of the behaviour of the q–profile during sawtooth activity. The most direct determination shows that q_0 remains well below unity during sawteeth, and does not return to unity at sawtooth collapses, a result which is supported by the observation of m=1 magnetic structures immediately following the sawtooth collapse. In contrast, measurements of shear at the q=1 surface, as inferred from observations of the 'snake' [13] and of pellet ablation [14], indicate that very low values of shear ($dq/dr \sim 5\times10^{-2}$) persist throughout the sawtooth cycle. Simple considerations of resistive diffusion suggest that such persistence implies the existence of a low shear region across the plasma centre, with q_0 within 1–2% of unity. Such a conclusion would also be consistent with the convective flow observed during the sawtooth collapse in JET.

4. Sawtooth Stabilization

Several techniques for sawtooth stabilization have been investigated in JET, and another, lower hybrid current drive, is currently being commissioned. Sawteeth have been suppressed for up to 5s following the injection of pellets, both in the current rise phase and during the flat–top. As is illustrated in figure 5, polarimetric measurements of q_0 indicate that sawtooth suppression is due to a broadening of the current profile, leading to $q_0 > 1$, which results from the substantial changes in electron temperature produced by pellet ablation. This is supported by observations of mhd activity with mode numbers (m,n) = (3,2) and (2,1) deep in the plasma core.

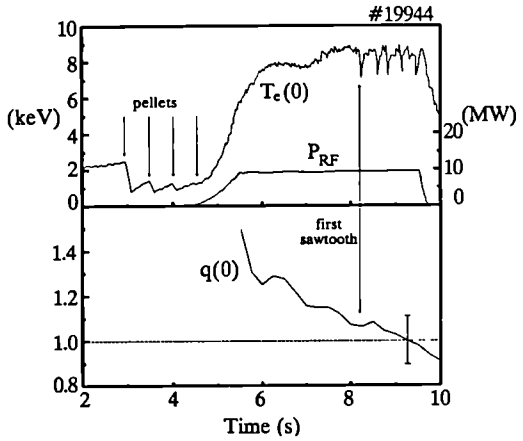

FIG 5: *Suppression of sawtooth activity following pellet injection in JET. Polarimetric measurements indicate that the suppression is due to q_0 remaining above unity.*

The 'monster' sawtooth regime [3], in which sawteeth are stabilized as a result of central heating, has been the subject of detailed investigations. By scanning the position of the ICRH resonance across the plasma centre, it has been found that stabilization is produced most efficiently (i.e. the longest stable periods are obtained for a given power) when the heating resonance is located at the magnetic axis. In addition, stabilization is achieved only for heating inside the sawtooth inversion radius. The results of this experiment are shown in figure 6, where the longest stable period observed is plotted against the major radius of the heating resonance. In each case, the corresponding sawtooth inversion radius is indicated. It has also been observed that stabilization is most probable at low ICRH minority concentrations, when the stored energy in the fast particle population is maximized.

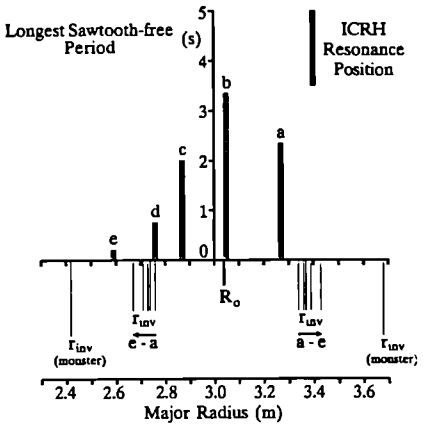

FIG 6: *Results of a scan of the ICRH resonance position. The longest sawtooth–free period at each resonance position is plotted against the resonance major radius. The sawtooth inversion radius (r_{inv}) is indicated for each case, as is the inversion radius of the longest 'monster' sawtooth.*

In 3MA discharges with $q_\psi \sim 4$, stable periods of up to 5s have been obtained and previously reported observations [1] that q_0 is significantly below unity ($q_0 \sim 0.6–0.8\pm0.15$) have been confirmed. In addition, long

sawtooth–free H–modes are now produced routinely during ICRF and ICRF/ NBI combined heating of X–point plasmas. However, stabilization by this technique becomes more difficult as the edge safety factor decreases ($q_\psi < 4$). To extend the regime to higher current, therefore, auxiliary heating has been applied during the current rise phase, either just before or just after sawteeth start. The high electron temperature attained is expected to slow the inward diffusion of current, but the smaller radius of the q=1 surface at such times may also be a significant factor. This approach has succeeded in extending stabilization to plasma currents of 5–6MA (see e.g. [15]).

5. Interaction of Sawteeth and Energetic Particles

Interactions between the sawtooth instability and energetic particle populations, produced either by auxiliary heating or by fusion reactions, are of growing importance as fusion plasmas approach breakeven conditions. For example, considerable attention has been given to the suggestion [16] that energetic ions, accelerated by RF fields, might be responsible for sawtooth stabilization in the 'monster' sawtooth regime. This process can occur when the average fast ion energy, E_h, is such that the bounce–averaged magnetic drift frequency of deeply trapped fast ions, $\omega_{Dh} = E_h/Z_h eB_\varphi R_o r_1$, exceeds the mode frequency in the plasma rest frame (Z_h is the hot ion charge, B_φ the toroidal magnetic field, R_o the plasma major radius and r_1 the radius of the q=1 surface).

A growing body of experimental evidence is now consistent with this interpretation. Not only is it known that ICRF minority heating in JET can accelerate minority ions to energies of order 1MeV, well above the relevant energy threshold (<100keV), but several experimental observations are as expected from theory. The result that stabilization is produced most efficiently with on–axis heating is consistent with the requirement that the hot ion pressure profile be peaked. As noted previously, low minority concentrations, corresponding to high stored energy in the fast ions, are also optimal for attaining stabilization. The difficulty experienced in producing stabilization as q_ψ falls below values ~4 can be associated with the prediction that the maximum stable values of β_p and β_{ph} scale as $(r_1/a)^{-\alpha}$, where $\alpha = 1.5$ for β_p and $2.0 < \alpha < 2.5$ for β_{ph}. Moreover, this observation stimulated the development of the current–rise heating scenario, which takes advantage of the smaller q=1 radius in the initial phase of plasma development to extend the stabilization to higher currents and lower values of q_ψ. Perhaps the most direct evidence for the role played by fast ions is the observation that, following switch–off of RF heating, a sawtooth collapse terminates the stable period within 200ms (often far less), i.e. on a timescale which is of the order of the average fast ion slowing down time within the q=1 radius.

Quantitative investigation of the theory is limited by difficulties associated with the determination of the fast ion distribution in space and energy, with uncertainties in the q–profile and with the general uncertainty surrounding the nature of the sawtooth instability. Nevertheless, by making several simplifying assumptions, essentially that certain local quantities can be approximated by global parameters, such a quantitative comparison between theory and experiment has been performed [17]. The analysis is performed in the (Γ, H) plane, where,

$$\Gamma = \frac{\gamma_{mhd}}{\omega_{Dh}^{max}} \qquad H = \frac{r_1}{s_o R_o} \frac{\omega_A}{\omega_{Dh}^{max}} <\beta_{ph}>_a. \qquad (1)$$

γ_{mhd} is the ideal mhd growth rate, ω_{Dh}^{max} the maximum fast ion precession frequency as defined previously, ω_A the Alfvén frequency, s_o the shear at the q=1 radius and $<\beta_{ph}>_a$ the poloidal beta associated with the perpendicular fast ion energy (which, for central ICRH, is a reasonable measure of the fast ion energy within the q=1 radius).

Results of this analysis are shown in figure 7, where the area enclosed by the curve represents the stable region and the dashed lines indicate the trajectories followed by discharges as the q=1 radius expands during a sawtooth–free period. Closed circles represent discharges in a variety of conditions ($4 \le q_\psi \le 9$, $7 \le P_{RF} \le 10MW$, $<n_e> = 2–3\times10^{19}m^{-3}$) where stabilization is readily obtained. The closed triangle corresponds to a pulse in which stabilization was obtained at the lowest power to date (P_{RF} ~ 1.2MW) and the open symbol to one of the longest sawtooth free periods (5s). Both pulses had q_ψ ~ 4.5. As is indicated, the experimental uncertainties in the calculations are large, and significant approximations have been applied to the theory to facilitate the analysis. Nevertheless, in the light of the more detailed experimental observations outlined above, the theory provides a working hypothesis for the development of an understanding of the stabilization mechanism.

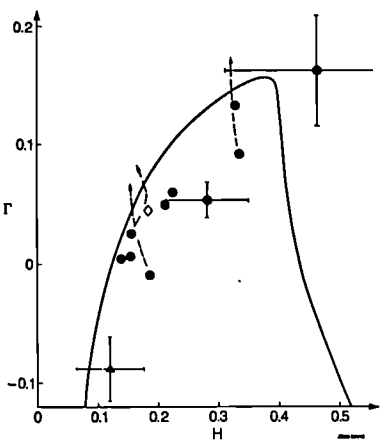

FIG 7: *Analysis of a series of sawtooth–free discharges in terms of the fast–particle stabilization theory [16,17]. Γ and H are defined in the text. The solid curve encloses the region predicted to be stable. The dashed lines indicate the trajectories of the discharges in the stability diagram as the q=1 radius expands during the sawtooth–free period.*

In JET plasmas with ohmic and ICRF heating, nentron emission is modulated in accordance with expectations based on the redistribution of ion thermal energy at the sawtooth collapse. However, the major contribution to the fusion yield of high performance discharges is non–thermal in nature and is due to beam–plasma and beam–beam reactions. The modulation of the reactivity due to m=1 activity and, in particular, the way in which m=1 instabilities affect energetic ions is, therefore, central to the optimization of fusion reactivity. While 'fishbone'–like bursts are observed in both NBI– and ICRF–heated plasmas [18], only at the highest β_t values is there evidence of detectable (<10%) modulation of neutron production. However, recent studies of neutron emission profiles derived by tomographic analysis of measurements obtained from orthogonal arrays of neutron detectors has revealed a strong modulation of central neutron production due to sawteeth [19].

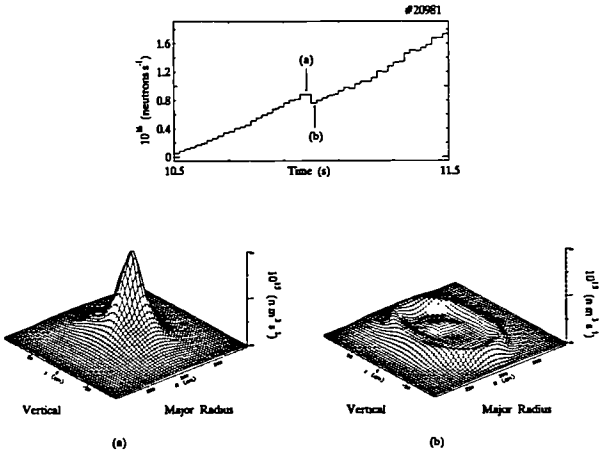

FIG 8: *Comparison of local neutron emission profiles measured before and after a sawtooth collapse. Although the global neutron emission falls by only 18%, the axial emission falls by a factor of 6.*

Figure 8 shows neutron emission profiles calculated at timeslices just before and just after a sawtooth collapse in a JET hot–ion H–mode plasma heated with 18MW of NBI. While the modulation of the global neutron yield is small, ~18%, it is found that the emission profile is changed dramatically, the FWHM broadening from 0.36m before to 1.2m after the collapse. In addition, the axial neutron emission falls by a factor of 6, from $1.9\times10^{15}m^{-3}s^{-1}$ to $2–3\times10^{14}m^{-3}s^{-1}$. Calculations show that, in this case, the emission is almost entirely non–thermal and that the ratio of beam–plasma to beam–beam reactions is 2:1. The fall in central emission can be explained, therefore, by a substantial redistribution of the fast, beam–injected ions to large minor radii, the redistribution occurring on a timescale of < 1ms.

6. Discussion

A complete understanding of the sawtooth instability remains elusive, but several key diagnostic observations of the sawtooth collapse phase have been confirmed. Thus, the initial phase of the collapse, which resembles the convective behaviour predicted by the 'quasi–interchange' model, has now been observed in SXR and ECE reconstructions. However, the rapid timescale of the collapse and, more fundamentally, the rapid switch–on of the instability, are not understood.

Measurements of the q–profile show that q_o remains well below unity throughout the sawtooth cycle. The persistence of a q=1 surface is further confirmed by observations of the 'snake' and of other long–lived m=1 structures. However, the topology of the sawtooth collapse implies that $q_o \simeq 1$, as does the observation, derived from pellet ablation measurements, that a region of very low shear exists close to the q=1 surface at all phases of the sawtooth. More precise measurements of the evolution of the q–profile during sawteeth are required to resolve this basic inconsistency.

Sawtooth stabilization, lasting for up to 5s, is now routinely obtained in L– and H–mode plasmas and at currents of up to 6MA. Its importance has been emphasized by recent demonstrations of local modulation of fusion reactivity and the redistribution of high energy ions due to sawteeth. In

cases where stabilization follows pellet injection, the dominant effect is the modification of the current profile, due to pellet ablation, which causes q_0 to rise above unity. On the other hand, in the 'monster' sawtooth regime q_0 is below unity and there is growing evidence that the stabilization is due to an energetic particle population.

7. Acknowledgements

It is a pleasure to acknowledge contributions to this work and many helpful discussions with our colleagues in the JET Project.

8. References

[1] Campbell, D.J., et al, *"Sawtooth activity and current density profiles in JET"*, Plasma Physics and Controlled Nuclear Fusion Research 1988 (Proc. 12th Int. Conf. Nice, 1988) Vol. 1, IAEA, Vienna (1989) 377.

[2] Söldner, F.X., et al, *Suppression of sawtooth oscillations by lower hybrid current drive in the ASDEX tokamak*, Phys. Rev. Lett. 57 1137 (1986).

[3] Campbell, D.J., et al, *Stabilization of sawteeth with additional heating in the JET tokamak*, Phys. Rev. Lett. 60 (1988) 2148.

[4] Schmidt, G.L., et al, *"Heating of peaked density profiles produced by pellet injection in JET"*, ibid. [1] Vol. 1, 215.

[5] Edwards, A.W., et al, *Rapid collapse of a plasma sawtooth oscillation in the JET tokamak*, Phys. Rev. Lett. 57 (1986) 210.

[6] Wesson, J.A., et al, *"Sawtooth oscillations"*, Plasma Physics and Controlled Nuclear Fusion Research 1986 (Proc. 11th Int. Conf., Kyoto, 1986) Vol. 2, IAEA, Vienna (1987) 3.

[7] Kadomtsev, B.B., *Disruptive instability in tokamaks*, Fiz. Plazmy 1 (1975) 710.

[8] Wolfe, S.W., et al, *"The detailed topology of the m=1 instability in the JET sawtooth collapse"*, Controlled Fusion and Plasma Heating (Proc. 17th Euro. Conf., Amsterdam, 1990) Vol. 14B(I), Euro. Conf. Abstracts (1990) 335.

[9] Campbell, D.J., et al, *"Sawteeth and the m=1 mode in JET"*, Controlled Fusion and Plasma Heating (Proc. 16th Euro. Conf., Venice, 1989) Vol. 13B(II), Euro. Conf. Abstracts (1989) 509.

[10] Westerhof, E., et al, *Observations of sawtooth postcursor oscillations in JET and their bearing on the nature of the sawtooth collapse*, Nucl. Fus. 29 (1989) 1056.

[11] Wesson, J.A., et al, *Spontaneous m=1 instability in JET sawtooth collapse*, JET Preprint JET–P(90)03, 1990 (to be published).

[12] O'Rourke, J. and Lazzaro, E., *"Faraday rotation measurements on JET, and the change in the safety factor profile during a sawtooth collapse"*, ibid [8] Vol. 14B(I), 343.

[13] Weller, A., et al, *Persistent density perturbations at rational–q surfaces following pellet injection in the Joint European Torus*, Phys. Rev. Lett. 59 (1987) 2303.

[14] Gill, R.D., et al, *Determination of the shear on the q=1 surface of the JET tokamak*, Nucl. Fus. 29 (1989) 821.

[15] Lomas, P.J., et al, *"Optimisation of performance in JET Limiter Plasmas"*, Paper IAEA–CN–53/A–6–2, this Conference.

[16] Pegoraro. F., et al, *"Theory of sawtooth stabilisation in the presence of energetic ions"*, ibid. [1] Vol. 2, 243.

[17] Porcelli, F., et al, *"Sawtooth stabilisation by fast ions: comparison between theory and experiments"*, ibid [8] Vol. 14B(I), 327.

[18] Nave, M.F.F., et al, *Fishbone activity in JET*, JET Preprint JET–P(90)32, 1990 (to be published).

[19] Marcus, F.B., et al, *"JET neutron emission profiles and fast ion redistribution from sawteeth"*, ibid [8] Vol. 14B(I), 331.

Self-Consistent Magnetic Chaos Induced by Electron Temperature Gradient

Abstract

Two mechanisms for the self-sustainment of magnetic islands are studied in cylindrical geometry. The first one is based on the different behaviour of electrons and ions in the presence of the islands as a result of their different Larmor radii. This mechanism could maintain magnetic turbulence resulting from a mixture between islands of the size of the ion Larmor radius and chaotic regions. The second mechanism is a pseudo-gravity, used here as a simple analogue for pressure gradient/field curvature modes. It could sustain islands much larger than the ion Larmor radius.

1. INTRODUCTION

There is no agreed explanation of the observed particle and energy losses in tokamaks. One possible cause for these losses is magnetic turbulence, which allows transport along chaotic field lines linking different regions of the plasma [1,2]. The magnetic turbulence could result from a mixture of small islands and chaotic regions [3].

This paper investigates two mechanisms for the self-sustainment of magnetic islands in a collisionless plasma in the cylindrical case. The first one results from the different response of electrons and ions to the islands due to their different Larmor radii. This effect requires a minimum threshold, since it is dependent on the presence of magnetic chaos [4]. The second one is a pseudo-gravity, which is here used as a simple analogue for pressure gradient/field curvature modes. The electron and ion drift velocities, associated with the pseudo-gravity, combine to produce the current sustaining the island. As this mechanism does not depend on the existence of magnetic chaos, it has no threshold. These effects have been also studied for non linear microtearing modes with a transverse particle diffusion [5].

The magnetic topology is first defined: it consists of islands separated by nested magnetic surfaces or by a chaotic region. Quasi-neutrality is imposed both inside and outside an island to determine the perturbed potential. This potential produces a net diamagnetic current and the divergence of this current drives an electron current along the field lines thus maintaining the island. Finally, Ampère's law for the island leads to the self-sustainment condition.

2. MAGNETIC TOPOLOGY

The calculation is made in a slab geometry with the coordinates $x = r - r_s$ and $y = r_s(\theta - z/q_s R) = \theta/k_y$, where r, θ and z are the cylindrical coordinates. r_s is the radius of the resonant surface, R is the major radius of the plasma and q_s is the safety factor at $r = r_s$. The poloidal wave number is $k_y = m/r_s$, where m is the poloidal mode number.

The overlapping parameter γ is the ratio of the virtual island width 2ε to the distance between two island chains $\Delta = 1.5q^2/q'm\delta m$, where q' is the shear and δm is the range of poloidal mode numbers around m . For $\gamma < 0.75$ the topology consists in islands separated by nested magnetic surfaces, for $0.75 < \gamma < 1.50$ the islands are embedded in a chaotic zone and for $\gamma \gtrsim 1.50$ the system is fully chaotic [6]. Fig.1-a shows part of a Poincaré map computed by integrating the field line equations with $\gamma = 1.05$. The island is defined by its poloidal extension $2\theta_0/k_y \leq 2\pi/k_y$ and its radial width $2b_0 \leq 2\varepsilon$. It is assumed to be thin, that is $k_y b_0 \ll 1$.

A first integral does not exist in the chaotic zone shown in Fig.1-a. However, the vector potential needs to be defined in this region to calculate the effect of both mechanisms investigated here. This is done by modelling the region outside the island by nested surfaces as represented in Fig.1-b. This defines an approximate magnetic flux $\mathcal{A}^*_z$, which is only used to calculate the perturbed electric potential imposed by the presence of the island:

$$\begin{cases} \mathcal{A}^*_z(x,y) = \dfrac{B'_0}{2}\,x^2 + \dfrac{\tilde{B}}{k_y}\,A(x,y) = \left(-\dfrac{\tilde{B}}{k_y}\right) A(x,y) \\ A(x,y) = 2\,\dfrac{x^2}{b_0^{\,2}} - A(x,y) \end{cases} \qquad (1)$$

where $B'_0 = (r_s q'(r_s)/Rq_s^{\,2})B_z$ is the shear factor, B_z being the toroidal field, and $\tilde{B}$ is the amplitude of the perturbing radial field. From symmetry, A(x,y) is an even function of y with a period $2\pi/k_y$. It is independent of x and equal to $a(y)$ inside the island. The last closed surface of the island is defined by $\mathcal{A}^*_z(x,y) = 0$ and its radial coordinates are given by:

$$b(y) = b_0\sqrt{a(y)/2} \qquad (2)$$

3. QUASI-NEUTRALITY CONDITION

The particles have a charge q_j (j = e,i) and are assumed to experience a fictitious gravitational potential ϕ_{Gj}, which is given by:

$$\phi_{Gj} = -G_j x \qquad \text{with:} \quad q_j G_j > 0 \qquad (3)$$

For $\gamma \gtrsim 0.75$, quasi-neutrality is ensured in the chaotic region by equating the electron to the ion flow. This leads to the radial electric field E_0 in the reference frame rotating with the islands:

$$E_0 = \frac{KT_e}{q_e}\left(\frac{n'_e}{n_e} + \frac{1}{2}\frac{T'_e}{T_e}\right) - G_e \qquad (4)$$

K is the Boltzmann constant. n'_e and T'_e are the average gradients of electron density n_e and temperature T_e.

When the ion Larmor radius $\rho_i = \sqrt{m_i KT}\,/\,q_i B_z$ is of the order of the island half-width b_0, the potential ϕ_i experienced by

the ions can be expressed as:

$$\phi_i = - E_0 x + b_0 (E_0 + G_i) \int_{-\infty}^{+\infty} G(x-x') \tilde{\varphi}(x',y)\, dx' \qquad (5)$$

The perturbed potential $\tilde{\varphi}(x,y)$ is dimensionless and the integral containing G(x-x') is the finite ion Larmor radius operator. This operator is derived by averaging the Fourier components of the perturbed electric field over a gyroperiod and the phase of the motion of a single ion and over a maxwellian distribution of velocities.

As the electron Larmor radius is much smaller than b_0, the electric potential ϕ_e felt by the electrons is given by:

$$\phi_e = - E_0 x + b_0 (E_0 + G_i) \tilde{\varphi}(x,y) \qquad (6)$$

The ion density n_i is a function of the potential $\phi_i + \phi_{Gi}$ and the electron density n_e depends on $\phi_e + \phi_{Ge}$ and on the approximate magnetic flux $\mathcal{A}_z^*$. $\mathcal{A}_z^*$ is an even function of x (see Eq.(1)) and only the part of $\tilde{\varphi}(x,y)$, which is odd with respect to x, contributes to the current sustaining the island (see Section 4). A function of $\mathcal{A}_z^*$, odd with respect to x, is formed by taking the square root of A(x,y) defined by Eq.(1). As A(x,y) is negative inside the island and positive outside, n_e is assumed to be independent of $\mathcal{A}_z^*$ inside the island, but to depend on the odd function $\pm\sqrt{A}$ outside, where the upper symbol refers to $x \geq b(y)$ and the lower symbol to $x \leq -b(y)$.

The perturbed potential $\tilde{\varphi}(x,y)$ is determined by imposing quasi-neutrality $n_e = n_i$ inside and outside the island. n_e and n_i are expanded at first order as a function of $\phi_e + \phi_{Ge}$ and $\pm\sqrt{A}$ and of $\phi_i + \phi_{Gi}$ respectively in the vicinity of 0. Replacing these quantities by their definitions given by Eqs.(1), (3), (5) and (6) leads to two integral equations satisfied by $\tilde{\varphi}(x,y)$. A good approximation for the solution of these equations writes:

$$\tilde{\varphi}(x,y) = \frac{\frac{1}{2}\frac{T'_e}{T_e}}{\frac{n'_e}{n_e}\left(1 - \overline{J_0^2}\right) + \frac{1}{2}\frac{T'_e}{T_e} - \left(\frac{q_e G_e + q_i G_i}{KT_e}\right)} \frac{x}{b_0} \left(1 - \mathcal{P}\sqrt{1 - \frac{b_0^2 \alpha(y)}{2x^2}}\right) \qquad (7)$$

with: $\mathcal{P} = \begin{cases} 0 \text{ for } -b(y) \leq x \leq b(y) \\ 1 \text{ for } x \leq -b(y) \text{ and } x \geq b(y) \end{cases}$

$\overline{J_0^2}$ is an approximation for the finite ion Larmor radius operator, which is defined by:

$$\overline{J_0^2} = e^{-(\rho_i/b_0)^2} I_0\left[(\rho_i/b_0)^2\right] \qquad (8)$$

where $I_0(z)$ is one of the modified Bessel functions of zeroth order. $\overline{J_0^2}$ is equal to 1 for very small Larmor radii ($\rho_i \ll b_0$) and tends toward zero for very large ρ_i ($\rho_i \gg b_0$).

Eq.(7) shows that the perturbed potential $\tilde{\varphi}(x,y)$ is a function, which is odd with respect to x and which is independent of y inside the island.

The system of integral equations has been solved by numerical iteration. The result for $\tilde{\varphi}(x,y)$ is plotted versus x/b_0 in Fig.2 in the case of y = 0, $\rho_i/b_0 = 1$, $n'_e/n_e = 1\ m^{-1}$, $T'_e/T_e = 2\ m^{-1}$ and $G_e = G_i = 0$.

4. CURRENT DENSITY SUSTAINING THE ISLAND

The perturbed current density sustaining the island $\delta J_{\parallel}(x,y)$ is obtained from current conservation in steady state:

$$\nabla\cdot(J_{\parallel}\mathbf{e}_{\parallel} + n_i q_i \mathbf{v}_{Di} + n_e q_e \mathbf{v}_{De}) = 0 \qquad (9)$$

$J_{\parallel}$ is the electron current density along the field lines, being the sum of the constant plasma current density and $\delta J_{\parallel}(x,y)$. $\mathbf{e}_{\parallel}$ is equal to B/B. $\mathbf{v}_{Di} = [-\nabla(\phi_i + \phi_{Gi}) \times \mathbf{B}] / B^2$ is the ion drift velocity and $\mathbf{v}_{De}$, the electron drift velocity, is given by a similar expression.

The leading term of $\nabla\cdot(J_{\parallel}\mathbf{e}_{\parallel})$ is $(-B'_0 x/B)\nabla_y \delta J_{\parallel}(x,y)$. In the limit of low β, $\nabla\cdot(n_i q_i \mathbf{v}_{Di})$ is zero, because n_i is a function of $\phi_i + \phi_{Gi}$. Taking account of quasi-neutrality $n_e = n_i$, it follows that:

$$\nabla\cdot(n_e q_e \mathbf{v}_{De}) = - \frac{q_e}{B^2} \mathbf{B}\cdot\left(\nabla n_i \times \nabla(\phi_e + \phi_{Ge})\right) \qquad (10)$$

where, since $n_i = n_i(\phi_i + \phi_{Gi})$, ∇n_i is equal to $dn_i/d(\phi_i + \phi_{Gi})\ \nabla(\phi_i + \phi_{Gi})$ with $dn_i/d(\phi_i + \phi_{Gi}) = -n'_i/(E_0 + G_i)$. From the expressions for the potentials given by Eqs.(3), (5) and (6), it can be shown that the right-hand side of Eq.(10) depends on $\nabla_y \tilde{\varphi}(x,y)$. Eq.(9) is integrated with respect to y. The perturbed current density sustaining the island $\delta J_{\parallel}(x,y)$ is then given by:

$$\delta J_{\parallel}(x,y) = \frac{n'_e}{B'_0}\left(-KT_e\left(\frac{n'_e}{n_e} + \frac{1}{2}\frac{T'_e}{T_e}\right)\left(1-\overline{J_0^2}\right) + (q_e G_e + q_i G_i)\right)\frac{b_0}{x}\tilde{\varphi}(x,y) \qquad (11)$$

where an additive function of $\mathcal{A}_z^*$ due to integration is omitted. This function is determined by taking into account other effects such as collisions: the resistivity is assumed to be the same inside and outside the island. Finally, $\delta J_{\parallel}$ has been computed using the data of $\tilde{\varphi}(x,0)$ shown in Fig.2 and normalised values are plotted as a function of x/b_0 in Fig.2. $\delta J_{\parallel}(x,y)$ is an even function of x.

5. MAGNETIC ISLAND SELF-SUSTAINMENT

Ampère's law for thin islands ($k_y b_0 \ll 1$) can be written as:

$$\frac{\tilde{B}}{k_y} \nabla_x^2 A(x,y) = - \mu_0\, \delta J_{\parallel}(x,y) \qquad (12)$$

The jump in the derivative of the vector potential across the region associated with the island is equal to the integral of $\delta J_{\parallel}(x,y)$ with respect to x. This leads to an equation in y and θ_0, which is solved by computing the Fourier components of the vector potential with respect to y for different values of θ_0 [4]. Eq.(12) then becomes:

$$\mu_0 \frac{n_e KT_e}{B'^2_0} \frac{1}{2}\frac{T'_e}{T_e}\frac{n'_e}{n_e} \frac{\left(\frac{n'_e}{n_e} + \frac{1}{2}\frac{T'_e}{T_e}\right)\left(1-\overline{J_0^2}\right) - \left(\frac{q_e G_e + q_i G_i}{KT_e}\right)}{\frac{n'_e}{n_e}\left(1-\overline{J_0^2}\right) + \frac{1}{2}\frac{T'_e}{T_e} - \left(\frac{q_e G_e + q_i G_i}{KT_e}\right)} \frac{1}{k_y \Delta} = F(\theta_0) \qquad (13)$$

The left-hand side of Eq.(13) is proportional to the

poloidal β and is independent of the sign of the shear q'. The numerator of the large fraction contains two terms. The first one is due to the finite ion Larmor radius effect and is maximum, when $\overline{J_0^2}$ is zero for island widths much smaller than ρ_i. Note that $\overline{J_0^2}$ is close to 1/2 for an island width equal to $2\rho_i$. This effect has a threshold, because it is switched off, when $n_e'/n_e + (1/2)\, T_e'/T_e$ is zero, that is when islands are separated by nested magnetic surfaces for $\gamma \lesssim 0.75$ (see Eq.(4)). The second term results from the pseudo-gravity effect. It is generally smaller in modulus than the absolute values of T_e'/T_e and n_e'/n_e. This effect is therefore dominant, when $\overline{J_0^2}$ is close to 1, that is when the island is much larger than ρ_i. It can sustain islands even when they are separated by nested surfaces for $\gamma \lesssim 0.75$, since it has no threshold. An example of pseudo-gravity is given by the interchange instabilities in the cylindrical approximation: $(q_e G_e + q_i G_i) n_e'$ is identified with $2rP_s'/(q_s R)^2$, where $r/(q_s R)^2$ is the inverse of the radius of curvature of an helix on the resonant surface at $r = r_s$ in the limit $r \ll q_s R$ and P_s' is the gradient of plasma pressure at $r = r_s$. In this case, Eq.(11) with $\overline{J_0^2} = 1$ gives the same perturbed current outside the island as the MHD equations [7].

$F(\theta_0)$ is determined from Poincaré map computation using the Fourier components of the vector potential calculated above. Table I shows that $F(\theta_0)$ increases, as θ_0 decreases, that is as the island is destroyed. The minimum threshold for turbulence self-sustainment by the finite ion Larmor radius effect is $F(\theta_0) = 0.20$, which corresponds to an overlapping parameter $\gamma \simeq 0.75$.

6. CONCLUSION

Two mechanisms have been proposed for the self-sustainment of magnetic islands. Both produce a net diamagnetic current in the region associated with the island.

The first effect is due to the difference between the electron and ion drift velocities as a result of their different Larmor radii. It could maintain a magnetic turbulence in which islands with a width of the order of the ion Larmor radius are embedded in a chaotic region. The turbulence is self-sustained, when the left-hand side of Eq.(13) is larger than 0.20.

In the second mechanism, the current results from the addition of electron and ion drift velocities associated with the pseudo-gravity. This effect has no threshold and could sustain islands much larger than the ion Larmor radius. This result can be also directly demonstrated from the MHD equations in cylindrical geometry [7] and could be extended to ballooning modes in toroidal geometry.

7.REFERENCES

[1] Rechester A.B. and Rosenbluth M.N., Phys. Rev. Lett. 40 (1978) 38-41.

[2] Kadomtsev B.B. and Pogutse O.P., Proc. 7th Int. Conf. on Plasma Physics and Controlled Nuclear Fusion Research, Innsbruck, 1978, Vol.1, IAEA, Vienna (1979) 649-663.

[3] Rebut P.H., Brusati M., Hugon M. and Lallia P.P., Proc. 11th Int. Conf. on Plasma Physics and Controlled Nuclear Fusion Research, Kyoto, 1986, Vol.2, IAEA, Vienna (1987) 187-196.

[4] Rebut P.H. and Hugon M., submitted to Plasma Phys. Contr. Fusion.

[5] Garbet X., Mourgues F. and Samain A., Plasma Phys. Contr. Fusion 30 (1988) 343-363.

[6] Rebut P.H. and Brusati M., Plasma Phys. Contr. Fusion 28 (1986) 113-124.

[7] Rebut P.H. and Hugon M., to be published.

8.ACKNOWLEDGEMENTS

The authors are very indebted to Dr. J.Wesson for valuable comments. They also acknowledge with thanks fruitful discussions with Dr. D.Baldwin.

Table I

Numerical results for $F(\theta_0)$ obtained from the Poincaré map computation as a function of θ_0 and of the overlapping parameter γ.

γ	0.4	0.7	1.0	1.2	1.4
θ_0	0.91π	0.70π	0.44π	0.32π	0.13π
$F(\theta_0)$	0.16	0.20	0.30	0.46	2.04

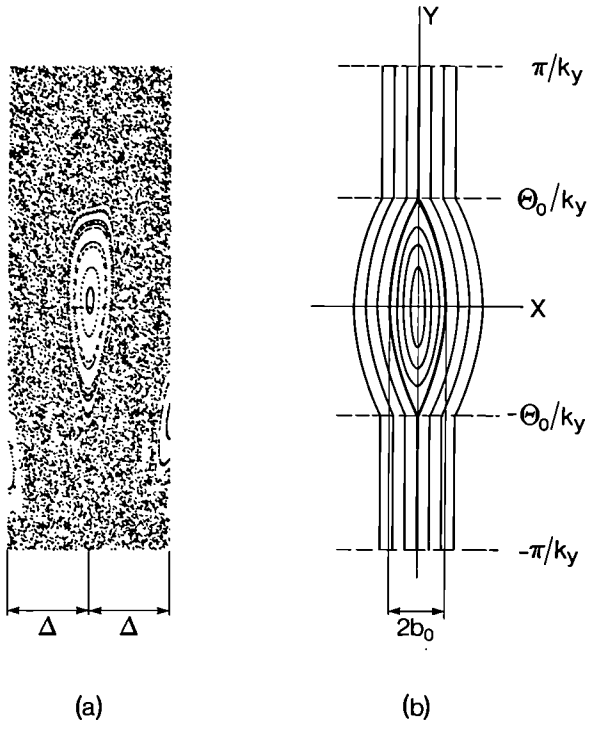

Fig.1: (a) Poincaré map computed for an overlapping parameter $\gamma = 1.05$ showing magnetic islands in equilibrium in a chaotic region; the island is defined by its poloidal extension $2\Theta_0/k_y \leq 2\pi k_y$ and its radial width $2b_0$; Δ is the distance between two island chains ; (b) The chaotic zone is modelled by nested magnetic surfaces to define the vector potential outside the island.

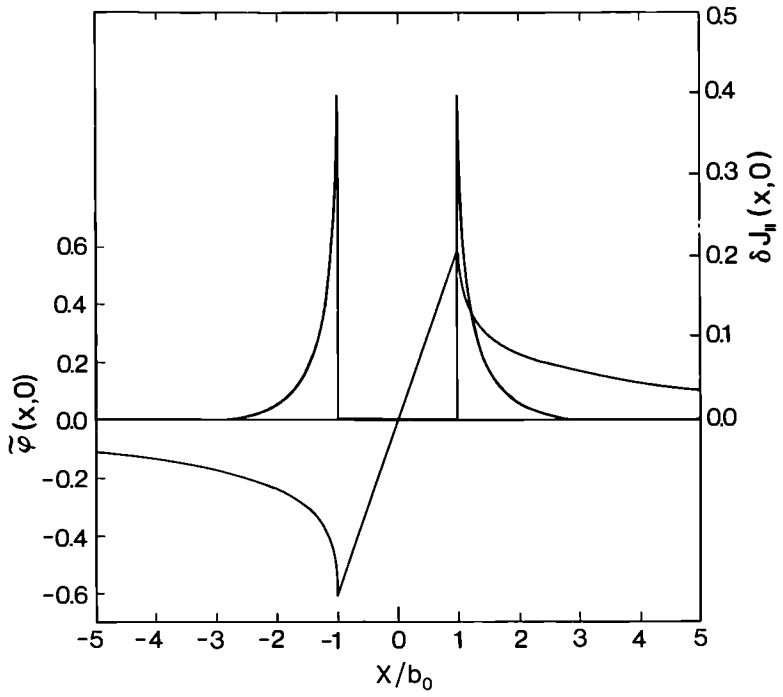

Fig.2: Result of computation of the peturbed potential $\tilde{\varphi}(x,0)$ and normalized current density, $\delta J_{\parallel}(x,0)$, sustaining the island versus x/b_0. The island lies between $x = -b_0$ and $x = b_0$. The ratio of ion Larmor radius ρ_i to island half-width b_0 is unity.

Sawtooth Reconnection

J.A. Wesson

JET Joint Undertaking, Abingdon, Oxon., U.K.

Abstract

Resistive mhd is inappropriate to describe tokamak sawtooth reconnection. It is found that under usual conditions the electric field resulting from flux reconnection is very large. The resulting acceleration of the electrons is such that reconnection is determined by electron inertia rather than electron collisions.

Introduction

It is well known that sawtooth oscillations are not understood. There are several features which are not in agreement with theoretical predictions based on resistive mhd. One of the discrepancies is that, in large experiments, the sawtooth collapse is an order of magnitude faster than predicted by Kadomtsev's model which is based on Sweet-Parker reconnection.

The natural response to this situation has been to examine the assumptions underlying both the theory and the experimental procedures. This has led to the realisation that use of the resistive form of Ohm's law is incorrect.

In the m=1 instability the core of the plasma is expected to behave as perfectly conducting fluid. The core moves toward the q=1 surface and drives a narrow current layer at this surface. In the layer the perfect conductivity equation is invalid and reconnection takes place. It is the behaviour in this reconnection layer which we shall examine.

Reconnection Layer

Figure 1 shows the basic geometry. The core moves toward the reconnection layer with a velocity v. The plasma enters the narrow layer, of thickness δ, and then flows out into the island region with a much higher velocity u. The pressure driving the flow comes from the perturbed helical field B^* and the strong gradient in this field implies the layer current mentioned above. The electric field which drives this current is determined by the rate of change of the helical flux.

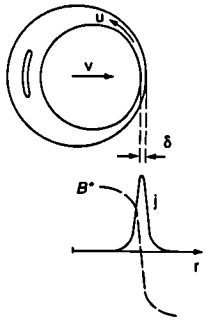

Figure 1. Diagram of reconnection model and the associated current layer.

Helical Flux

The helical flux which is reconnected is given by the magnetic field which crosses an imaginary sheet for which $d\theta/d\phi = 1$, where θ and ϕ are the poloidal and toroidal angles. Such a sheet is shown in Figure 2.

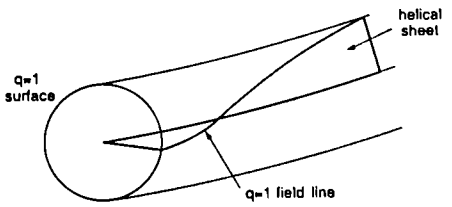

Figure 2. Helical sheet having $d\theta/d\phi = 1$.

For typical JET values (with $(1-q_o) \sim 0.3$) we find

$$v_d \sim 3\times10^8\ ms^{-1}\ \ (=c)\ .$$

It is clear therefore that the resistive model is inappropriate and that under these conditions the electrons would undergo strong runaway.

Electron Behaviour

At first sight it would appear that the runaway electron current would be "superconducting" and would prevent reconnection. However the situation is very different as can be seen from Figure 3.

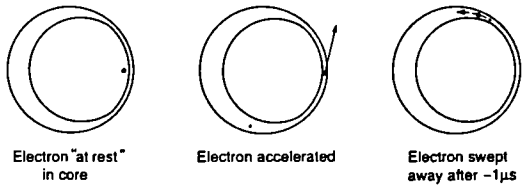

Figure 3. Behaviour of electron during reconnection.

Before entering the layer an electron is effectively stationary. Once in the layer the electron has to move with the required high drift velocity along the direction of the q = 1 field lines. But almost immediately (in ~ μs) the electron is swept out of the layer into the island. Thus the high current density has to be maintained by the continuous acceleration of electrons entering the layer. It is clear therefore that, rather than presenting a low impedance, this form of reconnection gives a high impedance.

Field lines having q = 1 lie in this sheet, and the equilibrium helical flux inside the q = 1 surface, at $r = r_1$, is given by

$$\Phi = \int_o^{r_1} (1-q)\, B_\theta\, dr$$

For a parabolic q profile

$$\Phi \equiv \tfrac{1}{4}(1-q_o) B_{\theta 1}\, r_1 \qquad (1)$$

where $B_{\theta 1} = B_\theta(r_1)$.

Electric Field

The electric field in the layer resulting from the reconnection of the helical flux can be estimated by noting that, in a full reconnection, this flux is removed in the time, τ_c, of the sawtooth collapse. Then, since there is no electric field in the frame of the core, we have

$$E \sim \frac{\Phi}{\tau_c} \qquad (2)$$

Resistive Model

The current density which would be expected from the resistive model is

$$j = \sigma \frac{\Phi}{\tau_c} \qquad (3)$$

where σ is the electrical conductivity.

Using equations (1) and (3) together with $\sigma = 2\,ne^2\tau_e/m$, where τ_e is the electron collsion frequency, the corresponding electron drift velocity is

$$v_d \sim (1-q_o)\frac{r_1}{R}\frac{\tau_e}{\tau_c}\omega_c r_1$$

In the resistive model $\delta \sim (\tau_A / \tau_R)^{\frac{1}{2}} r_1$, where $\tau_R = \sigma \mu_o r_1^2$, and substitution in to relation (5) gives the Kadomtsev reconnection time

$$\tau_K \sim (\tau_A \tau_R)^{\frac{1}{2}} \cdot$$

In the present model $\delta \sim c/\omega_p$ and the resulting reconnection time is

$$\tau \sim \frac{r_1 \omega_p}{c} \tau_A \cdot$$

Taking JET as an example of a large tokamak, $\tau_A \sim 1\ \mu s$, $\tau_R \sim 10s$, $c/\omega_p \sim 1$ mm and $r_1 \sim 0.3$m. These values give the Kadomtsev reconnection time

$$\tau_K \sim 3ms$$

and the inertial reconnection time

$$\tau \sim 300 \mu s \cdot$$

The observed collapse time on JET is ~ 100 μs and it is clear that the new model is in closer agreement.

Qualifications

The calculation given above indicates that the inertial effect is predominant. The numerical values, however, are clearly imprecise. Furthermore the calculation assumes that reconnection takes place in a particular way, whereas other types of behaviour are in principle possible. Also, we have not included other physical effects such as finite Larmor radius and a possible anomalous electron viscosity [2].

There are two other features which should also be borne in mind. One is that it appears in some experiments [3, 4] that only a fraction of the flux is reconnected, q_0 not being restored unity. In this case we might expect a corresponding reduction of the 300 μs reconnection time calculated above. Another effect is the velocity space instability of the runaway electrons. Simulations [5] indicate that this might increase the effective electron mass, again reducing the calculated reconnection time.

Inertial response

When electron inertia dominates, the corresponding term in "Ohm's law" is (m/e) dv/dt. The dominant term is (m/e) v.∇v and neglecting the density gradient the resulting equation is

$$E + v \times B = \frac{m}{ne^2} v \cdot \nabla j \cdot \qquad (4)$$

The electric field in the layer is given by the rate, vB*, at which flux is brought into the layer, where B* is here the helical field at the edge of the layer. Thus, using Ampere's law,

$$\nabla j \sim \frac{B^*}{\mu_o \delta^2}$$

and equation (4) gives

$$\delta \sim \frac{c}{\omega_p} ,$$

that is the layer thickness of the order of the collisionless skin depth.

Reconnection Time

We use the same calculation of flow continuity and momentum balance as the conventional model [1]. This gives the core velocity

$$v \sim \frac{\delta}{\tau_A}$$

where $\tau_A = r_1 / \left(B^* / \sqrt{\mu_o \rho}\right)$ · Then, defining the reconnection time

$$\tau = \frac{r_1}{v} ,$$

we obtain

$$\tau \sim \frac{r_1}{\delta} \tau_A \cdot \qquad (5)$$

Conclusion

The above analysis should be regarded as a clarification of the conventional reconnection model rather than an attempted description of the experimental behaviour. With so many uncertainties regarding the physics of sawtooth oscillations it is not clear that the reconnection is of this type. However it might be that examination of the consequences of the theory presented here could lead to better understanding of the experimental observations.

References

1. Kadomtsev, B.B., Fiz Plasmy 1, 710 (1975) Sov. J. Plasma Physics 1, 389 (1976).
2. Aydemir, A.Y., Phys. Fluids B2, 2135 (1990).
3. Soltwisch, H., et al.l Proc. 10th IAEA Conf., Kyoto 1986, Vol 1 p263.
4. JET Team (presented by D.J. Campbell), this Conference.
5. Wesson, J.A. and Sykes, A., Proc. 5th Eur. Conf. on Controlled Fussion and Plamsa Physics, Grenoble 1972, Vol. 1, p170.

Neutral Beam Heating and Current Drive Systems

D.Stork

Invited Paper presented to
16th Symposium on Fusion Technology,
London, UK., 3rd-7th September 1990

SOFT 1990 Invited Paper

NEUTRAL BEAM HEATING AND CURRENT DRIVE SYSTEMS

D. Stork

JET Joint Undertaking, Abingdon, Oxon. OX14 3EA, England

ABSTRACT

Several Neutral Beam Injection (NBI) systems are now capable of injection of powers greater than 20MW, some for pulse lengths in excess of 5 sec. These high power NBI systems have demonstrated the flexibility and utility of neutral beam heating; coupling easily to many plasma configurations; providing heating, fuelling and current drive capability and allowing access to new, improved plasma confinement regimes. All the high power NBI systems have now achieved routinely high reliability and system availability (≥ 80-90%).

The current status of NBI systems is reviewed and successful solutions to the technological problems encountered in design of high power beams, ranging from high heat transfer elements to large area cryopumps, are discussed. The interface to Tokamak operations such as the drift duct, stray field cancellation and fast interlock mechanisms are presented, emphasising the considerable progress in these areas.

The upgrading of NBI systems for tritium injection on JET and TFTR is reviewed.

The possible parameters for a 'Next Step' injector are presented, showing the choice of negative ion beams as an attractive option. With reference to the existing conceptual designs for ITER/NET it is shown that the main areas of uncertainty exist in the source and accelerator stack designs. The beamlines themselves should be able to take advantage of the properties of negative ions to lead to some marked simplifications.

1. INTRODUCTION

The past decade has seen significant advances in Neutral Beam Injection (NBI) systems. There are now several systems (on JET [1], TFTR [2], JT-60 [3] and DIIID [4]) capable of injecting more than 20MW of fast neutral atoms into the Tokamak plasma. The TFTR system has been operated successfully up to 30.5MW. These high power systems have developed into a flexible and useful experimental 'tool' for the fusion physicists. They have demonstrated the capability of neutral beam heating in terms of its ability to couple easily to many plasma configurations and to provide simultaneously heating, fuelling and current drive for the plasma.

NBI has been in the forefront of demonstrating access to new improved regimes of plasma performance such as the 'H' mode of Tokamak confinement, first seen in ASDEX [5] and subsequently in many other Tokamaks, and the 'supershot' regime in TFTR[6]. The dominance of NBI over other heating schemes is demonstrated by the list of record plasma parameters achieved by its use on the major experiments. Amongst the notable achievements are:

- record peak ion temperature of 28-30 keV in TFTR with 13.5 MW NBI into a low density plasma (Bitter et al. [6])
- record value of toroidal beta (β_{TOR}) ~ 10.7% achieved with 17-20MW NBI into a Double-Null H-mode in DIIID (Stambaugh et al. [7])
- record fusion product $n_d(0)\cdot T_i(0)\cdot\tau_E(0)) \sim 9\ 10^{20}$ m^{-3} keV sec achieved with 17 MW NBI into a Double-Null, hot ion H-mode in JET. This latter performance would extrapolate to a predicted $Q_{DT} \sim 0.8$ if the same conditions were obtained in a 50:50 D:T plasma mixture (Keilhacker et al. [8]).

The constituent elements of the high power beam systems of 1990 are the same as those of a beamline of 10 years ago and are shown in block diagram form in Fig.1. The performance of the elements of the beamline has improved substantially over the 10 years, however, and this has taken the technology from the most powerful beamline unit of 1980, the PLT injector delivering 0.75MW to the plasma for 0.3 seconds, to the most powerful beamline unit of 1990, the JET injector delivering up to 10.4MW to the plasma for 10 seconds.

In this paper we given an overview of important aspects of the technical status of positive ion injection systems. Due to lack of space, power supply systems will not be reviewed. The upgrades of positive ion beamlines to inject helium and tritium beams will then be discussed. We then show that the requirements for the injection systems on the 'Next Step' devices will necessitate the development of negative ion beamlines and review the status of negative ion source and accelerator development, highlighting the issues which must be addressed in the near future.

2. TECHNICAL OVERVIEW OF THE STATUS OF POSITIVE ION INJECTION SYSTEMS

2.1 Ion Sources

Ion source development has been driven by the twin needs of trouble-free source operation and high percentage yield of monatomic ions. The latter requirement arises in order both to maximise the penetration of the neutral atoms into the plasma (as shown in section 5) by maximising the full energy component (E_b) of the beam; and to limit the complication of ion dumps needed to cope with the ions of energy ($E_b/2$) and ($E_b/3$) produced by the breakup of diatomic and triatomic ions accelerated from the source.

Most present generation systems have adopted the magnetic multipole or 'bucket' source. An example of this (from the JT-60 injector [10]) is shown in Fig.2(a). A permanent-magnet cusp field surrounds the source body. The majority of the volume of the source has a low magnetic field (< 10-20 10^{-4}T.). The characteristics motivating the choice of the bucket source are its reliable and noise-free operation at high arc efficiency (~ 0.5A/kW) at low gas pressure (~ 0.25 Pa); the high volume with low magnetic-field which enables it to illuminate large extraction areas uniformly; the ease of obtaining a high monatomic species fraction (the JT-60 source gives ~ 92% H^+ : 6% H_2^+: 2% H_3^+ at a current density of ~ 2.5x10^3 Am^{-2}).

To obtain the best monatomic fraction yield, it is necessary to use a weak 'magnetic filter' (Ehlers and Leung [11]) to prevent the primary electrons from the filaments approaching the region near the extraction grids. This prevents the production of H_2^+ (or D_2^+) in this region. As H_2^+ production is prevented, H_3+ (resulting from $H_2^+ + H_2 \rightarrow H_3^+ + H.$) should also reduce. The low temperature electrons near the grids also result in enhanced destruction of $H_2^+(D_2^+)$ by disassociative recombination. The source is thus separated into a 'driver' region, where the ions are produced and an 'extraction' region. Large volume sources operating successfully on this principle are operational on JET [12], JT-60 [10] and TFTR [2]. An example of the siting of the filaments relative to a 'supercusp' filter is shown for the JT-60 source in Fig.2(b) [13].

2.2 Accelerator Systems

The most significant development for accelerator systems has been the success of multi-aperture, water-cooled extraction systems capable of DC operation. These were realised in slot geometry during the US Common Long Pulse Source (CLPS) program [14] and also in multi-circular aperture form for the JET injectors [15]. In operational experience the JET grids have accumulated an unrivalled performance. These grids, manufactured with water cooling channels passing between the rows of circular apertures (with 262 apertures over an extraction area ~ 0.45 × 0.18 m^2), have accumulated

> 10^5 (accelerator.pulse.seconds) since 1984. There have been no on-load or off-load failures in the system. The grids are manufactured by a sandwich process involving copper electrodeposition onto an OHFC copper base into which the apertures and water channels are machined. Beam pulses of up to 17 secs pulse length (80 kV, 60 A, Hydrogen) have been extracted from these grids with the plasma-facing (80 kV) grid being capable of DC operation at 75 kW power loading (~ 1% of extracted power + ~ 20% arc power).

Other important development programs have contributed to the improvements in terms of the optical quality of the beams accelerated by sources, especially the joint JET/Culham Laboratory/CEA Fontenay-aux-Roses development for the JET system which produced low divergence (9-10 mrad) multiple beams in 3 and 4 grid systems [1].

For its relevance to 'Next Step' injection systems, the radiation resistant, remote handleable JET Positive Ion Neutral Injector (PINI) source/accelerator system is noteworthy. This all-ceramic/metal injector is shown in cutaway form in Fig.3.

2.3 Deflection and Dumping of Un-Neutralized Ions

On most of the large NBI systems, the residual ions are dumped by magnetic means. The neutralisation of positive ions is a very inefficient process (the equilibrium, or infinite gas target, fraction of neutrals for deuterium beams at 140 keV is only ~ 30%) and a large amount of ion power with power densities in the range 30-100MW m^{-2} (perpendicular to the beam) is common in beamline designs. Inclination of dump elements yields only partial advantage due to space restrictions.

The two successful solutions to which have been realised on operational beamlines can be separated by their differing coolant water systems. The Low Pressure approach is represented by the 'HYPERVAPOTRON' elements used in the JET Ion Dumps, calorimeter and scrapers [1]. In these elements, a low pressure (0.6 MPa) water supply is passed through channels internally-profiled to increase both the turbulence and surface area. The elements can accept power densities up to ~ 15MW m^{-2} [16] with an overall coolant pressure drop of ~ 0.03 MPa. The High Pressure approach is represented by the High Heat Flux panels used on the ASDEX Long Pulse Neutral Injection (LPNI) system [17] and also on TEXTOR NBI. The panels, with their internally-finned tubes, are based on data from the US Neutral Beam Energy Test Facility (NBETF) at LBL [18]. They require water at 1.2 MPa, with 0.6 MPa pressure drop, but are capable of a DC operation at 25MW m^{-2} (and have been to 45MW m^{-2} without burnout). There is, of course, the accompanying drawback of the high stresses in components such as bellows associated with a high pressure system.

A notable development which may yield advantages on future systems has been that of the Electrostatic Beam Dump (ESBD) pioneered by the NBI group at CEA Cadarache. The ESBD is generally an in-line system surrounding the mixed neutral-ion beam passing through it. In positive ion systems, the ions are 'peeled-off' by allowing their space charge expansion to deflect them onto the beam dump. The resulting small angle deflections lead to low power densities. The ESBD can be coupled with an Energy Recovery System (ERS). This is planned for the TORE-SUPRA NBI system and has been tested at 75keV for 0.5 secs [19]. A schematic of the combined ESBD-ERS is shown in Fig.4. The system is unusual in having an ion source at ground potential and a neutraliser at HV potential. The ions are accelerated from the source and after the neutraliser, are decelerated to land on the recovery electrode at a potential ($-V_r$) around 5% of the beam energy. In this way only a fraction of the acceleration voltage is expended on these ions and energy is recovered. The system also features an electrode to suppress the emission of secondary electrons caused by the ions hitting the dump. Such electrons would be accelerated towards the ground potential parts of the system. The gain of the ERS is clearly higher if neutralisation of the beam is low (at high positive ion energies), also since only the full-energy ions are recovered, a source with a high monatomic fraction is required. The gains from an ERS of this type have been estimated as a function of beam energy (E_b) and monatomic fraction (α_1) and are shown in Fig.4(b). It can be seen that for the present deuterium injectors in the 100-140keV range (TFTR, JET, JT-60) the system does not lead to significant gains.

2.4 Beamline Pumping

The present large Tokamak NBI systems all use cryopumps for beamline pumping. Most designs feature conventional chevron-baffles. The requirements for low background pressure (~ 10^{-3} Pa) in the final drift region of the JET beamline [1] in order to limit re-ionization of the neutral beams (see 2.5), in the presence of high gas flows (~ 26Pa.m^3.s^{-1}) were too stringent for chevron-baffled cryopumps and stimulated the design of the JET 'open structure' cryopumps [20]. The JET Open Structure design shown in Fig.5 increased the transparency of the pump by having an unobstructed opening, and by shielding the Liquid Helium (LHe) panels in a nested fashion behind Liquid Nitrogen (LN_2) panels to protect the LHe surfaces from line-of sight incidence of 'thermal' gas molecules. The cryopump thus achieved ~ 47% of the theoretical 'black hole' pumping speed, ie ~ 200 m^3 s^{-1}/m^2, which is nearly twice the value achieved by chevron pumps. The installed pumping capacity on the JET beamline could thus be increased to 8 10^3 m^3 s^{-1} (H_2) for the 40 m^2 area of pump.

Probably even more relevant to the 'Next step' injectors is the development of low-loss cryo transmission lines and large, continuously operational cryoplants. The overall system at JET gives a good example of what can be achieved in this respect. The system features ~ 60 m long low-loss coaxial cryo-transmission lines [21] in which the LHe supply is shielded by successive vacuum; cold He boil-off gas; LN2 supply; cold N_2 boil-off gas and vacuum layers. The measured losses are ≤ 10 mW m^{-1} (LHe) and ≤ 150 mW m^{-1} (LN_2). The cryogenic plant has a LHe refrigerator for gas'boil off' recovery [22] and is capable of supplying 800 W at 4.4°K and a LN_2 storage system which delivers 1.5 m^3 hr^{-1} (equivalent to 65kW at 78°K). The plant supplies two JET beamlines and a pellet injector.

Developments such as these have allowed cryopumps to outstrip the performance of large-scale Titanium getter pumps even though there have been significant developments in regenerable versions of these [23]. Titanium getter pumps still retain the disadvantage that their pumping behaviour tends to depend on their previous history. Their capacity for H_2/D_2 (and hence T_2) retention before regeneration is also at least 2 orders of magnitude below that of the cryopump which typically can operate for two weeks between regeneration.

2.5 Drift Duct

The geometric access to the Tokamak plasma for NBI is generally very tight. The beams have to pass between the toroidal field (TF) coils of the Tokamak the distance between which must be kept small in order to minimise field ripple and the resulting loss of fast ions from the plasma. Access is also generally in a non-perpendicular direction in order to maximise beam deposition in the plasma and minimise shine-through onto the Tokamak inner wall. This situation is likely to exist in the Next Step machines and reactors where penetrations in the first-wall/blanket systems will be at a premium and hence will be kept as small as possible.

This restricted access leads to severe challenges in the design of Drift Ducts. In the drift region the beam neutrals are subject to reionisation reactions ($D_f^0 + D_2 \rightarrow D_f^+ + ...$) and high powers can accumulate from this in the long drift ducts necessary to penetrate coils, blanket etc. Long, narrow ducts have low vacuum conductance and are difficult to keep at low pressures to minimise reionisation.

The fringe field from the Tokamak has a strong spatial variation in the duct region and can act to focus the reionised power from the beams as is shown in an example from JET in figure 6. Extensive work has been done on this problem at JET [24], [25] following earlier accidents where duct protection was melted by the focussed power [24]. The recent work by de Esch et al. [25] shows good agreement between the simulated trajectories and the profiles of reionised power measured by *in situ* thermal instrumentation. This allows confident prediction of the safe operating conditions of the present (inertially cooled) duct protection which will accept peak reionised power loadings of $\leq 4.4 MW\ m^{-2}$ for pulse lengths of up to 10 seconds.

Reionised beam particles hitting the duct protection will release gas molecules. These form an increased gas target which will lead to enhanced reionisation and the situation will spiral out of control unless the gas release is kept to a minimum. Early work on this problem [26], [27] recognised the exponentially-deteriorating situation termed 'BEAM BLOCKING'. This occurs if the gas re-emission coefficient Γ (molecules per incident ion) exceeds a critical value Γ_{crit} and results in loss of the entire beam in reionisation. Γ_{crit} can be written in terms of beam and duct parameters as:

$$\Gamma_{crit} = \frac{C}{\sigma_{01} L \phi_B} \qquad (1)$$

where C is the duct conductance; L the duct length; ϕ_B is the beam flux through the duct and σ_{01} is the reionisation cross-section.

For long pulse systems where low reionisation power is required, $\Gamma << \Gamma_{crit}$ is needed and improvements in beamline pumping and materials evaluation have moved towards this situation. Bickley et al. [28] have shown in a study of the JET duct that metal (copper) ducts yield a static situation of $\Gamma \sim 0.5$ (1 atom emitted per incident ion) after conditioning with beam and that the conditioning of a metal duct continuously improves with accumulated beam-on time. The JT-60 NBI team also report a continuously improving situation with a metal duct and find that only ~ 40 beam-seconds are required to bring duct-reionisation power losses below ~ 5% of the incident power [29]. In the JET study the static situation was reached in < 1000 MW.secs of beam through the duct. For carbon or carbonised ducts on the other hand, it has been found that conditioning takes much longer (~ factor 5 ×) and the de-conditioning by H_2 or D_2 absorption onto the carbon/carbonised surfaces can take place if conditioning is suspended for a significant period (~ 1-2 days).

A measure of success in overcoming the duct problem is provided by the 3-dimensional plot in figure 7. Here the critical gas re-emission coefficient of the duct (Γ_{crit}) is plotted against the percentage duct reionised power loss (W_R) for a conditioned system and the peak neutral power transmitted through the duct (P_0). Since low Γ_{crit} is a measure of minimum disturbance to the Tokamak system, success can be defined as simultaneous achievement of low Γ_{crit}, low W_R and high P_0. The achievement of this separates those beamlines (eg. JET) which are pushing into reactor-relevant regions, from the more conservative designs (eg. JT-60).

It can be shown [28], that the percentage reionised power W_R is, to first order, proportional to pre beam gas pressure Pg and Γ/Γ_{crit}

Low Γ/Γ_{crit} can be achieved via a clean metal duct and a low Pg is achieved by good differential pumping of the beamline such (with reference to Fig.7) the ratio (S_L/C_{DD}) is as high as possible, where S_L is the pumping speed of the last beambox chamber and C_{DD} is the drift duct conductance.

2.6 Interface to Tokamak Operations

In general, the 'coupling' of NBI power into a Tokamak plasma causes few physics problems and it is now easily understood how to design out *a priori* such effects as, eg, field ripple loss of fast ions. The 'Engineering Coupling' problems which are encountered have been successfully overcome on the operational NBI systems. In addition to the Drift Duct already mentioned, there have been significant developments in handling beam shine-through and the adverse effect of the Tokamak stray magnetic field.

2.6.1 Beam Shine Through Protection

Unattenuated beam powers impinging on the Tokamak Inner Wall can be high in the absence of plasma (eg, up to 31 MW m^{-2} in JET). The protection of the inner wall has been facilitated by the development of graphite armour tiles . Progress here has often had a spin-off in the development of, eg. carbon fibre composite tiles for graphite bumper limiters or divertor targets. The large-Tokamak NBI systems have shine-through detector interlock systems to terminate the beams if excessive temperatures are detected on the Tokamak inner wall. These systems have employed a variety of technologies including pyrometers on DIIID [4] and TFTR [30], infra-red diodes on JET [31] and CCD cameras on JT-60 [29].

2.6.2 Tokamak Stray Magnetic Field

The earlier generation of plasma ion sources, such as the periplasmatron (eg. on ASDEX) and the 'field-free' source (eg. on the early TFTR NBI system) were often susceptible to Tokamak stray magnetic fields even at levels as low as $0.5\ 10^{-4}$ T. Such systems often had their own 'bucking coils' local to the plasma source.

In general, multipole sources are less susceptible to these fields. For many of the current beamlines, shielding 'passively' by using large assemblies of soft iron has been sufficient to reduce stray fields to low levels at the sources and in the beam transport regions. Fields ~ $5\ 10^{-4}$ Tesla at a multipole source are found to cause few problems for the source's uniformity or optics.

Two Tokamak NBI systems, those of JT-60 and JET, have successfully developed active feedback controlled field compensation systems. JT-60 is an air-cored Tokamak with high stray fields at the source, accelerator and dump regions. The decision was made at an early stage to rely on local passive shielding only in the source/neutraliser region and to actively shield the transport region to the dumps using cancellation coils under feedback control from sensors measuring the Tokamak stray field. With this system the JT-60 group were able to develop the first successful large-volume cancellation system [32], the performance of which is illustrated in Fig.8

On the JET NBI system, the passive shielding surrounding the beamline proved insufficient to shield the sources and neutralisers at plasma currents (I_p) above the original JET extended performance figure ($I_p = 4.8$ MA). At $I_p = 7$MA, the stray field measured at the JET PINI sources reached ~ $17\ 10^{-4}$ T. The high fields are caused by the saturation of the iron core of JET and also arise at the onset of the H-mode when the current in the vertical field poloidal field-coils rises strongly to counteract the strong increase in plasma β. These dynamic situations cause problems of deflection of the un-neutralised beam ions in the gas neutralisers which leads to beam deflection outside the tight geometrical requirements of the

JET system (allowed deflection ~ 1 mr horizontally). This can result in excessive power being intercepted by the beam scrapers. The problem has been solved by the successful development of a feedback controlled active field compensation system (AFCS) [33]. The JET AFCS is capable of backing-off up to 20 10^{-4} T over a volume of ~40 m^3. The magnetic field in rapidly changing plasma situations can now be maintained constant to an accuracy ~ ± 0.2 10^{-4} T [33].

2.6.3 Control, Diagnostics and Interlock

There are now completely computerised control and diagnostic systems on the beamlines of JET [34], JT-60 [3] and TFTR [35] with considerable operational experience. More interestingly, for future reactor-like operations, the large beamline systems on these machines and on DIIID have extensive interlock systems which terminate the beams in the event of out-of-normal conditions.

An example of the complexity of problems which can now be considered as solved in this area would be provided by the JET NBI system. This has a two-level basic-interlock network with a fast-response (10-20 ms) Fast Beam Interlock System (FBIS) backed up by a slower timescale (125 + ms) subsystem of the JET Central Interlock and Safety System (CISS) which is devoted to NBI. FBIS is a hardwired system which operates by gating sustaining pulsetrains (1 kHz) through to the NBI power supplies [36]. In the event of an out-of-normal event (eg, a pressure excursion in the beamline or disappearance of the Tokamak plasma) the pulsetrain is terminated which switches off the power supplies. This is an inherently failsafe concept and all parts of the system will be upgraded to provide redundancy and failsafe action prior to the start of D-T operations on JET. The CISS network is Programmable Logic Controller (PLC) based and acts both to backup FBIS and to Pulse Inhibit the injectors when dangerous conditions (eg, lack of water cooling) occur out-of-pulse [34]. Operationally, the FBIS has been called upon to act mainly on disappearance or malfunction of the Tokamak plasma itself (> 95% of trips) . The system has not failed to act correctly since its commissioning in January 1986.

Reliability and Availability

In general all the large NBI systems now report >90% availability and reliability of >80%. Extensive statistical exercises have been undertaken to justify these claims on JET [37], JT-60 [38] and TFTR [39], spurred on by the approach of the D-T phase on the large Tokamaks in which access to the beamlines for repair and maintenance will be severely restricted.

JET and TFTR have devised essentially similar performance indicators to measure reliability of their NBI systems. This 'shot' parameter (ρ_{SHOT}) [39] is essentially the ratio

$$\rho_{SHOT} = \frac{\text{NBI Energy delivered to the plasma}}{\text{NBI Energy requested for the shot}} \qquad (2)$$

Using the measure indicated in (2) the TFTR performance gave ρ_{SHOT} ~ 0.83-0.98 for 1988 operations at 95-110kV, whilst JET achieved $\bar{\rho}_{SHOT} \simeq 0.82$ for 1989 operations with 10 80keV PINIs and 6 140keV PINIs.

Most of the unavailability in these large systems is still dominated by the Power Supplies (over 50% of causes on DIIID, JET and TFTR). Considerable effort has been put into removing specific causes of unreliability which is proving to be successful.

The improved availability and reliability owes much to the improved quality of the injectors themselves and to the improved techniques of accelerator conditioning. Improved quality has benefited from the adoption of the common development programs of the 1980s. The two most successful of these were the European PINI joint development for JET (subsequently adopted by TEXTOR and ASDEX-upgrade) and the US Common Long Pulse Source (CLPS) for TFTR, DIIID and MFTF-B [40]. These have had the worthwhile spin-offs of involvement of industry, improved QA and the (often unmentioned) necessity of having to share with others (and hence really understand) the database for an injector.

Improvements in injector conditioning have followed the deployment of core snubber assemblies [41] which dissipate the stored energy in the long injector HV transmission lines and prevent it damaging the accelerator grids in the event of breakdown.

2.8 Technical Spin-offs

The data accumulating on the mechanical engineering aspects of the large, high-power beamlines is providing valuable materials information across the Fusion Technology field. The 'multiple-unit' nature of most beamline systems and the large number of elements per beamline allow the possibility of meaningful statistical analyses. The power densities handled are also in the reactor-relevant regime and this leads to the use of beamline data as evidence of the pulsed capability of Next Step Tokamak designs (see e.g: the review by Watson [42]). Ion beam dumps give the most comprehensive information on the behaviour of high heat flux structures under pulsed loads in addition to their associated components such as bellows [43]. Structures such as the JET NBI Test Bed beam dump [1] have now accumulated > 3.5 10^4 pulses without problem.

There has also been a valuable study by Papastergiou [44] of the *Reliability Growth* experienced on a beamline design (the JET line) after design changes were made to rectify early failures in the bellows and neutraliser cooling systems. The study involved the use of the 'Duane model', a curve fitting model for the time evolution of fault occurrences. Reliability improvements can be statistically quantified in this way.

Regarding specific technical spin-offs, the extensive operational experience of the JET 'Hypervapotron' dump element design (section 2.3) has provided sufficient confidence in the design for it to be chosen for the actively-cooled target elements of the JET pumped divertor [45], [46]. Cardella [47] has also performed optimisation studies of the Hypervapotron design for Next Step divertor applications.

3. HELIUM INJECTION SYSTEMS

Several of the positive ion NBI systems originally built as H/D injectors are now in the process of establishing reliable facilities for Helium injection. The injection of ^{4}He beams can provide an accurately known, centrally deposited source of ^{4}He ions which can be used to simulate the centrally produced α-particles in a reactor.

Transport studies of thermalised α's and the behaviour of pumping and exhaust systems in the removal of α- particles can thus be studied. JT-60[48] have already used long-pulse (3 sec), ^{4}He beams at the 0.4 MW level in studies of divertor 'enrichment factors' for helium. TEXTOR have a working long-pulse ^{4}He injection system (45keV, 1.1MW, 2 sec.) [49] which is producing initial results. DIIID has also injected 75keV, 0.5 sec ^{4}He beams in studies of the Isotope effect in H-mode confinement [50].

Plans are now well-advanced for the injection of long pulse (≤5 secs.) helium beams on JET, with a demonstration expected in October 1990. Due to constraints imposed by the beam deflection magnet designed for D^+, ^{4}He is limited to 120kV. ^{3}He operation is limited to 155keV by the 30A limit of the accelerator power supply. Whilst the ^{4}He will be used in the thermal helium transport studies previously mentioned, the ^{3}He beams are expected to provide interesting physics in several areas. These include the efficient central heating of plasma ions using the monoenergetic, highly penetrating ^{3}He beams (ion

temperatures of 50-60keV might be possible with 10MW of ^{3}He neutrals); the realisation of high fusion yield experiments using the D-^{3}He reaction. The acceleration of injected ^{3}He ions by the JET Ion Cyclotron Radio Frequency (ICRF) could further increase the ^{3}He energy towards the maximum in the D-^{3}He cross section (at nearly 300keV ^{3}He energy), and would enhance the fusion yield still further.

3.1 Pumping of Helium

Injection of helium neutrals has been made possible by the development of 'cryosorption' techniques for the pumping of helium. Helium gas is pumped in the NBI lines by its cryosorption onto a layer of gas previously condensed onto the LHe cooled panels. The gases which can be used for this effect have been found to be Argon [49], [51], 52]; SF6 [53] and N_2 [49]. Pumping speeds ~ 20-30% of that obtained for H_2 have been achieved for He in these systems. The ice layer typically needs to be renewed between shots in order maximise the pumping speed for He. The optimum quantity of cryosorbing gas which must be pre-condensed onto the LHe panels is about 20-50 times the total quantity of helium to be pumped during the injection shot.

4. TRITIUM INJECTORS

The Tokamaks with planned D-T operation phases (JET and TFTR) have firm plans to upgrade their NBI systems to provide injection of tritium beams. On JET this is planned for 1992, although if the JET Pumped Divertor proposal proceeds, the D-T phase will be delayed until 1995-6 [54]. For TFTR the planned dates are 1993-4 [55].

The injection of tritium beams provides a method of controlling the central isotope mixture in a D-T plasma. This should be especially important for the low recycling 'supershot' regime in TFTR where the fuelling by NBI (S_N) approaches that from recycling neutrals at the limiter (S_R) with typically $S_N/S_R \sim 0.3$.

Some of the design issues on the upgraded tritium beamlines such as integrity of interlocks and reliability of equipment inside the biological shield, were already being tackled as part of NBI designs for the planned D-T Tokamaks. Other design issues specific to the operation of T$^+$ beams are:

- tritium gas supply to the Ion Sources and neutralisers, including gas efficiency
- tritium inventory (especially stringent for TFTR)
- breakdown of HV insulators in the presence of a β-emitter
- tritium permeation through ion dumps
- water and vacuum leaks on the beamlines.

We will make a brief survey of progress in this area, much of which is being achieved in a collaborative fashion by the JET and TFTR groups.

4.1 Tritium gas supply

The TFTR and JET injectors both have separate source and neutraliser gas feeds for flexibility of operation. The source gas feed passes through an SF6 shrouded HV insulator to enter the ion source at high voltage potential. This carries the small but finite risk of breakage of the insulator leading to SF6 contamination in the T_2 cycle and concomitant poisoning of the T_2 recovery catalysts. To avoid this an efficient single gas feed has been developed for the sources which introduces gas at ground potential into enclosure where it can access the accelerator grid interspace [56] and keep the plasma source from gas starvation. The replacement of the HV gas feed should lead to at least a 30% reduction in the Tritium inventory for a shot.

4.2 Tritium Inventory

The tritium gas will be supplied to the injectors from Uranium beds. For each experiment there are site-inventory limits for tritium with a fraction of typically ½ to ¼of these limits being allowed for in the injection systems. The beamline inventory accumulating on the cryopumps will be recovered daily by regeneration of the LHe panels. On JET the 9 gr. (~ 85 10^3 Curie) T_2 inventory per beamline would yield ~ 17 shots per day (10 sec. beam pulse length). On TFTR the requirements are more stringent with only ~ 25 10^3 Curie allowed out of the Tritium vault [57].

The TFTR Ion Sources require interpulse conditioning (unlike on JET) and much work has gone into optimising this conditioning scenario to investigate isotope exchange in the Ion Sources to enable tritium-less conditioning scenarios [84].

Tritium trapped in the ion dumps from ion beam 'drive-in' effects will form a non-regenerable component of this inventory. Tests done for TFTR with 10keV molecular deuteron beams [58] show that the trapping efficiency in copper exceeds that estimated from diffusion models by ~ 2 orders of magnitude. The excess has been attributed to lattice damage by the beams [58], [59] and agrees with results from drive-in neutron targets. It has been estimated [59] that about 50 10^3 Curie would become trapped in the JET Ion Dumps in this manner which would limit the operational scenarios. The 'pumping' due to trapping of beam ions in the dumps is illustrated by the drop in tank pressure when a beam is extracted in the JET Neutral Beam Test Bed (see Fig.9).

4.3 Breakdown of HV Insulators

The breakdown characteristics of the TFTR and JET gridstack insulators have been tested in a tritium atmosphere at Sandia Laboratories and found to pose no problem [60].

4.4 Tritium Permeation

The tritium permeation through the beam dump structures into the water cooling channels appears to cause no problem. Falter [61] has estimated only ~ 1 mg (~ 10 Curie) of tritium permeating into the water in this manner. This estimate is based on diffusion models for hydrogen in solids however, and in view of the high surface concentrations expected due to lattice damage (section 4.2) it appears to be wise to test the permeation behaviour at high concentration gradients.

4.5 Beamline Vacuum and Water Leaks

The only types of vacuum leaks on the beamlines which need to be considered as tritium release hazards are those which result in a catastrophic venting to atmosphere. In practice such leaks have not occurred on either system which gives confidence for future operations. The use of tritium makes it necessary to consider even highly-improbable scenarios however, therefore the main weak links in the vacuum system have been identified and their integrity is being discussed with the appropriate regulatory authorities.

An *in vacuo* water leak in a beamline with tritium-loaded cryopumps would risk the production of large quantities of tritiated water when the cryopumps regenerated. The JET Exhaust Detritiation System (EDS) would safely handle such quantities [62] and active drains will be fitted to the beamline. However, the probability of water leaks must be kept as low as possible. In this respect the improved reliability of the beamlines gives confidence. There have been no in-pulse water leaks on the JET beamline since February 1988 and only 1 small out-of-pulse water leak since August 1988. Previous water leak problems have now been eliminated for all practical purposes by improvements in the mechanical engineering [44] and

physics [25] designs. Similar experiences have occurred on TFTR. Nevertheless, design studies are now in progress at JET on methods for early water-leak detection. Because the water resulting from small or even modest leaks is deposited as ice/snow inside the beamline, fast regeneration scenarios of the cryopumps are being studied which would enable condensed T_2 be recovered and hence minimise the production of tritiated water.

4.6 Upgrades to the JET Beamline for T° Operation

Operation with T° beams at 160keV should yield ~ 12MW of neutral power to the JET plasma with f(E):f(E/2):f(E/3) ~ 0.7:0.18:0.12. Upgraded designs for the beamline deflection magnet [56] and the drift duct protection [28] have been necessary to safely transport this power. The JET deflection magnet (designed for 160kV D^+) will have to operate at high currents to deflect 160 keV T^+. This would have resulted in excessive stray field in the neutraliser region due to saturation of the magnet iron yoke. This has been successfully solved by shimming the magnets and beam tests with 120keV ^4He beams to simulate the 160keV T, have shown the ion dump power profiles to be safely inside the dump envelope. There is evidence that the power profiles do not exactly match code predictions however, indicating that the beams have undergone space charge expansion [63].

The upgraded duct protection is designed with integral scrapers as a more robust unit with less in vacuo bellows and pipes. Although not designed for continuous operation, it will be capable of accepting peak reionisation power loadings ~ 5MW m^{-2} for pulse lengths of up to 14 seconds. The duct will be instrumented with a full array of thermocouples which will allow accurate validation of the reionisation power profiles calculated from the measured stray magnetic field [25].

5. PARAMETER RANGE FOR NEXT STEP INJECTION SYSTEMS

'Next Step' Tokamak devices such as ITER, NET and FER are physically-large systems in order to take advantage of the size-scaling of energy confinement seen in L-mode plasmas [64] and over a more limited database in the H-mode [65]. There is also an increasing body of experimental evidence to support the view that the 'effectiveness' of additional heating, in terms of the achievement of higher central plasma parameters, is improved if the power is deposited centrally [66]. Since it can be shown that in the plasma ion temperature range from 7 to 25 keV, the fusion yield (Q) of an ignited plasma increases with ~ $\gamma_n\gamma_T$ where γ_T is the temperature profile peaking factor $(T_i(o)/<T_i>)$ [67], ignited plasmas would clearly be more easily achieved by the application of central ion heating. Highly penetrating NBI systems seem prime candidates for the task of 'starting up' an ignited machine.

For DC operation of a Tokamak, non-inductively driven current is necessary with a profile peaked towards the axis. For the high plasma densities ($n_e \sim 10^{20}$ m^{-3}) foreseen for a Next Step machine, Lower Hybrid Current Drive (LHCD) would be effectively excluded from the plasma centre [68]. Penetrating NBI remains as the only experimentally-validated method of axial non-inductive current drive. Current drive studies on present generation Tokamaks have experimentally validated the theoretical efficiencies of NBI current drive [69], [70] even though present NBI systems were not optimised to drive current. On DIIID, a plasma has also been sustained entirely non-inductively by NBI [71].

Highly penetrating neutral beams require high energies because the trapping cross-sections of ionisation and charge-exchange of neutral atoms decline rapidly with energy (see Fig.10(a)). In order to obtain a beam with a mean penetration distance similar to the minor radius of the ITER machine (2.15m) in a 10^{20} m^{-3} spatially-constant plasma ($\bar{\lambda}_{20}$) one must have deuterium neutral beams with energy ~ 1MeV (see Fig.10(b)). At such energies, the neutralisation efficiency for positive ions has dropped to infinitesimal values (<0.5%, see Fig.10(c)). The neutralisation efficiency for negative ions in ordinary gas targets remains high at ~ 60% for energies above 1MeV (Fig.10(c)). Thus it is clear that injectors on the Next Step devices must feature negative ion beamlines. The exact energy of injection has quite a wide margin of uncertainty at the moment as simulation of current drive efficiencies for typical ITER conditions show that the predicted current drive efficiency varies by $< \pm 5\%$ from a value of over the beam energy 800keV to 3MeV [72].

6. NEGATIVE ION SOURCE AND BEAMLINE DEVELOPMENT

Studies of Next Step injectors show that in order for the dimensions of the plasma ion source to be kept to a reasonable size, sources capable of supplying negative ion current densities ~ 200-500 A m^{-2} are required. Such sources are being realised, at least in small-scale experiments. Two basic lines of source development are evident; the 'surface conversion' source where negative ions are produced by double-charge exchange of positive ions incident onto a surface having low work function and 'volume production' source where the negative ions are produced within a low density plasma.

This paper will not review in detail the development of negative ion sources. For this the reader is referred to the review by Alessi [73] for surface conversion sources and by Green [74] for volume production sources. Below we give only a brief overview of the present status.

Surface conversion sources for many years relied upon the introduction of Caesium vapour to produce the low work function surface. This produces problems with voltage holdoff in accelerator stacks, and because of the general undesirability of Caesium impurities in a system attached to a Tokamak, the sources declined in status when the negative ion content of volume sources was identified. Recently, successful experiments with a Barium cathode conversion surface [75] have revived the prospects for such sources although the sputtering of Barium still seems to be an issue. In addition, as the conversion surface is biased at ~-300 to -400V, the negative ions are emitted from the surface with fairly high transverse energies (~10eV) causing problems for the design of the focussing optics for beam transport from such systems.

Volume production sources became serious contenders for production of negative ions with the observation by Bacal et al [76] of significant H^- densities in the low pressure discharges in magnetic multipole sources. The fact that these sources were becoming the standard for positive ion beams (see section 2.1) stimulated development [74]. The negative ions are thought [77], [78] to be produced in a 2-step process via an intermediate highly-excited molecular vibrational state viz:

$$e^- + H_2 \rightarrow H_2^*(6 \leq v \leq 14) + e^- \quad (3)$$

$$e^- + H_2^* \rightarrow H^+ + H^- + e \quad (4)$$

since electron energies > 10eV are most favourable for reaction (3) but low energy electrons (~1eV) are needed for reaction (4) to proceed we are thus faced with the familiar '2 temperature region' situation as in the positive ion sources (section 2.1) and indeed the insertion of a magnetic filter into the bucket source was shown to enhance the negative ion yield in the extraction region [79]. Recently the observation by Leung et al [80] that a 'one-off' puff of Cs vapour into a volume production source enhances the negative ion yield has been adopted by the Japanese JAERI group to enable extraction of 10A of H^- from a multi-aperture source (209 holes), corresponding to ~360 A m^{-2} [81]. Volume sources still have the poorly-understood problem that the yield in deuterium (D^-) plasmas is substantially reduced from the yield in hydrogen (H^-) plasmas, where most of the present experimental work is carried out. Also the maximum current density which can be extracted from the source reduces as the size of the extraction aperture increases an effect possibly due to stripping losses near the extraction grid [74].

6.1 Advantages of Negative Ion Beamlines

In addition to the high neutralisation efficiency (η_o) *per se*, negative ion beamlines have other advantages.

Arising from the high η_o, the gas flow required for negative ion beamlines are lower. This enables more conventional 'chevron-baffled' cryopumps to be envisaged and also reduces the power loading from neutral beam reionisation ($D_f^o + D_2 \rightarrow D_f^+ .....$) which must be handled from devious particles in the beamline. The spacecharge in a negative ion system, with its reduced current densities, is lower than in the equivalent positive ion system. This leads to reduced space charge expansion near the ion dumps and also to less heating of the gas in the neutraliser. This latter effect, which reduced the effective neutralisation target in positive ion systems and increased gas loads, was first identified by Paméla [82]. It has been seen in reduced neutralisation efficiency measurements found on many positive ion systems, eg. [83], [84]. As an effect which is directly related to beam current density, it should not play a significant role in negative ion systems.

Negative ion systems are also intrinsically resistant to space charge expansion. The spacecharge neutralisation for a negative ion beam, which depends on confinement within the beam envelope of slow positive ions produced in beam-gas collisions, is more easily achieved than in the equivalent positive ion beam where it must be achieved by confinement of the highly mobile electrons which are similarly produced. Negative ion beamlines with very low divergence are hence possible and 3mr. at 90keV/nucleon energy has been achieved. [85].

Negative ion beamlines can thus, if required, be very long. This has the advantages of;

- remote positioning from the Tokamak, reduction of the neutron and tritium problems;
- long regions of beamline are available for the dumping of residual ions at low power densities;
- long pumping regions are available, increasing further the conservative aspects of the pump designs.

6.2 Disadvantages of Negative Ion Beamlines

The disadvantages depend upon the type of source adopted.

Surface conversion sources have the disadvantages associated with the effect of the sputtered/condensed low work-function material (caesium or barium) on the voltage hold-off of the accelerator stacks.

Volume production sources tend to operate at relatively high pressure (~1.3Pa) when compared to positive ion equivalents. Stripping losses of the D^-beam ($D_f^- + D_2 \rightarrow D_f^o + ...$) can occur with high probability in the long accelerator stacks leading to beam-losses. Consequently the accelerator stack pumping has to be very efficient and a working demonstration of this has not yet been produced.

For all negative ion sources, electrons would be extracted in copious quantities unless suppressed ($n_e/n(H^-) \geq 40$ in a volume source). This would severely limit beamline efficiency. Fortunately electron suppression techniques have been developed, pioneered by Holmes et al [86]. Their system is shown in Fig.11. Electrons are first suppressed by a magnetic filter field using magnets inserted in the extraction electrode. Electrons which still leak through are trapped at low potential by an electron trap in the second grid. Thus only a fraction (f) of the full accelerating voltage is wasted on their acceleration. If the current of electrons leaking through I_e is given by $\delta \times I^-$ (I^- is the negative ion current) then the beamline efficiency is reduced by a factor

$$\frac{e}{e_o} = [1-\delta f] \qquad (5)$$

for practical systems f cannot be lower than ~ 0.05 to 0.1 and thus the initial filter needs to ensure $\delta \leq 1$. This has been achieved on a working system [86].

6.3 Large Scale Negative Ion Beamline Demonstrations

Clearly, large scale demonstrations of working negative ion beamlines are desirable before proceeding to a Next Step device. In the next 5 years, two demonstrations are currently funded.

i) Within the European Community's (CEC) fusion program the 'DRAGON' facility at AEA Culham will come into operation at the beginning of 1991 [87]. This will have a 4A D^- volume production source, coupled to a 200kV pre-accelerator stack (4 grids). The design aims to produce 2.4 A equivalent of D^o atoms (110A m^{-2} equivalent) from a 288 aperture system.

DRAGON will represent the first demonstration of D^- extraction and will demonstrate the following aspects of the CEC's ITER NBI proposal (see below)

- operation of a grounded plasma source
- operation of a neutraliser at high voltage with segmented construction
- operation of an electrostatic beam dump
- operation of the 200kV pre-accelerator
- the predicted stripping losses for the CEC D^- accelerator.

ii) Within the Japanese fusion program, the negative ion development is aimed at the realisation of a negative ion injector for JT-60U. This system will culminate in a 500keV accelerator feeding a 10MW (neutrals), 10 second pulselength beamline [88], shown in Fig.12. Notable features are the cryopumps at the accelerator stack position and the extremely long (~10m) gas neutraliser. The beamline is conservative, using a source at HV potential and magnetic deflection for the ions. The dumping field is feedback-controlled in strength depending on the Tokamak stray field but the source and neutraliser are shielded passively. The system aims to demonstrate 2MA NBI current drive.

This system will test many of the features of the Japanese ITER NBI proposal (see below). In its original conception it does not rely on the enhancement in negative ion yield coming from caesium vapour puffing. An intermediate step system (350keV, 0.1A, 9 apertures) will test the H^- yield enhancement from Cs vapour on a large system and is due to come into operation at the end of 1991. The full JT-60U negative ion system is foreseen for 1995 operation.

7. NBI PROPOSALS FOR ITER

Within the context of the ITER proposals [89], the Technology phase foresees a steady state Tokamak with a 2 week burn period. This machine would have a plasma current up to 11 MA and an installed current drive capability of up to 150MW. Approximately 50% of the current drive capability would come from NBI.

The common parameters for the NBI system for ITER are given in Table 1. Of particular note are the requirements for the system to operate at 50% and 75% of full energy during the start-up phase of the plasma, and the ambitious requirement to have a vertical power profile control at the plasma so that control of the current profile in the Tokamak could be achieved.

On the basis of this parameter choice, 4 design proposals for the NBI system have been received from the CEC [90],Japan [91], USA [92] and USSR [93]. At the overview level all the proposals are essentially similar and an overview drawing of the Japanese proposal is shown in Fig.13.

7.1 Issues in the ITER NBI proposals

In general, most of the contentious issues in the proposals involve the source/extraction and accelerator stack section of the beamline. A reflection of the uncertainties is given by the fact that the 4 proposals differ radically in this area and each has unproven features.

All designs feature electrostatic d.c. accelerators and the problems of avoiding electrical breakdowns in these structures must be addressed. A particular problem for negative ion systems is, as already indicated, the acceleration of larger quantities of electrons than in the positive ion case. The impact of these electrons on grid structures and the resultant X-ray and UV production with its impact on further ionisation in the grid volume poses severe challenges. The designs are probably approximately 2 orders of magnitude from previous successful demonstration in terms of their specific X-ray and U.V. production.

For the CEC concept [90] which proposes a high pressure (0.9 Pa) volume production filter source, the stripping losses and electron acceleration problems are postulated to be minimised by the operation of the source at ground potential, with the accelerator stack and neutraliser being at increasingly positive voltages. Operating a source at ground will enable stronger pumping in this area as pumping access can be achieved up at relatively high pressures without the risk of long path breakdowns. The operation of the source at ground potential also simplifies source replacement enormously. (The source is identified in all the proposals as the item for most frequent replacement). As already stated, the DRAGON facility will test the source/extraction to 200kV and the concept of the HV potential neutraliser including the 'onion skin' type shielding around this to prevent acceleration of field-emission electrons from the beamline walls towards the neutraliser [87].

The Japanese concept [91] proposes a 'Cs-seeded' volume production source operating at HV potential with a gas neutraliser at ground potential. The Cs is proposed to enable source operation at lower pressures (~0.5 Pa) and hence reduce the gas load stripping and x-ray production problems. The voltage hold-off in the presence of caesium and the long term behaviour of the caesium D^- enhancement are the major issues. Unlike the EC concept, which accelerates beamlets in rows to keep an open structure for pumping, the Japanese concept forms a sheet beam after the 4 grid extraction has acce;erated the ions to ~ 180kV. Plasma may form in the centre of this sheet beam and increase the space charge effects with deterioration of beam optics [94]. As already stated, a successful demonstration of the JT-60U negative ion system would answer many of the uncertainties about this concept.

The US concept [92] proposes to use a Barium converter, surface conversion source based on the work at FOM [75] now being pursued further at LBL. The accelerator in the US concept differs from the others in being an Electrostatic Quadrupole (ESQ) accelerator [95]. The long term behaviour of the Barium in the converter and the handling of the large quantities of sputtered barium (over 1 kg. in the 2 week pulse) and its effects on the extraction system voltage holdoff are clearly issues here. The optics problems arising from the initial high transverse negative ion temperatures (section 6) also need to be overcome. The ESQ is claimed to have strong advantages in preventing breakdowns. The ESQ transverse focussing fields offer the possibility of steering electrons born in the accelerating stack off to the side of the assembly. X-ray production and breakdown problems should thus be reduced. The transverse focussing enables longer acceleration stacks thus reducing the voltage gradient and the probability of breakdown. It is essential for this concept that a demonstration of ESQ acceleration of currents ~1A is performed. At present 45mA of H^- has been accelerated to 200keV. [96].

The USSR concept [93] proposes a 'ring-extraction' hollow-cathode Cs-assisted source. Source uniformity and its effects on optics are the key issues here in addition to all the usual problems associated with caesium.

7.2 General Comments on the ITER Beamline Design

In many aspects the ITER beamline designs are all conservative and this gives confidence in the practicability of realisation.

In comparison to the equivalent '10MW module' of the JET NBI system, a lower quantity of gas (about ⅓) is required leading to a lower installed pumping requirement (~1 - 1.2 10^3 m^3 sec^{-1}) and the adoption of conventional chevron baffled cryopumps. The ion dump power densities are also much lower. A quantity of ion power ~ 45% of that dumped on the 80keV JET beamline is spread over a much larger area. This increases the safety margins against burnout and reduces the erosion and surface damage problems on these dumps which will help to offset the problems inherent in the long pulse operation. The drift duct problems also appear to be less severe. On the JET beamline 10.8 MW of neutral power is transmitted through a 0.22 m^2 aperture. On ITER the equivalent figures are ~ 32.4MW transmitted through 2.72 m^2.. An approximate evaluation of the beamline parameters shows Γ_{crit} ~ 13 - 14 for ITER compared to ~ 4 for JET. Reionisation power loading and duct conditioning should therefore be less of a problem.

Reionisation focussing studies similar to those carried out on JET by de Esch et al [25], have not yet been performed for the ITER design. This seems an important and timely topic now that the design is more firm.

The Tokamak stray field from the 22MA, air cored ITER will be very high at the sources/neutralisers (70-120 10^{-4}T) and has been recognised as a problem. Heavy double-layer passive magnetic shielding is foreseen in all the design proposals. In view of the success of feedback-controlled active compensation on JT-60 and JET (section 2.6.2) it seems advisable to review its use in the ITER beamline. Savings in weight, cost and radioactive material inventory can be identified and the active compensation systems are more easily upgradable and changeable to meet parameter extensions of the system.

8. FURTHER DEVELOPMENTS FOR NEXT STEP INJECTORS

Two developments which lack comprehensive funding programs but which appear to offer significant technical advantages are those of the plasma neutraliser and the RF excited multipole source.

8.1 Plasma Neutralisers

It is well known that the charge stripping interaction between negative hydrogen and positive ions (A^{+}) in a plasma ($H^- + A^{n+} \rightarrow H^\circ + A^{(n-1)+}$) proceeds with a high probability. Recent measurements [97] have shown that the cross-section enhancement coming from having multiple-charged ions from high-Z elements is not as high as previously thought, scaling approximately as $Z^{1.3}$ instead of Z^2. Thus it now appears that plasma neutraliser cells which concentrate on the efficient production of dense hydrogenic ions are competitive with the previous heavier gas designs. Hydrogenic neutralisers are also more compatible with Tokamak NBI systems.

Plasma neutralisers using deuterium can result in a substantial increase in the conversion probability of D^- to D° above the gas-neutraliser case from ~ 60% to about 85% as shown in Fig.14. The gas load is also substantially reduced in these devices.

Given these advantages, the demonstration of a working full-scale plasma neutraliser would seem a high priority. Moses and Trow [98] have

experimented successfully with r.f. driven Argon plasma neutralisers attaining $n_e \sim 5\ 10^{19}\ m^{-3}$ over a 0.5m length in a 50kW discharge. There is now growing evidence that r.f. excited multipole sources can obtain very high efficiencies (see section 8.2). Using this Holmes et al [90] have proposed an r.f. driven plasma neutraliser with a cusp containment field. A schematic of this proposal is shown in Fig.15. The containment is nearly completely 6-sided as the D^-/D^0 beams are able to pass through the rows of containment magnets at the neutraliser entrance and exit. Using the figures from the RF buckets, Holmes et al calculate only ~ 0.2MW is needed to drive such a neutraliser at nearly 95% fractional ionisation.

Such a neutraliser inserted in the EC ITER concept would increase the overall beamline efficiency from an estimated 45% to 66%. The increased efficiency could either be used to decrease cost (omit one of the beamlines) or increase safety margins and decrease power supply provision and would be more than enough to compensate the lost current drive efficiency if the accelerator voltage had to drop below (say) 1MV because of breakdown considerations.

8.2 RF Excited Plasma Sources

One major problem in long-pulse injectors would be filament lifetime and it would clearly be disadvantageous to keep replacing ion sources regularly in the remote-handleable conditions of the ITER beamline. Also the de-excitation reactions which are thought to destroy negative ions in volume production sources are enhanced [77], [78], by the presence of dissociated atomic neutrals which produce associative detachment of the negative ions:

$$H^- + H \rightarrow 2H + e \qquad (6)$$

Wall materials which enhance the recombination of neutrals to molecules are hence desirable. Production of the vibrationally excited molecules from which negative ions can be formed (reaction (3)) are also thought to be enhanced by differing wall materials. The problem with the conventional tungsten-filamented volume source is that after a period of operation the walls are covered with Tungsten and surface optimisation cannot be pursued.

These problems would be overcome by the successful large-scale development of r.f.-excited multipole sources. Successful r.f.-excited, multi-pole containment sources have been run with very high efficiencies obtaining positive ion values as high as ~4 A/kW in the case of Di Vergilio et al [99] using a multipole source with internal r.f. antenna. Successful positive ion rf sources have also been developed at IPP Garching [100] where recently a JET PINI source has been converted to r.f. excitation and a factor 4 efficiency enhancement over the filamented version has been achieved [101].

With this background a clear case exists for substantial funding being channelled into r.f. excitation sources to demonstrate their efficiency as negative ion generators. Work is already under way at AEA Culham Laboratory on small scale demonstration projects with this aim [102].

9. CONCLUSIONS

Positive ion NBI systems now represent a mature and robust technology which has provided an invaluable tool in the progress of research of Fusion Physics in recent years.

The operation of high power NBI systems (> 20MW) composed of high power beamline units (~ 10MW) has shown that the design issues surrounding the realisation of such beamlines can now be considered solved. With current technology, it is possible to design a working d.c. beamline at these high power levels. Indeed it is only the non-d.c. aspects of the JET drift duct which prevent the most powerful extant beamline unit (the JET system capable of delivering 10.4MW) from being such a beamline. The 'engineering-coupling' problems of interfacing such beamlines to Tokamak operations are also now solved in essence.

The upgrade of NBI systems to inject helium and tritium beams is well advanced maintaining the importance of the fuelling aspects of current systems. Helium pumping by cryosorption has been successfully realised on large systems for long pulses. The design issues for tritium beams have been addressed, in the main, and solutions established.

The success of positive ion beamline realisation gives confidence in proceeding to the Next Step where negative ion systems will be required because of the high beam energies needed to penetrate large Tokamak plasmas. With their high neutralisation efficiency, low spacecharge and inherent resistance to spacecharge expansion, negative ion systems can be remote from the Tokamak. This gives advantages in radioactive inventory and also allows dumped power densities to be low. Pumping requirements are also lower than for the positive ion beamlines. Such conservative tendencies in the design enhance the prospects of success.

Negative ion sources are being developed to the stage where they can yield current densities in the range 200-500 A m^{-2}, suitable for the Next Step device. Demonstration of large scale extraction system remains to be performed however and stripping losses in extraction systems could be high.

The most serious design issues to be resolved in the 4 proposals for the ITER NBI system are all in the area of the ion source/extraction system/accelerator stack. All 4 proposals have potential major problems here. Demonstrations on a large scale are in prospect for most of the crucial design concepts in the CEC and the Japanese proposals.

A considerable upgrade in the overall efficiency of a negative ion beamline (from ~45% to ~66%) could be achieved by the successful realisation of large plasma neutralisers. A similar comprehensive program should also be instigated to develop r.f. excited multipole sources for negative ion production.

Finally, one should observe that, in the space of a review article, it is not possible to indicate all the pitfalls which have been overcome on the route to the success of the positive ion systems. In all cases, in retrospect it has been shown that the building of Test Bed units, of the maximum possible realism, is invaluable. In this way the 'surprises' of the positive ion physics program (e.g. spacecharge effects in multiple beams, neutraliser gas heating effects) have been identified and accommodated. The engineering coupling problems (e.g. stray field on JT-60) have also been solved. It would be very unwise to economise in the provision of a full beamline Test Bed unit for ITER, in spite of confidence in the outcome!

ACKNOWLEDGEMENTS

In the preparation of this paper, I have benefited from discussions with many colleagues, some of whom have provided me with unpublished data.

It is a pleasure to acknowledge their contributions, especially discussions with Drs. C D Challis, R S Hemsworth, H D Falter and E Thompson (JET) and A J T. Holmes (Culham). Useful material has been provided by Drs. M Akiba and M Kuriyama (JAERI); F Bottiglioni and C Jacquot (CEA, Cadarache); A P Colleraine (G A Technologies); M Löchter (K F A, Jülich); E Speth (IPP Garching) and M Williams (PPPL). I would like to express my thanks to them all.

Finally I would like to thank Mrs S Humphreys, Mrs D Noyes and Mrs P Millward for the preparation of this manuscript.

Table 1

- Common parameters for the 1990 ITER NBI system.

INJECTED POWER (D^0)	:	75MW
ENERGY (MAXIMUM)	:	1.3MeV
PULSE LENGTH (MAXIMUM)	:	350 hrs
OVERALL SYSTEM EFFICIENCY	:	> 40%
ENERGY OPERATION POINTS	:	50%, 75%, 100% FULLENERGY
ENERGY STEP CHANGE RATE	:	10 secs.
POWER PROFILE CONTROL AT PLASMA*	:	HOLLOW, FLAT or PEAKED
POWER STEPS IN PROFILE CONTROL	:	10%
POWER CHANGE RATE	:	10MW S^{-1}
AIMING TANGENCY RADIUS	:	6.2m (cf. R_o = 6.0m)
PORT DIMENSIONS	:	0.8m(W) x 3.5m(H)
TRITIUM ACCUMULATION (TOTAL)	:	< 10 grams
NO. OF PORTS 3		BEAMLINES MODULES/PORT . 3
INJECTED POWER/MODULE	:	10 MW @ 1.3 MeV
BEAMLINE DIMENSIONS	:	4M (OD) x 15M (L)

REFERENCES

[1] G Duesing et al., Fusion Technology 11 ,(1) (19870, 163.

[2] L R Grisham et al., Nucl. Instr. and Methods B10/11 (1985), 478.

[3] S Matsuda et al., Fusion Eng. and Design 5 (1987), 85.

[4] A P Colleraine et al., Proc. 11th Symp. on Fusion Engineering (SOFE), vol.2, (IEEE, New York, 1985), 1278.

[5] F Wagner et al., Phys. Rev. Letts. 49 (1982) 1408

[6] M Bitter et al., Plasma Phys. and Contr. Fusion 29 (10A), (1987), 1235.

[7] R D Stambaugh et al., contrib. paper 13th IAEA Conf. on Plasma Physics and Controlled Nuclear Fusion Res., Washington (1990) IAEA-CN-53/A1-1-5.

[8] M Keilhacker and the JET Team, Phys. Fluids B2(6), (1990), 1291.

[9] G Schilling et al., Proc. 11th Symp on Fusion Technology, (SOFT), Oxford (1980). In 'Fusion Technology 1980' vol. 2, (Pergamon, 1980), 967.

[10] Y Okumura et al., Rev.Sci.Instr. 55 (1984), 1.

[11] K W Ehlers and K N Leung, Rev.Sci. Instr. 53 (1982), 1423

[12] T S Green et al., Proc. 10th IAEA Conf. on Contr.Fus. and Plasma Phys., London (1984), IAEA-CN-44/H1-I-5.

[13] S Tanaka et al., Rev.Sci.Instr. 57 (2) (1986), 145.

[14] J A Paterson et al., ibid.[4], Vol.1, 153.

[15] A.P.C. de Vere et al., Proc. 12th SOFT, Jülich (1982), in 'Fusion Technology 1982' (Pergamon 1982), Vol. 2, 1534.

[16] R B Tivey et al., Proc. 12th SOFE, Vol. 2 (IEEE, Monterey, 1987), 1122.

[17] J H Feist et al., Proc. 14th SOFT, Avignon (1986) in 'Fusion Technology 1986' Vol 1, (Pergamon 1986), 115.

[18] J A Paterson et al., Proc. 9th SOFE, Vol. 2, (IEEE, Chicago 1981), 1666.

[19] M Fumelli, F Jequier and J Paméla, Plasma Phys. and Contr.Fus. 31 (1990), 495.

[20] W Obert et al., Proc. 13th SOFT Varese (1984), In 'Fusion Technology 1984' Vol. 1 (Pergamon 1984), 311.

[21] W Obert et al., Proc. 9th Int. Cryogenic Eng.Conf., Kobe (1982), 100.

[22] R Roberts et al., JET-P(85)14 (1985).

[23] Z Sledziewski et al., ibid [20], Vol 1, 343-346.

[24] A P H Goede et al., ibid [16], 1115.

[25] H P L de Esch, T T C Jones and D Stork, Proc. 16th SOFT London (1990), to be published.

[26] A C Riviere and J Sheffield, Nucl. Fusion 15 (1975), 944.

[27] R S Hemsworth, CLM-R162, UKAEA Culham Laboratory (1977).

[28] A J Bickley et al., Proc. 13th SOFE, Vol. 2, (IEEE, Knoxville 1989) 1438.

[29] M. Mizuno et al., ibid [16], Vol 1, 281.

[30] S S Medley et al., Rev.Sci.Instr. 57 (8) (1986), 2063.

[31] D Cooper, A Staebler and D Stork, ibid [16] 1483.

[32] S Matsuoka et al., ibid [16] 1153.

[33] D Cooper et al., Proc. 16th SOFT London (1990), to be published.

[34] D Stork et al., ibid [17], Vol. 2, 1451.

[35] T O'Connor et al., ibid [16], Vol.1, 306.

[36] D Cooper et al., ibid [16], Vol.2, 1096

[37] E Thompson et al., JET 1989 Progress Report, Vol I, p.26, (EUR 12800 EN (EUR-JET-PR7))

[38] M Kuriyama et al., IAEA Tripartite Workshop on Reliability and Availability of Large Tokamaks, Culham (1988).

[39] T Stevenson et al., ibid [28], Vol. 1, 292.

[40] W Lindquist and S Staten, ibid [16], Vol 2, 1130.

[41] T H Fink, W R Baker and H M Owen, IEEE Trans. Plas. Sci. 8 (1) (1980, 33.

[42] R D Watson, Proc. 9th Plasma Surface Interactions Conf., Bournemouth (1990), to be published in Journal of Nuclear Materials.

[43] K H Berkner et al., ibid [20], Vol. 1, 685.

[44] S Papastergiou, ibid [28], Vol 1, 416.

[45] E Deksnis et al., Proc. 16th SOFT, London (1990), to be published.

[46] H D Falter et al, Proc 16th SOFT, London (1990), to be published.

[47] M Cardella, Proc. 16th SOFT, London (1990), to be published.

[48] H Nakamura et al., contrib. paper, IAEA Technical Committee Meeting on Alpha particle confinement and heating, Kiev (1989).

[49] R Uhlemann et al., Proc. 16th SOFT, London (1990), to be published.

[50] D P Schissel et al, Nucl. Fusion (1989).

[51] J Kimet al., General Atomics Report GA-A 19792 (1989).

[52] P Massmann et al., Proc. 16th SOFT, London (1990), to be published.

[53] M Kuriyama et al., ibid [28], Vol. 2, 996.

[54] P H Rebut, Proc. 16th SOFT, London (1990), to be published in Fusion Engineering and Design.

[55] M D Williams, ibid [28], Vol. 1, 1.

[56] H.D. Falter et al, Bull Am Phy Soc 33 (9) (1988), 2032

[57] L.R. Grisham, private communication.

[58] K.L. Wilson et al., J. Vac. Sci. and Tech. A5 (1987), 2319

[59] H.D. Falter et al., Proceedings 9th PSI Conference, Bournemouth (1990), to be published in J. Nuclear Matls.

[60] L.R. Grisham et al., JET-P(90)07, submitted to Rev. Sci. Instr.

[61] H.D. Falter et al, private communication

[62] A.H. Dombra et al., Proceedings 15th SOFT, Utrecht (1988) in 'Fusion Technology 1988', vol 2 (North-Holland 1988) 1301.

[63] R.S. Hemsworth, private communication.

[64] see eg: R. Goldston, Plasma Physics and Contributed Fusion 26 (1984), 87.

[65] D.P. Schissel et al.

[66] see eg: J.D. Callen et al., Nucl. Fusion 27 (1987), 1857.

[67] eg: A. Gibson and the JET Team, Plasma Physics and Controlled Fusion 30 (1988), 1375.

[68] C. Gormezano, Proceedings 16th SOFT, London (1990), to be published in Fusion Engineering and Design.

[69] C.D. Challis et al., Nucl. Fusion 29 (4) (1989), 563.

[70] M. Zarnstorff et al., Phys. Rev. Lett 60 (1988), 1306.

[71] T. Simonen et al, Phys. Rev. Lett. 60 (1988), 1720.

[72] C.D. Challis, private communication.

[73] J.G. Alessi, Proceedings 4th International Symposium on Production and Neutralisation of Negative Ions and Beams, Brookhaven (1987), 208.

[74] T.S. Green, Plasma Phys and Contri Fusion 30 (11) (1988), 1505.

[75] C.F. Van Os et al, ibid [62], vol. 1, 598.

[76] M. Bacal, E. Nicolopoulu and H.J. Doucet, Proceedings Symposium on the Production and Neutralisation of Negative Ions and Beams (Brookhaven, NY) (1977), 26.

[77] M. Bacal, Physica Scripta T2/Z, (1982), 467.

[78] J R. Hiskes, Comments on Atomic and Molecular Physics 19 (1987)

[79] K.N. Leung, K.W. Ehlers and R.V. Pyle, Rev. Sci. Instr. 56 (1985) 366

[80] K.N. Leung et al., Rev. Sci. Instr. 60 (4) (1989), 531.

[81] Y. Okumura et al., Proceedings 16th SOFT London (1990), to be published.

[82] J Paméla, Rev. Sci. Instr. 57 (6), (1986), 1066-1068.

[83] R.S. Hemsworth et al., Contributed paper 13th European Conference on Controlled Fusion and Plasma Heating, Schliersee (1986), Europhysics Conference Abstracts 10C, II, 297-300

[84] J.H. Kamperschroer et al., J. Vac. Sci. Techn A7 (1) (1989), 83.

[85] A.J.T. Holmes et al, ibid [73] (1987)

[86] A.J.T. Holmes, R. McAdams, proc. IAEA Technical Committee Meeting on Negative Ion Beam Heating, Culham (1987) (Culham Laboratory Report).

[87] A.J.T. Holmes et al, Proceedings 16th SOFT, London (1990), to be published.

[88] Y. Ohara et al, ibid [28], Vol 1, 284.

[89] 'ITER Conceptual Design Report', IAEA, Vienna (1990)

[90] EC ITER NBI Proposal, A.J.T. Holmes et al, Report 3/73/89-5/FU-UK/NET (Culham Laboratory) (1990)

[91] Japanese ITER NBI Proposal, Y. Ohara et al, ITER-IL-HD-4-0 11, (JAERI) (1990)

[92] USA ITER Proposal, ITER-IL-HD-4-0-16 (1990).

[93] USSR ITER Proposal, ITER-IL-HD-4-0-13 (1990).

[94] J.H. Whealton et al., 3rd European Conf. on the Production and Application of Negative Ions (Amersfoort, Netherlands) (1988).

[95] O.A. Anderson et al., Lawrence Berkeley Report LBL-25339 (1988)

[96] J.W. Kwan et al., Bull. Am. Phys. Society 34 (9) (1989) 2066.

[97] E. Salzborn, Proceedings 5th Symposium on Negative Ions and Beams, Brookhaven (1989), p.40 (AIP Conf. Proc. N° 40).

[98] K.G. Moses and J.R. Trow, ibid [94], (1988).

[99] W.F. DiVergilio, H. Goede and V.V. Fosnight, Rev. Sci. Instr 57 (1986) 1254.

[100] W. Kraus and M. Kaufmann, ibid [62], Vol 1, 495

[101] J.H. Feist, private communication.

[102] A.J.T. Holmes, R. McAdams, private communication.

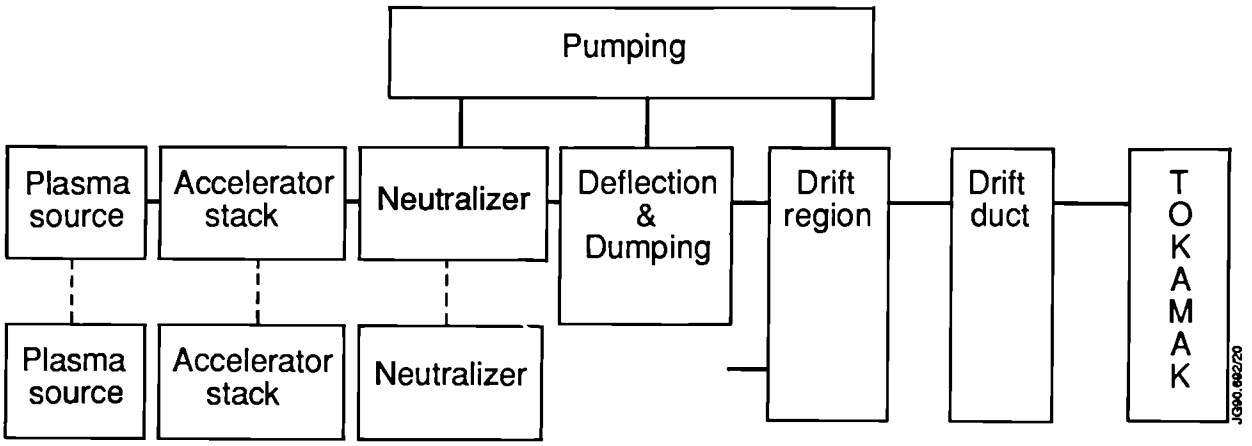

Fig.1 Block Diagram of the Elements of a Neutral Injector.

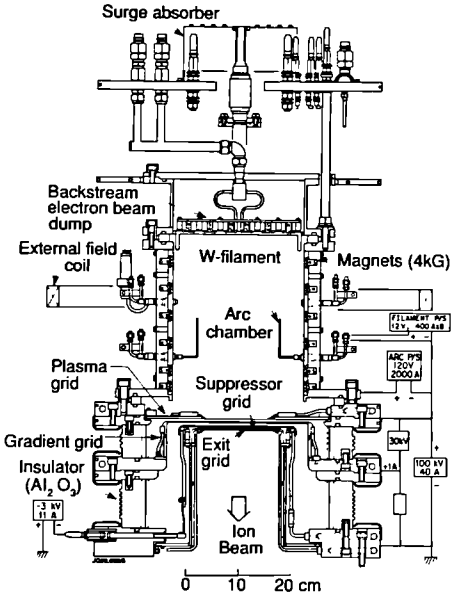

Fig.2 (a) Engineering drawing of the Magnetic Multipole source and extraction system for JT-60 NBI. The source illuminates an extraction area 0.12x0.27 m^2 and the accelerator unit is capable of delivery 70A at 75keV when operating in hydrogen (from ref [10]).

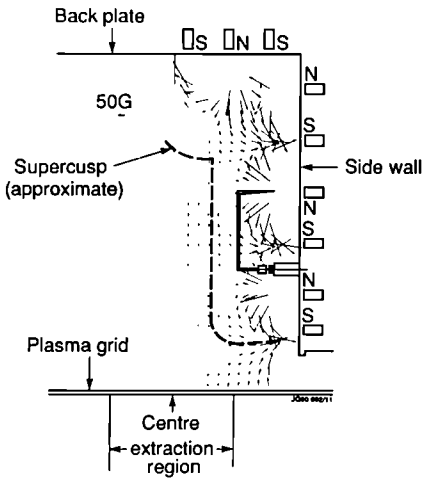

(b) Magnetic field distribution plot in a plane of the JT-60 magnetic multipole source, measured *without* the filaments energised (taken from ref.[13]). Also shown is the approximate position of the 'supercusp' field relative to the filaments.

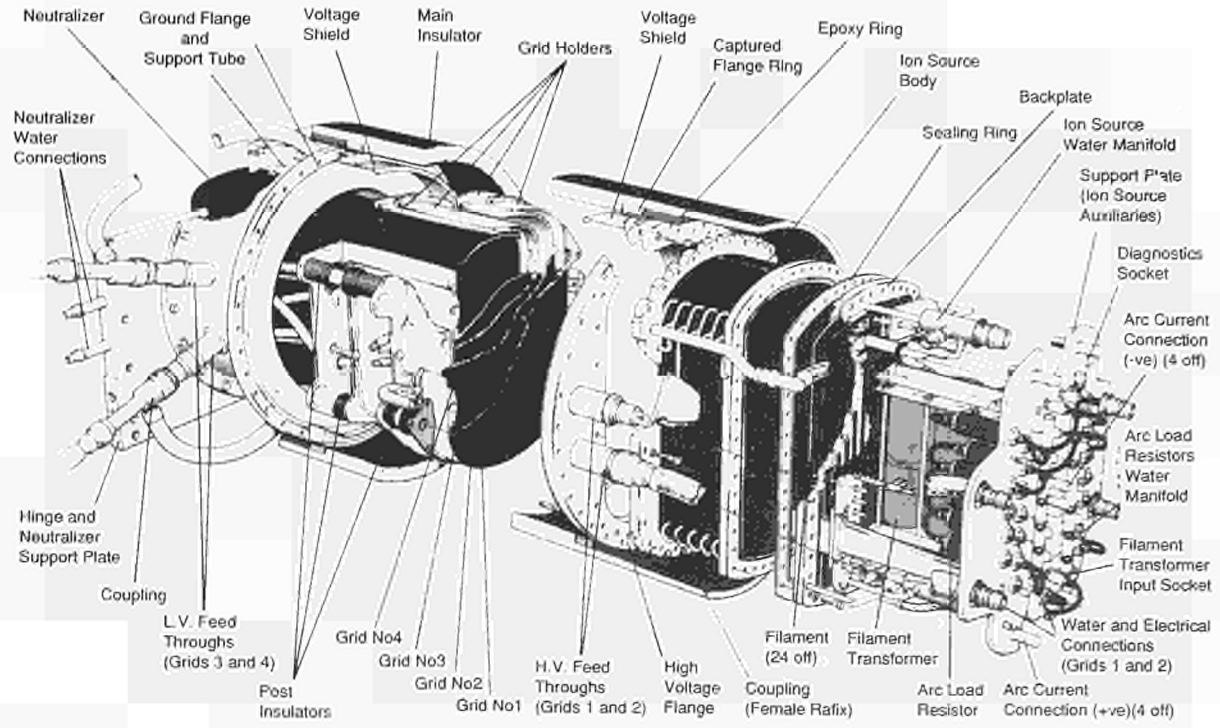

Fig.3 Cutaway view of the JET Positive Ion Neutral Injector (PINI) in its 4 grid 80kV form.
This 4 grid unit is capable of operation at currents of 60A (Hydrogen) or 42A (Deuterium) from an extraction area of 0.18x0.45 m². The higher voltage version has a revised 3 grid accelerator stack and has currently been operated up to 160kV, 37A in deuterium.

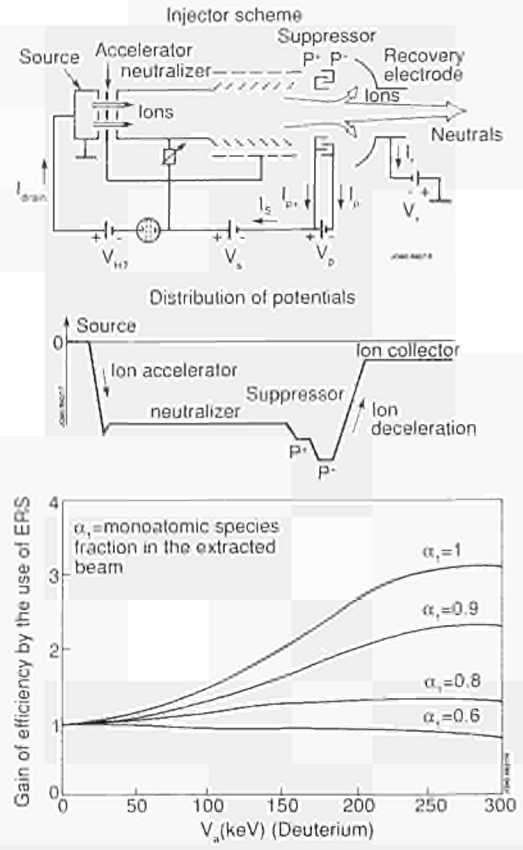

Fig.4(a) Schematic of the TORE-SUPRA injector including the Electrostatic Energy Recovery Electrode. Also shown is the distribution of potentials along the beamline (taken from ref.[19]).

(b) Calculated gain in energy efficiency using the Energy Recovery Electrode for a positive ion-derived neutral deuterium beam. The efficiency is plotted for different monatomic beam fractions (α_1) from the ion source assuming a neutraliser gas target of 10^{20} m^{-2}.

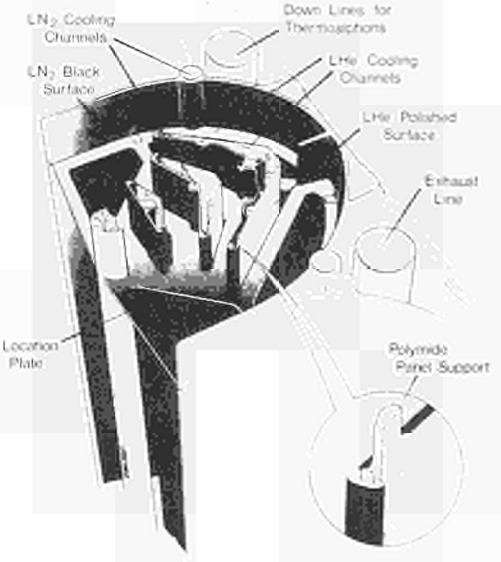

Fig.5 Detail of the JET Open Structure Cryopump module. The JET beamline has 10 such modules lining each side wall of the Neutral Injector Box.

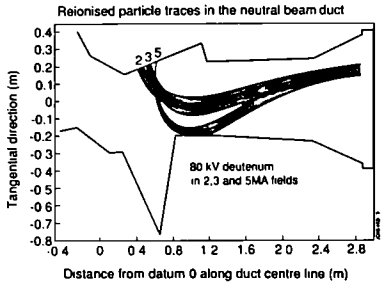

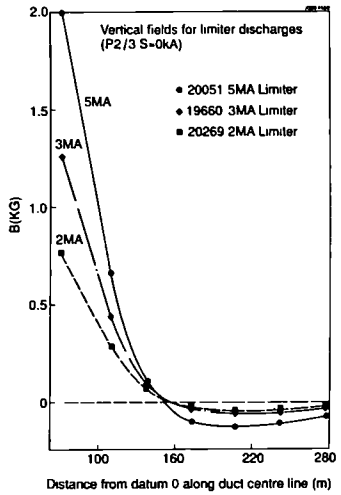

Fig.6(a) Reionised particle trajectories from 1 PINI simulated in the JET drift duct (plan view). The simulation has been done for field maps for 2,3 and 5MA JET plasmas (Fields as in 6(b))

(b) Measured vertical fringe fields in the JET drift duct for JET limiter plasmas of various currents. The vertical fringe fields arise mainly from the stray field of the vertical position control coils of the JET poloidal field system. Extra fields come into play when the poloidal shaping coils (P2/P3) are also energised.

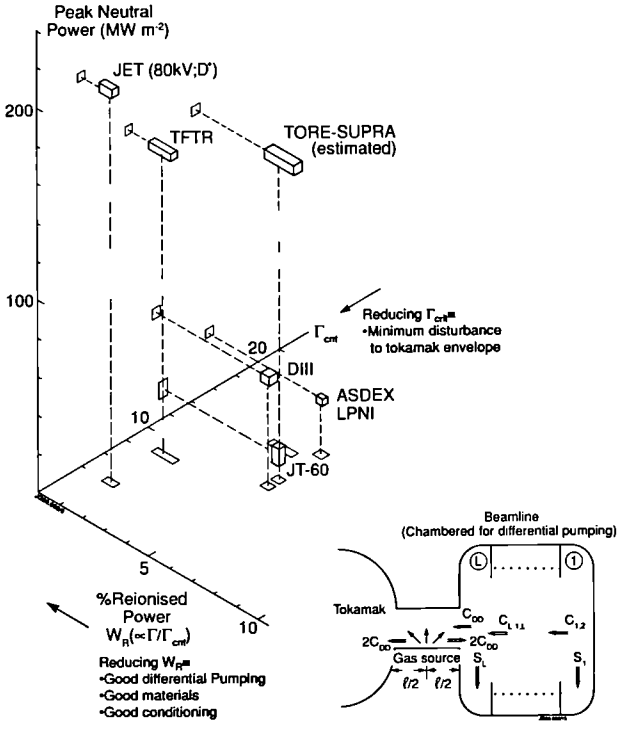

Fig.7 3-Dimensional plot showing comparative performance of different NBI Drift Duct designs for various Tokamak NBI systems. The positions of the ducts in the 3-D space are represented precisely. In reality for all systems the error bars on a particular co-ordinate are of the order ± 10-20% of the given value. Duct conductances used in the determination of Γ_{crit} (via equation (1) of the text) are multipled by 4 from the measured values on the approximation that the reionised gas source is produced mainly at the longitudinal ***centre*** of the duct and hence, can be pumped out by the 2 halves of the duct acting in parallel (see inset).

As described in the text, a low gas pressure in the duct (p_g) can be achieved by maximising the ratio of the last drift chamber pumping speed (S_L) to the duct conductance (C_{DD}).

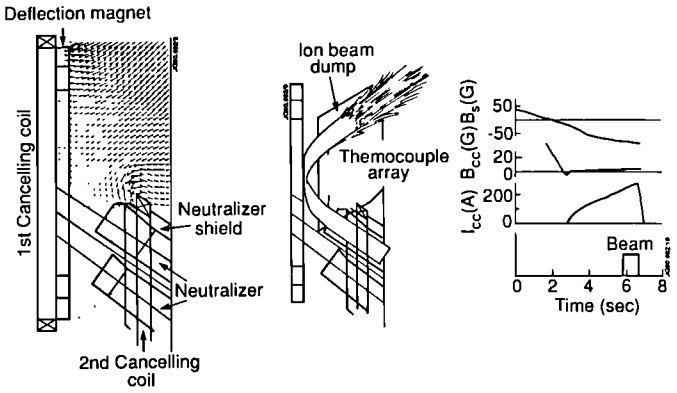

Fig.8(a) Schematic of JT-60 NBI beamline showing a magnetic field vector plot with the cancellation coils energised. The large volume of zero field is evident (from ref.[32]).

(b) As Fig.8(a) but indicating the ion beam transport envelopes and their relationship to the cancelled field volume.

(c) Waveforms showing the cancelled field (B_{cc}) and the current in the cancellation coils (I_{cc}) during a JT-60 discharge with NBI. The stray field in the absence of cancellation (B_s) is also shown.

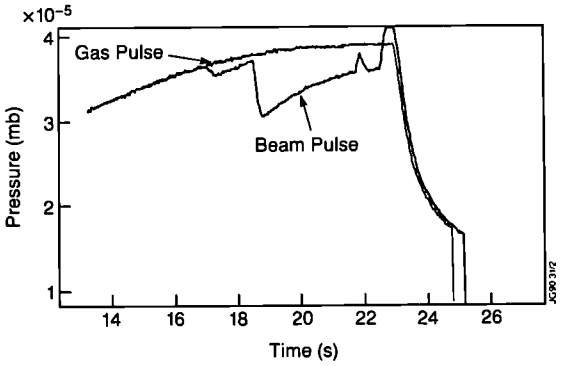

Fig.9 Measured pressure variation in the JET Test Beam Line showing the effect during a beam pulse. The reduction in pressure indicates 'pumping' of the plasma source and by beam trapping in the ion dumps.

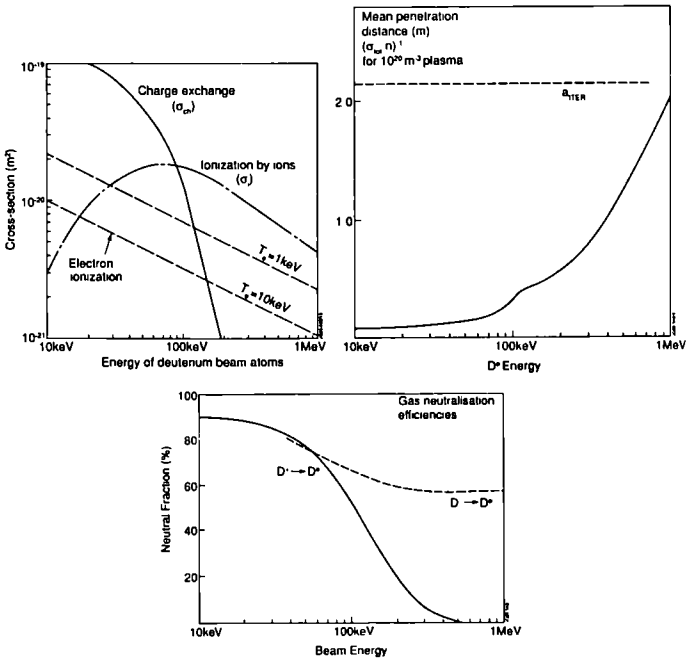

Fig.10(a) Cross sections for charge exchange (σ_{ch}) and ionisation (σ_i) of deuterium beam neutrals by plasma ions and the effective cross section $\langle\sigma_{ei}u\rangle$ for ionisation by electron impact in a Maxwellian plasma of varying temperatures (T_e).

(b) Mean penetration distance ($\lambda \approx (\sigma_{tot}n_e)^{-1}$) for a deuterium neutral in a spatially constant plasma with density (n_e) = 10^{20} m^{-3} and Maxwellian average electron temperature = 10keV. a_{ITER} indicates the minor radius of the proposed ITER Tokamak.

(c) Neutral fractions for positive (D^+) and negative (D^-) beams as a function of ion beam energy emerging from:
- an infinite gas target (D^+)
- the finite optimum gas target (D^-)

Note the optimum gas target for D^- varies from ~0.4 10^{20} m^{-2} at 160keV to ~ 2 10^{20} m^{-2} at 1MeV.

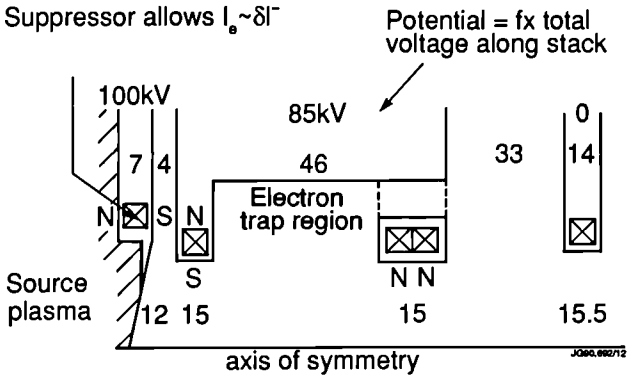

Fig.11 Schematic of the extraction system for the prototype negative ion accelerator of Holmes et al. used for development of electron suppression and electron trap concepts [86] (Dimensions in mm).

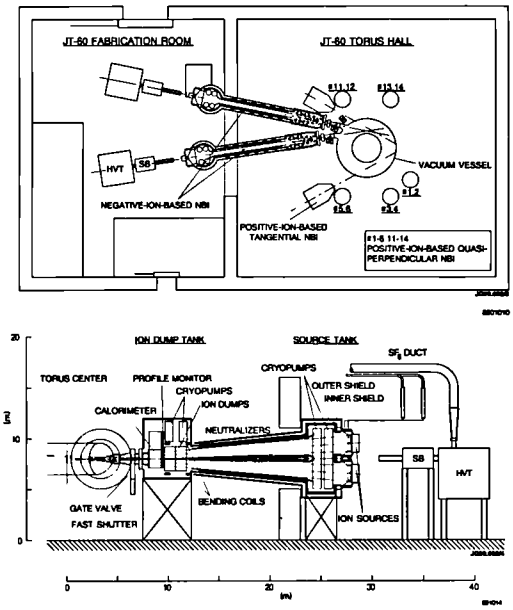

Fig.12 Overview of JT-60U negative ion system.
(a) Plan view indicating the system's position relative the Positive Ion injectors on JT-60. (b) Elevation view.

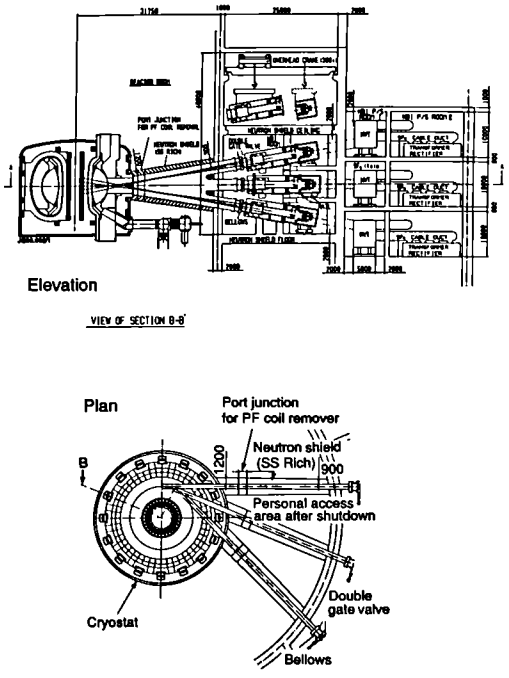

Fig.13 Overview of the Japanese ITER NBI proposal showing the relationship to the ITER plasma (Ohara et al. ITER-IL-HD-4-0-11).

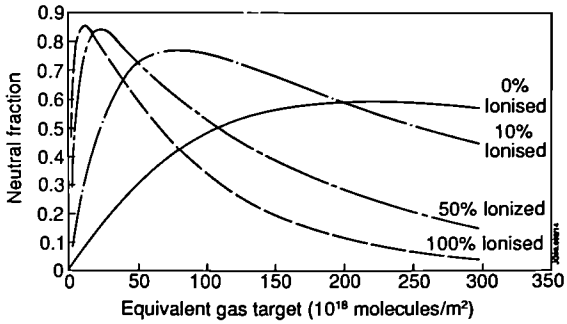

Fig.14 Neutral fraction obtained from a D^- beam at 1.3MeV as a function of equivalent gas target of a plasma neutraliser. The curves are drawn for each value of the percentage ionisation in the neutraliser (0% corresponds to a conventional gas neutraliser). At high equivalent gas targets for high ionisation percentages the neutral fraction falls rapidly due to D^0 reionisation to form D^+.

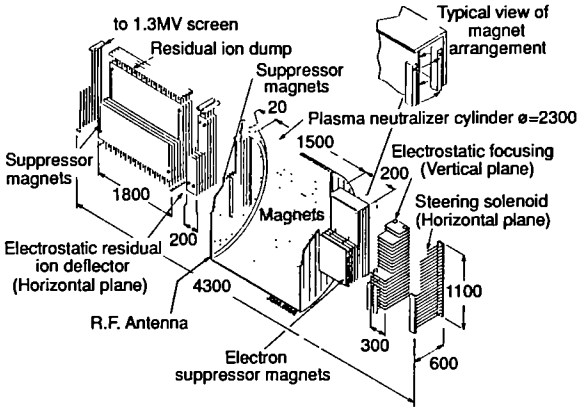

Fig.15 Schematic of r.f. excited plasma neutraliser with cusp-field containment as proposed by Holmes et al for the CEC ITER NBI beamline [90] (Dimensions i n mm).

Radio Frequency Heating and Current Drive Status and Prospects for the Next Step

C.Gormezano

Invited Paper presented to
16th Symposium on Fusion Technology,
London, UK., 3rd-7th September 1990

RADIO FREQUENCY HEATING AND CURRENT DRIVE STATUS AND PROSPECTS FOR THE NEXT STEP

C GORMEZANO

JET Joint Undertaking, Abingdon, OX14 3EA, UK

Additional heating is a necessary requirement on all tokamaks and stellarators. All the major devices are now equipped with large additional RF heating systems and the actual data base both on the physics aspects and on the technical aspects is large and still expanding /1/ /2/.

Radio Frequency techniques in the Ion Cyclotron (ICR), Lower Hybrid (LH) and Electron Cyclotron (ECR) range of frequency have proved to be very effective for one or more of their potential applications: heating, profile control, bulk current drive, non-inductive current ramp up and plasma initiation and are planned to be used on the next step facility.

Although other RF methods are being developed, such as Ion Bernstein wave heating and current drive and Alfvén wave heating, we will restrict the discussion to the most promising and well documented methods. The corresponding main results to date and some of the relevant physics basis will be discussed first. The technical status of coupling structures, transmission lines and generators will then be given.

RF techniques cover a large domain both in the physics and in the technical aspects, as illustrated in fig.1, and consequently only highlights of the different methods will briefly be indicated.

1 MAIN RESULTS TO DATE

Large amounts of RF power have been launched in many experiments:

- 18 MW of ICR power for a few seconds and 6 MW for 20 seconds in JET
- 9 MW of LH power for a few seconds in JT-60
- 2.2 MW of ECR power for 0.2 s in T-10 and 1 MW for about one second in DIII

Record achievements with RF methods have been obtained:

- the largest fusion yield: 100 kW from ^{3}He -D reactions in JET with energetic ions created from ICRH minority heating /3/
- the largest electron temperature: 12 keV in JET with ICRH /3/
- the largest and longest non-inductive current drive plasma currents: 2 MA in JT-60 /4/ and 35 kA for more than one hour in Triam-1M, both with LHCD /5/.

The basic relevant physics is given as follows.

1.1 Electron Cyclotron Range of Frequencies

The resonance occurs along the layer:

$$\omega = \omega_{ce} = e\,B/m_e$$

which corresponds in today's experiments to a very high frequency range: 60 - 140 GHz. It is to be noted that strong absorption occurs in a localised heating zone and that relativistic and Doppler shifts allow the possibility of power absorption at values of the magnetic field different from resonance (up-shifted and down-shifted resonances).

Electron Cyclotron Current Drive results from the asymmetric collisionality generated by a selective absorption of EC waves, preferentially on fast electrons for a good efficiency. Wave injection at an oblique angle is preferred.

1.2 Ion Cyclotron Range of Frequencies

The resonance occurs along the layer:

$$\omega = \omega_{ci} = e\,B/m_i$$

corresponding to a very low frequency range: 20 -120 MHz. The absorption is weak for a pure plasma at $\omega = \omega_{ci}$. A strong absorption in a localised heating zone is obtained either at the first harmonics or at the cyclotron layer of a minority species like hydrogen or helium minority in a deuterium plasma or deuterium minority in a tritium plasma.

Ion Cyclotron Current Drive might result either from asymmetric heating of minority ions, with a low efficiency but capable of producing highly localised current, or from direct interaction between fast wave and electrons (Electron Landau Damping or Transit Time Magnetic Pumping) for which predicted efficiency can be very large in dense and hot plasmas. Localisation of driven current is close to the plasma centre and does not depend upon the density.

1.3 Lower Hybrid Range of Frequencies

LH waves represent the slow wave branch of the plasma dispersion relation in the frequency range:

$$\omega_{ci} < \omega < \omega_{ce}$$

Contrary to the other RF methods, there is not a magnetic resonance but a kinetic resonance.Damping of the waves depends upon many plasma parameters such as the plasma density, the magnetic field, the plasma temperature and upon wave parameters, the main one being the parallel index of refraction which is determined by antenna geometry.

There is a density threshold (proportional to f^2) above which damping occurs on fast ions and below which occurs on fast electrons.

Lower Hybrid Current Drive results from the creation and the damping of the wave on fast electrons. High efficiency driven currents are obtained when a unidirectional wave is launched. Efficiency is directly proportional to the velocity of LH induced fast electrons, ie can be very high at low values of the parallel wave index.

For current drive application, the high frequency range of LH waves is preferred.

1.4 Main Results to Date

The following main results can be noted from the large present experimental data base on heating and current drive:

- high grade H-modes have been obtained with RF techniques alone:
  - ICRH on JET
  - ECRH on D III
  - LHCD on JT-60
- long sawteeth free discharges (ICRH "monsters" in JET, TEXTOR)
- no RF specific impurities problem
- increase of density limit (ICRH and ECRH)
- low voltage start up of tokamak discharge (ECRH on CLEO, DIII)
- ionisation and start-up of stellarator discharge (ECRH on Heliotron E, W VII, ATF)
- mode control through local heating (ECRH on CLEO, DITE, TFR)
- ECR current drive is demonstrated (CLEO, DITE, DIII, WVII) but with a rather low efficiency
- bootstrap current compensation in stellarator (W VII-AS)
- ICR current drive is observed in small size tokamaks. The basic physics elements for current drive in large machines has been demonstrated in JET
- LH current drive is observed in all LH experiments. Efficiencies close to those needed for a reactor have been obtained in JT-60.
- mode control and profile control through current drive has been achieved in many LH experiments (with corresponding large central T_e values)
- substantial volt second saving with LHCD during current ramp-up (JT-60)

2 COUPLING STRUCTURES

Antennae are a very sensitive part of any RF system since they have to launch the desired wave structure and constitute the interface with the plasma.

ECRH antenna load is insensitive to the plasma density and the antenna can be located far away from the plasma. There is no need for a tuning device since the coupling is very good.

LHCD launcher coupling is sensitively determined by the density at the plasma-antenna interface. No tuning device is needed due to the achieved good coupling efficiency (> 90%)

ICRH antenna impedance is very sensitive to the density of the scrape-off plasma which might vary with many parameters such as: distance antenna-plasma, MHD activity, plasma density and H-mode transition. Tuning devices are needed to take into account the substantial reflected power.

2.1 ECRH Antennae

They are the most simple of the RF systems since they can be the direct output of a waveguide, which is already widely used.

Mirrors can be used to reflect and/or to focus the wave from a penetration port and to transform the incident radiation pattern. Rotatable mirrors and polarization control are in use in the W-VII as stellarator.

For high power operation and/or long pulse operation, active cooling might be needed. In Tore Supra, losses for a 400 kW incident RF power at 110 GHz have been estimated to be of the order of 1 kW.

2.2 LHCD Antennae

They are made from a phased array of open-ended waveguides located in the scrape-off plasma (grill). The parallel wave spectrum is determined by the width of the waveguide and the phase between adjacent waveguides.

To date antennae use a large number of waveguides per antenna:

JT-60	96 waveguides at 2 GHz
ASDEX	48 waveguides at 2.45 GHz
Tore Supra	128 waveguides at 3.7 GHz
JET	128 waveguides at 3.7 GHz
JET	384 waveguides at 3.7 GHz (in preparation)
JT-60U	192 waveguides at 2 GHz (in preparation)
FT-U	48 waveguides at 8 GHz (in preparation)

An important practical problem is the RF breakdown which might occur in open-ended evacuated waveguides due to:

- multipactor (resonance of secondary electrons trajectories which is a severe problem at ω_{ce}, $\omega_{ce}/2$, $\omega_{ce}/3$,...
- impact ionisation of residual gas (if p> 10^{-5} torr)

The usual remedies are the following:

- coatings: Carbon, Ti pulverisation, rough gold
- glow discharge cleaning
- baking at high temperature
- magnetic shielding
- vacuum windows between plasma and cyclotron layer
- large pumping (100 000 l/s being developed for JET)
- RF conditioning (aging)

allowing substantial power handling densities to be achieved, ranging from 2 kW/cm^2 at 1 GHz to 10 kW/cm^2 at 10 GHz.

The trend to operate at high frequency is favourable for power density capability, but the corresponding reduction in dimensions impose the use of very large number of waveguides.

In order to reduce the number of associated vacuum windows, the power can be split by passive elements into small waveguides in the evacuated section of the antenna. With the "multijunction" technique (Petula, Tore Supra, JT-60, JET) the power has been split in up to 8 waveguides per window. It is to be noted that the use of built-in phase shifters impose a good mechanical accuracy in the construction of the antenna and that the relative phasing between waveguides is less flexible.

The preferred waveguide material is copper to minimize resistive losses. Disruption induced forces are very high due to the proximity of the grill mouth to the plasma. In Tore Supra, Zirconium copper (good mechanical qualities) and electrical insulation between waveguides has been used. In JET and JT-60, copper coated stainless steel and strong shielding box to reduce eddy currents have been used. Cooling is required for long pulse operation: gas cooling in JT-60 and water cooling at 200° C in Tore Supra.

Matching is achieved by moving the antenna radially using large bellows and hydraulic actuators. A good location accuracy (1 mm) is needed. Position control systems can be rather complex owing to the weight of the launcher (15 tonnes in JET), the protection of the vacuum moving system against disruption induced forces and the safety aspects. Programmed movement during a plasma shot is needed with eventually a feedback control (in preparation in JET).

2.3 ICRH Antennae

To date they are made from inductive loop antennae carrying poloidal RF current. A Faraday shield is required to impose wave polarisation, to avoid parasitic loading into other wave modes and prevent direct streaming of particles into antenna.

Optically closed screens made of Nickel or Titanium Carbide have been used in ATC, PLT, TFR, JET, ASDEX, TFTR. The corresponding RF losses entail the use of active cooling, as in JET with Nickel screens. Optically open screens and the use of a good conductor allow to reduce RF losses and to use only radiation cooling, as in JET with Beryllium screens.

For long time, application of large ICRF power induced metallic impurities. Coating techniques (carbonisation, boronisation) have beneficial effects. Tilting the screen parallel to the magnetic field and the use of Beryllium (low self-sputtering yield) have solved the problem of impurity release, in good agreement with theoretical predictions /6/.

To achieve a good matching it is possible to fit the antenna within a port and to move radially the launcher (JT-60, TFTR, Tore Supra). In such a way, a small area of the tokamak is used, in competition with other port requirements, and large RF fields can be produced in front of the antenna.

The other possibility is to move the plasma-antenna distance as in JET. Antennae can then be located between main ports allowing to use a substantial part of the outer wall (8 antennae in JET) and to operate with much lower RF fields in front of the antenna. In addition, the plasma movement reaction is much faster than with a mechanical movement.

A feedback system on the radial position of the plasma has been successfully tested in JET allowing a constant impedance to be maintained even during the large change in the scrape-off plasma density which occurs during an H-mode transition.
In practice, the antenna electrical performance is usually limited to a maximum voltage reached in the antenna and its feeds, which can be improved by increasing the plasma loading resistance, for instance by placing the structure closer to the plasma, or by increasing the capacitance of the loop coupler.

It is to be noted that the new A2 antennae which are being prepared for JET will allow improved coupling properties by making use of the space created by the new pumped divertor configuration. More-over they will incorporate ICR current drive features such as a septum to decouple adjacent conductors (to allow arbitrary phasing) with a better directivity, up to 80%.

3 TRANSMISSION LINES

The two main elements of a transmission line are the following:

- the vacuum windows as the interface with the antenna
- the pressurised section

The vacuum windows constitute a very sensitive item of the system since they have to ensure the vacuum integrity of the torus, to have good mechanical qualities and obviously good RF properties.

They are usually made from flat ceramic discs that are brazed into a section of the waveguide or of the coaxial transmission line. The following material are used:

- alumina
- beryllium oxide
- boron nitrate
- quartz
- sapphire

Sapphire is the preferred material at high frequency, ie above a few GHz.

The main role of the pressurised section is to allow transport of RF energy from generators which can be located far away from the torus and along transmission path which include usually a large number of bends. They have to transmit power with low RF losses and to launch the wave with the required pattern.

3.1 Vacuum Windows

3.1.1 Dimensions of ECRH windows are not directly linked to the wavelength of the EC waves. The average power density is usually in the range of 6 to 8 kW/cm^2 but the dielectric losses are high and cooling is a problem.

For short pulse operation, cooling is achieved through conduction at the edge. For high power and/or long pulse operation, the actual technique is to use double sapphire disks with a stable liquid (fluorinated hydrocarbon) flowing between disks. The associated thermo-mechanical stresses are important, specially taking into account the small thickness of the disks.

To date, ECRH windows are a weak link in the power chain and limit the energy handling capability. 200 kW of power for a few seconds at 60 GHz have been achieved during tokamak operation. Higher power handling is obtained on sources:

60 GHz	CW	200 kW
140 GHz	CW	100 kW
140 GHz		400 kW for 0.5 s.

Development of high power windows is going on for the new generation of sources, as it will be discussed later.

3.1.2 An important aspect in the design of LHCD windows is linked to their location.

Windows with a small width have to be used if they are located between the plasma and the cyclotron layers. In spite of difficult technical problems, this technique has been successfully applied to several experiments: PLT, FT, ASDEX, FT-U. But, this technique is not felt to be practical for use in future machines due to damages to the window from neutron irradiation and gamma bombardment.

Larger windows located far from the plasma have to be used in order to develop similar techniques than foreseen in future machines. Distance between the antenna mouth and the vacuum interface can then reach 6 to 8 metres: JT-60, Tore Supra, JET. Power handling capability of 300kW to 1MW for long duration time have been achieved, depending upon the frequency and upon the degree of reliability which is needed.

It is to be noted that techniques relevant for future machines such as double containment and remote handling installation have been tested in JET.

3.1.3 ICRH windows are made of a coaxial transmission line and their power handling capability has been found to be very large: 1 to 2 MW for long duration time.

The main problem for their design is the limit in voltage capability. Special attention has to be devoted to the shape and the design of the ceramic windows in order to withstand the required large voltage. To day, currents up to 1 kA and voltages up to 50 kV have been achieved.

3.2 Pressurized Transmission Lines

3.2.1 One of the main achievement in the design of ECRH transmission lines has been to produce a low loss system (Stuttgart, Culham). Such systems consist of a large number of components, including:

- overmoded waveguides
- mode converters to use low loss propagating modes (0.3dB/km for the HE11 mode and 0.43 dB/km for the TE01 mode)
- mode converters to launch the required mode structure
- mode filters
- bends and tapers required by the geometry

As an example, the 50m long transmission line for COMPASS at 50 GHz has a 10 to 15% transmission loss. CO_2 gas purging is sufficient for reliable operation.

It is to be noted that quasi-optical transmission lines (quasi-gaussian beams and focusing mirrors) will have to be used for frequencies above 140 GHz.

3.2.2 LHCD transmission lines are more conventional since they are made from standard waveguides which are pressurised with SF6 in order to reach their maximum capability, whicb is in the range of 1MW at a few GHz.

Resistive losses are important when the frequency exceeds 3 GHz and overmoded waveguides are eventually used to reduce losses. A 95% transmission loss has been achieved on Tore Supra with a 30m long transmission line at 3.7 GHz.

Low losses and realiable components such as DC break, hybrid junctions and flexible waveguides to accommodate launcher movement have been developed in several experiments. Remote handling flanges and HF connectors have been developed in JET.

3.2.3 ICRH transmission lines are made of large diameter coaxial transmission lines in order to withstand the large RF voltages. These coaxial transmission lines have very low losses when they are matched.

The significant amount of power which is reflected back to the generator is transformed into circulating power by matching units (stubs, trombones). Their location close to the antenna minimises losses.

In JET, some of the matching units are located close to the torus and a fully automated matching system is used allowing matching to be obtained in a large range of plasma conditions.

In the ORNL design for TFTR and Tore Supra antennae, variable vacuum capacitors are part of the antenna itself.

4 GENERATORS

Requirements for RF sources for fusion include high power, long pulse duration time and reliability. These requirements are close to those of other applications in the low frequency range (f < 1GHz), for instance in the domain of broadcasting. But specific developments have been needed in order to meet these specifications at high frequencies.

4.1 Development of high power ECRH sources is very challenging and still on-going. Today, high power sources available for pulse operation duration longer than one second are limited to frequencies up to 60 to 84 GHz.

The preferred source in almost all fusion experiments is the gyrotron. The radiation is produced through the interaction of an electron beam (with a large proportion of transverse energy) with an r.f.electric field in an overmoded cavity operating at high order mode. The electron beam is shaped to conform to the desirable mode structure, usually azimuthally symmetric modes.

Steady state gyrotrons have been operated at 60GHz on DIII (Varian) and 70 GHz on W VII AS (Varian) at a power level of 200 kW. 350 kW gyrotrons at 81 GHz have been operated for 0.2 second on T-10 (Gorky).

At higher frequency, the following gyrotrons have been developed:

1.5 MW for 0.2 sec at 81 GHz (Gorki)
200 kW for 0.1 sec at 100 GHz (Thomson)
120 kW for 0.1 sec at 140 GHz (KFK)
500 kW for 0.3 sec at 140 GHz (Toriy, USSR)
400 kW for 0.5 sec at 140 GHz (Varian)

Development to achieve long pulse operation (10 to 60 seconds) is proceeding for a 110 GHz gyrotron (Thomson) and for 110 and 140 GHz gyrotrons (Varian), all at power level of about 400 kW. Their efficiency is rather low: 30 to 34%. A Gyrotron concept with special separation of RF and e-beam might allow energy recovery resulting in shifting efficiencies up to 40 - 50% (under investigation).

To be noted is the use of superconducting magnets to provide the required magnetic field: up to 6 Tesla.

Another possible microwave source is the free electron laser. Radiation is produced by the interaction of a relativistic electron beam with a spatially periodic magnetic "wiggler" field and an electromagnetic wave that is propagating as a waveguide mode in a drift tube. It is to be noted that they can be tuneable in frequency which can be advantageous for several possible applications.

Using a relativistic e-beam at 6 MeV, an RF power pulse of 200 MW for 10Ns has been launched in the MTX experiment at Livermore through an evacuated transmission line.

It is to be noted that the progress of ECRH studies is closely linked to the development of sources. The following generators are:

-	running	W VII AS	1 MW	70 GHz	3 sec
		T-10	4 MW	81 GHz	
-	in preparation	COMPASS	2 MW	60 GHz	5 sec
		DIII	2 MW	60 GHz	5 sec
		T-15	12 MW	81 GHz	0.5 sec
-	in development	Tore Supra	2 MW	110 GHz	30 sec
		FT-U	2 MW	140 GHz	1 sec
-	proposed	ASDEX U	2 MW	140 GHz	
		DIII	5 MW	110 GHz	
		W VII X	10 MW	140 GHz	

for the plasma current, plasma densities exceeding 10^{20} m^{-3} and time duration of at least 200 seconds.

The estimated power required for heating the plasma to ignition is: 50 MW for 50 sec, and for burn control is: 20 MW for 200 sec.

The estimated power for non-inductive current drive ranges from 100 to 150 MW, depending upon the density, for time duration ranging from 200 sec to steady state.

Requirements for steady-state operation are very demanding. For all the methods which are possible candidates, including neutral beam current drive, a substantial part of the plasma current (25% to 50%) has to be driven by "natural" non-inductive plasma currents such as the bootstrap current.

For steady-state current drive, the efficiency is obviously a very critical parameter:

- a large "technical" efficiency, ie including power supply, source, transmission line and antenna efficiencies, is required to minimise the power from the grid which can be considered as recirculating power from the fusion output:
- a large "physics" efficiency, ie the ratio between the amount of produced driven current to the power effectively coupled to the plasma minimises power requirements. The required "physics efficiency" value has to be in the range of:

$$n R I/P = 0.4\ 10^{20}\ m_z^{-2}\ MA/MW$$

for the next steps, n being the plasma density and R the major radius of the tokamak, and significantly in excess of that value for reactors if operating density has to be high.

Actual domain of efficiencies are shown in fig. 2 /8/. The gap between required and actual efficiencies is quite small for LHCD, especially at relatively low density, larger for ICR driven methods, coming experiments on ICRD are aimed at bridging this gap, and quite large for all other methods. To be noted that experiments with MeV-beams are prepared (JT-60 U) allowing NBI current drive and efficiencies to be assessed in conditions closer to Next Step conditions than actual NBI current drive experiments.

4.1 ICRH for Next Step

ICRH is prime candidate for heating plasma to ignition and for burn control. ICR current drive is a promising method whose predicted efficiency is slightly smaller than for LHCD and for Neutral Beam current drive, but can be balanced by a high "technical efficiency".

The main advantage of the method is its independence to the density of the plasma and to its flexibility associated with the tuneability of the generator.

Required frequencies are the following:

- plasma heating to ignition: 44 MHz for minority heating on ^3He and for harmonic heating on tritium
- 33 MHz for burn control at $\omega = \omega_{cd}$
- 17 MHz for current drive (frequency below all main species resonances and highest efficiency range)

A 17 to 60 MHz tuneable system is proposed /9/ and no specific problems on generator and transmission line are anticipated, even if the frequency has to be varied during a plasma pulse in order to be tuned to different heating schemes. "Technical efficiencies" ranging between 50% and 60% are envisaged.

The antenna being a plasma facing component, it is proposed to make the antenna an integral part of the blanket modules. The main characteristics of the proposed system are the following:

- to use a large array of antennae: 30 to 60 if they can be mounted above port location, as sketched in fig. 3, 18 if they have to cross port location.
- the Faraday shield is made of water cooled tubes, avoiding welds
- the first ceramic insulator is placed after the first bend avoid neutron damages.

4.2 LHCD for the Next Step

The main role for the LHCD system is:

- to provide off-axis current drive
- to assist the ramp-up of the plasma current
- to provide some control of the plasma current profile

The proposed frequency of 5 GHz is a compromise between conflicting requirements. A higher frequency would avoid coupling to alpha particles and to have a good wave penetration even at high density. A lower frequency would avoid prohibitive resistive losses and to avoid reducing too much the distance between plasma and the antenna.

For this frequency, Klystrons are a preferred source because they are robust and can easily be controlled in phase. Units with an output power of 1 MW are considered. With actual technology a "technical" efficiency of: 45% (from the grid) is achievable. This efficiency can be increased up to 51% by developing more efficient klystrons. Different techniques are considered such as:

- a depressed collector
- hollow beams klystrons

Gyrotrons (6GHz, 1 MW CW) with high efficiency are under consideration in USSR.

A critical issue is related to the ability of the plasma facing parts of the launcher to withstand first wall conditions such as:

- erosion
- disruption induced forces

which can be quite severe because the launcher has to be located within a few cm from the plasma in order to achieve a good match.

The main characteristics of the proposed system, as sketched in fig. 4, are the following:

- coupler composed of 3000 waveguides made from glidcop or ZiCo using multijunction technique, located in two main ports.
- a "compact design" to avoid cyclotron layers
- replaceable grill mouth

4.2 LHCD sources are more conventional. Klystrons have been used at frequencies up to 4.6 GHz. They are robust, reliable with good efficiencies: 45% to 65% and can easily be controlled in phase which is quite important for current drive application. In particular, the phase has to be controlled and adjusted during a plasma pulse.

Klystrons can be operated in large nubers:

24 1 MW klystrons at 2 GHz for 10 sec in JT-60
16 0.5 MW klystrons at 3.7 Ghz for 30 sec in Tore Supra
24 0.6 MW klystrons at 3.7 GHz for 10 to 20 sec in JET

At higher frequency, gyrotrons or gyro-klystrons have to be used in order to have a significant power output per source.

An 8 GHz gyrotron for a pulse duration time of 1 second is being prepared for FT-U at a power level of 1 MW (Thomson), 500 kW (Varian). The control in phase is more difficult since gyrotrons are not amplifier tubes such as klystrons.

4.3 ICRH sources are high power tetrodes which are also reliable and robust sources with a very good efficiency: 60% to 80%. The following tetrodes have been operated:

1.5 MW for 20 sec (Eimac)
2 MW for 20 sec (Thomson)

and 2.5 to 3 MW units are in preparation. They can be tuneable in frequency. For instance, the following range has been achieved:

23 - 57 MHz in JET
30 - 114 MHz in ASDEX

A plant made of 16 units of 2 MW is routinely in operation in JET.

5 RF METHODS FOR NEXT STEP

The current drive and heating system for the Next Step has to be a multi-function system /7/. A list of the envisaged functions is as follows:

- heat the plasma to ignition with enough flexibility for burn control	ICRH (ECRH)
- drive all, or a portion of the plasma current for steady state or very long pulse operation	LHCD ICRD (ECRH)
- assist start-up of the plasma	ECRH
- assist ramp-up of the plasma current	LHCD
- control plasma current profile and plasma disruptions	ECRH LHCD

together with the RF methods which are considered to be very good candidates for the task. The brackets indicate the case for which the method is only a supplementary system.

Although the parameters of the Next Step are still under discussion, it is possible to assume some guide-lines to discuss the design of RF methods, such as a magnetic field of 5 Tesla, 20 to 25 MA

- stainless-steel frames to protect against disruption forces
- water cooling at the cooling temperature of the vessel, or slightly higher
- large pumping in the range of 100 000 l/s
- a 20 cm stroke, the weight of the launcher being in the range of 40 to 80 tonnes.

5.1 ECRH for Next Step

The main role for ECRH is to provide:

- preionisation
- assistance in ramp-up
- mode control

The required frequency range for these tasks is from 120 GHz to 170 GHz. Tasks for which ECRH can be a supplementary method: core heating and current drive, would require a higher frequency range: from 140GHz to 260 GHz, mainly because up-shifted frequencies are more effective for current drive.

It is proposed to use a large number of channels from sources at 140 GHz delivering 1 MW with mode converters integrated in the source, via a 50 m long corrugated waveguide transmission line. As shown in fig. 5, focusing mirrors are used as well as moveable mirrors to keep track of mode surfaces.

The main critical issues for the procurement of such a system are the windows and the sources.

Cryogenically cooled windows are under study for the ECRH Tore Supra programme at 100GHz. A possible problem is the water condensation at the window. An alternative is to develop an evacuated transmission line with a fast valve to protect the source.

Gyrotrons operating with different mode structure: whispering gallery, volume and quasi-optical modes are under study in many laboratories. The main difficulties is to obtain long duration pulses and good efficiencies, as a consequence of operating multi megawatt electron beams passing through small diameter cavities.

New concepts are developed such as CARMs where the radiation is an induced cyclotron emission from an electron beam which decreases also its longitudinal velocity during interaction with the wave. Potential efficiency can be high but these tubes are in the early stage of their development.

A free electron laser (FEL) is very attractive for its tuneability and its large power output. There is a large development for short pulse operation which is not very useful for tokamak fusion reactors. DC operation is much more difficult since high efficiency operation requires a sophisticated recirculation recovery scheme. A long pulse FEL at 200 GHz is under development at FOM laboratory.

6 SUMMARY AND CONCLUSIONS

RF systems are mature systems which have obtained main achievements in fusion oriented experiments. They are flexible systems with synergistic and complementary actions between different methods. The good theoretical understanding together with the large data base allow a good level of confidence in the extrapolation of the existing RF systems to the systems required for the Next Step. In particular operation on JET with powerful system at parameters close to those required for ICRH and LHCD for the Next Step provide operational experience for large machines

with constraints such as reliability and remote handling operation. A summary of the main features of the RF systems is as follows:

	ICRH	LHCD	ECRH
	very effective heating	very effective current drive	very effective heating
	technical efficiency: 50% to 60%	technical efficiency: 45% to 51%	technical efficiency: 30%
	P_{hf} up to 18 MW	P_{hf} up to 8 MW	P_{hf} up to 1.5MW
	promising current drive method localisation independent on density	actual physics efficiency close to required value for next step	localisation of heating
	possible in-blanket antenna		very simple launching structure
critical issues			
	demonstrate effective current drive	launcher close to plasma surface	high power sources and windows to be developed
Next Step			
	50 MW 17-60 MHz for heating to ignition and central current drive.	50 MW 5 GHz for off-axis current drive, ramp-up, profile control	20MW 140 GHz for plasma start-up and mode control

Rf systems are playing an increasing role in almost all of today's experiments and will certainly play an important role in Next Step devices. Next Step requirements for RF techniques will take into account the final parameters for the Next Step facility (magnetic field, divertor configuration), the anticipated mode of operation (H-mode operation, steady-state operation, etc..)and their consequence on important physics parameters such as electron temperature, plasma density and density profile.

ACKNOWLEDGEMENTS

Many contributions are gratefully acknowledged, in particular from G.Tonon, L.Rebuffi, J.G.Wegrowe, D.Swain, V.Erckmann, G.Faillon and M.Guidee. Discussions with T.Riviere and J.Jacquinot have played an essential role in the preperation of this paper.

REFERENCES

/1/ England, A.C., Eldrige, O.C., Knowlton, S.F., Porkolab, M., Wilson, J.R., Nucl. Fusion 9 (1989)1527.

/2/ Review papers in Course and Workshop on Applications of RF Waves to Tokamak Plasmas, S. Bernabei, V. Gasparino, E. Sindoni, Editors, Varenna, Italy (1985).

/3/ Gibson, A., et al in Proceedings 17th EPS Conf. on Controlled Fusion and Plasma Heating, Amsterdam (1990)

Start, D. et al, in Proceedings 17th EPS Conf. on Controlled Fusion and Plasma Heating, Amsterdam (1990).

/4/ Ushigusa, K., et al in Proceedings 17th EPS Conf. on Controlled Fusion and Plasma Heating, Amsterdam (1990).

/5/ Itoh, S., Hiraki, N., Nakawura, Y., Nakamura, K., Nagao, A., et al in Proceedings 12th Conf. on Plasma Physics and Controlled Nuclear Fusion Research, Nice (1988) Vol. I, p.629.

/6/ Bures, M., Jacquinot, J., Lawson, K., Stamp, M., et al, Report JET-P(90)49, submitted to Plasma Phys. and Contr. Fusion.

D'Ippolito, D.A., Myra, J.R., Bures, M. and Jacquinot J., Report Lodestar Research Conp. LRC-90-18 Submitted to Plasma Phys. and Contr. Fusion.

/7/ Tomabechi, K., in Proc. 12th Conf. on Plasma Physics and Controlled Nuclear Fusion Research, Nice (1988), Vol. IV, p.215-273.

/8/ Report on the Meeting on the Expert Group for an Integrated Development Program for Lower Hybrid Waves System for Next Step., Chairman GF Tonon (April 1990).

/9/ Ion Cyclotron Fast Wave Current Drive and Heating System for ITER, (ITER Report) D.W. Swain, J. Jacquinot, H. Kimura et al (1990).

/10/ Report on the Meeting of the Expert Group for an Integrated Development Programme for Electron Cyclotron Wave Systems for NET, Chairman MQ Tran (1990),

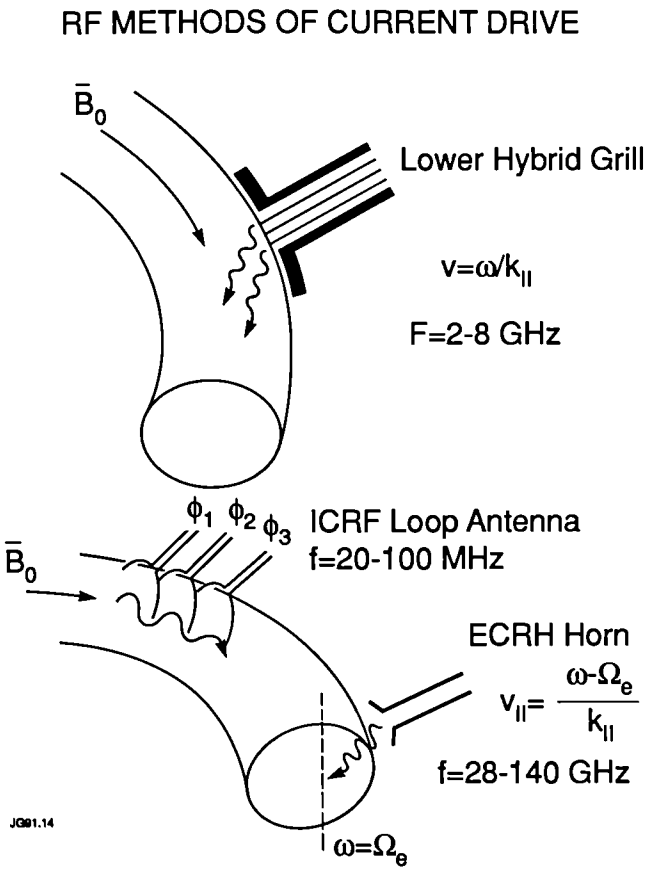

FIG.1 SCHEMATIC OF VARIOUS RF TECHNIQUES

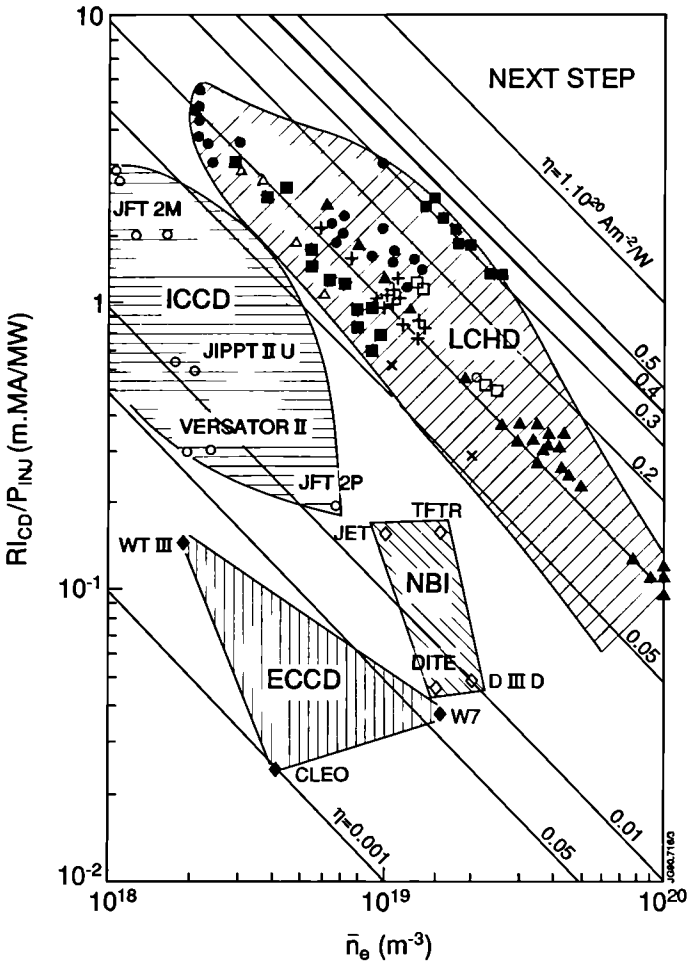

FIG.2 Domain of efficiencies for current drive methods: Lower Hybrid Current Drive (LHCD), Ion Cyclotron Current Drive (ICCD), Electron Cyclotron Current Drive (ECCD), Neutral Beam Current Drive (NBI). (from G Tonon, report of the expert meeting on LHCD for the Next Step, April 1990)

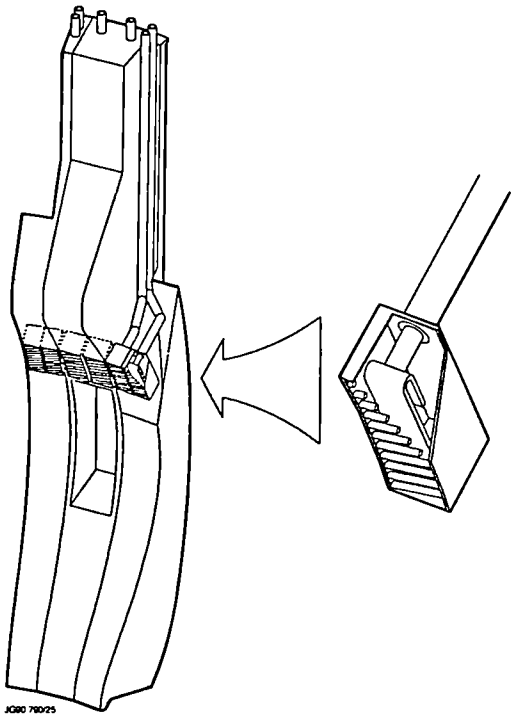

FIG.3 SCHEMATIC OF AN ION CYCLOTRON RESONANCE ANTENNA ON ITER

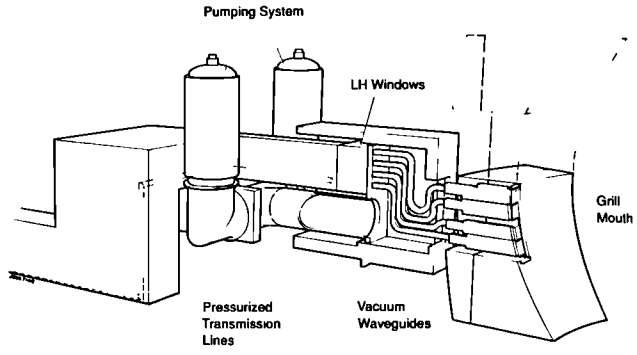

FIG.4 SCHEMATIC OF A LOWER HYBRID CURRENT DRIVE COUPLER ON ITER

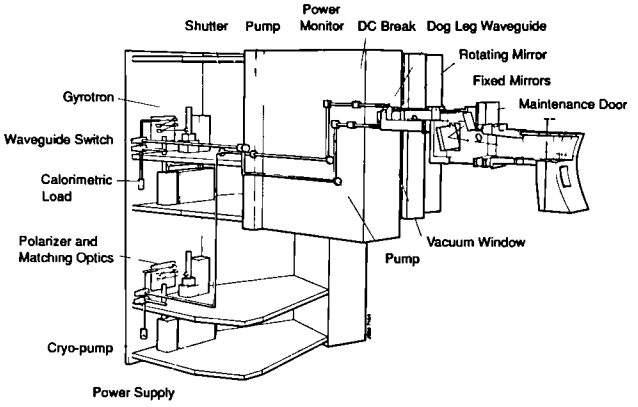

FIG.5 SCHEMATIC OF AN ELECTRON CYCLOTRON HEATING SYSTEM ON ITER

Appendix III (j)
JET-P(90)66

Future Prospects for JET and Next Step Tokamaks

P.H.Rebut

Invited Paper presented to
16th Symposium on Fusion Technology,
London, UK., 3rd-7th September 1990

Future Prospects for JET and Next Step Tokamaks

by

PH Rebut

JET Joint Undertaking, Abingdon, Oxon. OX14 3EA, UK.

ABSTRACT

Latest results from the JET tokamak, with beryllium as the first wall material facing the hot plasma, have shown substantial improvements in plasma purity and corresponding reductions in plasma dilution. This has allowed a fusion product ($n_D\tau_E T_i$) of 8-9x10^{20}m^{-3}skeV to be reached (within a factor of 8 of that required in a fusion reactor), albeit only transiently. Even so, at high heating powers, an influx of impurities still limits the achievement of better performance and steady state operation.

A New Phase for JET is planned in which an axi-symmetric pumped divertor configuration will be used to address the problems of impurity control, plasma fuelling and helium ash exhaust in operating conditions close to those of a Next-Step tokamak with a stationary plasma of thermonuclear grade. The New Phase should demonstrate a concept of impurity control; determine the size and geometry needed to realise this concept in a Next-Step tokamak; allow a choice of suitable plasma facing components; and demonstrate the operational domain for such a device. With an efficient axi-symmetric pumped divertor, ignition should occur in a tokamak reactor of about 2 to 3 times the size of JET.

It seems prudent to envisage international collaboration on a Next Step Programme, which could comprise several complementary facilities, each optimised with respect to specific clear objectives. There could be two Next Step tokamaks, and a Materials Test Facility. Such a programme would allow division of effort and sharing of risk across the various scientific and technical problems, permit cross comparison and ensure continuity of results. A single Next Step device (such as the ITER Project as currently conceived) has higher scientific, technical and management risks and does not provide such comprehensive information, particularly in the areas of ignition, reactor performance and blanket testing. Further details of these facilities, expected costs and timescales are discussed.

1. INTRODUCTION

The Joint European Torus (JET) is the central project in the European Fusion programme. This programme is coordinated by the European Atomic Energy Community (EURATOM). The EURATOM Fusion Programme is designed to lead ultimately to the construction of an energy producing reactor. Its strategy is based on the sequential construction of major apparatus such as JET, the next European Torus (NET), and DEMO (a demonstration reactor), supported by medium sized specialized tokamaks.

The objective of JET is to obtain and study a plasma in conditions and dimensions approaching those needed in a thermonuclear reactor [1,2] involving four main areas of study:

(i) various methods of heating plasmas to the thermonuclear regime;
(ii) the scaling of plasma behaviour as parameters approach the reactor range;
(iii) the interaction of plasma with the walls and methods of fuelling and exhausting the plasma;
(iv) the production of alpha-particles generated in the fusion of deuterium and tritium and the consequent heating of plasma by these alpha-particles.

JET is now in the second half of its experimental programme. The technical design specifications of JET have been achieved in all parameters and exceeded in several cases (see Table I). The plasma current of 7MA and the current duration of up to 30 seconds are world records and are more than twice the values achieved in any other fusion experiment. The neutral beam injection (NBI) heating system has been brought up to full power (~21MW) and the ion cyclotron resonance frequency (ICRF) heating power has been increased to ~18MW in the plasma. In combination, these heating systems have provided 35MW power to the plasma.

During its experimental programme, JET has devoted particular attention to studying the interaction of the plasma with the vessel walls. This paper summarises results obtained when JET was operated with carbon and then with beryllium as the first-wall to provide a low-Z material facing the plasma. Even though impressive results were obtained, at high heating powers, an influx of impurities still limits the achievement of better performance and prevents the attainment of steady state. A planned New Phase for JET [3] is presented: an axi-symmetric pumped divertor configuration would be used to address the problems of impurity control, plasma fuelling and helium ash exhaust in operating conditions close to those of a Next-Step tokamak with a stationary plasma of thermonuclear grade. Finally, the requirements for a Demonstration Fusion Reactor are set out and proposals are made on how international collaboration on a Next Step programme could be envisaged. This should comprise several complementary facilities, each optimised with respect to specific clear objectives.

2. JET SCIENTIFIC RESULTS AND ACHIEVEMENTS

The performance of JET, as indicated by the fusion triple product ($n_D\tau_E T_i$), has increased significantly since beryllium was introduced into JET as a first-wall material, in two different ways: initially as a thin evaporated layer on the carbon walls and limiters; and later, in addition as a limiter material. The consequence of these different regimes of operation on each plasma physics parameter in the fusion triple product is detailed below. Of particular significance is the effect of improved plasma purity, which previously, with a carbon first-wall, had impeded progress towards a reactor.

Recently, it became apparent that impurities and density control were the main obstacles to improved JET performance. Graphite components had been developed to mechanically withstand the power loads encountered. However, the interaction of the plasma with these components, even under quiescent conditions, caused unacceptable dilution of the plasma . In addition, imperfections in the positioning of the components led to localised heating during high power which caused enhanced impurity influxes. These influxes produced a condition called the 'carbon catastrophe', in which the plasma concentration, plasma temperature and neutron yield collapsed.

Density: With a carbon first-wall, the plasma density was limited. In general, this occurred when the radiated power reached 100% of the input power, leading to the growth of MHD instabilities and ending in a major disruption. The density limit was dependent on plasma purity and power to the plasma.

With a beryllium first-wall, the maximum operating density increased significantly by a factor of 1.6 - 2. A record central density of 4 x 10^{20}m^{-3} was achieved by strongly peaking the density profile using a sequence of 4mm frozen deuterium pellets injected at intervals throughout the current rise phase of an X-point discharge. Moreover, the density limit increased with increasing total input power, approximately as the square root of the power (see Fig.1). Furthermore, the nature of the density limit changed and the frequency of disruptions at the density limit were much reduced. Disruptions did not usually occur, and the limit was associated rather with the formation of a poloidally asymmetric, but toroidally symmetric radiating structure (a "MARFE"), which clamped the plasma density. These results constitute a substantial enhancement of the operating capability of JET.

Experiments were performed in which heating and fuelling were varied systematically, using NBI, ICRF, gas and pellet fuelling. With pellet injection and additional heating, more peaked density profiles were established. Pellet fuelled discharges at the same edge density as gas fuelled discharges had considerably higher central densities. Fig.2 shows density profiles just before a density limit MARFE occurred (cases (a) and (b)) and far away from the density limit (case (c)). Density profiles are very similar near the edge, but the gas fuelling profile is remarkably flat. These flat profiles are difficult to reconcile with an anomalous particle pinch and pose important questions related to particle transport, and in particular, the transport and exhaust of helium ash products. With deep pellet fuelling and additional heating, peaked profiles are obtained (cases (a) and (c)). These studies suggest that the edge density may be correlated with the density limit which, under beryllium conditions, may be considered as a limitation of edge fuelling. These observations endorse the view that the density limit is determined by a power balance at the plasma edge. This suggests that the cause of disruptions is related to radiation near the q=2 surface. Furthermore, when the radiation is low, or confined to the outermost edge, there are no density limit disruptions.

Operation with beryllium gettering allowed improved density control (due to high wall pumping). A beryllium first-wall offered the additional advantages of improved plasma purity and reduced radiation. These factors allowed higher input powers, greater fuel concentrations (n_D/n_e) (see Fig.3.) and improved fusion performance. On the longer timescale (minutes to hours), very little deuterium was retained in comparison with a carbon first-wall; over 80% of the neutral gas admitted to JET is recovered, compared to about 50% with a carbon first-wall. This has important advantages for the tritium phase of JET operation.

Temperature: High ion temperatures have been obtained at the low densities possible with a beryllium first-wall and with the increased neutral beam penetration afforded by operation at an energy of 140kV. Record ion temperatures were achieved: up to 18keV in material limiter plasmas and up to 30keV in magnetic limiter plasmas, for powers up to 17MW. A typical example is shown in Fig.4 in which the central ion temperature reached 28keV for about 15MW input in a magnetic limiter configuration. The ion temperature profile is sharply peaked and the electron temperature is significantly lower than the ion temperature, by a factor of 2-3. The central ion temperature is shown in Fig.5 to increase linearly with power per particle up to the highest temperatures so far achieved; the central electron temperature, on the other hand, is seen to saturate at about 12keV. At higher densities ($n_e(0)>2x10^{19}$m^{-3}), experiments with combined neutral beam and ICRF heating result in central ion and electron temperatures both exceeding 11keV in a 3MA plasma for an input power of 33MW (21MW NBI and 12MW ICRF heating).

Extensive studies have been performed in the 'monster-sawtooth' regime in which sawteeth oscillations have been suppressed for up to 5s by central ICRF heating. Peaked temperature profiles (with both central ion and electron temperatures above 10keV) were maintained for several seconds, which, in the equivalent D-T mixture, would result in a significant enhancement in the time-averaged fusion reactivity over that obtained in a sawtoothing discharge.

These observations indicate that electron thermal losses are anomalous, with electron confinement degrading substantially with increasing input power. The ions, on the other hand, behave quite differently; although ion thermal transport is also anomalous, ion confinement degrades little with increasing input power. This suggests that the electrons are the fundamental cause of anomalous transport. This is in-line with the critical electron temperature gradient model for confinement [4].

Energy Confinement: With either a carbon or beryllium first-wall, the energy confinement time on JET improves with increasing current and decreases with increasing heating power, independent of the type of heating.

In the X-point configuration, H-modes [5] with high power heating (up to 25MW) have been studied. In comparison with limiter plasmas, the confinement is about a factor of two better, but the dependences on current and heating power are similar. Although the experiments with a beryllium first-wall were conducted with carbon X-point target plates and the confinement times were similar to those obtained with a carbon first-wall, better plasma purity

(central values of fuel concentration (n_D/n_e) were in the range 0.7-0.9) allowed substantially improved fusion performance.

With a carbon first-wall, H-modes with ICRF heating alone were not obtained; with a beryllium first-wall, H-modes were successfully obtained with ICRF heating alone. This was mainly possible because of beryllium evaporation onto the nickel antennae screens, which lead to a lower impurity production. With beryllium antennae screens, H-modes were achieved with either monopole or dipole phasing of the ICRF antennae The confinement in H-modes with ICRF alone was similar to that with NBI.

In summary, the global confinement time degraded with input power for both ICRF and NBI heating in the range 4 - 25MW. The dependence of the confinement times on heating power in both material and magnetic limiter configurations is shown in Figs.6(a) and (b), respectively. Typically, H-mode confinement is about twice L-mode confinement.

These observations indicate that the transport in the H- and L-regimes are similar, except for an edge thermal barrier which is easier to establish with X-points and high shear. Furthermore, energy confinement does not appear to be affected by the impurity mix (carbon or beryllium in deuterium plasmas).

Beta Limits: Experiments have explored the plasma pressure (as represented by the β-value) that can be sustained in JET and investigated the plasma behaviour near the expected β-limit in a double-null H-mode configuration, at high density and temperature and low magnetic field (B_t = 1 T). Values of β_t up to ~ 5.5% were obtained. The β_t limit is close to the Troyon limit [6] $\beta_t(\%) = 2.8\ I_p(MA)/B_t(T)a(m)$, where I_p is the plasma current and a is the plasma minor radius, as shown in Fig.7. Significantly, it is found that the limit in JET does not appear to be disruptive. Rather, a range of magneto-hydrodynamic (MHD) instabilities occur and these limit the maximum value of β without causing a disruption.

The behaviour near both the density and β-limits may be reconciled in terms of resonant instabilities, which have the magnetic topology of islands.

Impurities: With a carbon first-wall, the main impurities in JET were carbon (2-10%) and oxygen (1-2%). With beryllium evaporation, oxygen was reduced by factors >20, and carbon by >2. Although beryllium increased, carbon remained the dominant impurity for this phase. With beryllium limiters, the concentration of carbon was reduced by a further factor of 10, but beryllium levels increased by about a factor of 10, and became the dominant impurity. Due to the virtual elimination of oxygen, and the replacement of carbon by beryllium, impurity influxes were reduced significantly, in line with a model [7] which takes account of impurity self-sputtering. As shown in Fig.3, it had not been possible to maintain (n_D/n_e) much above 0.6 with carbon limiters even for moderate input powers, but values greater than 0.8 were routinely achieved with beryllium limiters. Correspondingly, the effective ionic charge, Z_{eff}, was reduced significantly, already with the beryllium evaporation , and then more so with beryllium limiters. Z_{eff} as a function of line density for the three phases of operation is shown in Fig.8.

The improved plasma purity contributes significantly to improved fusion performance, which otherwise could be achieved only with a substantial increase in energy confinement.

Fusion Performance: The use of beryllium resulted in the elimination of oxygen, the reduction in the carbon influx and the increase in the plasma purity, with the fuel concetration (n_D/n_e) increasing to 0.9. Since the X-point tiles remained as carbon, the carbon catastrophe was not affected significantly with a beryllium first-wall. However, the duration of the H-mode was extended by up to 50% either by sweeping the X-point (both in the radial and vertical directions) to reduce the X-point tile temperatures, or by using strong gas puffing in the divertor region. Improved plasma purity and increased ion temperatures ($T_i(0)$ in the range 20 - 30keV) resulted, leading to improved plasma performance. In a particular case, the central ion temperature reached 22keV, the energy confinement time, τ_E, was 1.1s, with a record fusion product ($n_D(0)\tau_E T_i(0)$) of 8–9x10^{20}m^{-3}skeV. The neutron yield for this discharge was also the highest ever achieved on JET at 3.5 x 10^{16} ns^{-1}, with Q_{DD} = 2.4 x 10^{-3}. A full D-T simulation of this pulse showed that 12MW of fusion power could have been obtained transiently with the 16MW of NBI, giving a fusion product value ($n_D\tau_E T_i$) within a factor of 8 of that required in a reactor. The overall performance of the fusion product, as a function of ion temperature, T_i, is shown in Fig.9. for a number of tokamaks.

Summary of Scientific Achievements: Substantial progress has been made with beryllium as a first-wall material, affecting impurity influxes such that:

- oxygen impurities were essentially eliminated;
- the effective ionic charge, Z_{eff}, was significantly reduced in ohmic plasmas (down to 1.2) and with strong additional heating (down to <1.5);
- a severe carbon influx ('carbon catastrophe') persisted for inner wall and X-point plasmas, and represents a serious limitation in H-mode studies.

Reduced impurity levels allowed prolonged operation at higher densities and improved the general JET performance, as follows:

- the pumping of deuterium with a beryllium first-wall was more efficient than with a carbon first-wall and provided improved density control. This permitted low density and high temperature (up to 30keV) operation for times >1s;
- the density limit increased, with a record peak density of 4x10^{20}m^{-3} with pellet fuelling. This limit is principally a fuelling limit and not a disruption limit, as found with carbon limiters;
- sawtooth free periods exceeding 5s were achieved, but the stabilisation mechanism remains unclear.
- H-modes of 1s duration were created with ICRF heating alone. Their confinement characteristics were similar to those with NBI heating alone;
- β values up to the Troyon limit were obtained in low field double-null X-point plasmas;
- the neutron yield doubled to 3.5x10^{16}s^{-1} and the equivalent fusion factor Q_{DT} increased to ~0.8;
- the fusion product ($n_D\tau_E T_i$) increased to 8-9x10^{20}m^{-3}skeV for both high (>20keV) and medium temperatures (9keV), reaching near breakeven conditions and was within a factor of 8 of that required in a reactor.

However, the results were obtained only **transiently** and could not be sustained in a steady state. Ultimately, the influx of impurities caused a degradation in plasma parameters.

3. IMPURITY CONTROL: A PLANNED NEW PHASE FOR JET

So far, JET has concentrated on **passive** methods of impurity control, reducing impurity production by proper choice of plasma-facing components (such as beryllium or beryllium carbide), sweeping the magnetic configuration across the target plates and benefitting from the formation of a highly radiating zone in front of the target plates. Studies of **active** impurity control represent a natural development of the JET programme and accordingly, a New Phase for JET is planned to start in 1992 [3], with first results becoming available in 1993 and continuing to the end of 1996.

The aim of the New Phase is to demonstrate, prior to the introduction of tritium, effective methods of impurity control in operating conditions close to those of a Next Step tokamak, with a stationary plasma of 'thermonuclear grade' in an axisymmetric pumped divertor configuration. Successful impurity control would lead also to an increase in alpha-particle power by more than a factor of two.

Specifically, the New Phase should demonstrate:

- the control of impurities generated at the divertor target plates;
- a decrease of the heat load on the target plates;
- the control of plasma density;
- the exhaust capability;
- a realistic model of particle transport.

Principal concepts of active impurity control

Since the sputtering of impurities at the target plates cannot be suppressed, such impurities must be retained close to the target plates for effective impurity control. This may be achieved by friction with a strong plasma flow directed along the divertor channel plasma (DCP) towards the target plates [8]. The plasma flow will be generated by a combination of gas puffing, the injection of low speed pellets and the recirculation of some of the flow at the target plates towards the X-point. The connection length along the magnetic field line between the X-point and the target plates must be sufficiently long to allow effective screening of impurities.

Hypervapotron elements will be used for the high heat flux components of the target plates, and these are expected to accommodate power fluxes up to 15MWm^{-2} at the copper-beryllium interface. Of course, rapid sweeping (4Hz) of the target plates to limit the localised heat load, to limit erosion and to affect redeposition will be important. Methods of ensuring that a substantial fraction of input power can be radiated in a controlled way in the DCP will be key features.

In the vicinity of the target plates, a pumping chamber (with a cryo-pump) is introduced to control the main plasma density by exhausting and pumping a relatively large fraction ~10% of the plasma flow created by fuelling. The fuelling and exhaust capability of a Next Step will be dependent on whether deuterium and impurities (including helium ash) accumulate in the plasma centre. The production and transport of helium ash towards the plasma edge (where it must be exhausted) will depend on the relative importance of energy and particle confinement (D/χ ratios), the effect of sawteeth and the effect of an edge transport barrier forming in the H-mode. To assess fully these issues requires detailed modelling of particle transport and while this forms already an important part of present JET studies, a substantial experimental and modelling effort is envisaged for the New Phase.

Modelling Impurity Control

The plasma behaviour in the scrape-off-layer (SOL) and divertor channel plasma (DCP) can be understood qualitatively by considering the basic steady state equations for the particle flux, F, and the total plasma pressure, p, along the magnetic field line direction, x. Fig.10 shows isothermals and isoflows in the pressure (p) versus impurity density (n_z) plane. These curves intersect at two points, above and below a pressure $p_0/2$, corresponding to subsonic and supersonic flows, respectively. For a given plasma temperature, the maximum isoflow compatible with the steady state momentum equation is tangent to the isothermal at $p_0/2$.

Impurity retention in the divertor is determined from the steady state momentum equation for impurity ions, which for the simplest, realistic case gives the impurity density, n_z, decaying exponentially with distance from the target on a scale length, λ_z, given by

$$\lambda_z^{-1} = \lambda_F^{-1} - \lambda_e^{-1}, \qquad \text{with} \quad \lambda_F^{-1} = \frac{m_z v_z}{T\tau_z} \quad \text{and} \quad \lambda_e^{-1} = \alpha_z \frac{1}{T}\frac{dT}{dx}$$

The temperature gradient scale length is given by the heat transport equation with electron heat conductivity parallel to the magnetic field ($\kappa=\kappa_0 T^{5/2}$) being dominant and is primarily dependent on the input power. To ensure impurity control, the frictional force must exceed the sum of the pressure and thermal forces, that is, $\lambda_F^{-1} > \lambda_e^{-1}$.

A high density, low temperature plasma in front of the target plates increases the friction between the hydrogen and impurity flows and facilitates impurity control [8]. Furthermore,

such a plasma limits the surface erosion and thereby increases the lifetime of the target plates. However, such operation will lead to high densities at the separatrix and this will be unfavourable for non-inductive current drive using neutral beams or lower hybrid waves.

To solve the full set of classical fluid equations for the conservation of particles, momentum and energy in the SOL and DCP, a numerical 1-1/2 D transport model has been developed. Monte Carlo methods are used for neutral particles in the flux surface geometry of the planned pumped divertor configuration. The model shows that impurities can be retained near the target plates for plasma flows, typically ~$10^{23}s^{-1}$. The steady state distribution of beryllium impurities, for conditions with and without flow, are shown in Fig.11.

The Pumped Divertor Configuration

The aims of the New Phase can be realised with the internal multi-coil configuration shown in Fig.12. The design allows a large plasma volume at 6MA and the operational flexibility to modify the magnetic configuration in the vicinity of the X-point independent of the plasma current and separately on the high and low field sides. In contrast to the normal configuration for a divertor, all divertor coils carry current flowing in the same direction as the plasma current. With this configuration, single null X-point operation is possible for performance and impurity control studies, including plasmas with 6MA for 10s, a volume ~$93m^3$ and a connection length from the X-point to the target plates of 3m and with 5MA for 10s, a volume ~$80m^3$ and a connection length ~10m. In addition, it should be possible to run 3MA double null X-point plasmas for up to 20s at 3.4T and for up to 1 minute at 2.1T.

4. REQUIREMENTS FOR A DEMONSTRATION FUSION REACTOR

Fusion Research Programmes are directed ultimately to the construction of a Demonstration Fusion Reactor - DEMO. From physics considerations and present technology constraints, the size and performance of a thermonuclear reactor can be largely defined. The minor radius of the plasma needs to be twice as large as the tritium breeding blanket thickness, so it must be ~3m and the elongation can be as large as 2. Therefore, there is no need to operate at a toroidal field greater than 5T, in order to fulfil the plasma physics requirements. A practical aspect ratio of 2.5 sets the plasma major radius to 8m. Safe operation can be assumed for a cylindrical safety factor 1.6-1.8. This defines a reactor with a plasma current of ~30MA. Such a DEMO would produce power in the range 3-6GW thermal or 1-2GW electrical power.

The construction of a DEMO must be preceded by an extensive test of the concepts and technologies needed for incorporation into a DEMO design. In particular, tests and developments of plasma facing components and first-wall materials with a high resilience to 14MeV neutron radiation at a power flux of 2-3MWm^{-2} must be carried out in parallel with tests and developments of divertor target materials with high power handling capability and low erosion (eg. low Z materials, beryllium, carbon and carbide fibres, silicon carbide). The concept of a D-T fuelling system with a high speed pellet injector (v≥10km/s) would need to be demonstrated. In the areas of helium ash exhaust, pumping and the divertor configuration, besides the forthcoming tests in the New Phase of JET, progress is still needed to prove the viability of present or emerging concepts. Tritium breeding blankets are required to operate at high temperatures and have not yet been tested. Furthermore, in the area of superconducting technologies, viable high critical temperature superconducting materials are desirable for sufficient safety margins and these need thorough testing. Finally, a credible physics concept still needs to emerge for current drive, to sustain continuous plasma operation. However, this last requirement may prove to be unnecessary when semi-continuous operation (~2 hours) has been demonstrated, which maybe sufficient for a commercial reactor.

In view of the time needed to develop and incorporate emerging technologies required for a DEMO, a precisely defined or optimised engineering design cannot yet be proposed. A reasonably broad strategy would be to develop, partly in parallel, the main components of a fusion reactor. More than one DEMO seems desirable (as in the early development of fission). The Next Step needs to address all the physics and technological issues of a DEMO device.

5. THE NEXT STEP

The Next Step will provide the bridge from present devices to the position from which DEMO could be designed and constructed. As such, the aim of the Next Step is to demonstrate the scientific feasibility of ignition under conditions required for a DEMO device: that is, high power long pulse operation in fully ignited plasmas ($Q_{DT} = \infty$). It is also necessary to test hot blanket modules and the resistance of highly sensitive materials (eg insulators, first-wall) to high neutron fluences. Furthermore, semi-continuous or continuous operation and the viability of a fully superconducting tokamak must be demonstrated.

The variety of issues that the Next Step must address are expected to mature on different timescales. A single facility whose objectives cover all issues will have an unacceptable risk of failure unless a large safety margin is allowed on each component. In addition, it would not allow cross comparison of results nor permit continuity of data flow. To incorporate all innovations that are likely to reach maturity throughout the lifetime of a single facility requires a design which lacks the precise definition offered by well targeted objectives. There would also be an impact on the starting and construction times and on the consequential costs. A large degree of complexity would be introduced and this would place a practical limit on intended flexibility. A reactor strategy which would minimise risks and costs would be to address the different Next Step issues in several complementary facilities, each with separate objectives. This strategy requires a clearly defined Next Step Programme rather than a single device.

In such an optimised Next Step Programme, the three main issues of long burn ignition, superconducting coil technology and material testing are separated and addressed in three different facilities (P1, P2, P3) which are constructed on a timescale commensurate with the maturities of the technologies. The engineering design for each facility can be defined precisely, thereby allowing a high degree of confidence that objectives would be met.

The main details of such machines are the following:

- The primary objectives of P1 would be:
  - to demonstrate sustained high power operation of a fusion reactor core of 2-3GW thermal power produced for up to 12hrs per day for periods up to 6 days at a time;
  - to provide a testbed for the study and validation of tritium breeding blanket modules in full reactor conditions;
  - to achieve a cost/unit thermal output relevant to the establishment of fusion as a potential economic energy source (1ECU/thermal Watt).

  The design philosophy of P1 would be:
  - to make full use of the scientific and technical experience gained from JET and the rest of the tokamak programme;
  - to minimise the need for developments by using established techniques;
  - to reduce complexity and increase reliability at reasonable cost;
  - to provide a high safety margin in achieving design specifications for the magnetic field and plasma current.

  As a consequence, conventional coil technology could be used and this would allow an early start in 1994 once the results on impurity control become available from the New Phase of JET. These objectives could be achieved in a tokamak with 30MA, 4-5T, major radius 8m, minor radius 3m, and elongation of 2. Impurities would be controlled actively by high density operation and a pumped divertor. The approach to ignition would utilise ICRF heating with H-mode confinement and in the monster sawtooth regime, while long pulse ignition (> 30 mins) would be sustained with L-mode confinement at high power and also with high frequency low amplitude sawteeth. With sustained ignition conditions, blanket modules would be tested under neutron fluxes of up to 2MWm^{-2}.
- The primary objectives of P2 would be:
  - to demonstrate the viability of high power operation of a large tokamak with superconducting magnets;
  - to assess continuous operation at high density with current drive;
  - to assess profile control;
  - to assess advanced divertor concepts.

  The design philosophy would be to test, at a reasonable cost, superconducting and non-inductive current drive technologies in a low activation environment, so that flexibility could be built-in to incorporate innovations for concept development throughout the lifetime of the device. Some technological developments are still required and therefore, construction could start somewhat after P1, perhaps in 1998. The P2 objectives could be realised with a large tokamak operating at high power typically 10-12MA, 6-7T, minor radius 1.5m, major radius 5m, and elongation of 2. To control the density and impurities, an advanced exhaust and divertor concept would be used. To minimise activation, the tokamak would not operate in tritium and therefore would not ignite.
- The objective of P3 would be to test materials under very large neutron fluences. This could be realised in a test bed operating continuously and providing high fluxes of neutrons (2-10 MWm^{-2}) over surfaces of 0.04-0.05m^2. Its construction could start early in 1998, so that results should be available for the design of a DEMO in 2005.

A schedule for the design construction, and operation of Next Step and DEMO devices is shown in Table II. The overall cost for such a minimum Next Step Programme is estimated at 7bnECU, not including operation costs. This is similar to the cost of a single ITER device. However, for this cost, a single device would not cover all the issues of the Programme. Furthermore, the programme offers flexibility in location of the different facilities and in their starting dates.

6. CONCLUSIONS

- JET has successfully achieved or surpassed its original design aims and in doing so has produced and contained plasmas of thermonuclear grade.
- **Individually,** each of the parameters n, τ_E and T_i required for a fusion reactor have been achieved; **simultaneously,** the fusion product of these parameters is within a factor 8 of that required in a fusion reactor.
- However, these extremely good results were obtained only **transiently,** and were limited by impurity influxes due to local overheating of protection tiles.
- A New Phase is planned for JET, prior to the introduction of tritium, to demonstrate effective methods of impurity control in operating conditions close to those of a Next Step tokamak, with a stationary plasma of 'thermonuclear grade' in an axisymmetric pumped divertor configuration.
- Based on present progress, there is confidence that sufficient knowledge exists to begin the construction of the "core" of a fusion reactor within the next 3-4 years.
- However, a **single** Next Step facility (ITER) is a high risk strategy in terms of physics, technology and management, since **it does not provide a sufficiently wide base for a demonstration reactor.**
- A Next Step **Programme** comprising several facilities:
  - would make more effective use of resources;
  - is well within the capability of world research;
  - would provide a wider and more comprehensive data base; and
  - could even be accomplished without a significant increase in existing funding.
- With concerted effort and determined international collaboration, such a programme would provide sufficient results to allow the design of a DEMO to start in about 2005.

7. REFERENCES

[1] The JET Project - Design Proposal: EUR-JET-R5

[2] Rebut, P-H, et al, Fusion Technology, **11**, (1987), 13-281

[3] Rebut, P-H, et al, JET Contributions to the Workshop on the New Phase for JET: The Pumped Divertor Proposal (September, 1989), JET Report - JET R(89)16

[4] Rebut, P-H, Lallia, P, Watkins, ML, Proc. of the 12th Int. Conf. on Plasma Physics and Contr. Fusion Research (Nice, France, 1988), Nuclear Fusion Supplement (1989) Vol.2 p.191

[5] Wagner, F, et al, Phys. Rev. Lett. **49**, (1982), 1408

[6] Troyon, F, Gruber, R, et al, Plasma Phys. Controlled Fusion, 26, (1984), 209

[7] Summers, D.D.R., et al, J. Nucl. Mater., to be published (1990)

[8] Neuhauser, J, et al, J. Nucl. Mat., **121**, (1984), 194

8. ACKNOWLEDGEMENTS

The author is indebted to Drs DG Gambier, BE Keen and ML Watkins for assistance in preparation of the paper. In addition he is grateful to the JET Team, without whom the results in this paper would not be available.

Table I
JET Parameters

Parameters	Design Values	Achieved values
Plasma Major Radius (R_o)	2.96m	2.5-3.4m
Plasma Minor Radius horizontal (a)	1.25m	0.8-1.2m
Plasma Minor Radius vertical (b)	2.1m	0.8-2.1m
Toroidal Field at R_o	3.45T	3.45T
Plasma Current:		
Limiter mode	4.8MA	7.1MA
Single null X-point	not foreseen	5.1MA
Double null X-point	not foreseen	4.5MA
Neutral Beam Power		
(80kV, D)	20MW	21MW
(140kV, D)	15MW	8MW (only one box converted)
Ion Cyclotron Resonance Heating Power to Plasma	15MW	18MW

Table II: A Time Schedule for an ITER Programme

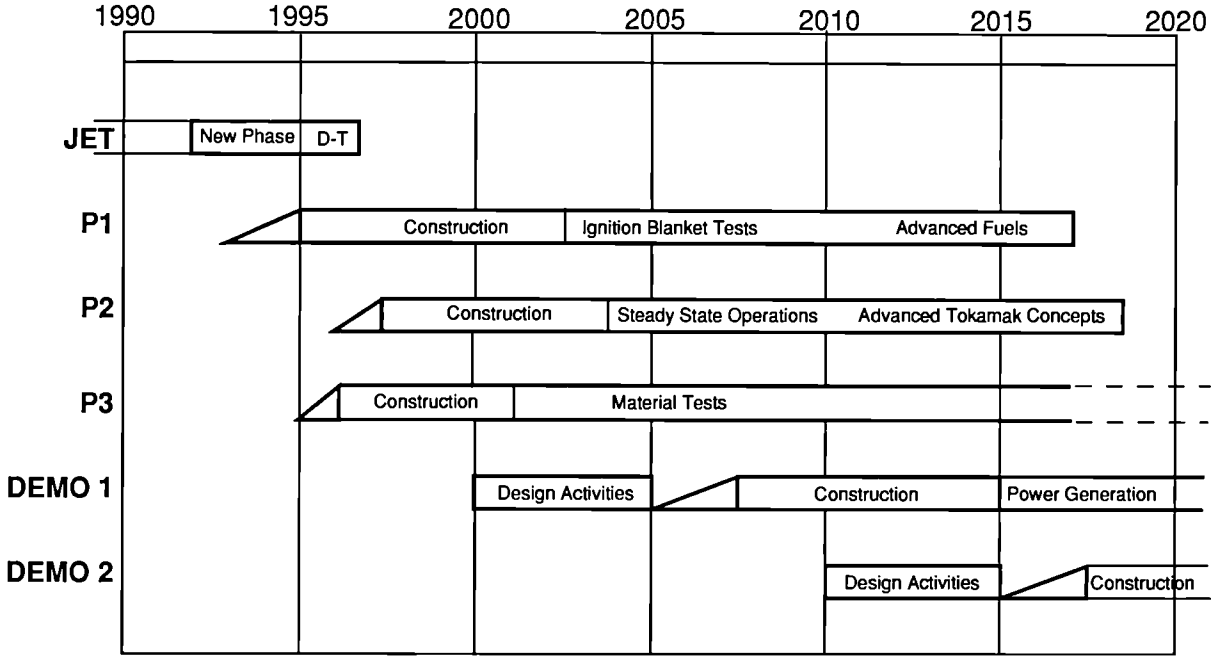

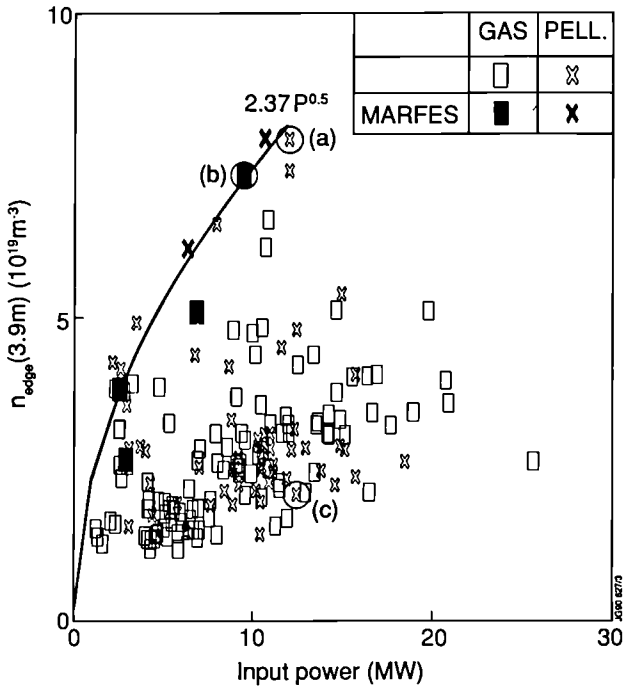

Fig 1 The edge electron density (n_{edge}) versus input power (P) showing that the density limit occurs at the boundary of the operational domain close to the curve n_{edge} ($\times 10^{19}$m^{-3}) = 2.37 $P^{1/2}$(MW). The profiles shown in Fig. 2 correspond to the three data points circled.

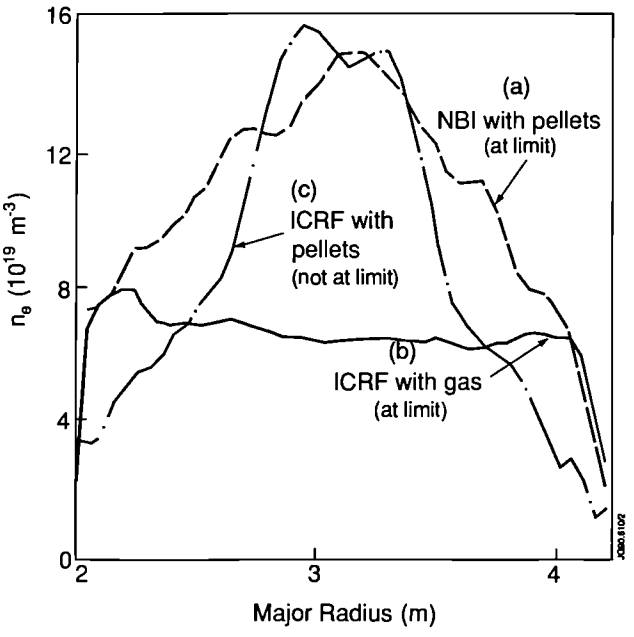

Fig 2 Electron density profiles for different fuelling and heating methods.

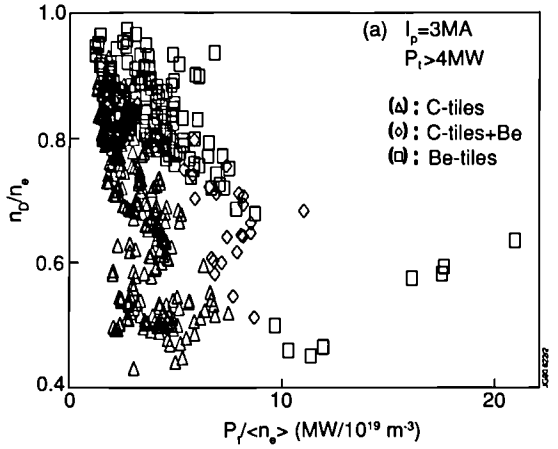

Fig 3 Fuel concentration, n_D/n_e, as a function of power per particle ($P_i/<n_e>$) for carbon limiter tiles, beryllium gettering and beryllium limiter tiles.

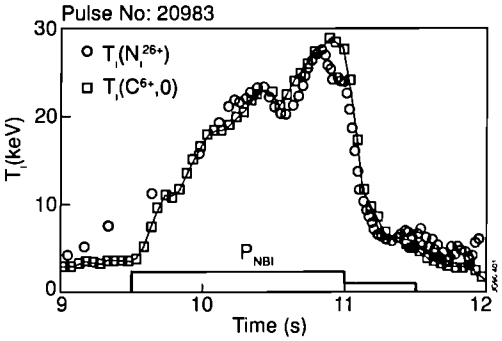

Fig 4 Ion temperature as a function of time during NB heating showing that temperatures of ~30 keV are reached.

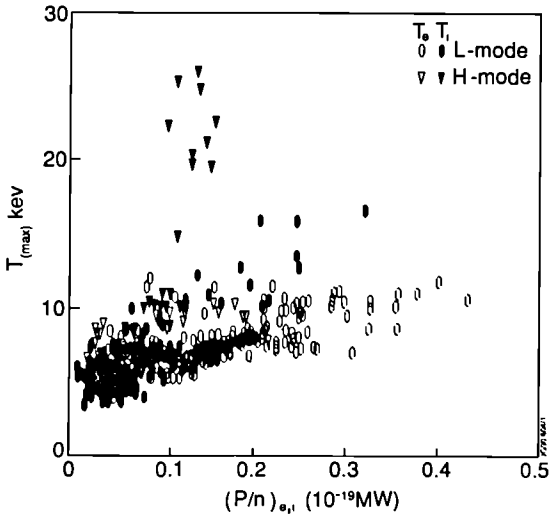

Fig 5 Central ion (T_i) and electron (T_e) temperatures as functions of power per particle $(P/n)_{e,i}$ to either species.

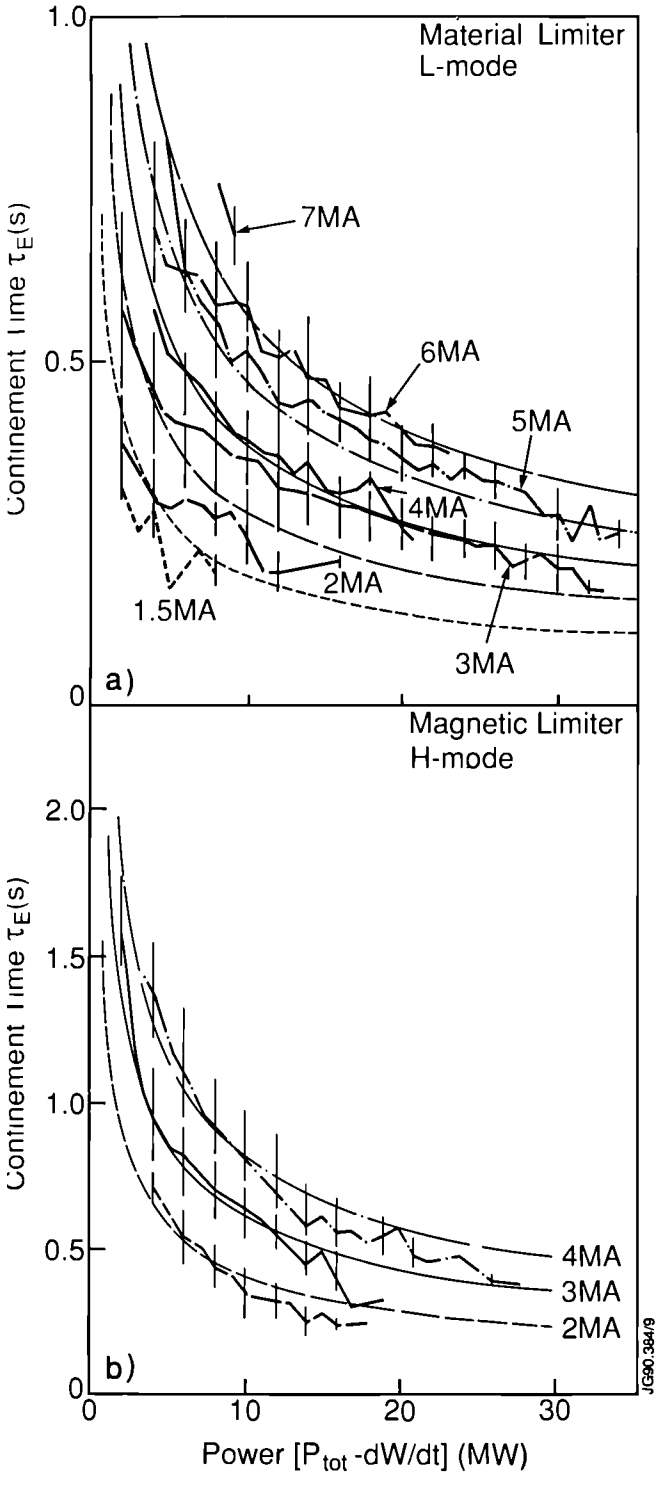

Fig 6 Global energy confinement time (τ_E) as a function of input power for (a) material limiters (L-mode) and (b) magnetic limiters (H-mode).

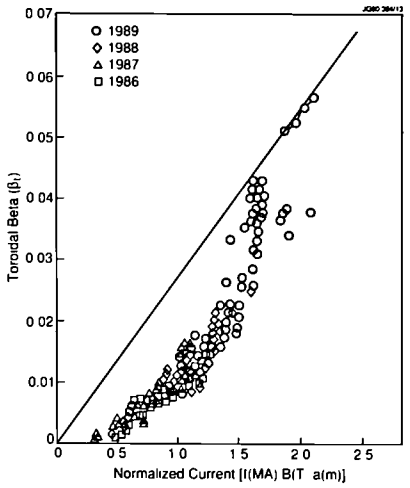

Fig 7 The maximum toroidal beta ($\beta_t=2\mu_0<p>/B_t^2$) as a function of normalized current $I_p(MA)/B_t(T)a(m)$.

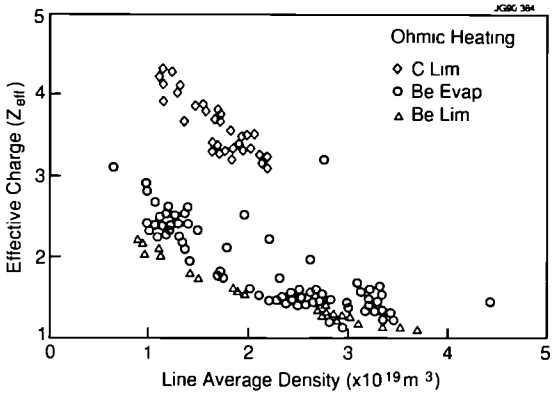

Fig 8 The effective ionic charge, Z_{eff}, as a function of line average density $<n_e>$.

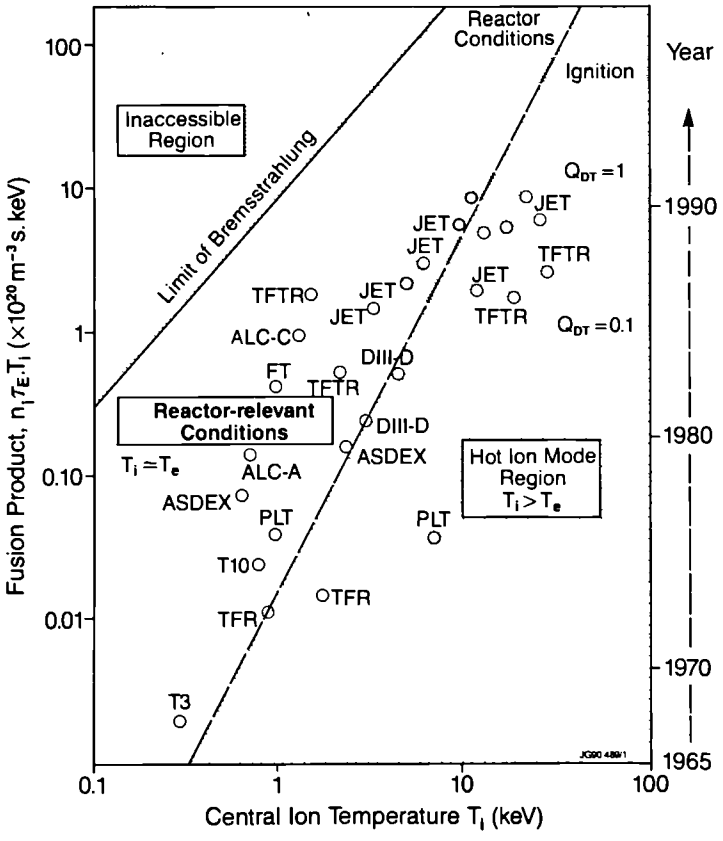

Fig 9 Overall performance of the fusion product ($n_D\tau_E T_i$) as a function of ion temperature (T_i), for a number of tokamaks.

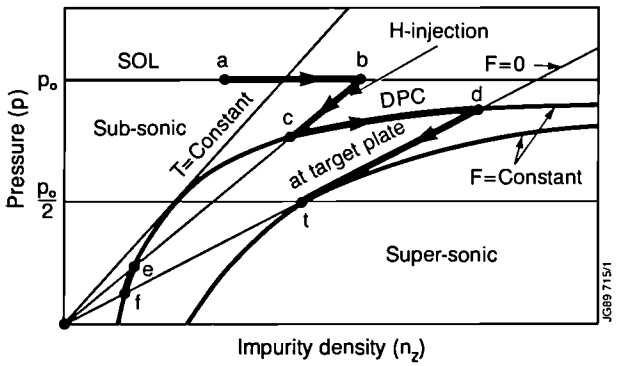

Fig 10 Diagram of pressure (p) versus impurity density (n_z) showing the qualitative behaviour of plasma parameters:

- in the SOL (section a-b where the flow F=0)
- at the X-point (section b-c)
- in the DCP (section c-d where F = constant)
- in front of the target plates (section d-t where the flow becomes transonic)

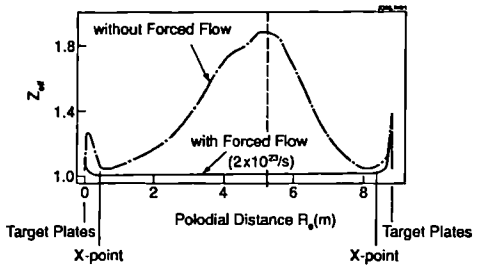

Fig 11 Poloidal distribution in the SOL and DCP between target plates of the effective ionic charge, Z_{eff}, for cases with and without flow

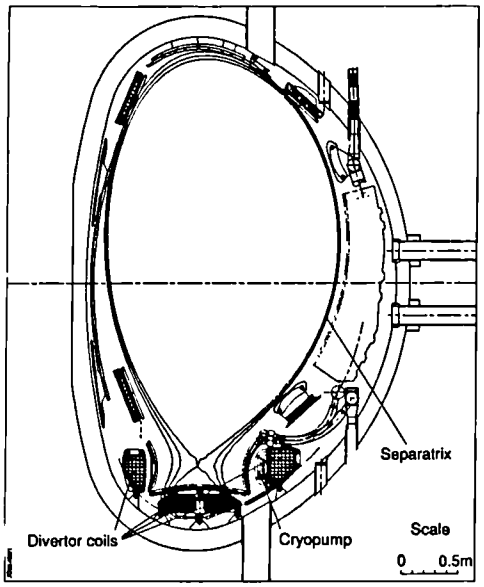

Fig 12 Poloidal cross-section of JET showing the plasma and main elements of the proposed pumped divertor.

Technical Aspects of Impurity Control at JET: Status and Future Plans

The JET Team
(presented by M.Huguet)

Invited Paper presented to
9th Topical Meeting on Technology of Fusion Energy
Oak Brook, USA., October 1990

TECHNICAL ASPECTS OF IMPURITY CONTROL AT JET: STATUS AND FUTURE PLANS

M. Huguet and the JET Team
Joint European Torus - JET
Abingdon, Oxon OX14 3EA, England

ABSTRACT

The salient feature of 1989-1990 operation at JET has been the use of beryllium as a first wall material. Technical and safety aspects of JET operation with beryllium are described.

The use of beryllium has substantially improved the plasma purity and as a consequence a record fusion product ($n_D T_i \tau_E$) of 9 x 10^{20} m^{-3}.keV.s has been achieved. Impurity influxes however prevent the achievement of higher plasma parameters and reaching steady state conditions.

A new divertor configuration has been proposed for JET with a view to study impurity control, fuelling and exhaust, in conditions relevant for the next generation of machines. The latest design features a multi-coil configuration which gives substantive operational flexibility. A technical description of the major components of the divertor including the internal coils, the target plates the pumping and fuelling systems is given.

I INTRODUCTION

The Joint European Torus (JET) is the central and largest project of the fusion programme of the European Community. This programme is coordinated by the European Atomic Energy Community (EURATOM).

The JET objective as defined in 1973 is to obtain and study a plasma in conditions and with dimensions approaching those required in a thermo-nuclear reactor [1]. This objective implies that deuterium-tritium (D-T) mixtures will be used in JET to study the production and confinement of alpha particles generated by fusion reactions and the consequent heating of the plasma by those alpha-particles. Technical aspects of and progress towards D-T operation at JET have already been reported [2, 3, 4].

A major area of research which has been identified since the beginning of the project is the study of plasma-wall interactions, the control of the plasma purity and the related requirements for plasma fuelling and exhaust.

Since the start of JET operation in 1983, a large and continuous effort has been made to minimise the detrimental effect of plasma impurities. Initially, the first wall facing the hot plasma was metallic (inconel). From 1984 to 1988, carbon was used as a first wall material. Graphite tiles were used to clad the walls and glow discharge techniques allowed to transform the remaining metallic surfaces into metal carbides or to coat them with hydrogenated carbon films. Graphite tiles were also used for limiters and X-point target plates[5].

Operation with a carbon first wall has been successful. The plasma current was raised to the record value of 7 MA. At lower plasma current (3 MA), quasi steady state conditions were achieved with T_i and T_e above 5 keV for 20 seconds. The plasma heating systems also performed up to their design specifications and were able to provide 35 MW of power to the plasma in combined operation. Physics results established JET at the forefront of fusion research and a fusion parameter ($n_D T_i \tau_E$) of 2.5 x 10^{20} m^{-3}.keV.s was achieved in H-mode operation[6].

With an all carbon first wall, the attainment of higher plasma parameters is however limited by impurities, mostly carbon and oxygen, coming from the walls. This effect can be characterised by the dilution factor n_D/n_e (n_D : deuterium density; n_e : electron density) which cannot be maintained much above 0.6 even with moderate heating power in the range of 5 to 10 MW. Carbon impurities from the graphite tiles simultaneously dilute the plasma, increase the radiated power and decrease neutral beam penetration.

Although plasma dilution is observed during long pulses at low plasma input power, the carbon influx is very strong at higher power when the surface temperature of the carbon tiles reaches temperatures of 1200-1300°C. In the latter case the carbon influx is thought to be due essentially to radiation enhanced sublimation and self sputtering. Self sputtering can increase the carbon influx in an avalanche like process when the self sputtering coefficient increases with temperature and reaches a critical value[7]. At JET this effect called the "carbon catastrophe" results in a sharp decay of all plasma parameters and a fall of fusion performance measured by the neutron yield from deuterium-deuterium (D-D) reactions.

For these reasons, beryllium was proposed as a first wall material as it was expected that it could provide superior performance because of its lower atomic number and its gettering properties for oxygen. A full comparison between carbon and beryllium as first wall materials and the rationale in favour of beryllium has been given in[8]. Also preparatory experiments conducted in the ISX.B[9] and UNITOR[10] tokamaks indicated that beryllium was a viable limiter material. Beryllium was first introduced into JET in 1989 and has been used with great success during the 1989 and 1990 experimental campaigns.

II STATUS OF FIRST WALL DURING THE 1989-1990 EXPERIMENTAL CAMPAIGN

Inboard Wall

The vessel configuration is shown on figure 1. The inboard wall is covered with graphite protection tiles. In the vicinity of the equatorial plane where the heat load is highest during normal operation and plasma disruptions, the tiles are fibre reinforced graphite and have a very much higher resistance to thermal shock than normal fine grain graphite tiles. The tiles have been aligned and can act as an inner bumper limiter with a power handling capability of 400 MJ. It should be remarked however that useful plasma discharges with an acceptable plasma dilution can only be sustained at much lower energy levels. Observations of the tiles showed that even though most tiles remained at temperatures below 600°C, some were heated sometimes up to 3000°C. Carbon sublimation often leads to plasma disruptions. Plasma energy inputs of about 20 MJ were able to produce this effect.

Figure 1 shows a discontinuity in the wall protection above and below the equatorial plane. This is due to the fact that internal saddle coils for the stabilisation of plasma disruptions have not been installed yet[5]. Installation of these coils is planned for 1992.

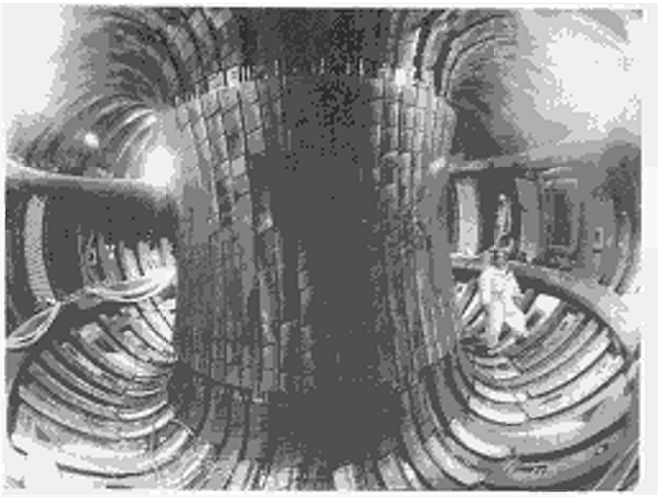

Figure 1: Present status of the JET vessel

X-point tiles

When the machine is operated in the X-point configuration, wall protections are also required where the magnetic separatrix intersects the vessel wall. It should be noted that JET can operate in a single-null configuration with the X-point at top or bottom, and also in a double-null configuration. The wall protections near the top X-point are fibre reinforced graphite tiles which have been carefully shaped and aligned to minimise local hot spots on the tiles. In particular the leading edge of each tile is shadowed by the adjacent tile. In addition, sweeping of the X-point position has been carried out in order to increase the effective strike area and reduce the surface temperature of the tiles. Sweeping in the radial direction (frequency $\simeq$1Hz, amplitude $\simeq$ 5 cm) was clearly effective at delaying the onset of carbon influx into the plasma. In the double-null configuration, vertical sweeping produced the same effect by alternatively loading the top and bottom tiles. A further improvement was achieved by injecting gas in the X-point region. This delayed the carbon influx and allowed the substainment of 5.3 seconds long H-mode discharges. With these precautions it has been possible to achieve an energy deposition of 30-40 MJ per pulse on these tiles before the onset of the "carbon catastrophe".

The wall protections near the bottom X-point consisted also of graphite tiles during the 1989 campaign. In 1990, these tiles have been replaced by beryllium tiles. The beryllium tiles which have been used for this purpose were designed to be protection tiles for the Ion Cyclotron Resonance Heating (ICRH) antennae and are therefore not an optimum design for an X-point target plate. Because of the curvature of the tile profiles and shadowing effects, the useful total strike length in the toroidal direction is only about 1.6m, whereas the toroidal circumference is 17m.

The decision to use these tiles as X-point protections was taken in order to gain experience with beryllium target plates prior to the installation of much larger and specially designed beryllium target plates by the end of 1990 (see section V). The beryllium X-point protection tiles can be seen in figure 1. There are a total of 32 radial rows of tiles distributed uniformly along the torus. There is so far only limited operational experience with these tiles. Some surface melting has been observed with an energy deposition of about 20 MJ per pulse. This surface melting produces surface irregularities but did not seem to affect operation. Melting was observed only at the outboard (low field) side of the X-point indicating a strong assymetry in power flow between the inboard and outboard sides. At these energy levels a beryllium influx was observed within a few hundred milliseconds after the start of X-point operation.

Limiter

When the machine is operated in the limiter configuration, the plasma is leaning against the belt limiter[11]. The belt limiter consists of two toroidal rings above and below the equatorial plane of the machine, at the outboard wall. It is designed so that the tiles are radiatively cooled by a radiator structure which can be water cooled. The tiles can be easily exchanged. In 1989 and 1990, beryllium tiles have been used rather than graphite tiles. The beryllium employed is S-65B (Brush Wellman) cold pressed and sintered. The front face of the beryllium tiles is castellated in order to avoid the deep propagation of surface cracks. Experiments carried out at Sandia Laboratory USA, have shown that thermally induced surface cracks do not propagate when castellations are provided.

Although the belt limiter was designed with a power handling capability of 40 MW during 10 seconds, its use has been limited by plasma behaviour[12]. The design value of the peak heat flux was about 5MW/m^2 but the actual peak heat flux in operation has reached much higher local values due to uneven loading between the top and bottom belts, scrape off thicknesses smaller than expected and edge loading of the tiles.

Beryllium influxes from localised hot spots at the limiter surface terminate low density high performance pulses. The reason for these hot spots is not clear even after a careful examination of the tiles during the 1989-1990 shutdown. The misalignments between adjacent tiles can be of about 0.3mm and this could perhaps explain hot spots at the exposed leading edge of some tiles. Local melting at the leading edge can produce irregularities or droplets on the tile surface, thus increasing the flux deposition and the damage can propagate from the edge across the tile surface. This scenario is supported by observation of melting at tile edges and at the tessalation cuts. About 10-15% of the tiles showed evidence of edge heating. Surface melting which did not seem to originate from the edge was also seen and was often associated with surface cracks. Surface cracks can only be initiated by large heat loads and it has been suggested they could be the result of disruptions. About 5% of the plasma facing area showed this kind of damage.

Melting of beryllium tiles was only superficial and did not affect the tile integrity or operation although surface unevenness of about ±1 mm was observed in some areas. Tile melting was not distributed uniformly along the toroidal direction, instead there was a clear correlation with the ripple of the toroidal field: most melt marks were found between toroidal field coils. This observation demonstrates that an accurate alignment of tiles is essential. The radial variation of plasma position due to field ripple is only 1.5 mm at the face of the limiter.

The energy deposition on the belt limiter has generally been kept well below the design value of 400 MJ. With a careful selection of the plasma shape so as to maximise the plasma foot print on the limiter, it has been possible to apply 90 MJ of heating energy with an acceptable beryllium contamination Moreover, at high plasma densities and by tailoring the gas feed during the discharge, it has been possible to feed into the plasma 30 MW of power for 6 seconds while keeping Z_{eff} at about 1.5 (dilution 0.83). This should be compared with the graphite limiter were a maximum of 50 MJ could be applied without carbon catastrophe but with a plasma dilution of about 0.5.

Evaporators

The evaporators are essential elements of beryllium operation[13]. Each evaporator consists of a bell shaped beryllium head (3kg) which is internally heated by a graphite resistor. During plasma operation the head is retracted inside a port but for evaporation it is pushed inside the vessel and heated up to a temperature close to 1200°C.

Initial operation of the evaporator was satisfactory but there was a sharp decrease in the evaporation rate only a few hours after the start of operation. This was attributed to a beryllium and beryllium oxide dust layer which was found on the head. The dust may be due to oxidation by residual gases in the vacuum vessel. Also the impurities present in the sintered material tend to accumulate on the surface when beryllium evaporates. The dust layer acts as a cold shroud which prevents evaporation. More recently, beryllium heads made of cast material (rather

than sintered), which is purer, have been used. There is still a small reduction of the evaporation rate after a few hours but much less than with sintered material. The beryllium heads have now all been replaced with cast material.

There are four beryllium evaporators equally spaced along the torus. The beryllium coat on the vessel walls and graphite tiles is of course not uniform but an average thickness of 20nm is achieved in one hour of evaporation. By the end of 1989 the average coverage of the vessel was about 0.8μm.

The beryllium coat on the graphite X-point tiles erodes within 1 to 5 discharges and then an equilibrium tends to establish between erosion and redeposition. The impurity reduction in the plasma remains however unchanged over tens of discharges. Evaporation sessions, typically 2 to 5 hours long have been carried out routinely, once or twice a week in 1989 and 1990.

Beryllium evaporation has also been found to be an extremely efficient and quick method to recondition the vessel for plasma operation after a vessel opening. The residual gas analyser shows a dramatic reduction of gazous contaminants in the vessel after a beryllium evaporation.

III TECHNICAL AND SAFETY ASPECTS OF BERYLLIUM HANDLING

Since the introduction of beryllium in the JET vessel in July 1989, there have been several interventions requiring personnel access inside the beryllium contaminated vessel, and one major shutdown during which one eighth (octant) of the machine was dismantled for the replacement of a faulty toroidal field coil[14]. This shutdown involved work in two shifts during 6 months and a total of 8,000 man-hours have been spent inside the vessel. There has been so far no safety incident involving beryllium on the JET site.

There is considerable experience available at JET on how to tackle work inside the contaminated vessel, and how to handle contaminated components, tools and protective clothing outside the vessel. It should be noted that the techniques developed for beryllium handling may also become useful in the future to protect workers against, and avoid the spread of contamination by activated dust from the vessel.

The central piece of equipment for work inside the vacuum vessel is the Torus Access Cabin (TAC) which includes all the facilities for the safe access of personnel inside the vacuum vessel[15]. The TAC can support 5 men working with full protective suits with an external air supply. Air locks are also provided for the transfer of small tools and components. During the 1989-1990 shutdown, the TAC operation has been generally satisfactory but many improvements were found necessary and implemented to the breathing air supply, ventilation plant and water wash system. Also extra cabins were docked onto the TAC to accommodate the flow of personnel, provide additional space for change facilities and additional storage space for components protection tiles taken out of the vacuum vessel.

Plasma operation produces significant quantities of fine beryllium dust which becomes easily airborne and would in the absence of respiratory protection be inhaled by workers inside the vacuum vessel. At the beginning of the October 1989 shutdown, the vessel was water washed to reduce the beryllium airborne and surface contamination. Following the wash, the airborne contamination was generally well below the statutory level ($2\mu g/m^3$) above which respiratory protection is mandatory. It was found, however, that sudden large rises in airborne contamination would occur when components inside the vessel were disturbed or dismantled. This was attributed to pockets of beryllium dust which may have escaped the water wash, or possibly dust which may have been collected by water during the wash and may have accumulated in certain areas. For this reason respiratory protection was worn at all times inside the vessel. Depending on potential contamination, full suits with external air supply or face masks with filters have been used. For grinding work, protective helmets with a powered filtered air supply have been worn. It was found that wearing suits did not affect the efficiency and speed of work of the personnel.

For work requiring an opening of the vacuum vessel but no access inside, bagging techniques have been developed to avoid the spread of any beryllium dust. A dedicated workshop with specialist equipment for welding PVC has been set up to manufacture tailor made isolators able to bag the components, mostly diagnostics, which have to be disconnected from vessel ports.

Large pieces of equipment cannot be introduced into the vacuum vessel through the TAC. Access is provided at another horizontal port, where the remote handling Articulated Boom is routinely used to introduce and accurately position heavy components inside the vessel[4]. The Articulated Boom is itself enclosed in an air tight PVC tent attached onto the vessel port. Components are transferred in and out of the tent through an air lock and a slight under pressure is maintained inside to ensure that contamination is well contained.

Beryllium related work on contaminated tools or components is carried out in a beryllium facility which has been erected inside the JET Assembly Hall. The facility has a working area of $72m^2$ and includes an access system, a component transfer air lock, a filtered ventilation plant and a waste water collection system.

Suits used for in-vessel work have to be decontaminated, cleaned and checked for damage before re-use. This work is done in a dedicated suit cleaning facility. During the shutdown 90 suits/week were used from a complement of 300 suits. After each working session the suits were double-bagged and transferred to the cleaning facility. Suits were cleaned with water and detergent inside and outside and then checked for residual beryllium contamination. Following an acceptable analysis result, the suits were then transferred to another area for repair and final inspection before re-use.

A beryllium analysis laboratory has been set up for the analysis of beryllium samples. Airborne contamination or surface contamination must be collected on filter paper which is then analysed by the Atomic Absorption Spectrometric Technique. During the shutdown, more than a hundred samples were analysed every day. The samples originated from in-vessel work where each man carries a personal air sampler, from fixed air monitors in various areas, from smear samples on protective suits after cleaning, and other smear samples required to clear decontaminated tools or components or entire work areas.

All solid and liquid beryllium contaminated wastes are carefully monitored and disposed of in accordance to strict procedures complying with regulations .

IV SUMMARY OF RESULTS ACHIEVED WITH A BERYLLIUM FIRST WALL

The chief effect of beryllium as a first wall material has been to reduce the plasma dilution. This effect is illustrated in Table 1 which gives the average impurity concentrations and dilution factor for various operating phases[16-17].

The gettering properties of beryllium removes oxygen from the plasma. The elimination of carbon sputtering by oxygen also results in a strong reduction of the carbon concentration.

Another beneficial effect of beryllium is that it pumps deuterium very strongly during the discharge. A recycling coefficient as low as 0.9 has been observed with the beryllium belt limiter, whereas values of 0.99 were obtained with an unconditioned graphite limiter. At the same time, beryllium retains after the discharge only a small proportion, about 10 to 20% (60% for graphite) of the deuterium injected in the vessel during the pulse.

Table 1. Average impurity concentrations (%) and dilution factor for the various operating phases

	C Phase	Be/C Phase	Be Phase	
			Limiter	X-point
Oxygen	1	0.05	0.05	0.05
Carbon	5	3	0.5	1.5
Beryllium	-	1	3	1
$n_d(o)/n_e(o)$	0.6	0.8	0.85	0.9

C phase = carbon first wall
Be/C phase = beryllium evaporation only
Be phase limiter = beryllium evaporation and solid beryllium tiles on the limiter
Be phase X-point = beryllium evaporation and graphite X-point tiles

It should be stressed that in contrast to beryllium, graphite behaves as a reservoir of hydrogenic atoms which are released by plasma contact. For this reason, graphite walls become an uncontrollable source of particles during the discharge. Graphite walls can only be depleted from the stored atoms by frequent and time consuming conditioning sessions with helium (glow discharge or tokamak discharges).

The properties of beryllium have a great impact on operation since density control is much easier, operation at low density becomes possible (hot-ion mode), and the wall is no longer deconditioned by disruptions.

From the improved plasma purity, an improvement of nearly all plasma parameters ensues. Details are given in[16-17] and the results can be summarised by the record values achieved in pulse No. 20981.

Table 2. Pulse No. 20981
(n_D, n_e and T_i are values at the plasma centre)
X-point double null configuration. H-mode
I_p = 4MA P_{NB} = 16 MW
$n_D = 3.7 \times 10^{19}\ m^{-3}$
T_i = 22 keV $n_D.T_i.\tau_E = 9 \times 10^{20} m^{-3}.keV.s$
τ_E = 1.1 sec
$n_D/n_e = 0.92$
D-D fusion power: $P_{D\text{-}D}$ = 40 kW
Computed equivalent D-T fusion power
P_{DT} = 13 MW* (for 0.1 second)
*Total power (thermal + beam/plasma) for injection of 140 kV D beams in a tritium plasma.

V THE PUMPED DIVERTOR: AN IMPURITY CONTROL CONCEPT RELEVANT FOR THE NEXT STEP

Although impressive, the results described in section IV were achieved in transient conditions. The high quality period of a plasma pulse lasts only for a second or less, and the D-D neutron count, which is a true measurement of fusion performance decays rapidly as impurities penetrate the plasma.

There is scope to improve the situation and lengthen the duration of the useful part of a pulse. X-point target plates carrying beryllium tiles will be installed in JET at the lower X-point position by the end of 1990. These dump plates have a much larger surface than the existing X-point tiles and will follow very closely the theoretical shape of the torus in both the toroidal and poloidal directions. Sweeping of the X-point position will also be performed as already explained in section II. This will result in a very substantial increase of the strike area and it is expected that useful X-point discharges will be sustained at higher power and for longer duration.

This approach may improve JET's performance but is however not relevant for the machines of the next generation which will operate for long pulses, a few 100 to a few 1000 seconds, and therefore require steady state conditions for the plasma.

It is also necessary to obtain more data on the operation of the divertor systems required by the next step devices. The problems of controlling the back-flow of impurities from the divertor target to the plasma, and of the target plate erosion have never been studied with plasma parameters and pulse durations which are of some relevance for next step machines.

Due to its size, plasma performance and long pulse capability, JET is in a unique position to carry out such studies.

The objectives of the new JET impurity control programme are "to demonstrate effective methods of impurity control in operating conditions close to those of the next step tokamak; that is a stationary plasma of thermonuclear grade in an axi-symmetric pumped divertor configuration".

VI TECHNICAL DESCRIPTION OF THE JET PUMPED DIVERTOR

Basic principles and main components

The key concepts of the pumped divertor have already been explained[7,18].

The impurities generated at the divertor target plates should be confined there by a flow of plasma particles directed towards the target plates. This confinement relies on friction forces between impurities and plasma particles, and to be effective requires a strong plasma flow which should be enhanced by recycling of neutrals from the target plates. The connection length along magnetic field lines and between the target plate and the X-point region should also be long enough, that is of the order of 3 to 10 metres[7].

A low temperature, high density target plasma should form in front of the target plate. This target plasma should:
a) Radiate some of the incident power and somewhat decrease the peak heat load on the target plates.
b) Screen the target plates from the plasma particles and reduce the impurity production.
c) Screen the plasma from the target plate impurities.

The main components of the pumped divertor are:
- The divertor coils which produce the required magnetic configuration.
- The target plates.
- The cryopump which will help in controlling the main plasma density.

The magnetic configuration

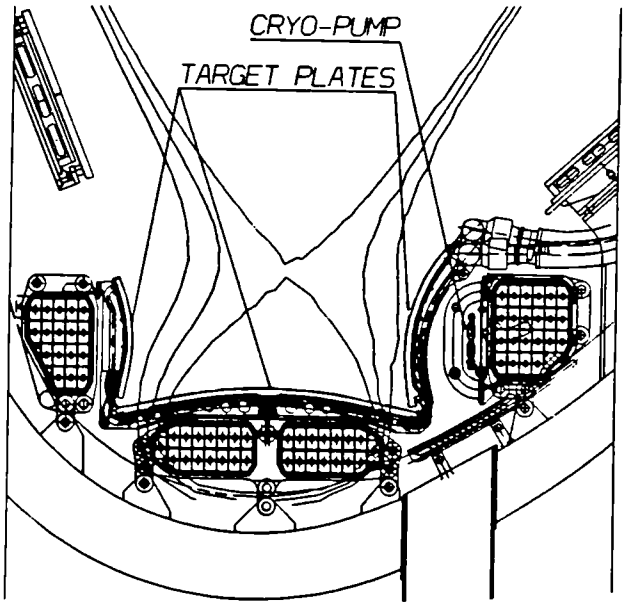

Figure 2: The JET pumped divertor components

The configuration features four divertor coils which allow many different configurations to be obtained (Figure 2)[19]. It should be noted that

all four coils carry currents in the same direction. The two bottom central coils produce the X-point and have been made as flat as possible to increase the volume available to the plasma. The two side coils allow a reduction of the poloidal field in the region between the X-point and the target plate, thus changing the pitch of the magnetic field lines and consequently increasing the connection length.

Since all four coils will have independent electrical supplies, a great flexibility can be achieved in the type of magnetic configuration. This is illustrated in Figures 3 and 4 and Table 3 which show two typical cases, the so called "fat" and "slim" plasma configurations.

Table 3: Parameters of X-point plasmas

Configuration	Fat	Slim
Plasma current (MA)	6	5
Plasma volume (m^3)	88	75
Connection length (m)	3.1	8.2
Safety factory q_{95}	2.2	2.4
Growth rate (s^{-1})*	270	800
Sum of divertor coil currents (MAt)	0.74	1.5

*Growth rate of plasma vertical instabilities in the absence of vertical position feed-back control.

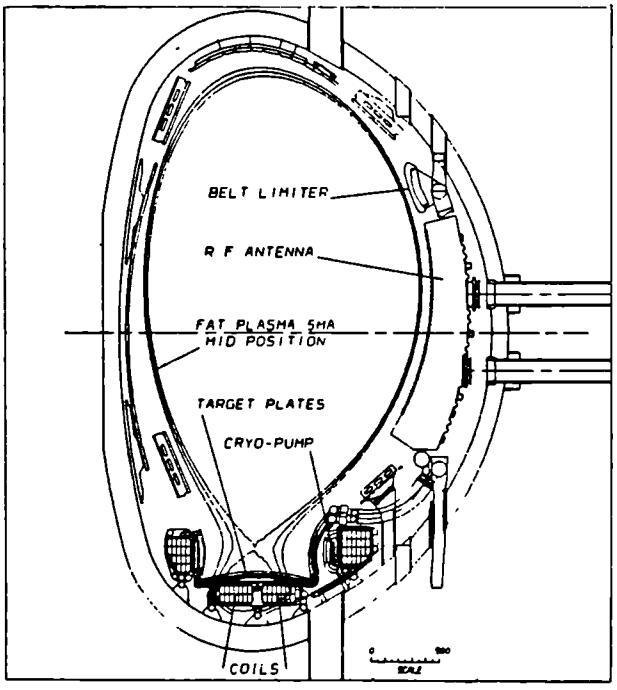

Figure 3: Fat plasma configuration at 5MA

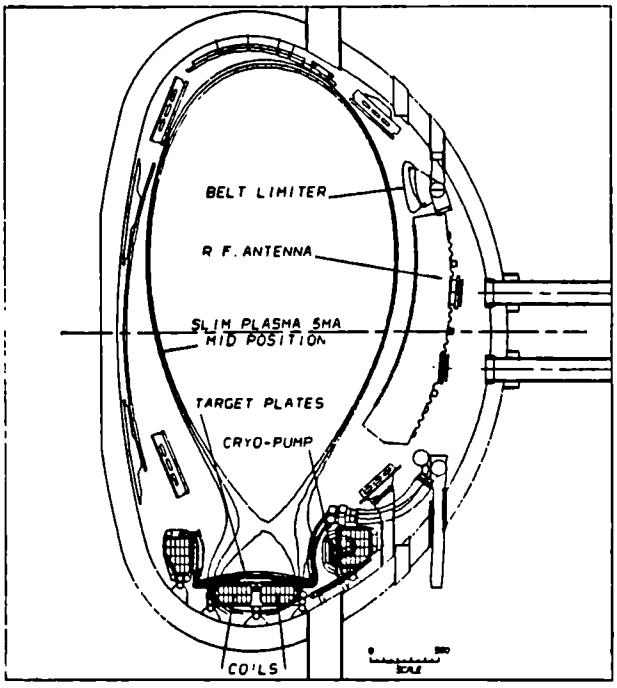

Figure 4: Slim plasma configuration at 5MA

The side coils also allow the connection length to be adjusted independently of the plasma current and separately on the inboard and outboard sides of the X-point.

Sweeping of the strike region on the target plates can be easily achieved by shifting radially the barycentre of the divertor coil currents. A total sweep amplitude of 20 cm is possible without significant changes of the connection lengths inboard or outboard.

Table 3 also shows the growth rate of vertical instabilities which is larger than the present values of 150 to 280 s^{-1}. The stabilisation of divertor plasmas requires a fast vertical position control system which is under development.

The divertor coils

The coils are conventional and use water cooled copper conductors with epoxy glass and kapton insulation. They are enclosed in thin vacuum tight inconel cases and will have to be cooled continuously when the vessel is at its operating temperature of 350°C. The coils will be assembled inside the vessel from preformed one-third turn segments. After assembly of the coil in the case and completion of the final welds on the case, vacuum impregnation with epoxy resin will take place.

The coils include 15 to 21 turns and carry typically 0.6 MA.t. The forces acting on the coils

can be large during vertical instabilities of the plasma when flux variations increase the coil currents. The vertical force can reach 400 tonnes on the outermost coil and the total net vertical force transmitted to the vessel is 900 tonnes. These forces are restrained by hinged supports which allow differential expansion between the vessel and the coils.

The target plates

The target plates are made up of three parts. The horizontal plates intersect the heat flux conducted along field lines while the vertical side plates receive the radiated power from the divertor target plasma. The horizontal and vertical plates are split into 384 segments grouped in 48 modules of 8 segments.

The target plates are designed for a total steady state conducted power of 40 MW which gives a maximum power flux density of 10-12 $MW.m^{-2}$ when sweeping of the X-point is taken into account[20]. The side plates may receive up to 5 $MW.m^{-2}$ in case the full power is radiated by the divertor plasma. These power density levels require the use of highly efficient heat sinks. Hypervapotrons have been used extensively for the JET Neutral Beam systems and can cope safely with steady state heat fluxes up to 15 $MW.m^{-2}$. Figure 2 shows the layout of the hypervapotrons and the cooling water pipework.

The surfaces facing the plasma will be clad with a 2 mm thick beryllium layer. The choice of beryllium is supported by the results achieved with a beryllium first wall in JET but is not ideal since beryllium impurities in the divertor plasma will only radiate a negligible fraction of the incident power. The choice of any other, higher Z, material would however entail the risk of impurities migrating back to the vacuum vessel and jeopardizing the benefits of a beryllium first wall.

The strength of the bond between the beryllium cladding and the copper-chromium of the hypervapotron is critical. Silver brazing at about 650°C is the preferred method of fabrication but the strength of the joint is strongly reduced when the temperature exceeds 350-400°C. In the longer term, other cladding techniques such as explosion bonding, or plasma spraying which has potential for in-situ repair, may be preferable.

Analytical studies have shown that an average flux density of 12 $MW.m^{-2}$ and a sweeping frequency of 2 Hz give acceptable temperature excursions (Figure 5) for both the beryllium surface and the beryllium copper interface. Hot spots, particularly at the edge of each segment must be avoided and, to this end, each segment is tilted so that the edge is shadowed by the adjacent segment. All segments will have to be aligned with an accuracy of 0.2-0.3 mm. The beryllium layer should be castellated to minimise the plastic strain. This will be achieved by brazing small tiles with dimensions of 6-10 mm.

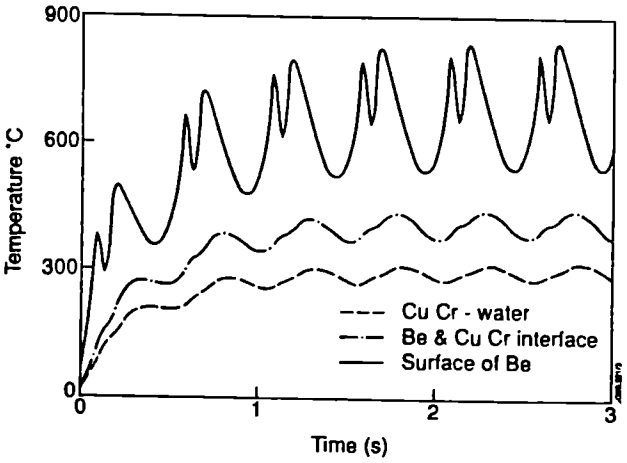

Temperature evolutions at the beryllium surface and copper-beryllium interface.

Large forces can act on the hypervapotrons due to currents flowing during disruptions. Some eddy current paths have been eliminated by a careful design of the mechanical attachments. However during vertical instabilities it is believed that currents flow in the poloidal direction and these currents can be shared between the vessel and the hypervapotrons. Forces of 2 tonnes per metre could be produced on each of the 384 segments. The hypervapotrons are firmly clamped onto steel beams which are themselves attached to the lower divertor coils.

The cryopump

For pumping, a cryopump has been selected because it has no tritium inventory after regeneration, it is reliable and there is experience and cryogenic systems available at JET.

The pump includes a chevron type liquid nitrogen cooled radiation screen and helium cooled pipes which cryo-condense the incoming gases. This pump is completely surrounded by water cooled structures which intersect the radiated power from the hot vessel and from the divertor plasma[21].

During plasma pulses the most severe heat load on the helium cooled pipes is expected to come from the neutrons and gamma rays produced during D-T operation. In the case of operation at $Q \simeq 1$ with a neutron production rate of $10^{19}\ s^{-1}$, a power of 4.5 kW would be absorbed by the helium and the stainless steel conduits. For

this reason, the helium tubes have thin walls and are slightly corrugated for increased strength. The heat capacity of the helium content (40 litres) is about 50 kJ for a 1°K temperature rise and may therefore limit the pulse duration but only if operation close to Q = 1 is achieved.

The cryopump itself has a nominal pumping speed for deuterium at 300°K of 500,000$\ell.s^{-1}$ but what really matters is the probability for neutrals emitted at the target plate to reach the pump. This has been estimated using a code provided by KFA-Jülich[22]. Neutrals can reach the cryopump through gaps between the hypervapotrons. The pumped fraction depends crucially on the target plasma temperature and varies from 0.5% to 3% for electronic temperatures between 70 and 10 eV.

The pump is split into quadrants in the toroidal direction and there will be two cryo-supplies common for two quadrants. The liquid nitrogen shield consists of blackened copper alloy baffles brazed onto stainless steel tubes for the forced flow of liquid nitrogen. The helium loop is supplied with a forced flow of supercritical helium and includes six thin-walled stainless steel tubes connected in series. The tubes are mounted in brackets which are plasma coated to reduce eddy currents. The brackets are supported from the radiation shield by thin stainless steel wires.

Fuelling

Pellet fuelling is expected to play a key role in controlling the plasma density profile, plasma flow and impurity and alpha-particle concentrations in the plasma. In order to provide operational flexibility and keep all options open a wide range of pellet velocities is foreseen.

Fast pellets at velocities of about 4km.s^{-1} should be used to fuel the plasma centre and flush impurities and alpha-particles towards the plasma edge. The development of fast guns at JET has now reached an encouraging state and such guns should be available for divertor operation[23].

Medium velocity (1.5 km.s^{-1}) pellets should fuel intermediate layers inside the plasma and help control the density profile and establish the plasma flow towards the target plate. Discussions are underway between JET and the US-DOE for the supply of adequate guns.

Low velocity (up to 500 m.s^{-1}) pellets should finally fuel the outermost plasma layers and enhance the flow of plasma particles towards the target plates.

In addition to pellet injection, gas injection nozzles are foreseen to increase if required the plasma flow towards the target plates. Gas nozzles are also foreseen inside the triangular region formed by the magnetic separatrix and the target plate so as to enhance the local flow of particles towards the target.

Ion cyclotron resonance heating

The Ion Cyclotron Resonance Heating (ICRH) system will include 8 antenna modules in 4 groups of two. As shown in figure 3 the antennae feature a deep housing to bring the RF conductor close to the plasma boundary for good power coupling. For the slim plasma configuration shown in figure 4, the antennae will be pushed forward and tilted. The housing supports and the RF conductor are designed to make this displacement. a relatively simple operation requiring only a short access inside the vacuum vessel.

Diagnostics

In view of the experimental nature of the pumped divertor experiment, an extensive range of diagnostics are being designed to obtain data on the target plasma temperature and density (langmuir probes, microwave interferometer, microwave reflectometer, electron cyclotron absorption, Thomson scattering), the impurities in this plasma (XUV/VUV spectroscopy, visible spectroscopy), the radiated power (bolometers), the neutral gas pressure (pressure probes), and the magnetic configuration at the target plates (flux loops and magnetic probes). Thermocouples at the target plates and cooling water pipes will yield data on temperature distributions and total incident power.

VIII CONCLUSIONS

Impurity control at JET has so far concentrated on the development and use of passive elements such as low Z materials for wall protection, limiter tiles and X-point target plates. Graphite and more recently beryllium have been used with great success but impurity influxes prevent the attainment of higher performances and steady state conditions.

A new pumped divertor configuration is proposed for JET which would address the problem of impurity control in operational conditions close to those of the next generation of machines. The construction and operation of the JET pumped divertor requires an extension to the JET Experimental Phase. It is planned that installation would take place in 1992 and operation with the pumped divertor would start in 1993. This extension if approved will allow essential data to be obtained on the operational domain of next step machines, the physics of the divertor and technological aspects such as the choice of materials facing the plasma.

REFERENCES

1 The JET Project. Design Proposal. Commission of the European Communities. EUR-JET-R5 (1975).

2 M. HUGUET, E. BERTOLINI, Main features implemented in the JET facility for D-T operation. Fusion Technology journal, Vol 10. No.3, p.1398-1403 (1986).

3 R. HAANGE et al, General Overview of the Active Gas Handling System at JET. Toronto Conf (1987).

4 T. RAIMONDI, The JET experience with remote handling equipment and future prospects, Fusion Eng. and Design 11 (1989) p.197-208 (North Holland, Amsterdam).

5 M. PICK et al, Integrated design of the new JET In-vessel components. Proceedings of the 15th Symposium on Fusion Technology vol 1, p.771 Utrecht (The Netherlands). (September 1988).

6 R.J. BICKERTON AND THE JET TEAM. Latest JET results and future prospects, 12th Int. Conf. on Plasma Physics and Controlled Nuclear Fusion Research, Nice (France) (October 1988) 9IAEA-CN 50/A-III.2).

7 P.H. REBUT, P.P. LALLIA, B.E. KEEN, Impurities in JET and their control. Proceedings of the 13th Symposium on Fusion Engineering. Vol 1, p.227, Knoxville (October 1989) IEEE catalog. 89 CH 2820-9.

8 P.H. REBUT et al, Use of beryllium as a first wall material in JET JET Report R(85)03.

9 R.C. ISLER et al, Nuclear Fusion 25 (1985) p.1635.

10 J. HACKMAN AND J. UHLENBUSCH, J.Nucl. Mater. 1280129 (1984) p.418.

11 G. CELENTANO et al, The JET belt limiter, Proceedings of the 14th Symposium on Fusion Technology, Vol 1. p.581, Avignon (France) (September 1986).

12 E. DEKSNIS et al, Damage to JET beryllium tiles, Proceedings of the 9th Symposium on Plasma Surface Interactions, Bournemouth (May 1990). To be published.

13 K. DIETZ et al, Beryllium in JET, A report on the operational experience, Proceedings of the 13th Symposium on Fusion Engineering, Vol.1, p.512, Knoxville (October 1989) IEEE catalog 89 ch 2820-9.

14 M.A. PICK et al, Toroidal field coil exchange and related octant exchange at JET, Proceedings of the 16th Symposium on Fusion Technology, London (September 1990). To be published.

15 S.J. BOOTH et al, Beryllium related maintenance on JET proceedings of the 16th Symposium on Fusion Engineering, London, (September 1990). To be published.

16 M. KEILHACKER AND THE JET TEAM, Overview of results from the JET Tokamak using a beryllium first wall, Phys. Fluids B2(6), June 1990, p.1291-1299.

17 K.J. DIETZ AND THE JET TEAM. Effect of beryllium on plasma performance in JET. Proceeding of the 17th meeting of the European Physics Society. Amsterdam. 1990. To be published.

18 M. HUGUET, E. BERTOLINI AND THE JET TEAM, Technical status of JET and future prospects, Proceedings of the 13th Symposium on Fusion Engineering, vol.1, p.491, Knoxville (October 1989). IEEE catalog 89 CH 2820-9

19 J.R. LAST et al, The JET divertor magnetic configuration and coil design. Proceedings of the 16th Symposium on Fusion Technology. London (September 1990). To be published.

20 E. DEKSNIS et al, Design of high heat flux components for the JET pumped divertor. Proceedings of the 16th Symposium on Fusion Technology, London (September 1990). To be published.

21 W. OBERT et al, The JET pumped divertor cryopump, Proceedings of the 16th Symposium on Fusion Technology, London, (September 1990). To be published.

22 D. REITER, E. DEKSNIS, EIRENE users manual, JET Report (in press).

23 P. KUPSCHUS et al, Upgrading the JET pellet injector with a two-stage light gas gun prototype and future planning. Proceedings of the 13th Symposium on Fusion Engineering, vol.2, p.1293, Knoxville (October 1989) IEEE catalog 89 CH 2820-9.

A Programme Towards a Fusion Reactor

P.H.Rebut

Invited Paper presented to 32nd Meeting of Division of
Plasma Physics, American Physical Society,
Cincinnati, USA., 12th-16th November 1990

A Programme towards a Fusion Reactor

ABSTRACT

Near breakeven conditions have been attained in the JET tokamak, with beryllium as the first wall material. A fusion triple product ($n_D\tau_E T_i$) of 8-9x10^{20}m^{-3}skeV has been reached (within a factor of 8 of that required in a fusion reactor). However, this has only been achieved transiently. At high heating powers, an influx of impurities still limits the achievement of better performance and steady state operation.

In parallel, an improved quantitative understanding of fusion plasmas has emerged from the development of a particular plasma model. Good quantitative agreement is obtained between the model and JET data. The main predictions are also consistent with statistical scaling laws. With such a model, we begin to have a predictive capability to define the parameters and operating conditions of a DEMO, including impurity levels. Present experimental results and model predictions suggest that impurity dilution is a major threat to a reactor. A divertor concept must be developed further to ensure impurity control, before a DEMO can be constructed.

A New Phase for JET is planned in which an axi-symmetric pumped divertor configuration will be used to address the problems of impurity control, plasma fuelling and helium ash exhaust. It should demonstrate a concept of impurity control and demonstrate the operational domain for such a device.

A single Next Step facility (ITER) is a high risk strategy in terms of physics, technology and management, since it does not provide a sufficiently sound foundation for a DEMO. A Next Step Programme is proposed, which could comprise several complementary facilities, each optimised with respect to specific clear objectives. In a minimum programme, there could be two Next Step tokamaks, and a Materials Test Facility. Such a programme would allow division of effort and sharing of risk across the various scientific and technical problems, permit cross comparison and ensure continuity of results. It could even be accomplished without a significant increase in world funding.

1. INTRODUCTION

Present Fusion Research Programmes are directed ultimately to the construction of a Demonstration Fusion Reactor - DEMO, which should be a full ignition, high power device. Moderate extrapolation of latest results and considerations of model predictions, taken together with the constraints of present technology, allow the size and performance of a thermonuclear reactor to be largely defined.

JET has successfully achieved and contained plasmas of thermonuclear grade, and has reached near breakeven conditions in single discharges. JET is well placed to oversee the route to a DEMO. Sections 2 and 3 of the paper set out the main results achieved in JET.

Furthermore, a clearer picture of energy and particle transport begins to emerge. The critical electron temperature gradient model is a particular model consistent with JET results. The implications of this model are considered in Section 4 and predictions are compared with JET results.

All aspects of plasma behaviour, impurity control and plasma exhaust must be included in the model used to define the size, toroidal field, plasma current and operating conditions of a DEMO reactor (see section 4). Such a reactor would produce power in the range 3-6GW thermal or 1-2GW electrical power. Most critical is the control of impurities and the exhaust of helium ash at high power. An acceptable solution is most likely to be achieved with a divertor at high densities.

To consolidate the model for density and impurity control, a New Phase is planned for JET with an axi-symmetric pumped divertor configuration to operate with a stationary plasma (10s-1minute) of thermonuclear grade. This is described briefly in Section 5.

The Next Step must bridge the gap from present knowledge to that required to construct a DEMO. This demands significant technological and scientific developments (see Section 6). these developments are expected to mature on varying timescales. Attempting to cover them all in a single device will limit the domain of investigation and lead to unacceptable risk of failure, unless a large safety margin is allowed on each component. This would impact on the start-time and construction time, with consequential effect on costs.

A Next Step Programme is needed to address these issues. It seems prudent to envisage international collaboration. The programme could comprise several complementary components, each optimised with respect to specific clear objectives. There could be two Next Step tokamaks, and a Materials Test Facility, each constructed in different locations with differing start dates. This theme is developed further in Section 7, where further details are presented of such a programme, and its timescale and cost.

2. JET PERFORMANCE RELEVANT TO A DEMO

JET is a high current, high power tokamak with a low-Z first wall [1-3]. Furthermore, JET operates with the configuration foreseen for a Next Step tokamak. The plasma current of 7MA in the limiter configuration [4] and the current duration of up to 30s at 3MA are world records and are over twice the values achieved in any other fusion experiment. 5.1MA and 4.5MA are also the highest currents achieved in the single-null and double-null divertor configurations, respectively [5]. NBI heating has been brought up to full power (~21MW) and ICRH power has been increased to ~22MW in the plasma. In combination, these systems have delivered 35MW to the plasma.

The overall fusion triple product as a function of central ion temperature is shown in Fig. 1 for JET and a number of other tokamaks.

2.1. Fusion performance

Better plasma purity was achieved in JET with a beryllium first-wall, by sweeping the X-point and by using strong gas-puffing in the divertor region. This resulted in high ion temperatures ($T_i(0)$ in the range 20-30keV) and improved plasma performance, with the fusion triple product ($n_D(0)\tau_E T_i(0)$) increasing significantly. Such improved fusion performance could otherwise have been achieved only with a substantial increase in energy confinement.

In the hot-ion H-mode regime, the central ion temperature reached 22keV, the energy confinement time, τ_E, was 1.1s, with a record fusion triple product ($n_D(0)\tau_E T_i(0)$) of 8–9x10^{20}m^{-3}keVs. The neutron yield for this discharge was also amongst the highest achieved on JET at 3.5x10^{16} ns^{-1}, with Q_{DD} = 2.4x10^{-3}. A full D-T simulation of the pulse showed that 12MW of fusion power would have been obtained transiently with 16MW of NBI power, giving an equivalent fusion amplification factor Q_{DT} ~ 0.8, reaching near breakeven conditions and within a factor of 8 of that required by a reactor. Similar results with ICRF were also obtained at medium temperatures, with $T_e \sim T_i \sim$10keV.

However, the best fusion performance was obtained only **transiently** and could not be sustained in steady state. Ultimately, the influx of impurities caused a degradation in plasma parameters. In fact, density and impurity control have been the main obstacles limiting JET performance.

2.2. General plasma performance

As a result of reduced impurity levels with a beryllium first-wall, the general JET performance improved and operation at higher densities was prolonged. In particular:

- the pumping of deuterium with beryllium was more efficient than with carbon walls and provided improved density control. This permitted low density and high temperature (up to 30keV) operation for times >1s;
- the density limit increased [6], and a record peak density of 4x10^{20}m^{-3} was achieved with pellet fuelling. The density is limited principally by fuelling and not by disruptions, as was found with carbon limiters;
- sawteeth were stabilized for periods exceeding 8s;
- in the absence of sawteeth, the central electron temperature appears to saturate at ~12keV, even though the central power to the electrons can exceed that to the ions;
- with beryllium antennae screens, H-modes were obtained for periods >1s using ICRH alone. The confinement characteristics were similar to those with NBI alone;
- β-values up to the Troyon limit were obtained in double-null X-point plasmas [6].

Thus, in JET, the parameters of a reactor plasma have been reached individually, and near breakeven conditions have been achieved in single discharges.

3. QUANTITATIVE UNDERSTANDING OF FUSION PLASMAS

The underlying JET results are presented with particular emphasis on their significance for the formulation of a model of transient and steady state plasmas that can be used for moderate extrapolation to a Next Step tokamak.

3.1. Density limit

With a beryllium first-wall, the maximum operating density increased significantly by a factor 1.6 - 2 compared with a carbon first-wall. Furthermore, the nature of the density limit changed and the frequency of disruptions at the density limit were much reduced. Disruptions did not usually occur, and the limit was associated rather with the formation of a poloidally asymmetric, but toroidally symmetric radiating structure (a "MARFE"), which limits the plasma density to within the stable operating domain.

Heating and plasma fuelling were varied systematically, using both gas and pellet fuelling. With deep pellet fuelling and either NBI or ICRH, peaked profiles were obtained (Fig. 2). Just before a density limit MARFE occurred, pellet fuelled discharges reached the same edge density as gas fuelled discharges, but the central densities were considerably higher. The central density depends, therefore, on the fuelling method used. The profiles are similar near the edge, but are remarkably flat with gas fuelling.

These observations suggest that the edge density may be correlated with the density limit and is found to increase approximately as the square root of power (Fig. 3). This endorses the view that the density limit is determined by a power balance at the plasma edge and the cause of disruptions is related to radiation and charge exchange near the q=2 surface. Thus, where beryllium is the only impurity and when the radiation is low, and confined to the outermost edge, density limit disruptions are not observed.

3.2. Density profiles and transport

Density profiles obtained with edge fuelling tend to be flatter with the lower Z_{eff} achieved with beryllium, in contrast to those obtained with carbon, which tend to be more peaked, even with edge fuelling. The occurrence of flat density profiles suggest that there is no need for an anomalous inward particle pinch, except, perhaps, on impurities.

The relaxation of the peaked density profiles achieved with pellet injection allows an estimate of particle transport. For a 4mm pellet injected into 3MA/3.1T plasma, the decay of the central electron density is shown in Fig. 4. Following injection, the decay constants are 1.8s for the ohmically heated discharge and 1s when ~8MW ICRH is applied, The global energy confinement times are in a similar ratio. Therefore, it is reasonable to assume that particle and energy transport are linked. The measurement of emissivity profiles by the soft X-ray cameras following the injection of laser-ablated, high-Z impurities provides evidence of better impurity confinement in H-modes. The temporal evolution of NiXXVI emission is shown in Fig. 5 for the L- and H-phases of two similar discharges with ~9MW of additional heating. In contrast to the decaying signal of the L-phase, the signal rises rapidly to a steady value which persists to the end of the H-phase. This shows that impurities have considerably longer confinement times in the H-phase and endorses the view that an edge transport barrier exists, which could be destroyed (for example, by Edge Localised Modes) and on transition from the H- to the L-phase.

3.3. Temperature

High ion temperatures have been obtained at the low densities possible with a beryllium first-wall and with the better penetration afforded by NBI at 140kV. Record ion temperatures were achieved of up to 18keV in limiter plasmas and up to 30keV in X-point plasmas (with powers up to 17MW). In this mode, the ion temperature profile is sharply peaked and the electron temperature is significantly lower than the ion temperature, by a factor of 2-3. The central ion temperature (as shown in Fig. 6) increases approximately linearly with power per particle up to the highest temperatures, indicating that ion thermal losses are anomalous, but ion confinement degrades little with input power. On the other hand, the central electron temperature saturates at ~12keV, even though with ICRH the central heating power to the electrons can apparently be higher than that to the ions. Electron thermal transport is also anomalous and electron

confinement degrades strongly with increased heating power. This suggests that electrons are primarily responsible for confinement degradation. However, this does mean that ion losses are necessarily small.

3.4. Electron heat and density pulse propagation

The propagation of temperature and density perturbations following the collapse of a sawtooth provide good measurements of energy and particle transport. The decay of the temperature perturbation at different radii in a 3MA/3.1T ohmically heated discharge is shown in 7(a). This can be modelled with an heat pulse diffusivity, χ_{HP}~3.2m^{2}s^{-1}, compared with χ_e~1m^{2}s^{-1}, obtained from power balance considerations. The results in an L-mode plasma, heated with 9.5MW of ICRH, are shown in Fig. 7(b) and indicate that, although χ_e~2m^{2}s^{-1}, the same χ_{HP}~3.2m^{2}s^{-1} can be used in the simulation to fit the data. Within experimental uncertainties, the same χ_{HP} can be used also for H-regime plasmas and does not depend on heating power.

Simultaneous measurements of the temperature and density perturbations indicate that the particle pulse diffusion coefficient, D_{DP}~D_e≈χ_{HP} [7]. This general behaviour must be reproduced by the model.

3.5. Global energy confinement

With a carbon first-wall, the energy confinement time improves with increasing current and degrades with increasing heating power, independent of the heating method and similar at high power. With a beryllium first-wall, energy confinement times and their dependences are effectively unchanged: energy confinement does not appear to be affected by the impurity mix (carbon or beryllium in deuterium plasmas).

In the X-point configuration, high power H-modes (up to 25MW) have been studied. In comparison with limiter plasmas, confinement is a factor ~2 better, but the dependences with current and heating power are similar (Fig. 8). These observations are consistent with the same basic mechanism applying over most of the radius, except perhaps near the very edge.

3.6. Plasma beta

Experiments have explored the plasma pressure (indicated by the β-value) that can be sustained in JET and investigated the plasma behaviour near the expected β-limit in the double-null H-mode configuration, at high density and temperature and low magnetic field (B_t = 1T). β_t values up to ~ 5.5% were obtained, close to the Troyon limit $\beta_t(\%) = 2.8 I_p(MA)/B_t(T)a(m)$, where I_p is the plasma current and a is the plasma minor radius [6]. These results are consistent with the highest values obtained on D-III(D) [8]. In JET, the limit does not appear to be disruptive at present power levels. Rather, a range of MHD instabilities occur, limiting the maximum β-value without causing a disruption. The behaviour near both the density and β-limits may be interpreted in terms of resonant instabilities which have the magnetic topology of an island. Ignition will therefore not be limited by β. Fusion power will be limited rather by the capability of the first wall and the divertor.

3.7. Alpha-particle simulations

The behaviour of alpha-particles has been simulated in JET by studying energetic particles such as 1MeV tritons, and ^{3}He and H minority ions accelerated to a few MeV by ICRH [9]. Triton burn-up studies show that the experimental measurements of the 14MeV neutron rate is in good agreement with that calculated from the 2.5MeV neutron (and hence the 1MeV triton) source rate and classical thermalization. The energetic minority ion population with ICRH has up to 50% of the stored energy of the plasma and possesses all the characteristics of alpha-particles in an ignited plasma, except that in the JET experiments, the ratio of the perpendicular to parallel pressure was above three, while in a reactor plasma the distribution will be approximately isotropic. The mean energy of the minority species was about 1MeV, and the relative concentration of the ^{3}He ions to the electron density was 1-2%, which is comparable to the relative concentration of alpha-particles in a reactor (7%). Under conditions with little MHD activity, no evidence of non-classical loss or deleterious behaviour of minority ions was observed, even though the ratio of fast ion slowing down time to energy confinement time in JET is greater than that expected in a reactor. The prospects for alpha heating in DEMO should therefore be good.

4. A TRANSPORT MODEL

4.1. Formulation of a plasma model

Any model used to predict the performance of a Next Step tokamak must be consistent with the foregoing JET data and with physics constraints. Experimental observations support a model for anomalous transport based on a single phenomenon and MHD limits. This **Critical Electron Temperature Gradient** model of anomalous heat and particle transport features

- electrons which determine the degree of confinement degradation;
- ion anomalous transport with heat diffusivity χ_i linked to electron heat diffusivity χ_e;
- anomalous particle diffusivities, D, for ions and electrons, proportional to χ;
- anomalous particle "pinch" for impurities alone.

Specifically, above a critical threshold, $(\nabla T_e)_c$, in the electron temperature gradient, the transport is anomalous and greater than the underlying neoclassical transport. The electrons are primarily responsible for the anomalous transport, but ion heat and particle transport are also anomalous. The general expressions for the anomalous conductive heat fluxes are:

$$Q_e = -n_e \chi_e \nabla T_e = -n_e \chi_{an,e} (\nabla T_e - (\nabla T_e)_c)$$

$$Q_i = -n_i \chi_i \nabla T_i$$

$$\chi_i = 2 \chi_e \sqrt{T_e/T_i} \times (Z_i/\sqrt{(1+Z_{eff})})$$

$$D_i \approx 0.6 \chi_i$$

The critical electron temperature gradient model of Rebut et al [10] specifies possible dependences for $\chi_{an,e}$ and D and this is explored further in [7].

$$\chi_{an,e} = 0.5c^2\sqrt{\mu_0 m_i}\left(1-\frac{r}{R}\right)\sqrt{1+Z_{eff}}\left(\frac{\nabla T_e}{T_e}+2\frac{\nabla n_e}{n_e}\right)\frac{q^2}{\nabla q}\frac{1}{B_T\sqrt{R}}\sqrt{\frac{T_e}{T_i}}$$

$$(\nabla kT_e)_{cr} = 0.06\sqrt{\frac{e^2}{\mu_0 m_e^{1/3}}}\frac{1}{q}\sqrt{\frac{\eta j B_T^2}{n_e (kT_e)^{3/2}}}$$

This model features:

- a limitation in the electron temperature;
- electron heat pulse propagation with $\chi_{HP} \sim \chi_{an,e} > \chi_e$;
- no intrinsic degradation of ion confinement with ion heating power;
- density decay following pellet injection and its dependence on heating power;
- similar behaviour of particle and heat transport;
- density pulse propagation as observed with $D_{DP} \sim D_i \propto \chi_{HP}$.

Furthermore, in the plasma interior, the same model applies to the L- and H-regimes and particle and energy confinement improve together. However, at the edge of an H-mode, an edge transport barrier forms and the transport might be classical over a short distance (~few cms). In fact, the H-mode may be the 'natural' consequence of the transport model, since $\chi_{an,e}$ depends on shear, reducing to zero near the separatrix. Furthermore, MHD activity reduces on making the transition from L → H phase. This may imply the stabilisation of some other instability at the edge, where the effect of impurity radiation and neutral influxes on MHD might be important in destroying, at least partially, the edge confinement barrier. This instability is apparently easier to suppress in an X-point configuration with high edge magnetic or rotational shear.

To complete the plasma model requires a description of the scrape-off layer (SOL), for which a rudimentary model is also included (see also Section 5.3). For example, the spontaneous improvement in edge confinement has yet to be modelled.

4.2. Application of the model to JET

Several examples are shown to illustrate the applicability of this plasma model to JET experimental results.

A comparison between experimental and computed density and temperature profiles for a 3MA/3T discharge heated with 8MW NBI is shown in Fig. 9. It is to be noted that the temperature profiles are well represented and that the electron density profiles are flat. The Z_{eff} of this discharge is low. No anomalous particle "pinch" is needed to describe adequately the density evolution.

The density and temperature profiles are also well represented for a 3MA/3T discharge heated with 8MW ICRF (Fig. 10). However, it should be noted that the electron density profile is more peaked. The Z_{eff} of this discharge is also higher. An anomalous particle "pinch" is required and in the model this may be attributed to impurities.

The model has also been applied to the propagation of heat and density pulses following the collapse of a sawtooth in JET. As shown in Fig. 11, the computed changes in T_e and n_e at various radii and times agree well with experiment.

The characteristics of an H-mode can also be modelled, assuming classical transport near the separatrix. As shown in Fig. 12, this leads to higher density and Z_{eff}, reduced edge flow (D_α signal simulated), higher stored energy and τ_E, lower χ_e and χ_i, as observed experimentally.

Thus, we have established good quantitative agreement between the model and JET data. Furthermore, the main predictions of the model are also consistent with statistical scaling laws [9]. With such a model, we begin to have the predictive capability needed to define the parameters and operating conditions of a DEMO, including impurity levels.

4.3. Application of the model to a First DEMO

The parameters of a first DEMO are defined by technology and physics predictions. The minor radius of a DEMO plasma needs to be twice the thickness of the tritium breeding blanket thickness, which makes it ~3m and the elongation can be up to 2. A practical aspect ratio of ~2.5 sets the plasma major radius to 8m. Safe operation can be assumed for a cylindrical safety factor 1.6-1.8. Plasma physics requirements can be fulfilled by operating at a toroidal field no greater than 5T. This defines a reactor with a plasma current of ~30MA.

The operating conditions will be such that:

- $T_i \sim T_e$;
- confinement is L - mode;
- D-T mixture, including helium ash;
- sawteeth (minimum internal control from outside);
- high density, flat density profile;
- full impurity control.

We now model DEMO plasmas using the L-mode transport model which has been tested against JET results, together with a model for sawteeth, β-limit instabilities and the divertor. A mixture of D-T is assumed and includes helium ash accumulation and pumping. Assuming the provision of adequate impurity control, ignition is maintained in DEMO (R_{major}=8m, a=3m, 4.5T, 30MA, κ=2) after switching off 50MW of ICRH (Fig. 13). At ignition, the slightly hollow density profiles (Fig. 14) with edge fuelling are sufficient to fuel the centre. However, helium poisoning alone can quench the ignition without adequate pumping. To exhaust sufficient helium and maintain ignition requires the pumping of about **1kg of D-T per hour. Exhaust and impurity control are essential.** In fact, while the H-mode has short term benefits for approaching ignition, the long term deficiencies due to helium poisoning are evident (see Fig.15). Steady ignition conditions can be achieved with a specific level of helium ash.

It is fundamental to control dilution in a reactor. There are two primary sources of dilution: target plate impurities and helium ash. With impurity control, ignition is achieved with edge fuelling and high pumping; high density and flat profile; sawteeth and L-mode

confinement; and recirculation of a kg of D - T per hour. The H-mode does not improve steady state ignition due to the better confinement of ashes. At present, impurity control is envisaged to require high density operation. Under these conditions, the use of current drive seems precluded. However, one hour steady state requires only 50Vs (~10% of inductive Vs) and this can easily be provided.

A divertor concept for impurity control must be developed further. The fuelling, impurity control and exhaust capability of a Next Step will be dependent on whether deuterium and impurities (including helium) accumulate in the plasma centre. The production and transport of helium ash towards the plasma edge (where it must be exhausted) will depend on the relative importance of energy and particle confinement, the effect of sawteeth, the effect of the edge transport barrier in the H-mode and the behaviour of the scrape-off layer plasma.

5. SOLUTION OF OUTSTANDING ISSUES

5.1. Impurity control and the New Phase planned for JET

Plasma dilution is a major threat to a reactor. Active impurity control represents a solution to this problem, and this will be tested in JET in a New Phase planned to start in 1992 [3]. First results should become available in 1993 and the Project should continue to the end of 1996.

The aim of the New Phase is to demonstrate, prior to the introduction of tritium, effective methods of impurity control in operating conditions close to those of a Next Step tokamak, with a stationary plasma of 'thermonuclear grade' in an axisymmetric pumped divertor configuration. Specifically, the New Phase should demonstrate:

- the control of impurities generated at the divertor target plates;
- a decrease of the heat load on the target plates;
- the control of plasma density;
- the exhaust capability;
- a realistic model of particle transport.

5.2. Key concepts of the JET pumped divertor

Sputtering of impurities at the target plates presents a major difficulty and such impurities must be retained close to the target plates for effective impurity control. This retention may be accomplished by friction with a strong plasma flow directed along the divertor channel plasma (DCP) towards the target plates [11, 12, 13]. The plasma flow will be generated by a combination of gas puffing, injection of low speed pellets and recirculation of a fraction of the flow at the target plates towards the X-point. The connection length along the magnetic field line between the X-point and the target plates must be sufficiently long to allow effective screening of impurities.

5.3. Modelling the edge plasma

Calculations for JET New Phase [13] show that impurities can be retained near the target plates for plasma flows, typically $\sim 10^{23} s^{-1}$ near the X-point. The steady state distributions of Z_{eff} (with beryllium impurities), for conditions in the SOL and DCP, with and without flow, are shown in Fig. 16(a). These results are obtained for an electron density $\sim 10^{20} m^{-3}$ at the target plates. At target densities approaching $10^{21} m^{-3}$, the reduction of erosion and the plasma flow associated with high recycling at the target plates ensures impurity control. In addition, the calculations show that the ion temperature in the SOL can be substantially larger than the electron temperature (Fig. 16(b)). In present JET discharges, probe measurements indicate, that at low density, the electron temperature at the target plates is lower than the ion temperature determined from broadening of H_α emission and power balance considerations [14].

5.4. JET programme in the New Phase

The New Phase of JET should demonstrate a concept of impurity control; determine the size and geometry needed to realise this concept in a Next-Step tokamak; allow a choice of suitable plasma facing components; and demonstrate the operational domain for such a device.

A schedule for the JET programme incorporating the New Phase is shown in [12]. The earliest date to have a pumped divertor in JET is 1993. By the end of 1994, all information on particle transport, exhaust and fuelling, first wall requirements and enhanced confinement regimes needed to construct a Next Step tokamak, should be available. This concept could be developed further towards lower temperature, higher density, eg cold radiating plasma or gas target. Such concepts would have to be proven further for the inclusion in a Next Step tokamak.

6. TECHNOLOGY OF A DEMO

DEMO is a large and complex device. It would include a magnetic system (with superconducting coils), a divertor with high power handling capability and low erosion, an exhaust system for impurities and helium "ash" products, a first wall that is highly resilient to 14MeV neutrons, a hot blanket to breed tritium, a plasma control system and a D-T fuelling system. Auxiliary heating systems are required for start-up. DEMO would operate either semi-continuously with long pulses (2hrs or so) or continuously with non-inductive current drive. It must achieve high reliability, high duty cycle and high safety level. Activation and tritium inventory must be minimised. A full remote handling maintenance capability is required.

The construction of a DEMO must be preceded by an extensive test of the concepts and technologies required. Plasma facing components and first-wall materials with a high resilience to 14MeV neutron radiation at a power flux of $2\text{-}3 MWm^{-2}$ must be developed and tested. Divertor target materials with high power handling capability and low erosion (eg. low Z materials, beryllium, carbon and carbide fibres, silicon carbide) must be developed and tested. An efficient, high flow D-T fuelling system with pellet injection needs to be demonstrated. The viability of present or emerging concepts for helium ash exhaust, pumping and energy exhaust still needs to be proved. Tritium breeding blankets must operate at high temperatures but have not yet been tested. Furthermore, in the area of superconducting technologies, viable high temperature superconducting materials are desirable for sufficient safety margin and these need thorough testing. A credible physics concept still needs to emerge for current drive, to sustain continuous plasma operation. However, this last requirement may prove to be unnecessary when semi-continuous operation (2hrs or so) has been demonstrated, since this would be sufficient for a commercial reactor.

In view of the time needed to develop and incorporate emerging technologies required for a DEMO, a precisely defined or optimised engineering design cannot yet be proposed. A reasonably broad strategy would be to develop, partly in parallel, the main components of a fusion reactor. In addition, it is clear that more than one DEMO will be required (as in the early development of fission). All the physics and technological issues for a DEMO must be addressed, so that it can be constructed from proven elements. A well defined Programme towards DEMO is essential.

7. A PROGRAMME TOWARDS DEMO

The scientific feasibility of ignition under conditions required for a DEMO device must first be demonstrated: that is, high power long pulse operation in fully ignited plasmas ($Q_{DT} = \infty$). Tritium breeding in hot blanket modules should also be tested. Advanced divertors and concept development aimed at improved efficiency must also be pursued.

Technology must still emerge on such items as pumping and helium extraction; the use of low-Z plasma facing materials (eg. beryllium, silicon carbide, carbon fibres, carbide fibres); the nature of breeding materials and coolant and structural materials for tritium breeding blankets. The resistance of highly sensitive materials (eg insulators, first-wall, etc.) to high neutron fluences should be evaluated. Industrial development is also required for superconducting coils which can withstand neutrons and AC losses. It is expected that the remaining technology can be scaled up from existing knowledge.

Many of these issues are expected to mature on differing timescales. A single tokamak addressing all these issues would be close to a DEMO. Even with a large safety margin on each component, the risk of failure would be unacceptable. To incorporate all innovations that are likely to reach maturity throughout the lifetime of a single facility requires a design which lacks the precise definition offered by well targeted objectives. There would also be an impact on the starting and construction times and on the consequential costs. A large degree of complexity would be introduced and this would place a practical limit on intended flexibility. We are not yet in a position to take such a large step. It is therefore not possible to address all issues on a single device.

An ITER programme is the way to address the different Next Step issues. Several complementary facilities, each with separate, clearly defined objectives, would

- reduce scientific and technological risks;
- allow flexibility to accommodate new concepts;
- allow cross-checking of results;
- be more practical in managerial and industrial terms;
- offer flexibility in location and time scheduling.

This programme towards DEMO would minimise the risks and overall costs and would ensure an efficient use of world resources.

In such an optimised Programme, the three main issues of long burn ignition, concept optimisation and materials testing would be separated and addressed in different facilities which would be constructed as technologies mature. The engineering design for each facility can be defined precisely, thereby allowing a high degree of confidence that objectives would be met. A minimum ITER Programme should comprise:

P1 - A thermonuclear furnace: the core of a first reactor;
P2 - An advanced tokamak for concept optimisation;
P3 - A materials test facility.

In support of this ITER Programme, "National Programmes" comparable in size will be needed.

The main details of such machines are set out below.

7.1 P1 - A Thermonuclear Furnace: the core of a first reactor

The primary objectives of P1 would be:

- to demonstrate sustained high power operation of a fusion reactor core of 2-3GW thermal power produced for up to 12hrs per day for periods of several days at a time (~2000 hrs total);
- to provide a testbed for the study and validation of tritium breeding blanket modules in full reactor conditions;
- to achieve a cost/unit thermal output relevant to the establishment of fusion as a potential economic energy source (1ECU/thermal Watt; 1ECU ≈ 1.4$);
- to achieve a high level of safety.

The design philosophy of P1 would be:

- to make full use of the scientific and technical experience gained from JET and other tokamaks;
- to minimise the need for developments by using established techniques;
- to reduce complexity and increase reliability at reasonable cost;
- to provide a high safety margin in achieving design specifications for the magnetic field and plasma current.

The objectives could be achieved in a tokamak with 30MA, 4-5T, major radius 8m, minor radius 3m, and elongation of 2. The main parameters of P1 are shown in Table I. Impurities would be controlled actively by high density operation and a pumped divertor. The approach to ignition would utilise ICRF heating with H-mode confinement and in the monster sawtooth regime, while long pulse ignition (0.5 - 1 hr) would be sustained with X-point L-mode confinement at high power and also with high frequency low amplitude sawteeth. With sustained ignition conditions, blanket modules would be tested under neutron fluxes of up to

$2MWm^{-2}$. Conventional coil technology should be used. An early start in 1994 would be possible, once the results on impurity control become available from the New Phase of JET.

7.2 P2 - An Advanced Tokamak for Concept Optimisation

The primary objectives of P2 would be:

- to develop advanced divertor concepts at high power;
- to improve plasma performance by profile and shape control;
- to test efficient continuous operation with current drive;
- to demonstrate the viability of advanced superconducting technology in a large, high power and high field tokamak.

The basic geometry and concept of DEMO would be expected to evolve due to the emergence of "new" physics, which would be demonstrated on P2.

The design philosophy would be to test new concepts in a low activation environment at a reasonable cost. Flexibility should be built-in to allow tests of new concepts throughout the lifetime of the device. This includes advanced divertor concepts (eg. gas target, radiative target, cold plasma target, etc.) and advanced superconductors. The P2 objectives could be realised with a large tokamak operating at high power (typically 200MW), 10-12MA, 6-7T, minor radius 1.5m, major radius 5m, and elongation of 2. The main parameters of P2 are shown in Table II. During the major part of the programme, the tokamak would not operate in tritium and therefore would not ignite. Some technological developments are still required and therefore, construction could start somewhat after P1, perhaps in 1998.

7.3 P3 - A Test Facility for Materials

The objective of P3 would be to test materials under very large neutron fluences. This could be realised in a test-bed operating continuously and providing high fluxes of neutrons (2-10 MWm^{-2}) over surfaces of 0.04-0.05m^2. Its construction could start early in 1995, so that results should be available for the design of a DEMO in 2005.

7.4 Time schedule and costs

A time schedule for the design, construction, and operation of devices within an ITER Programme is shown in Table III. The overall cost for such a minimum Programme is estimated at 7BioECU, not including operation costs, spread over 10 years. This is made up of capital costs of P1 at 3.5BioECU; P2 at 2BioECU; and P3 at 1.5BioECU.

In parallel, National Programmes would be expected to continue on scientific and technological development in support of the International Programme, which would cost a comparable sum (making a total of ~14BioECU over a 10 year period). This should be compared with present world funding of fusion research of 1.2BioECU/annum (ie. ~12BioECU over a 10 year period).

8. CONCLUSIONS

- Individually, each of the plasma parameters n, T_i and τ_E required for a fusion reactor have been achieved in JET; in single discharges, the fusion product of these parameters has reached near break-even conditions and is within a factor 8 of that required in a fusion reactor;
- However, these good results were obtained only transiently, and were limited by impurity influxes due to local overheating of protection tiles;
- The quantitative understanding of fusion plasmas has improved with the development of a specific plasma model, which is in good quantitative agreement with JET data The main predictions are also consistent with statistical scaling laws.
- With such a model, we begin to have a predictive capability to define the parameters and operating conditions of a DEMO, including impurity levels;
- Present experimental results and predictions of the model suggest the importance of controlling dilution in a reactor. The divertor concept must be developed further to provide sufficient impurity control;
- A New Phase is planned for JET, to demonstrate effective methods of impurity control in an axisymmetric pumped divertor configuration;
- Based on present progress, there is confidence that sufficient knowledge will exist to begin the construction of the "core" of a fusion reactor within the next 3-4 years;
- A single Next Step facility (ITER) is a high risk strategy in terms of physics, technology and management, and it does not provide a sufficiently sound foundation for a demonstration reactor;
- A Next Step Programme comprising several facilities:
  - would make more effective use of world resources;
  - is well within the capability of world research;
  - would provide a wider and more comprehensive data base; and
  - could even be accomplished without a significant increase in existing world funding;
- With concerted effort and determined international collaboration, we have the resources to proceed with such a programme, towards a DEMO starting operation in ~2015.

9. REFERENCES

[1] The JET Project - Design Proposal: EUR-JET-R5.

[2] Rebut, P-H., et al, Fusion Technology, **11**, (1987), 13-281.

[3] Rebut, P-H., Lallia, P.P., and Keen, B.E., Proc. of the 13th Symposium on Fusion Engineering, (Knoxville, USA, 1989), **1**, 227.

[4] Lomas, P.J. and The JET Team, Proc. of 13th Int. Conf. on Plasma Phys. and Contr. Nucl. Fus. Res., (Washington, USA, 1990), Paper IAEA-CN-53/A-6-2.

[5] Tanga, A. and The JET Team, Proc. of 13th Int. Conf. on Plasma Phys. and Contr. Nucl. Fus. Res., (Washington, USA, 1990), Paper IAEA-CN-53/A-4-1.

[6] Smeulders, P. and The JET Team, Proc. of 13th Int. Conf. on Plasma Phys. and Contr. Nucl. Fus. Res., (Washington, USA, 1990), Paper IAEA-CN-53/A-3-4.

[7] Taroni, A., et al, Proc. of 13th Int. Conf. on Plasma Phys. and Contr. Nucl. Fus. Res., (Washington, USA, 1990), Paper IAEA-CN-53/A-2-1.

[8] Taylor, T. S. et al, Proc. of 13th Int. Conf. on Plasma Phys. and Contr. Nucl. Fus. Res., (Washington, USA, 1990), Paper IAEA-CN-53/A-3-1.

[9] Start, D. F. H. and The JET Team, Proc. of 13th Int. Conf. on Plasma Phys. and Contr. Nucl. Fus. Res., (Washington, USA, 1990), Paper IAEA-CN-53/E-2-1.

[10] Rebut, P-H., Lallia, P.P., and Watkins, M.L., Proc. of 12th Int. Conf. on Plasma Phys. and Contr. Nucl. Fus. Res., (Nice, France, 1988) Nuclear Fusion Supplement, **2**, 191.

[11] Rebut, P-H, et al, JET Contributions to the Workshop on the New Phase for JET: The Pumped Divertor Proposal (September, 1989), JET Report - JET R(89)16

[12] Rebut, P-H, and The JET Team, Proc. of 13th Int. Conf. on Plasma Phys. and Contr. Nucl. Fus. Res., (Washington, USA, 1990), Paper IAEA-CN-53/A-1-2.

[13] Keilhacker, M., et al, Proc. of 13th Int. Conf. on Plasma Phys. and Contr. Nucl. Fus. Res., (Washington, USA, 1990), Paper IAEA-CN-53/A-5-1.

[14] Thomas, P. R. and The JET Team, Proc. of 13th Int. Conf. on Plasma Phys. and Contr. Nucl. Fus. Res., (Washington, USA, 1990), Paper IAEA-CN-53/A-5-3.

Table I
Parameters of P1

Parameters	
Plasma Major Radius (R_0)	8m
Plasma Minor Radius (horizontal)	3m
Plasma Minor Radius (vertical)	6m
Toroidal Field Strength at R_0	4.5T
Plasma Current	30MA
Flat Top Pulse Length	1000-4000s
Volt Seconds	425Vs
Additional Heating Power (ICRF)	50MW
Fusion Power	0.5-4GW

Table II
Parameters of P2

Parameters	
Plasma Major Radius (R_0)	5m
Plasma Minor Radius (horizontal)	1.5m
Plasma Minor Radius (vertical)	3m
Plasma Aspect Ratio	1.8-2
Toroidal Field Strength at R_0	6-7T
Plasma Current	12MA
Flat Top Pulse Length	up to continuous
Current Drive/Additional Heating Power	200MW

Table III: A Time Schedule for an ITER Programme

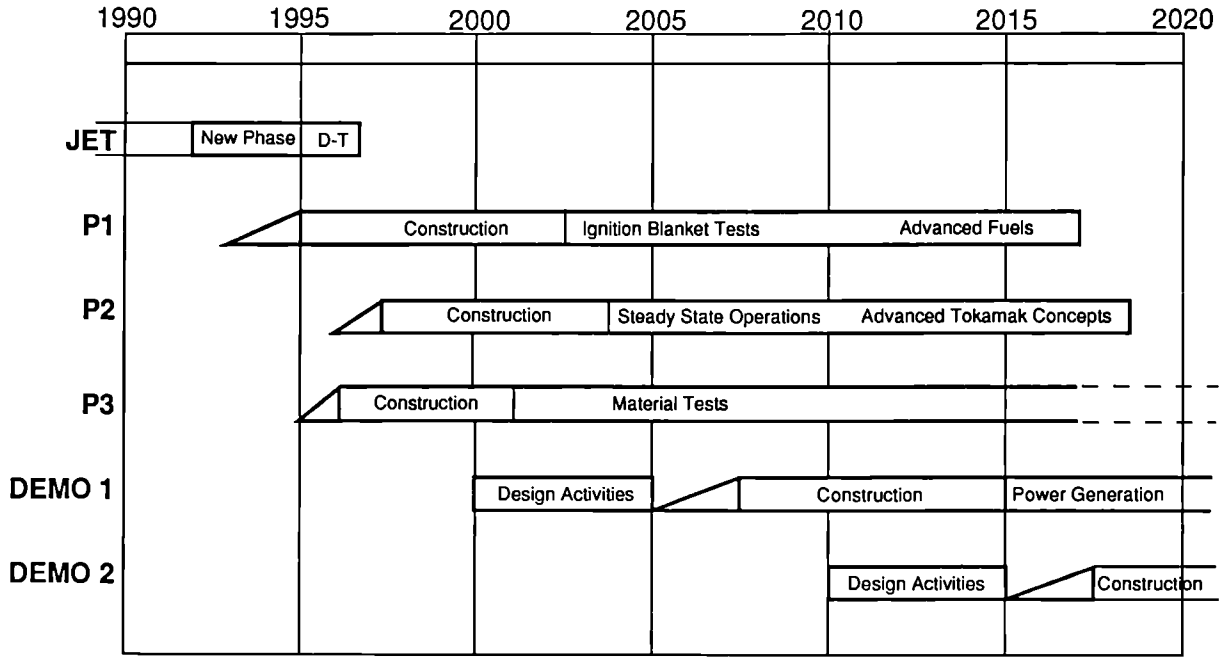

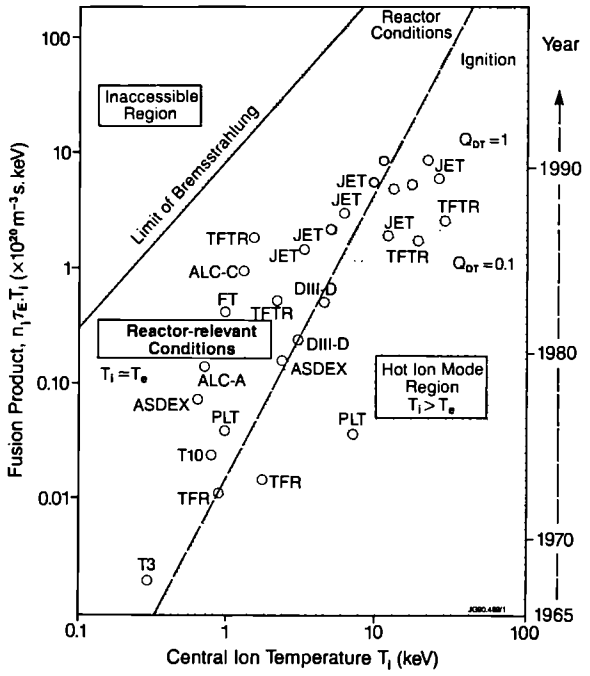

Fig. 1: Overall performance of the fusion product ($n_D(0)\tau_E T_i(0)$) as a function of central ion temperature ($T_i(0)$), for a number of tokamaks

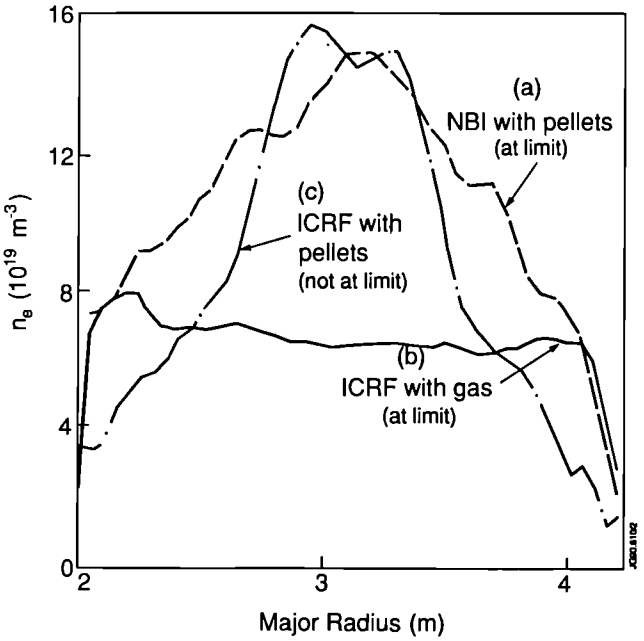

Fig. 2: Electron density profiles for different fuelling and heating methods. Profiles (a), (b) and (c) are correlated with their proximity to the density limit (see Fig.3)

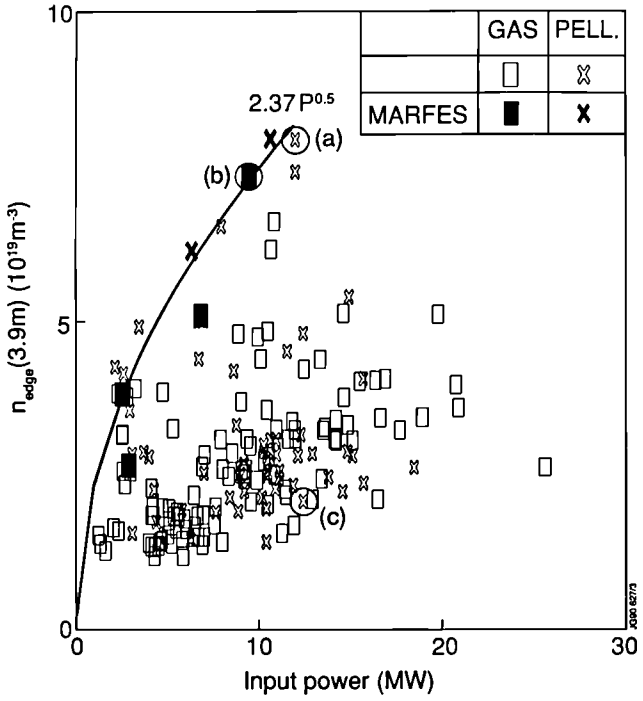

Fig. 3: The edge electron density (n_{edge}) versus input power (P) showing that the density limit occurs at the boundary of the operational domain close to the curve n_{edge} ($\times 10^{19} m^{-3}$) = 2.37 $P^{1/2}$(MW). The profiles shown in Fig.2 correspond to the three data points (a), (b) and (c)

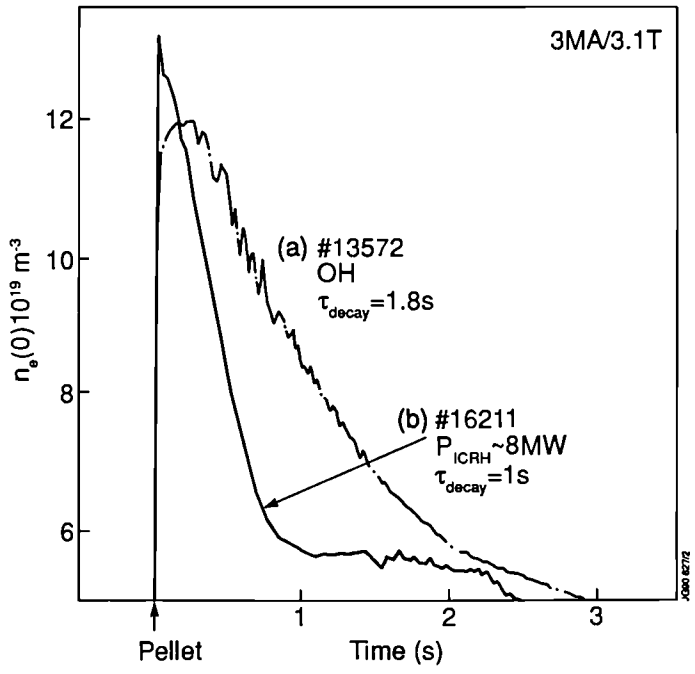

Fig. 4: Decay of central density following pellet injection into discharges with (a) ohmic heating only and (b) ~8MW ICRH

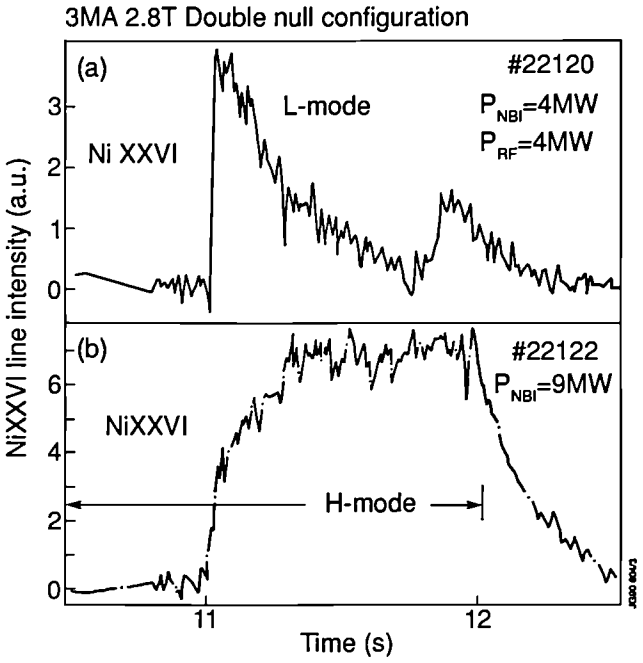

Fig. 5: Temporal evolution of NiXXVI emission in (a) the L-phase and (b) the H-phase of two similar discharges with ~9MW of additional heating

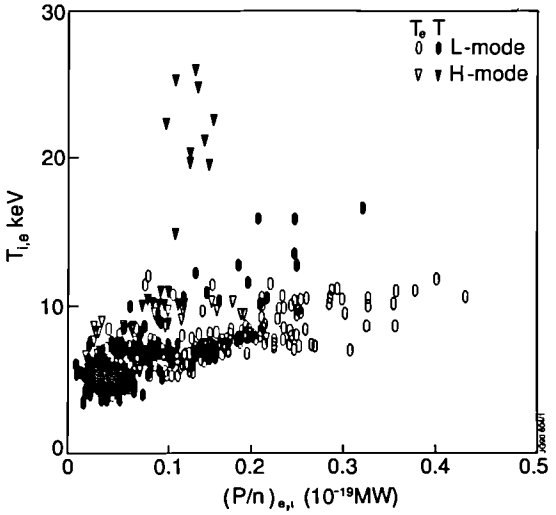

Fig. 6: Central ion (T_i) and electron (T_e) temperatures as functions of power per particle $(P/n)_{e,i}$ to either species

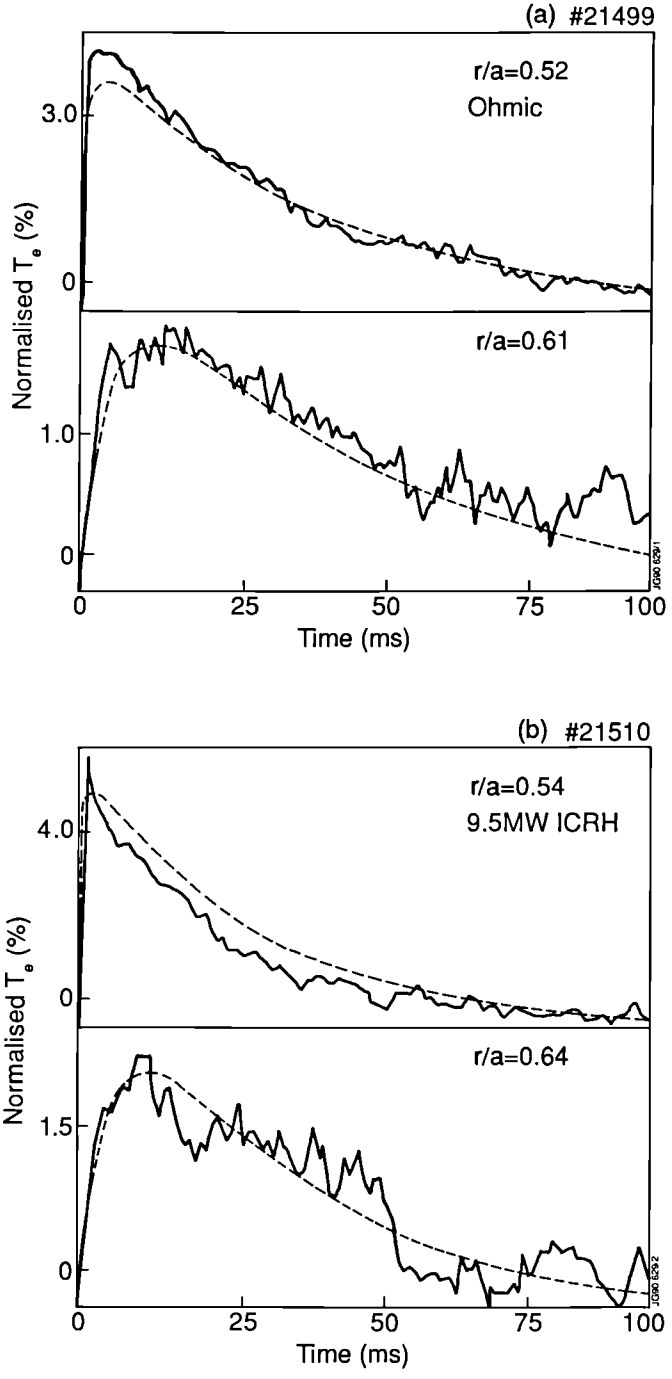

Fig. 7: Temporal evolution of electron temperature perturbations (normalised to the central electron temperature prior to the collapse of a sawtooth) at different radii for 3MA/2.8T discharges with (a) ohmic heating only and (b) 9.5MW ICRH. Dashed lines are from model calculations using $\chi_{HP}=3.2m^2s^{-1}$

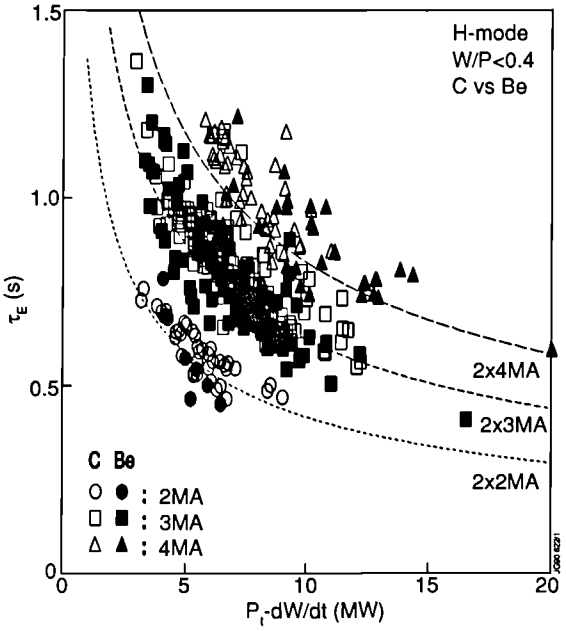

Fig. 8: Global energy confinement time (τ_E) during the H-mode as a function of net input power for different plasma currents and first wall materials

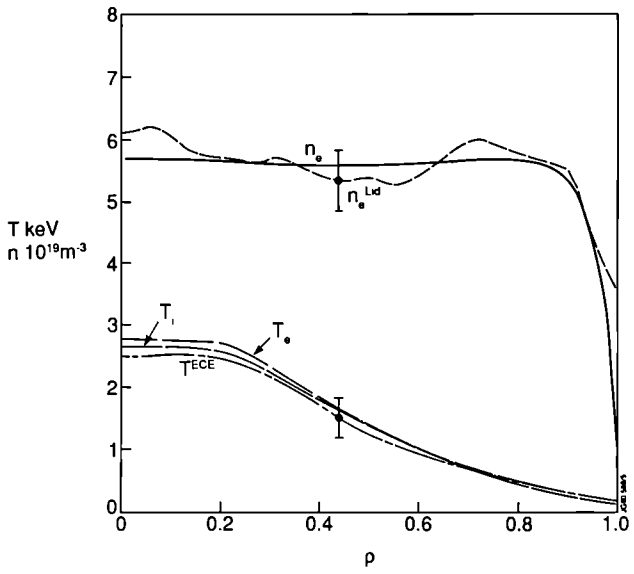

Fig. 9: A comparison between experimental and computed density and temperature profiles as a function of normalized radius, ρ, for a 3MA/3T discharge heated with 8MW NBI

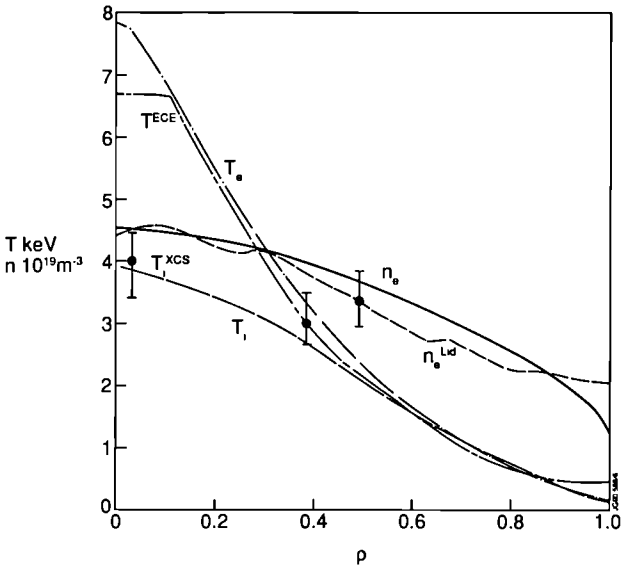

Fig. 10: A comparison between experimental and computed density and temperature profiles as a function of normalized radius, ρ, for a 3MA/3T discharge heated with 8MW ICRH

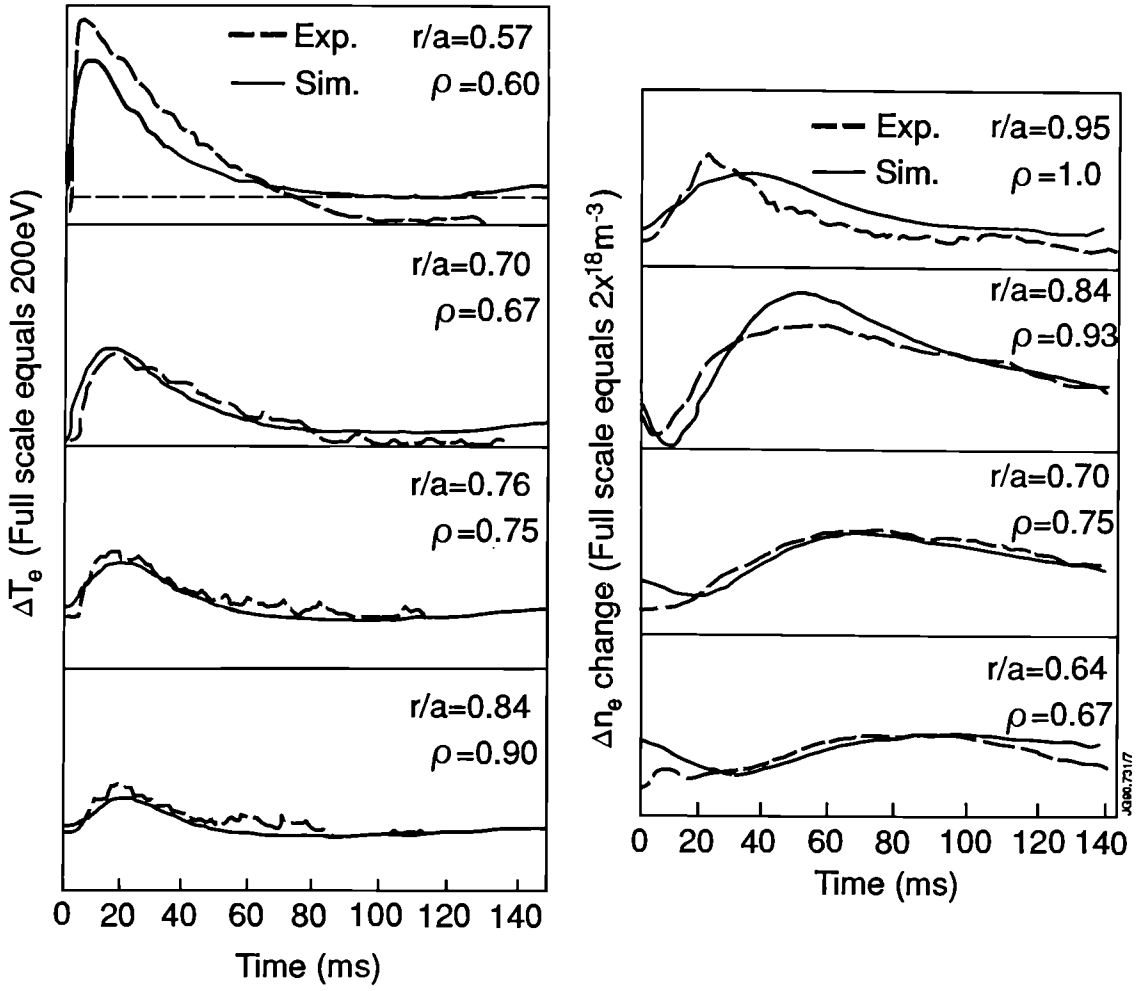

Fig. 11: Application of the model to the propagation of heat and density pulses following the collapse of a sawtooth in JET

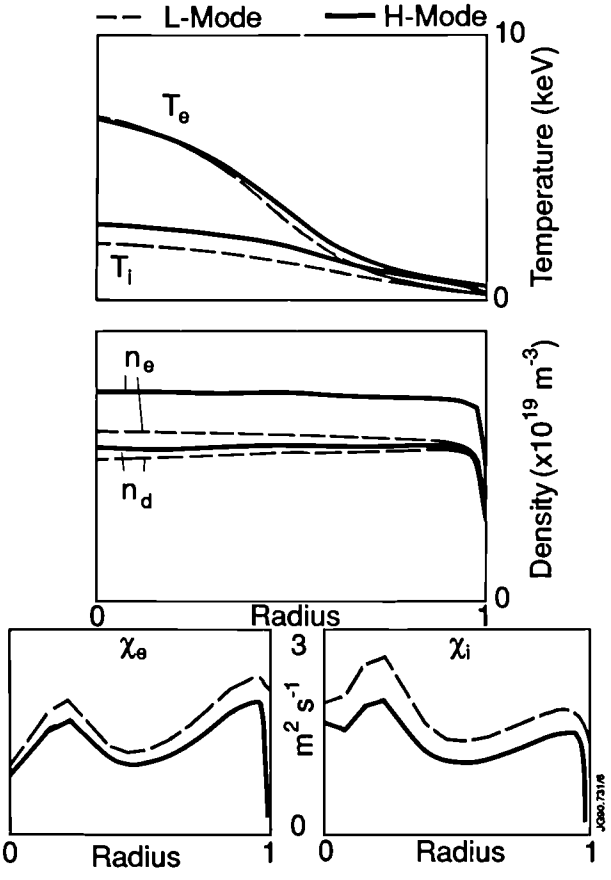

Fig. 12: The characteristics of an H-mode modelled, assuming classical transport near the separatrix

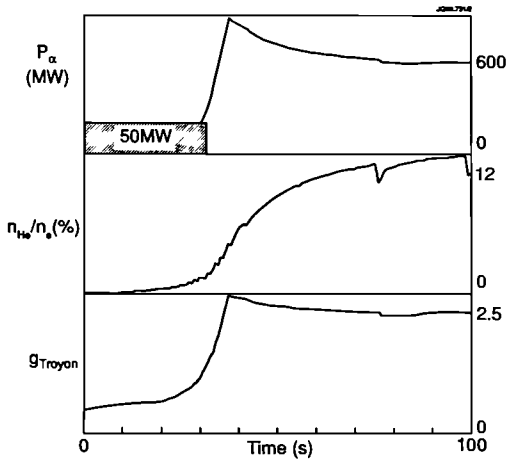

Fig. 13: Model of DEMO plasmas using the L-mode transport model which has been tested against JET results

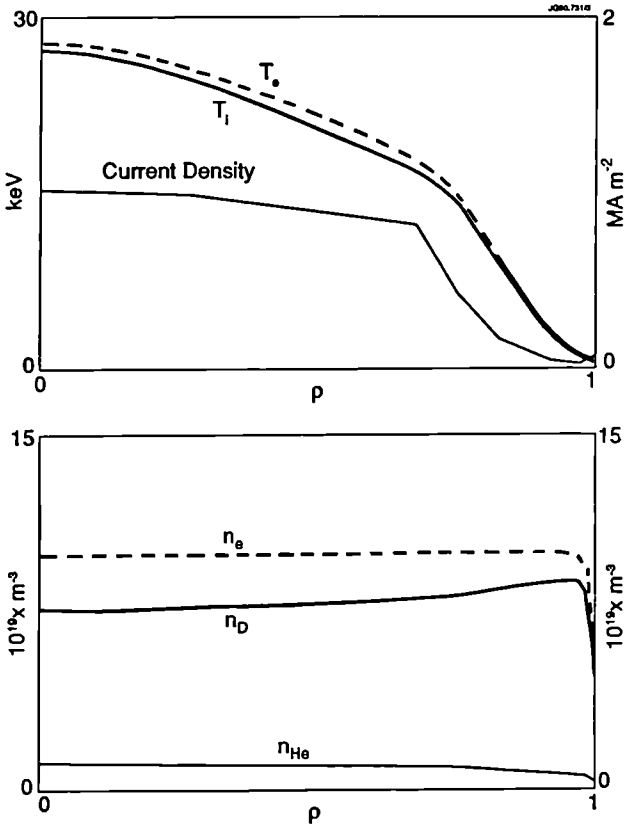

Fig. 14: DEMO profiles at ignition as a function of normalized radius, ρ

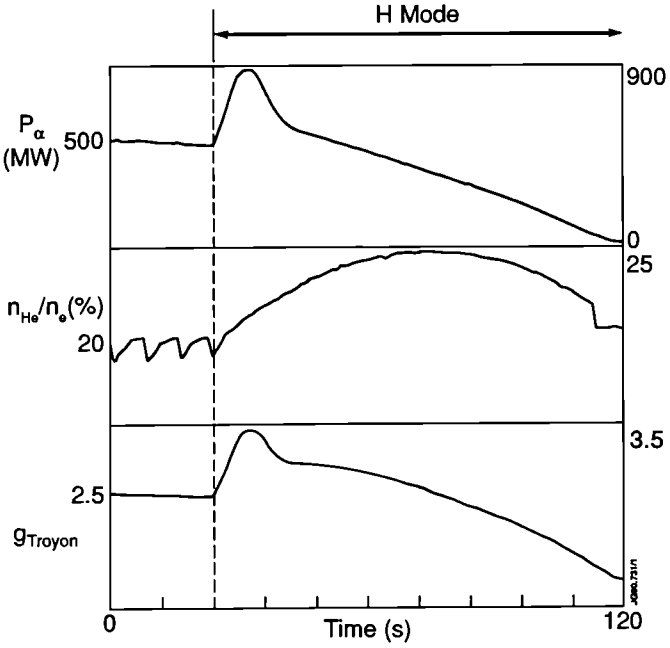

Fig. 15: Long term deficiencies due to helium poisoning in the H-mode

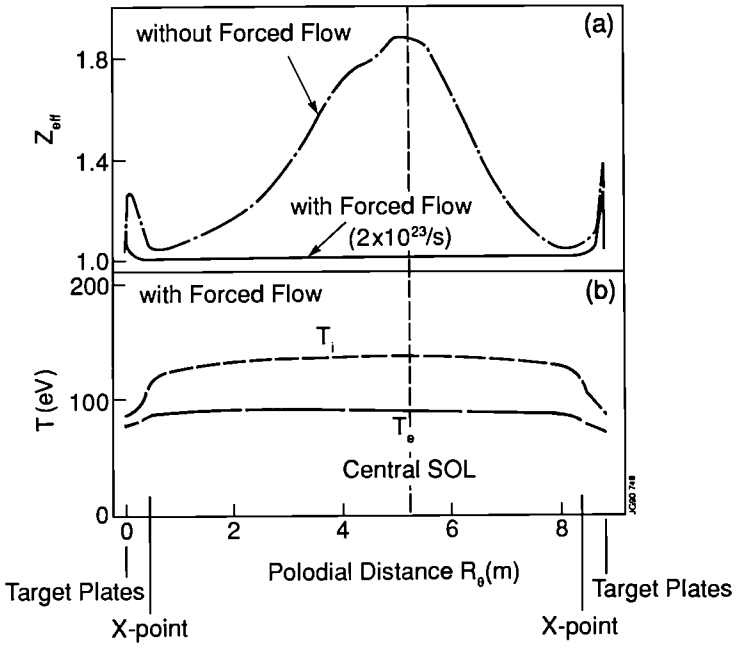

Fig. 16: Poloidal distribution in the SOL and DCP between target plates of (a) the effective ionic charge, Z_{eff}, for cases with and without flow and (b) the electron and ion temperatures for the case with flow


)66 426709 410066 426709 410066 426709 410066 4